



BCN

FINAL REPORT

CRC



Canstar Communications

Submitted To:

Government of Canada
Department of Supply and Services.

Prepared By:

Canstar Communications Division of
Canada Wire and Cable Limited
1240 Ellesmere Road
Scarborough, Ontario.

Title: BCN Project Final Report

Approvals:

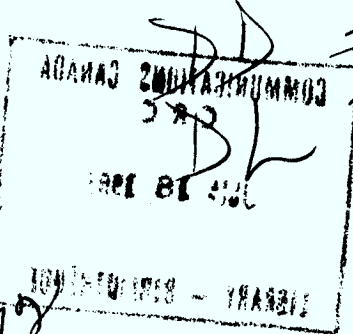
Leon Frank
BCN Project Manager

Dr. Ken Hill
DOC - Design Authority

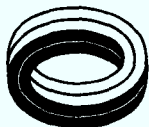
February 1982

1. REPORT NO. PR-110-000404	2. REPORT DATE February 8, 1982
3. TYPE OF REPORT AND PERIOD COVERED Final Report : June 1978 to June 1981	4. NO. OF PAGES
5. TITLE AND SUBTITLE Final Report - Broadband Communication Network (BCN) Project	
6. AUTHOR(S) Leon Frank - BCN Project Manager	
7. PERFORMING ORGANIZATION NAME AND ADDRESS Canstar Communications 1240 Ellesmere Road Scarborough, Ontario. M1P 2X4.	
8. SPONSORING AGENCY NAME AND ADDRESS Department of Supply & Services (DSS): Hull, Quebec Department of Communications (DOC) : Ottawa, Ontario BCN Fiber Optic Inc. : Toronto, Ontario	
9. CONTRACT OR GRANT NO. 82-750	10. SPONSORING AGENCY CODE DSS 1ST 77 00178
11. ABSTRACT <p>This Final Report is a consolidation of the final reports to be delivered following 30 day commissioning and the six months (ammended from one year) operation and maintenance phase. Covered in this report is a summary of the history and events of the complete project and includes a chronological record of the problems encountered, the solutions employed, engineering trade-offs required and results obtained.</p> <div data-bbox="387 1417 713 1649" style="border: 1px solid black; padding: 5px; width: fit-content;"> Industry Canada Library - Queen NOV 21 2013 Industrie Canada Bibliothèque - Queen </div> <div data-bbox="852 1466 1215 1748" style="border: 1px solid black; padding: 5px; width: fit-content; transform: rotate(-5deg);"> COMMUNICATIONS CANADA C R C JUL 18 1983 LIBRARY - BIBLIOTHÈQUE </div>	
12. SUPPLEMENTARY NOTES	13. DISTRIBUTION See attached list

P 91
C655
F73
1982



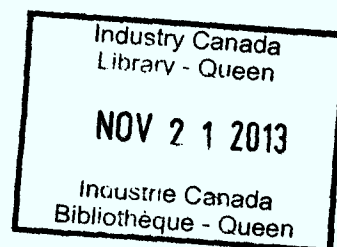
380 4649
381 2587



BCN FINAL REPORT

Distribution:

D.C. Mitchell	General Manager - Canstar
E. Mendell	Manager, Systems - Canstar
Dr. Ken Hill	Department of Communications
J.T. Boyle	Department of Supply & Services
D. Monteith	Canadian Cablesystems Engineering
BCN Members	



Rec'd from M. S. McCune Dept '82 mcp



BCN FINAL REPORT

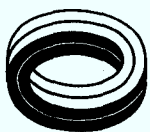
Table of Contents

PART I : EXECUTIVE SUMMARY

- 1.0 Introduction
- 2.0 Summary Description of BCN Project
- 3.0 Project Status
- 4.0 General Evaluation

PART II : TECHNICAL DESCRIPTION

- 1.0 Detailed System Description
- 2.0 History of Major Activities, Problems and Solutions
- 3.0 Test Results
 - 3.1 Performance Target vs Performance Results
 - 3.2 Fibre Optic Cable Transmission Characteristics
 - 3.3 Mean Time Between Failures
 - 3.4 Mean Time to Repair
 - 3.5 System Performance as a Function of Environment
 - 3.6 Digital Loop Thru Tests



PART III : TRAINING AND MAINTENANCE

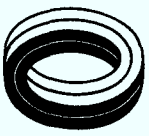
- 1.0 Cable Preparation and Splicing
- 2.0 Connectorization
- 3.0 Routine Maintenance - Fault Detection System
- 4.0 Periodic Maintenance - System Measurements

PART IV : CONCLUSIONS

- 1.0 General Conclusions
 - 1.1 Observations
 - 1.2 System Reliability
- 2.0 Economics of Fibre Optic Systems
 - 2.1 Fibre Optic Cost Projection
 - 2.2 Alternative Fibre Optic System Design

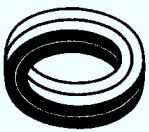
PART V : APPENDIXES

- 1.0 Appendix 1: The Phenomenon of Modal Noise in Analog And Digital Optical Fibre Systems by: R.E. Epworth
- 2.0 Appendix 2: Origin of Delay Noise in High Speed Digital System Using HLP1500 Injection Laser Diodes
- 3.0 Appendix 3: Study on Mechanical and Transmission Characteristics of Optical Fibre Cable During Installation
- 4.0 Appendix 4: Modal Noise in Optical Fibres: Open and Closed Speckle Pattern Regimes by: Y. Tremblay, B.S. Kawasaki and K.O. Hill.
- 5.0 Appendix 5: Optical Transmission Channel Noise Phenomena for High Bit Rate Fibre Optic Systems by: E.J. Miskovic and P.W. Casper.



PART I

EXECUTIVE SUMMARY



PART I : EXECUTIVE SUMMARY

1.0 INTRODUCTION

This final report describes the activities and results of the BCN Fibre Optic Project. The technical proposal prepared at the onset of this project has been carefully outlined detailing the work to be carried out, the expected results and what has been achieved.

At the birth of the BCN project optical fibre technology has already been progressing at an accelerating rate and this typical progression has not yet ceased. As an example in todays technology, designers may select between several techniques to transmit the same video capacity over half as many fibres and the necessity of intermediate repeaters for a 10 km link would be eliminated. Wavelength division multiplexing and transmission over single mode fibres are some of the prospective methods to be implemented in the near future. However, this report will indicate a need for further technological break-throughs in fibre and componentry even though todays technology is well into commercial feasibility. The overall performance vs cost effectiveness will greatly depend upon the technological advances, improved fibre manufacturing and handling, fibre cabling, splicing and connectorization, input-output devices and their associated circuitry.



1.0 (cont'd)

The controlling factor to all new technologies will be cost and as we learn that fibre optic cable is dropping 20 to 30% per year and inexpensive related components are being announced regularly contributing to link cost reduction by as much as 50% in the next two to three years we should expect the degree of penetration of fibre optic applications to increase accordingly.



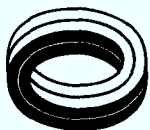
1.1 Technical Feasibility

1.1.1 General

The BCN project has provided an excellent learning experience to the CATV environment and as a result will allow them to enter into fibre optic solutions with greater ease. The BCN system has been plagued with disturbances of spurious noise and other problems related to the design, nevertheless, solutions have been incorporated to make the system operational and the effective design improvements required are discussed to obtain a more viable system.

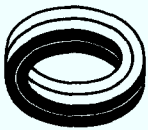
The transfer of technology into CATV operations has been performed satisfactory however, field connectorization of optical fibres, module level repairs of the electro-optic & codec hardware and system diagnostics have not been fully developed. This report discusses improvements which can be implemented in future systems to simplify maintenance work.

Digitally encoded baseband and digitally encoded VSB signals are the two techniques utilized to transmit video signals over the fibre optic cable. The digital approach has been selected over a) analog intensity modulation and b) FM analog intensity modulation because it offers better performance and increased capacity over longer repeater spacings.



1.1.1 General (cont'd)

The analysis behind selecting both digitally encoded BB and VSB is discussed in the following:



1.1.2 Digitally Encoded Baseband

The basic serial data rate requirement for an 8-bit system sampling at 10.74 MHz (3 x's the color sub-carrier - 3.58 MHz) is 86 Mb/s. It has been determined that program audio transmission synchronization can easily be provided with the addition of one bit plus a further bit for parity thereby making the data rate for one video channel 107.4 Mb/s. Thus a three channel system has a rate of about 322 Mb/s.

At high data rates the repeater spacings are determined by fibre cable dispersion or pulse spreading rather than optical losses. The dispersion limit is defined at the rate at which pulse spreading causes a 1 dB (optical) degradation in BER performance. Actual channel bandwidth required for a NRZ signal at 322 Mb/s is 150 MHz. It is common to use a bandwidth · length (MHz.km) product, B_o , as a measure of quality in comparing fibres. Theoretically,

$$B_o = B_m L_m^\gamma$$

where:

B_m = bandwidth measured

L_m = measured length in km

γ = 1 in case of no mode mixing

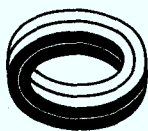
γ = 0.5 in case of complete mode mixing



1.1.2 (cont'd)

In practice γ varies between these extremes depending on the variation in mode mixing and modal compensation in the fibre and extrinsic factors such as measurement techniques and micro-bending due to cabling. γ equal to 0.8 is usually selected as a conservative value estimate of the bandwidth product.

For a 4.2 km repeater spacing and end to end bandwidth requirement of 150 MHz the bandwidth product requirement is therefore 473 MHz.km. Thus a three channel system at a rate of about 322 Mb/s appeared to be a feasible solution.



1.1.3 Digitally Encoded VSB

Normally when TV signals are received at a CATV head end site the signals are in VSB format. Equipment at the head end known as signal processors perform the required frequency conversion. Only in very specialized applications are the VSB signals demodulated to baseband video and then remodulated to VSB.

The process of demodulating and modulating is much more costly than frequency conversion and therefore the motivation in employing digitally encoded VSB in optical systems is significant. Since there are many locations along a distribution trunk where interfacing to VSB format is required there is a substantial cost saving realized in not having to perform the modulation at these points.

A TV channel received "off-air" is first frequency converted through double heterodyne processing with an IF of 45.75 MHz to a low frequency signal centered around 1.25 - 1.5 MHz. This VSB signal is then digitally encoded by the A/D converter which then drives the optical transmitter. At the distribution interfaces the opposite functions are performed.

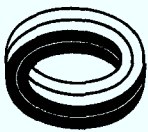
The sampling frequency of 16.11 MHz and a 10 bit word yield a serial data rate of 161.1 Mb/s. Thus a two channel system has a rate of about 322 Mb/s which is essentially equal to the data rate of a 3 channel baseband system. Furthermore, the repeater



1.1.3 (cont'd)

modules and other electro-optic modules are identical for both approaches. Repeater spacing calculations and optical design parameters are equally applicable for both cases.

Performance results of each approach are discussed in Part II.



1.2 Reliability

As a first generation developmental product it is inherent that improvements in equipment and system design would manifest from the test results and observations derived during the commissioning and six month operation and maintenance period.

Equipment failures have been recorded regularly as part of the routine maintenance activities. Nevertheless it has been difficult to ascertain a level of confidence for system reliability performance which will be discussed further in this report. Several recommended improvements in the system have evolved and include the following:

- a) General mechanical arrangement of optical and power supply modules is poor making maintenance lengthy and cumbersome.
- b) F-type electrical connectors mechanically unsuited causing intermittent operation on the associated channel.
- c) Implementation of higher reliability injection laser diodes.
- d) Implementation of higher performance optical connectors.
- e) Improve method of quality control on optical fibres before cabling as a result of brittle fibres on some sections.
- f) Improve design of timing and logic circuits causing frame sync losses due to heating problem.



1.3 Maintainability

The system maintenance philosophy is based on module replacement level only. The link test maintenance unit (on-line supervisory system) assists in isolating faults between stations and remotely reports to the master station triggering an alarm. Our observations have shown that maintaining a fibre optic system is in essence systematically comparable to coaxial or other transmission systems as will be discussed later. The repair philosophy may extend to component level however, for this sophistication, detailed test procedures would be required.

Fibre termination has not yet reached a simplistic and convenient level for field connectorization and it is recommended that the connector assembly work be carried out at the factory. On the other hand field splicing operations are easily accomplished.



2.0 SUMMARY DESCRIPTION OF THE PROJECT

2.1 General

The BCN fibre optic system consists of a six fibre video-supertrunk approximately 8 km in length, designed as an alternative transmission system paralleling the existing coaxial supertrunk. The major intentions of the BCN project were to achieve:

- . learning experiences in the field of fibre optics
- . cost and performance evaluations of fibre optic systems vs coaxial cable system for future broadband telecommunication services
- . reliability of the system
- . serviceability of the system
- . operating and maintenance cost

2.2 BCN Project Organization

Broadband Communications Networks (BCN) Ltd. is a consortium of five major Canadian cable TV companies who in conjunction with Canada Wire and Cable (CWC) Ltd. formed BCN Fibre Optics Ltd. for the purpose of supply and testing of a fibre optic transmission system for CATV point-to-point signal distribution.



2.2 (cont'd)

Canada Wire and Cable Ltd. performed as the prime contractor for the procurement and installation of the BCN supertrunk electro-optic equipment and fibre optic cable. The equipment was purchased from Harris Electronics Systems Division and the cable core from Siecor.

Subsequently, Canada Wire and Cable Ltd. formed Canstar Communications, a wholly owned division to manufacture and supply fibre optic cable systems.

2.3 BCN Project Objectives and Results

2.3.1 (a) Objective I

The construction of a six fibre transportation trunk approximately eight kilometers in length. The capacity to be 15 TV channels and 12 stereo FM channels. Looping will simulate rural trunking up to 48 kilometers. Digitally encoded video and digitally encoded vestigial sideband transmission systems will be tested.



2.3.1 (b) End Result of Objective I

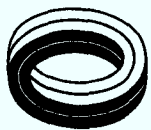
Construction of a six fibre transportation trunk approximately eight kilometers in length is completed, having a capacity of 15 TV channels and 12 stereo FM channels. Loop thru simulations have been attempted however, no conclusive results determined as discussed in Part II, Section 3.6 of this final report. Digitally encoded baseband video and digitally encoded vestigial sideband transmission systems have been tested and results documented in Part II, Section 3.1.

2.3.2 (a) Objective II

The accumulation of technical and economic data on the design, installation and operation of a digital fibre optic trunk.

(b) End Result of Objective II

Technical data has been accumulated as documented in Part II of this final report. It has been difficult to quantitatively appreciate the maintenance loading aspects due to the developmental nature of the project and the unforeseeable disturbances which have materialized during the field turn-up and commissioning phases. However, regardless of the above from our own observations and handling we have assessed preventive maintenance costs of a fibre optic system within same boundaries as that of a coaxial network and corrective maintenance, assuming module replacement level only, similarly equivalent.



2.3.3 (a) Objective III

The demonstration, both to Canadian and foreign markets, that Canada has the necessary capabilities, expertise and experience to engineer and deliver a complete fibre optic system.

(b) End Result of Objective III

The results, solutions and conclusions of this project are a major contribution to future projects involving high bit rate transmission over fibre optics.

2.3.4 (a) Objective IV

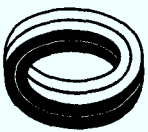
The design and manufacture of a fibre optic cable for pole mounting suitable for withstanding stress during installation and rigors of Canadian weather (London, Ontario).

(b) End Result of Objective IV

The design and manufacture of a fiber optic cable for pole mounting has been completed. Results of the installed cable are documented in Part II Section 3.0 of this report.

2.3.5 (a) Objective V

The design of a system to integrate the fibre optic cable with electro-optic and electronic equipment at data rates suitable for cable TV.



2.3.5 (b) End Result of Objective V

The design of a system to integrate the fibre optic cable with electro-optic and electronic equipment has been completed. Cable losses and optical output power used in the system design calculations proved to be inferior to that which was actually manufactured and as a consequence it became beneficial to re-configure the original system to one repeater.

2.3.5 (a) Objective VI

The construction and test in the laboratory of equipment prototypes (transmitters, repeaters, receivers, fault locators, etc).

(b) End Result of Objective VI

The construction and test in the laboratory of the equipment prototypes have been completed.

2.3.7 (a) Objective VII

The assembly and test of a representative system of equipment, cable and connectors in a laboratory environment.

(b) End Result of Objective VII

The assembly and test of a representative system of equipment, cable and connectors in a laboratory environment have been completed and accepted.



2.3.8 (a) Objective VIII

The installation, test and commissioning of the system in a cable TV network.

(b) End Result of Objective VIII

The installation, test and commissioning of the system in a cable TV network have been completed as detailed in Part II Section 2.0 of this report.

2.3.9 (a) Objective IX

The training of regular cable TV personnel in aspects of systems design, construction, operation and maintenance.

(b) End Result of Objective IX

The training of regular cable TV personnel in aspects of system design, construction, operation and maintenance has been completed as detailed in Part III of this final report.

2.3.10(a) Objective X

The operation and maintenance of the system for one year after commissioning and throughout the commissioning and operating periods, to perform a series of tests to measure technical performance and economic aspects of the system. A series of tests and assessments will also be made to gauge the ability of technical staff to cope with the technological changeover.



2.3.10(b) End Result of Objective X

The operation and maintenance of the system for one year after commissioning had been contractually amended to six months. This six months post-commissioning phase has been completed. During this period a series of tests have been performed to measure the technical performance of the system. Some economic aspects are discussed in Part IV. It has been assessed that there were no difficulties for the technical staff to cope with the technological changeover and therefore no special tests were created to evaluate personnel adaptability.

2.4 System Description and Configuration

The BCN supertrunk system utilizes fibre optic cable and terminal equipment to provide transfer of cable television signals from an antenna location (Head End) to the distribution point (Hub End).

The system is installed in London, Ontario on a route which is parallel to an existing coaxial system. The existing system consists of an antenna system on CFPL-TV tower with RF pre-amplifiers and frequency translation devices as required to provide a frequency division multiplexed cable television system. A one inch coaxial cable and broadband repeater amplifiers provide the transfer of vestigial sideband signal from the signal receiving terminal at CFPL-TV to the hub terminal at London Cable TV.



2.4 (cont'd)

The entire route represents approximately 8 km of aerial coaxial cable lashed to a messenger wire which is supported by utility poles.

The BCN fiber optic cable parallels the existing coaxial cable trunk system in that it is lashed either to the same messenger wire or to another messenger wire mounted on the same utility poles as the coaxial cable. The signal sources for the BCN fibre optic equipment is the same antenna system as that supplying the existing coaxial system. Whereas, the coaxial system uses frequency division multiplexing of the vestigial sideband signals for transfer of the multiple television signals on a single cable, the BCN fiber optic system employs two digital techniques.

One requires demodulation of the television signal to baseband where it is digitized, then time division multiplexed with two other serial, digitized television signals into a single 322 megabit data stream. This modulates an infrared laser and is fed down a graded index optical fiber cable.

The second technique requires a vestigial sideband television signal at I.F. frequencies. This signal is translated such that its picture carrier is about 1.75 MHz, and is then digitized. It is time division multiplexed with one other digitized VSB signal to modulate a laser diode with a 322 megabit data stream.



2.4 (cont'd)

In addition to the television signals, digitized FM signals and baseband audio signals are time division multiplexed where necessary to the data stream.

The optical levels along the fibre are augmented by an optical/electrical/optical, non-regenerative repeater mid-way between terminal ends.* At the hub or receiving end the serial optical signals are demultiplexed and converted to analog levels representing either baseband or vestigial sideband television signals. The baseband signal can now be fed to a standard modulator along with the decoded baseband audio to generate a vestigial sideband television signal. The output of the vestigial sideband units are translated up to the correct frequency, using standard converter units.

* The original system configuration of the 8km video link consisted of two non-regenerative repeater stations equally spaced apart between the terminal ends. This configuration manifested its vulnerability both to optical noise interference and high receiver input levels (excess system gain leading to overdriving of the receiver). Therefore, a one repeater station mid-way between terminals was selected as the most optimum solution to combat this interference. Details of the reconfiguration work are described in Part II.



3.0 PROJECT STATUS

3.1 Major Tasks Completed

- 3.1.1 The design and manufacture of fibre optic cable for aerial installation lashed to a messenger wire.
- 3.1.2 The system design of integrating the fibre optic cable with electro-optic and electronic equipment at an operating data rate of 322 Mb/s.
- 3.1.3 The construction, assembly and lab testing of a prototype system.
- 3.1.4 The factory acceptance testing of the system integrating both the equipment and the cable.
- 3.1.5 The manufacture, assembly, test and shipping to site of the complete system hardware and cable.
- 3.1.6 The installation, acceptance testing and commissioning of the system on site.
- 3.1.7 The operation and maintenance of the system for six (6) months after commissioning.



3.1.8 The performance of a series of tests to measure the technical performance of the system.

3.1.9 The training of regular cable T.V. personnel in aspects of system design, operation and maintenance.

3.2 System Operational Status

The operational status of the system as of June 1981 is given in Table 3.2.1.

TABLE 3.2.1 OPERATIONAL STATUS

Description	Status	Notes
1. Link #1 (baseband)	Operational	BER is high $\approx 10^{-5}$ and frame sync is lost at a rate of 2 to 3 counts per minute.
2. Link #2 (baseband)	Operational	BER is $\approx 10^{-7}$ and no loss of frame sync is experienced.
3. Link #3 (vestigial sideband)	Operational	BER is $\approx 10^{-7}$ and no loss of frame sync is experienced.
4. Link #4 (vestigial sideband)	Operational	BER is $\approx 10^{-7}$ and no loss of frame sync is experienced.
5. Link #5 (vestigial sideband)	Not Operational	Problem diagnosed in the VSB receiver drawer. Spares were not purchased for the VSB system.
6. Link #6 (baseband)	Operational	BER is high $\approx 10^{-5}$ and frame sync is lost at a rate of one count every 2-3 minutes.
7. FM Stereo Channel over baseband link	Not Operational	Problem not diagnosed.
8. FM Stereo Channel over VSB link	Operational	Two sound channels are inoperative.

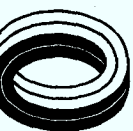


TABLE 3.2.1 OPERATIONAL STATUS (cont'd)

Description	Status	Notes
9. LTMU	Inhibited	LTMU is inhibited to allow the baseband channel associated with the LTMU information transfer to function normally. Minor repairs to the LTMU system internally are also required.
10. Spare BB Transmitter Drawer	Operational	
11. Spare BB Receiver Drawer	Not Operational	Spare modules used to replace failed modules in the system.
12. Spare Repeater Modules	Operational	Used to replace failed modules in the system
13. Spare Transmitter Modules	Operational	
14. Spare Receiver Modules	Operational	
15. Two Spare Fibres Between Head End & Repeater Site	Operational	
16. Two Spare Fibres Between Hub End & Repeater Site	Both Not Operational	One break located at a splice location. The other break located at the repeater site (determined by the OTDR).



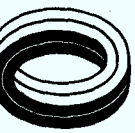
4.0 GENERAL EVALUATION

The tasks and expectations outlined in the technical proposal have been accomplished. Performance of the BCN system is documented in Parts II and III and the derived conclusions are discussed in Part IV.

The success of this project is measured by the contributions it has presented in familiarizing the CATV environment to fibre optics, keeping them in step with the upcoming technology and has provided guidelines for the systems design of future CATV applications.

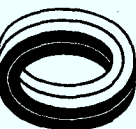
Unknown optical phenomena and design deficiencies have caused this program to extend much beyond the time frame originally planned. During this period fibre optic technology has progressed extensively. For example, production of graded index multi-mode fibre having attenuations lower than 3.0 dB per kilometer is commonly available therefore making the BCN cable virtually obsolete. This is an expected result for a technology entering into the commercial world. On the other hand, fibre optic system costs (both capital and operational) still remain higher than coaxial cable with comparable channel capacity.

A large effort has been exerted into making the system operational as well as completing the commissioning and testing phases of the system. The learning experiences obtained from this project have been tremendous, especially in areas such as, installation, handling, troubleshooting and designing fibre optic systems.



PART II

TECHNICAL DESCRIPTION



PART 2 - TECHNICAL DESCRIPTION

1.0 DETAILED SYSTEM DESCRIPTION

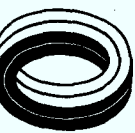
The BCN system consists of:

- a) Head-End Terminal
- b) Hub-End Terminal
- c) Repeater Site (located mid-way between Hub & Head Terminal Sites)
- d) Inter-connecting 8-Fibre Optic Cable

Figure 1.1.1 is a block diagram illustrating the system configuration and Figure 1.1.2 is a route map illustrating the locations of the Head-End Terminal, Hub-End Terminal and Repeater Site.

The equipment is connected to the cable by a fibre pigtail cord. The pigtail cord is connectorized at one end by a male optical connector which mates with its female counterpart mounted on the equipment frame. The other end of the pigtail cord is fusion spliced to the cable. The same holds true for the repeater site except that the pigtail cords are female connectorized and the repeater modules are male connectorized onto the modules' pigtail protruding from the repeater module itself.

The system is equipped for operation of six optical links with two additional fibres incorporated in the cable as spare.



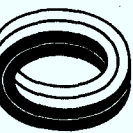
1.0 DETAILED SYSTEM DESCRIPTION (cont'd)

The terminal sites operate from 115V AC power brought to AC outlets mounted on the sides of the equipment bay. AC to DC converters are mounted in the equipment drawers. At the repeater site an AC to DC power supply is housed in a sealed box which is mounted on a pole. The repeater housing (water-tight) mounts on the messenger wire a few feet from the pole. A connectorized power cable is used to connect between repeater and power supply housings. The BCN system consists of the following integral components:

1.1 Terminal Equipment

The head end equipment consists of a double width electronic rack. The electronics required to interface with each fibre occupies a single drawer 7" high by 19". Each drawer has its own power supply and fan assembly, however, a master blower located at bottom of the rack provides vertical ventilation. Each drawer, with the exception of the FM drawer, can then be operated by itself, within the rack assembly. The FM encoder assembly feeds more than one encoder drawer and does not have an optical output.

The head end equipment supplied consists of three baseband video encoder drawers (one a spare), two vestigial sideband signal encoder drawers, one baseband video decoder drawer, one vestigial sideband signal decoder drawer, two FM encoder drawers and one remote link maintenance test unit (LMTU) drawer.



1.1 Terminal Equipment (cont'd)

The hub end equipment consists of one double rack with 3 baseband video decoder drawers (one spare), providing 3 video outputs each and 2 VSB video decoder drawers with 2 VSB signal outputs each.

One baseband encoder drawer and one VSB encoder drawer are included for the upstream link. The master link maintenance test unit (LTMU) is located in this rack. A fan assembly at the bottom of the rack provides for vertical air flow in the rack and a fan on each drawer gives horizontal air flow. As the head end equipment each drawer has its own power supply.

1.1.1 Baseband Video Encoder Drawer

This drawer has provisions to input three baseband video signals at a 1 volt p-p level. Internal A-D converters operating at a 10.7 MHz sample rate convert the video at an eight bit word. Two bits are added to include parity, synchronizing, audio and FM stereo information. Each of three serial digital data streams are scrambled and then interleaved to drive the optical transmitter modules. The data rate on the output is 322.2 Mb/s. The clock rate for the drawer is divided down to be phase-locked to an internal 3.58 MHz reference. In this system the sample frequency of A-D converters is not locked to the color subcarrier reference of the incoming video as each drawer is designed to handle three non-synchronous (to each other) video inputs.



1.1.1 Baseband Video Encoder Drawer (cont'd)

In addition to the video inputs, provisions are made for three balanced audio inputs which are again digitized in a 10-bit A-D converter. Three FM digital inputs are provided which interface with FM stereo encoder drawers. Clock and sync outputs from the baseband video drive the FM stereo encoder drawer. Other inputs provide for asynchronous digital data to be added to the data stream. Figure 1.1.3 shows the block diagram of the baseband encoder drawer.

An optical connector on the rear connector panel is connected to laser diode in the optical transmitter module by a fibre optic pigtail. Since there are no front panel gain controls, it is essential to ensure that the levels of the audio to video inputs are correct, i.e. 1V p-p for the video. Figure 1.1.4 shows the composition of the data signal format.

1.1.2 Vestigial Sideband Encoder

The encoder input is an I.F. frequency VSB signal at +30 dBmv level. The picture carrier is at 45.75 MHz with the video spectrum inverted. This signal is available from the CATV head end equipment.

Two VSB signal inputs are provided. Each of the inputs is down converted, such that the picture carrier is at 1.75 MHz and the sound carrier at 6.25 MHz. A 8-bit A-D converter operating at 16.1 MHz converts the down converted VSB signal into an 8-bit word.



1.1.2 Vestigial Sideband Encoder (cont'd)

Two bits, one a spare, the other with synchronizing and digitized FM information are added. The 10-bit words are serialized, scrambled and interleaved to form a 322.2 Mb/s data stream which drives the optical transmitter. The data format for the digitized and interleaved VSB signals is shown in Figure 1.1.5.

The optical transmitter (located at back of the drawer) uses infrared laser diode with a photo detector feedback system to regulate the output. A thermo-electric cooler maintains the laser temperature less than +35°C.

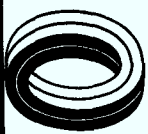
Modular power supplies are located in the rear area of the drawer.

Figure 1.1.6 shows the block diagram of the VSB encoder.

1.1.3 FM Stereo Encoder

The FM stereo encoder drawer has facilities for digitizing six FM inputs. Each FM input operates with an FM input level of +30 dBmV at a center frequency of 10.7 MHz.

The FM input at 10.7 MHz is down converted to a center frequency of 250 KHz. An A-D converter digitizes this signal to a 9-bit parallel word at 859.2 KHz rate. The 9-bit word is serialized at a 10.7 MHz rate. This serial output is connected to either a baseband or VSB encoder which adds the data to the selected data stream. The baseband or VSB encoder provides the synchronizing and strobe clocks to the FM encoder drawer. As the VSB drawer has facilities for 4 FM



1.1.3 FM Stereo Encoder (cont'd)

channels and each baseband drawer has facilities for 3 FM channels and the FM sampling rates are synchronous to the appropriate video A-D sampling rate, 3 pairs of inputs are required for FM synchronizing and FM strobe pulses. Each pair can be operated from separate encoder drawers as required. Internal to the system is an FM sync pulse and FM strobe pulse selection system where each FM encoder module will be fed from the FM sync and FM strobe pulse appropriate to the encoded data stream it will be feeding in the video encoding drawer. Figure 1.1.7 shows the block diagrams of the FM stereo encoder drawer.

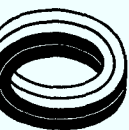
This drawer does not include optics as the output is added to the output of either a baseband or vestigial sideband encoder.

1.1.4 Baseband Video Decoder

This drawer accepts an optical signal in via an optical connector on the rear panel. This connector is connected to the optical receiver module via a fibre optic pigtail.

The optical receiver has an avalanche photodiode input with AGC capabilities to handle from 100 nW to 10 μ W (-40 dBm to -20dBm) average optical input.

The output of the optical receiver drives a phase lock oscillator system for clock recovery. The recovered clock is used to perform a logic decision on the input data stream.



1.1.4 Baseband Video Decoder (cont'd)

The 322 Mb/s data is demultiplexed into three data streams, one to each video decoder module. The 107 Mb/s serial data stream is descrambled and converted to a parallel format. Eight bits (of a 10 bit parallel word) are applied to the D-A converter which provides the video output, the remaining two bits, one of which is parity and the other is demultiplex to the FM digital port, the audio decoding circuit and the sync comparator circuit. Figure 1.1.8 shows the block diagram of the decoder drawer. The outputs are 3 baseband video channels at 1V p-p, 3 balanced audio channels, 3 FM digital data streams, the 3 FM sync and 3 FM strobe lines, the latter feed the FM decoder drawers.

1.1.5 Vestigial Sideband Decoder

The optical input is applied to the optical receiver module via a fibre optic pigtail from the optical connector on the rear panel to the optical receiver module.

A phase lock oscillator system locking to input data stream regenerates the clock. The input data is strobed by this clock and the regenerated data is de-interleaved into two data streams. Each stream is descrambled and converted to a 10-bit parallel format where 8-bits are applied to D-A converter. The output of the D-A is a vestigial sideband signal which is up converted to the I.F. frequency with its picture carrier at 45.75 Hz.

Figure 1.1.9 shows the block diagram of the VSB decoder.



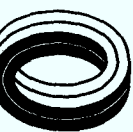
1.1.6 FM Stereo Decoder

The baseband or vestigial sideband decoders demultiplex a serial bit stream which is applied to the FM decoder drawer. This serial data stream is converted to a parallel 9-bit word using the strobe and sync information coming from the appropriate decoder drawers. The 9-bit word generates within a D-A converter, an analog output which is up converted to a 10.7 MHz I.F. signal. The output represents an FM stereo signal with a center frequency at 10.7 MHz at +30 dBmV. Figure 1.1.10 shows the block diagram of the FM decoder drawer.

1.1.7 Link Test and Maintenance Unit (LTMU)

The LTMU subsystem integrates into the system configuration as shown in Figure 1.1.11. The LTMU MASTER generates a command word consisting of an 8-bit command byte and an 8-bit data byte. This command word is then transmitted via PAM on the uplink channel. The FIDRIG module at the repeater site looks at the command word address and should the command address correspond to a FIDRIG's unique station code, the FIDRIG responds, loads the requested data into the data byte and retransmits the word uplink. If there is no address correlation, the FIDRIG retransmits the word without loading any data.

At station "0", the LTMU REMOTE retransmits the word, translates the word to ECL logic levels and feeds the word to all four downlink channels where the word is transmitted to station "2" via overhead bits of the channel bit stream. At station "2", the word is retranslated, processed and the requested data is displayed.



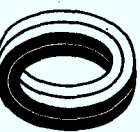
1.1.7 Link Test and Maintenance Unit (LTMU) (cont'd)

A command is sent once each second. The LTMU MASTER performs two functions, bit error rate (BER) monitoring, and the generation and decoding of interrogation command and response words to monitoring circuitry (FIDRIG's).

The BER circuitry continually monitors all four downlink fibers for bit errors. An error strobe is generated whenever a frame sync error is detected on the fibre bit stream by the decode circuitry. These error strobes are counted and time averaged with a time base determined by both LTMU controls, and the channel monitored. The following table defines these time bases:

<u>Channel</u>	<u>Short Mode</u>	<u>Long Mode</u>
1 Baseband	9.32 Sec	932 Sec
2 Baseband	9.32 Sec	932 Sec
3 VSB	6.21 Sec	621 Sec
4 VSB	6.21 Sec	621 Sec

At the end of each time base, the count is stored and counting circuitry is reset to zero. The count can be displayed as errors-as-they occur, or as a total error count which is updated at the end of each time base. Excessive BER conditions will activate the audio alarm and fault LED's.



1.1.7 Link Test and Maintenance Unit (LTMU) (cont'd)

The major differences between LTMU MASTER, LTMU REMOTE and Repeater FIDRIG are monitoring capabilities, transmission and reception schemes, and environmental. The LTMU MASTER and the LTMU REMOTE are capable of monitoring six voltages and one temperature. The Repeater FIDRIG can monitor twelve voltages and two temperatures. The LTMU MASTER receives NRZ bits and transmits PAM. The Repeater FIDRIG both transmits and receives PAM. The LTMU REMOTE receives PAM and transmits asynchronously to overhead bits. The Repeater FIDRIG is designed to operate over temperature extremes. The other two are designed for room temperature.

Once the FIDRIG has received a Manchester word, it decodes the word to NRZ and stores it in two eight-bit parallel input/output shift registers. The mux address is determined by the channel selected, etc., and the appropriate analog mux channel is turned on. The monitored signal is then scaled and analog to digital converted into an 8-bit data byte. This data byte is then loaded into the shift register, if an address correlation occurs. An address correlation occurs if the station code in the command word is identical to the FIDRIG's station code. If no address correlation occurs no data is loaded, and the command word is re-encoded, unmolested, and retransmitted.

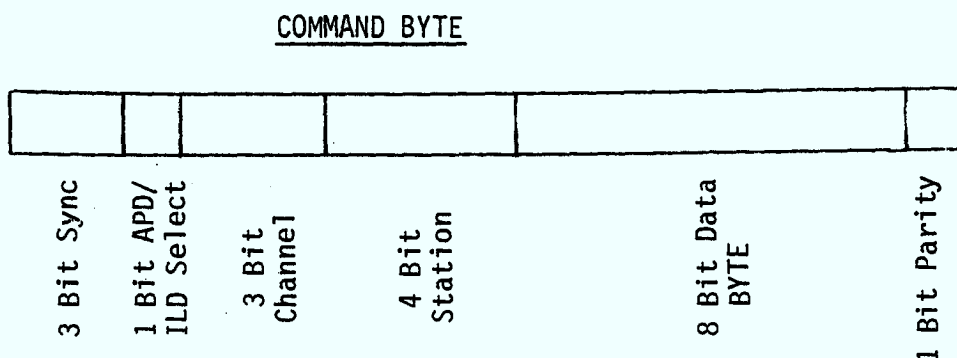


1.1.7 Link Test and Maintenance Unit (LTMU) (cont'd)

The interrogation command word is generated utilizing front panel controls. The LTMU MASTER, using a multiplex terminal unit (MTU), creates a 20 bit Manchester encoded command word.

The word is broken down as follows:

Manchester code transmits a logic one bit as 10 and a zero as 01:



If used with FIDRIG's, station, channel, and APD or ILD can be interrogated to obtain voltage or temperature data by selecting the appropriate control settings.

The response word comes from either an internal LTMU/FIDRIG or from overhead bits of the six optical bit streams. These six channels are multiplexed, and the response word is decoded by an MTU. The data byte is then extracted, processed and displayed on the front panel. Also, the received word's command byte is compared with the transmitted word's command byte. Any discrepancies are displayed on the front panel. If the received word has, due to bit error conditions invalid Manchester bits, the display will blank, indicating an invalid word was received.



Figure 1.1.1 BCN SYSTEM BLOCK DIAGRAM

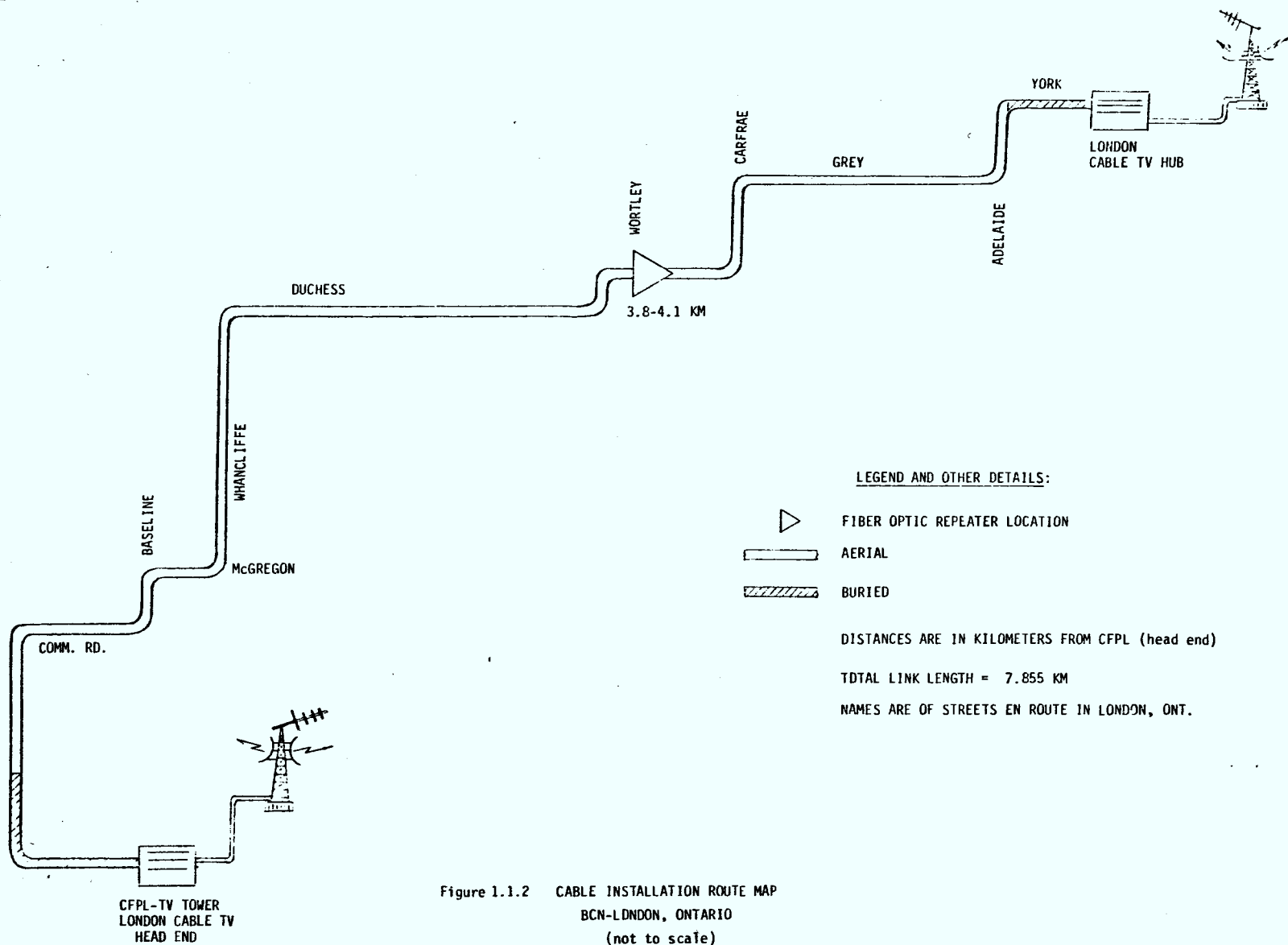


Figure 1.1.2 CABLE INSTALLATION ROUTE MAP
BCN-LONDON, ONTARIO
(not to scale)

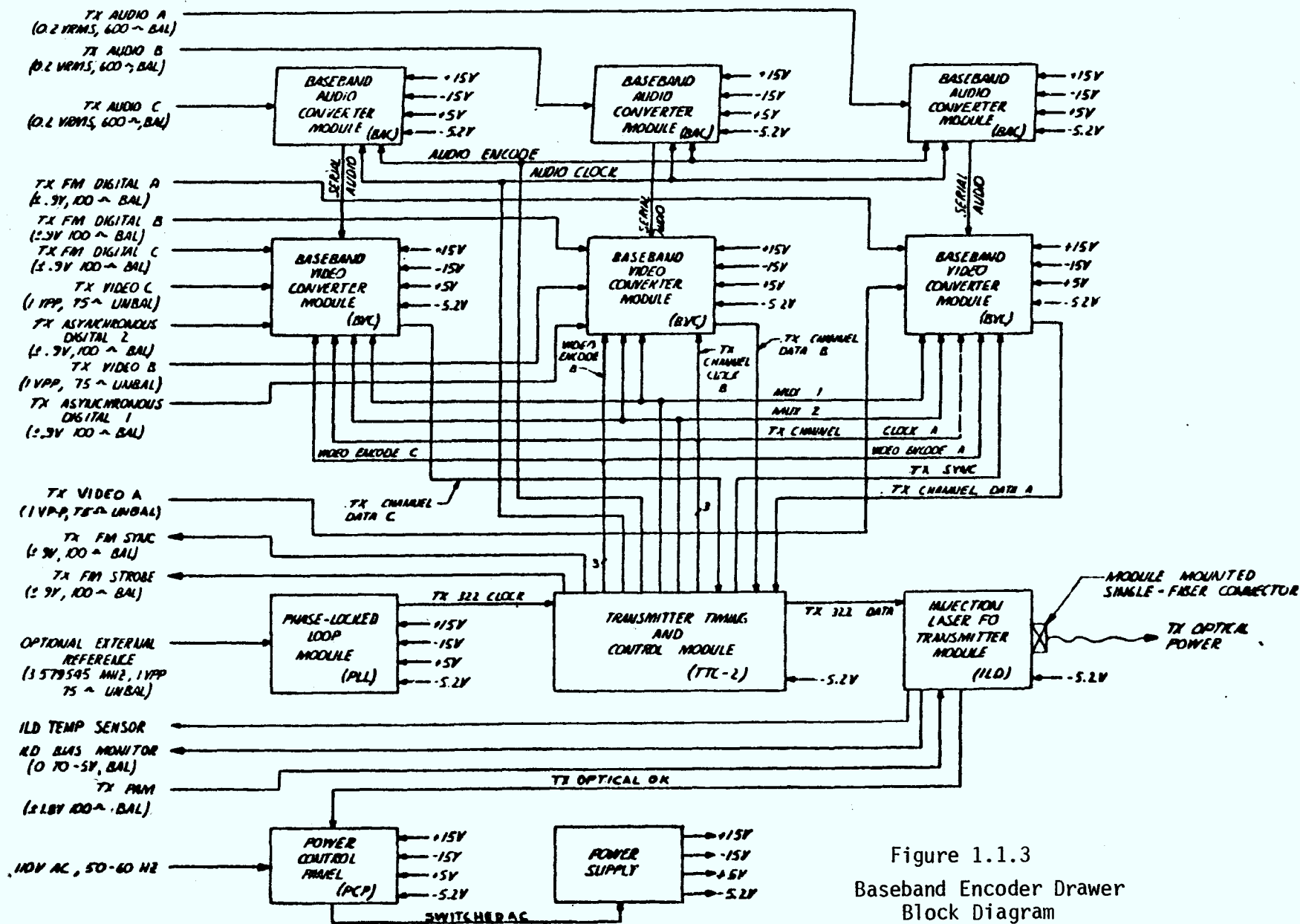


Figure 1.1.3
Baseband Encoder Drawer
Block Diagram

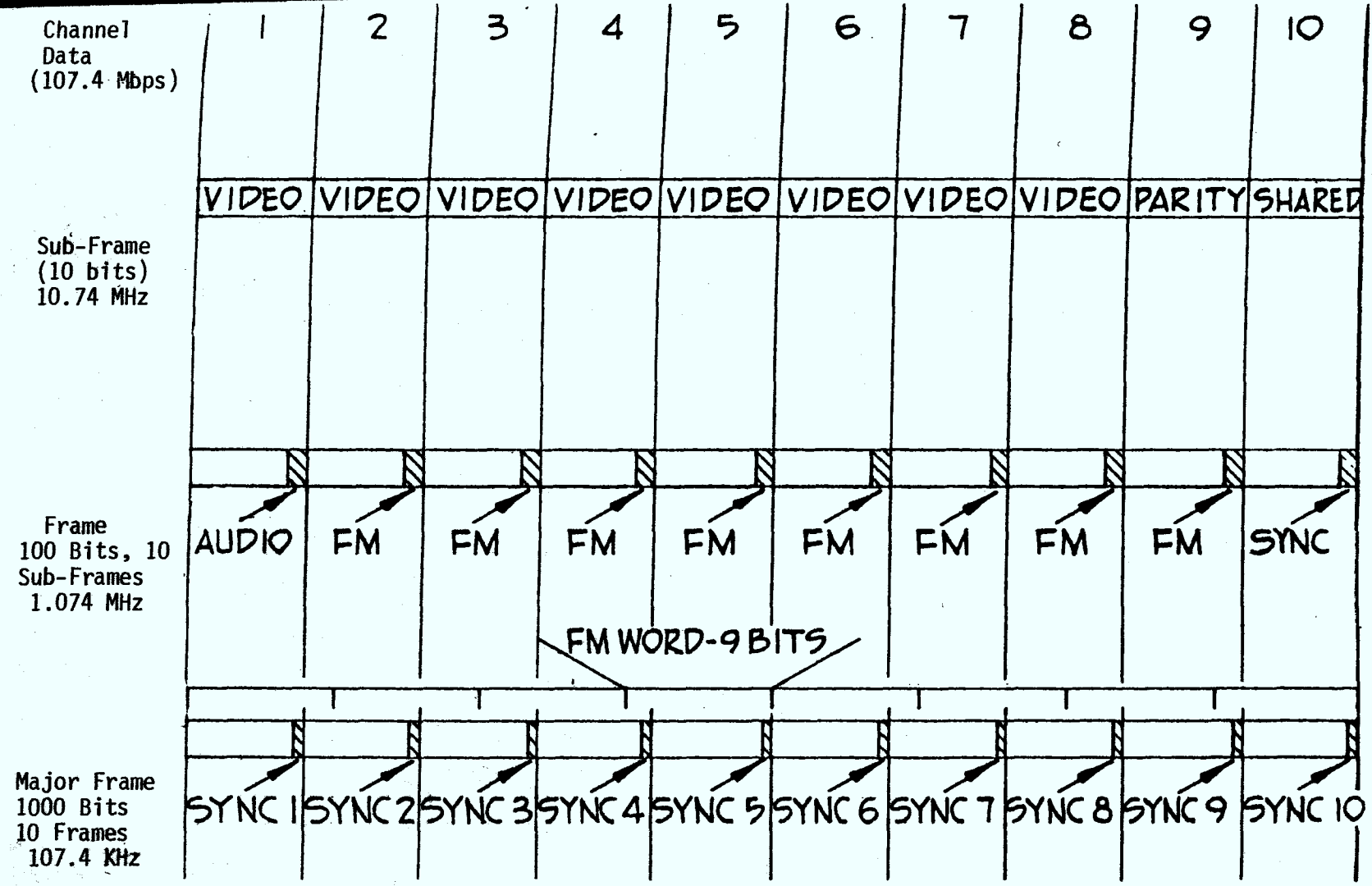


Figure 1.1.4
BB Channel Data Format

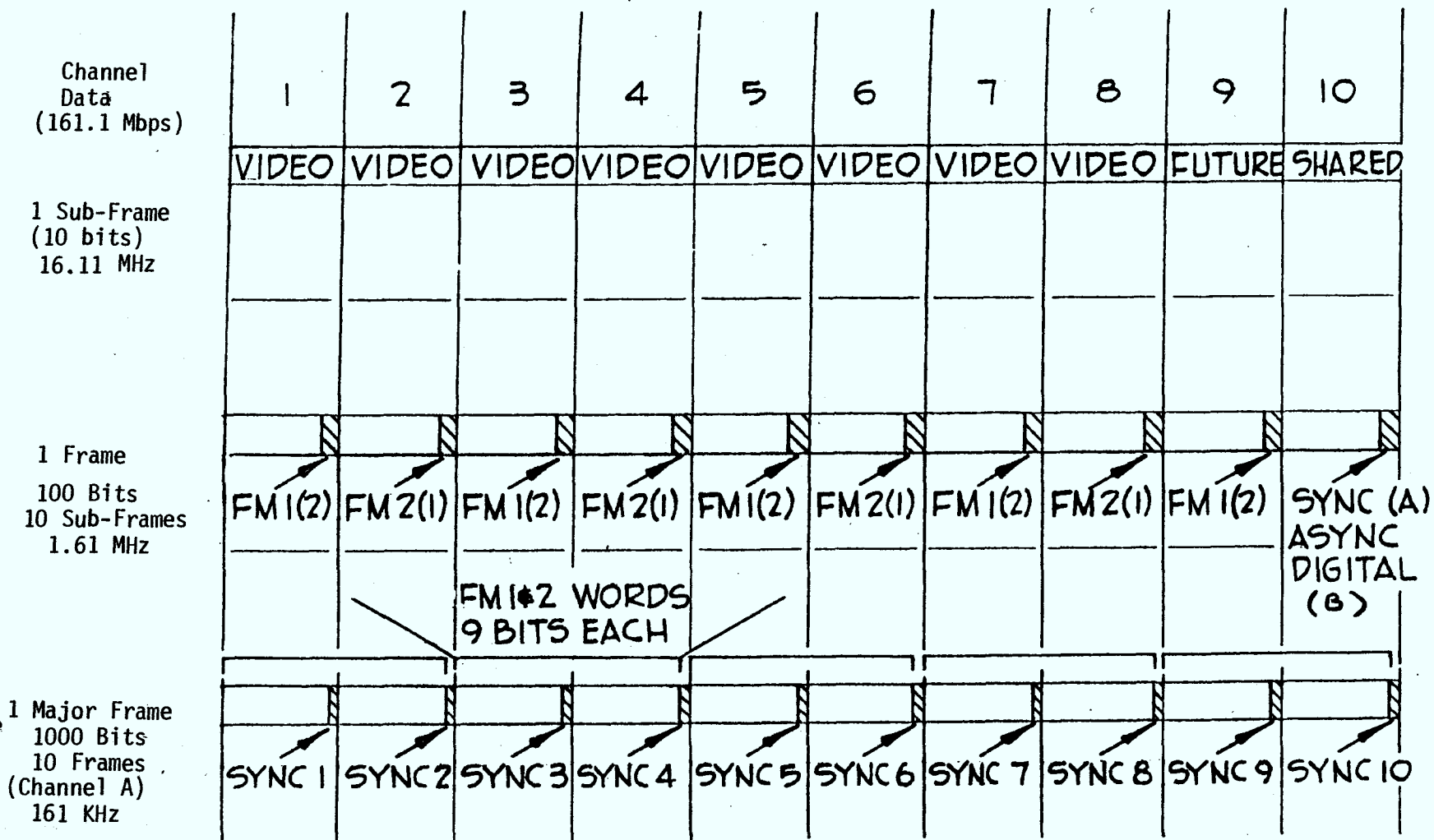


Figure 1.1.5
VSB Channel Data Format

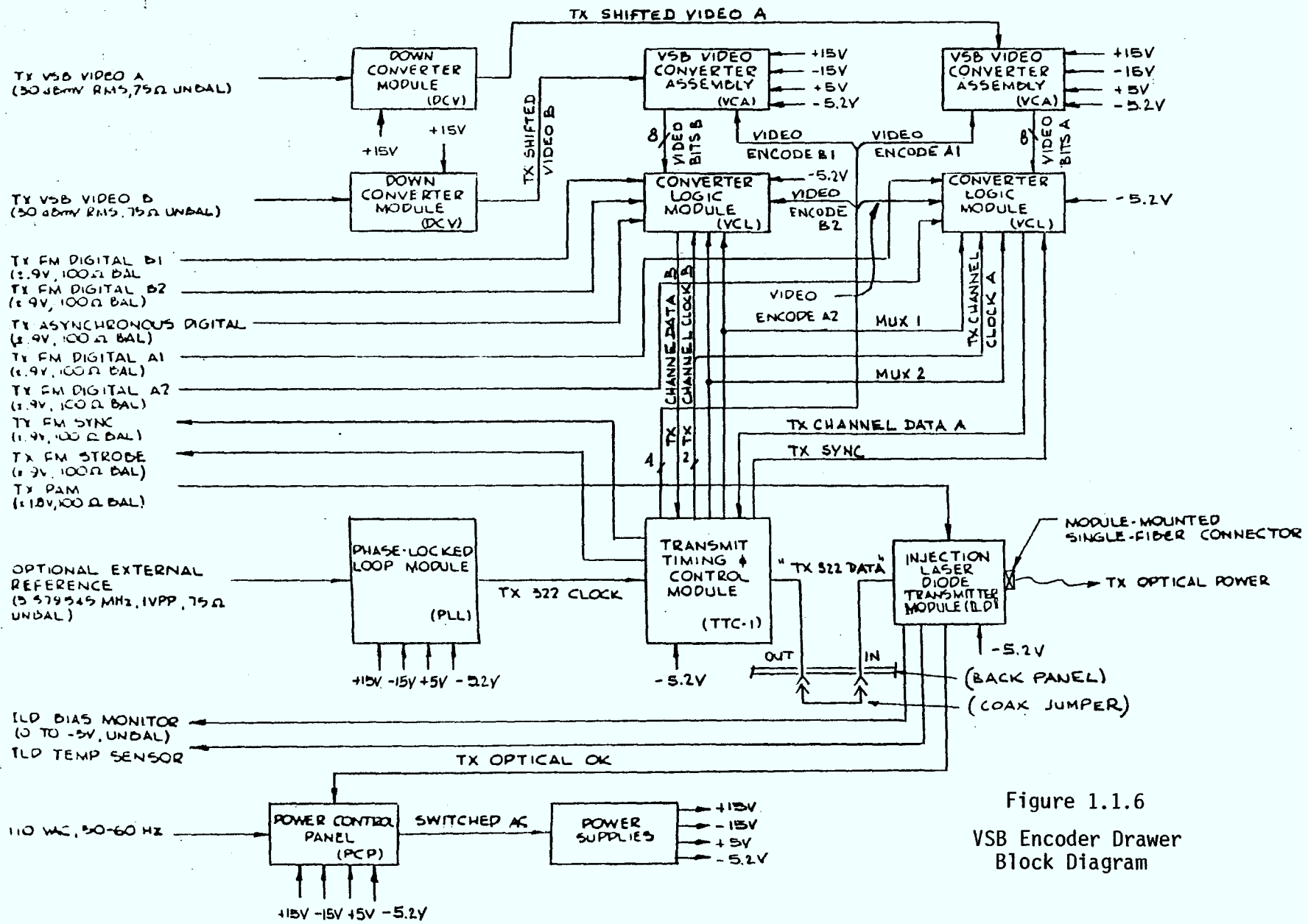
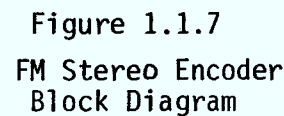


Figure 1.1.6
VSB Encoder Drawer
Block Diagram



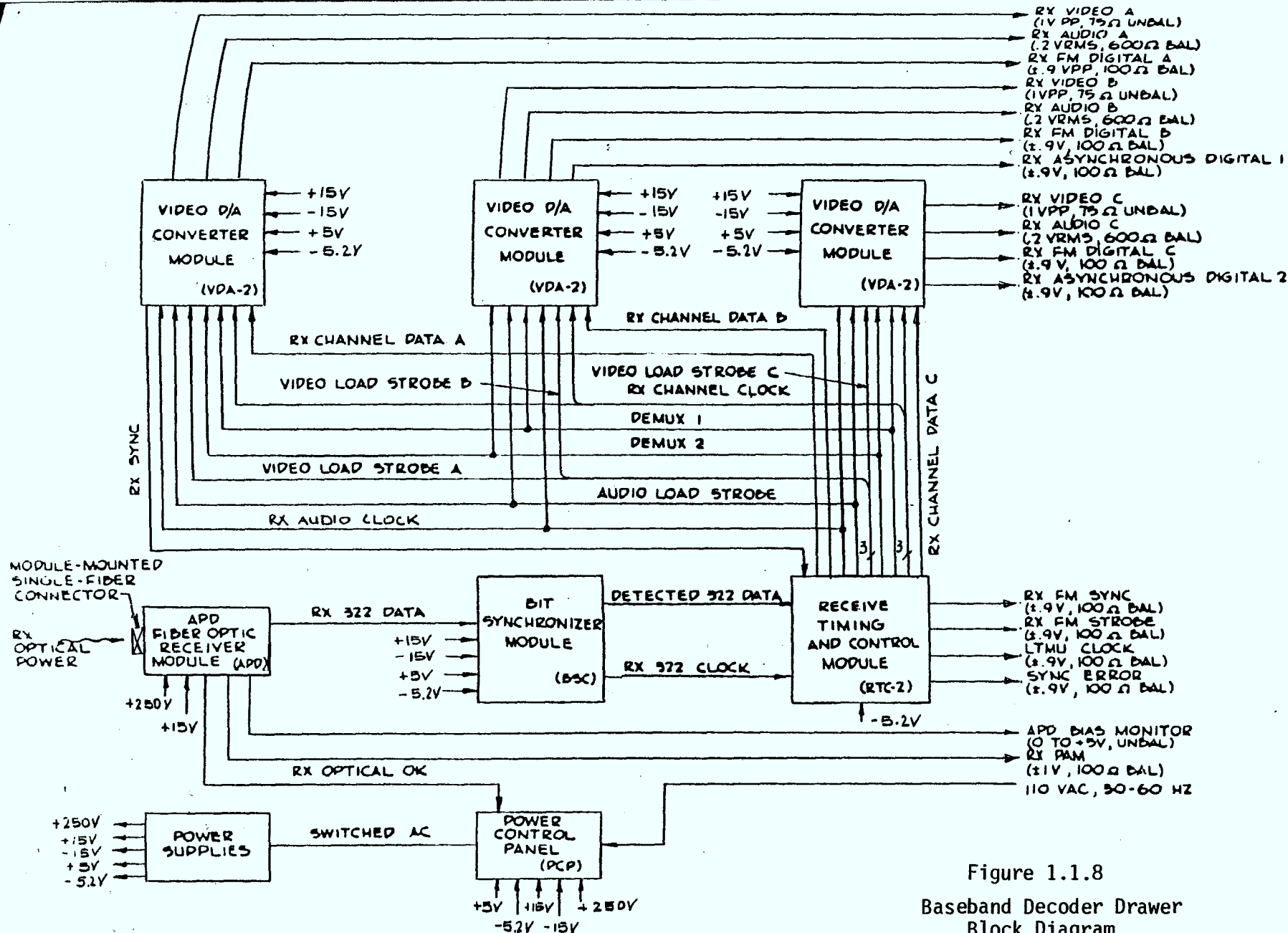


Figure 1.1.8
Baseband Decoder Drawer
Block Diagram

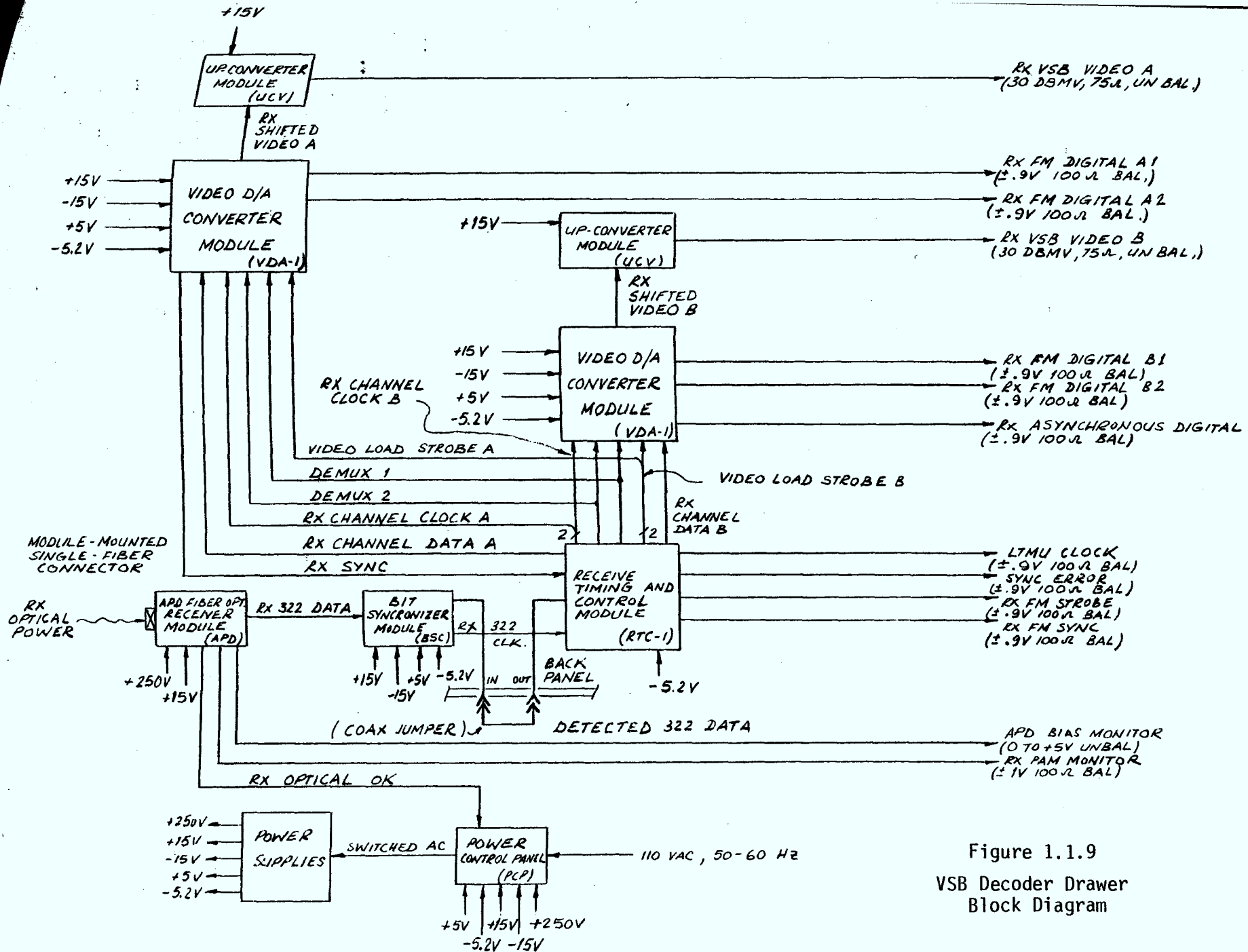


Figure 1.1.9
VSB Decoder Drawer
Block Diagram

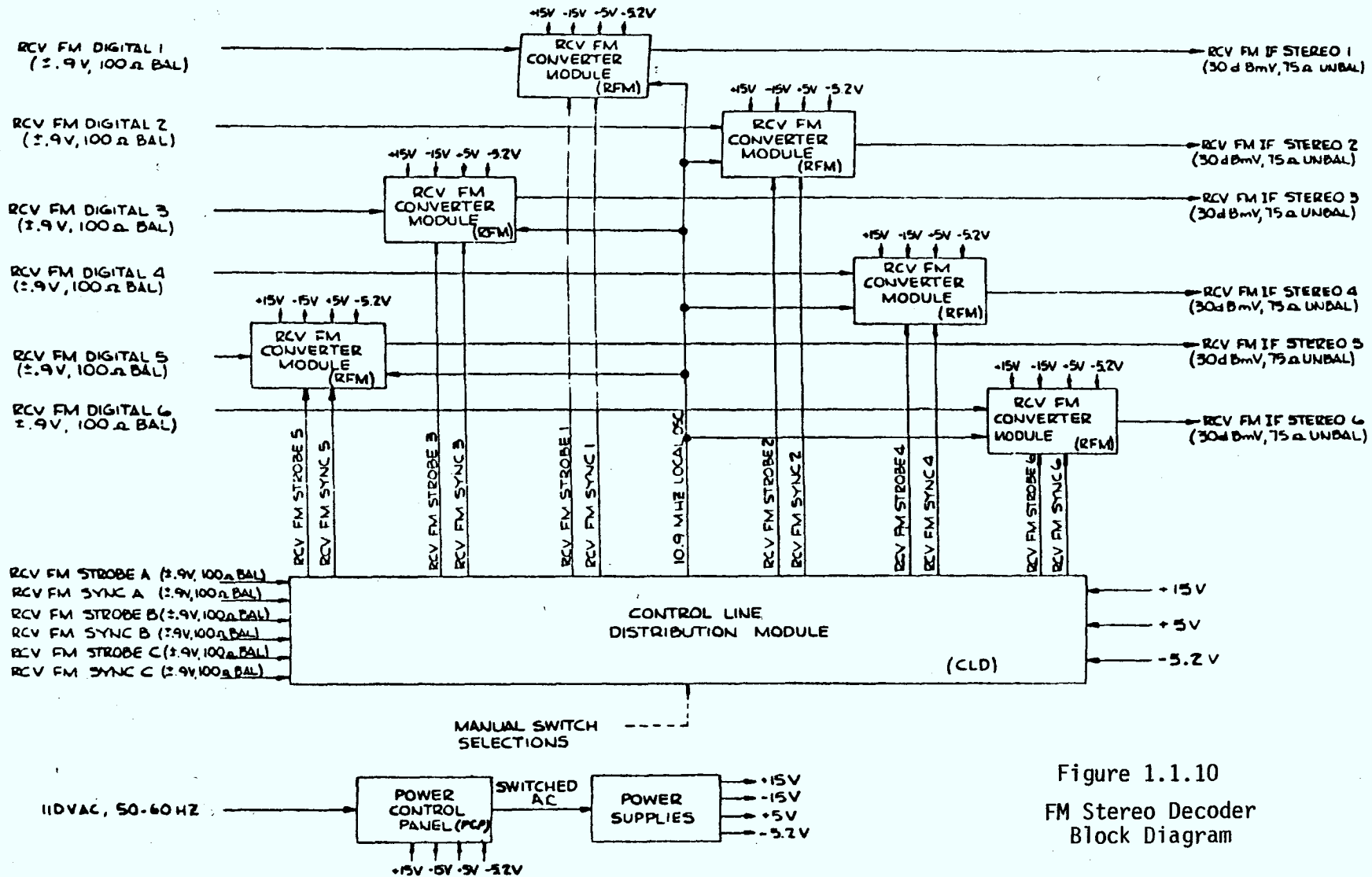


Figure 1.1.10
FM Stereo Decoder
Block Diagram



Downhill (Response)

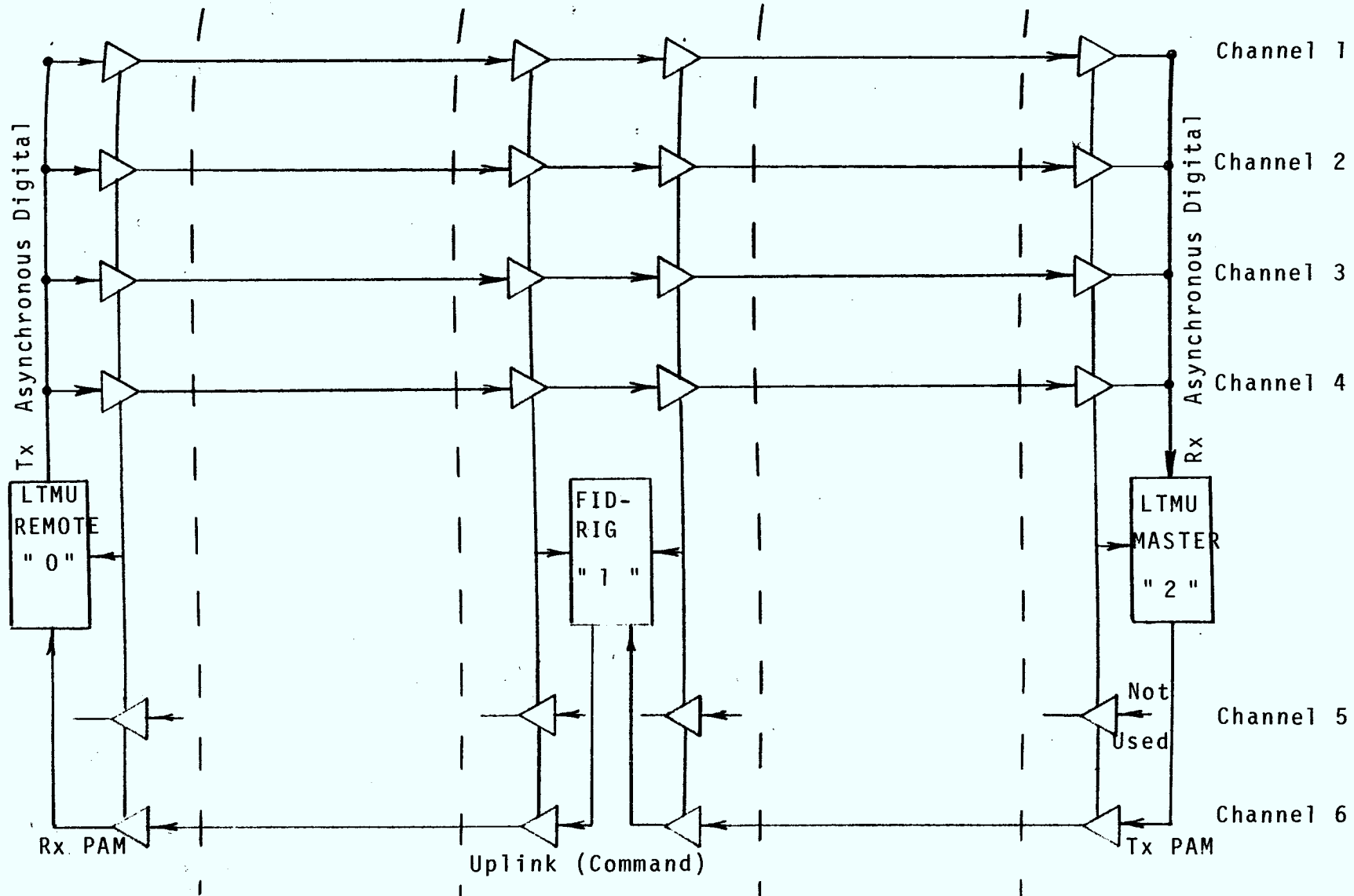


Figure 1.1.11
LTMU SYSTEM CONFIGURATION



1.2 Repeater Equipment

The repeater is mounted in a cable TV repeater housing. A modified Jerrold entrance connector is used to provide a cable entrance seal. Individual repeater modules are used for each fibre. The modules themselves are similar in operation to the optical receiver and transmitter used in the baseband Video Encoder Drawer. They are of a non-regenerative type. The block diagram of the repeater module is shown in Figure 1.2.1.

A pole mounted power supply provides the D.C. voltages required.

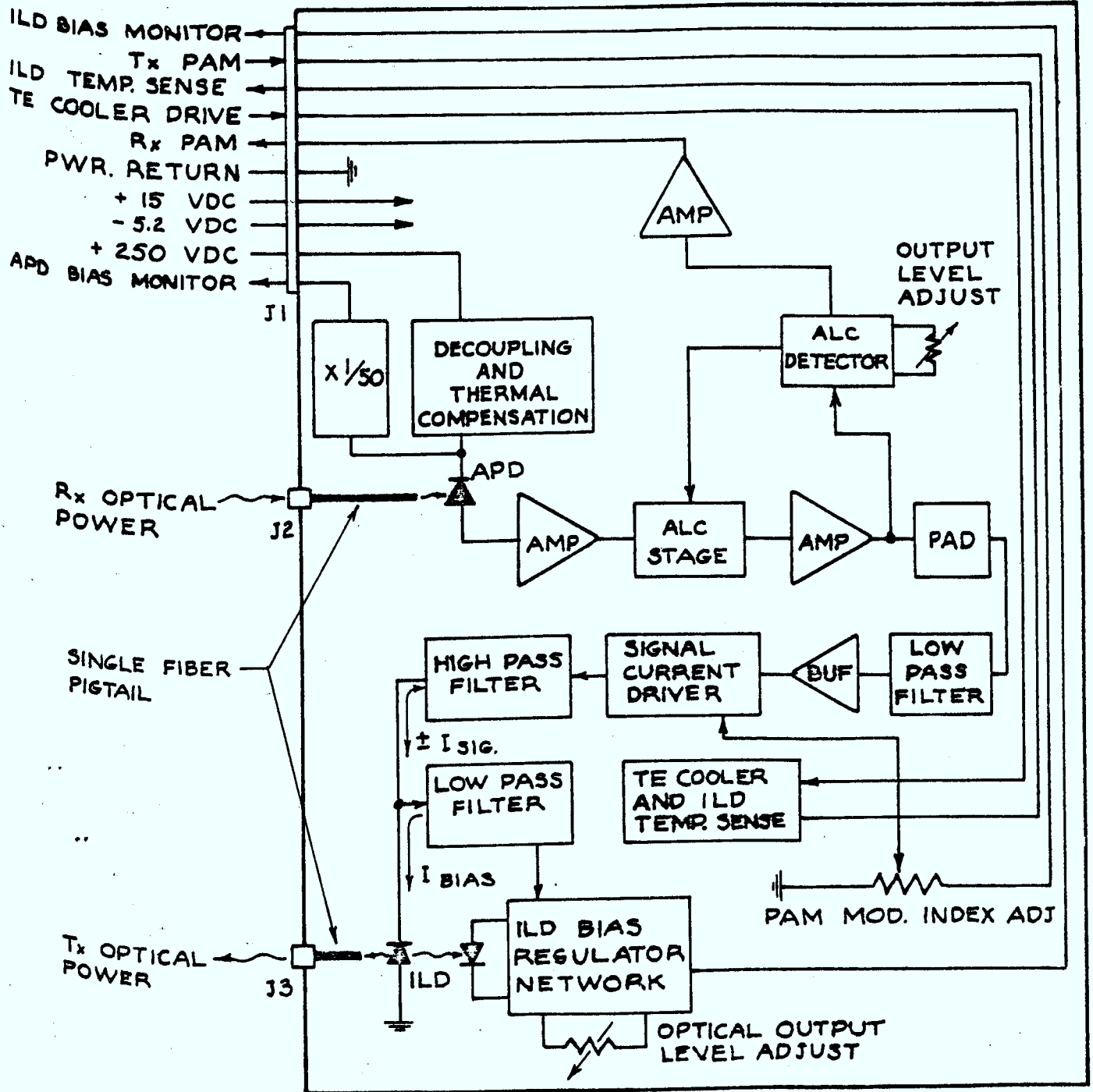


Figure 1.2.1
Repeater Block Diagram



1.3 Fiber Optic Cable

The cable consists of 8 fibres, each fibre enclosed in a buffer tube. The 8 buffered fibres are stranded concentrically around a plastic coated steel strength member. A non-hygroscopic core wrap encloses the buffered fibre and a layer of polypropylene yarn is stranded over the buffered fibre core to provide a cushioning layer. The outer sheath consists of an aluminum shield bonded to a polyethylene jacket providing an effective moisture barrier. Figure 1.3.1 illustrates the cross-sectional layout of the fibre optic cable.

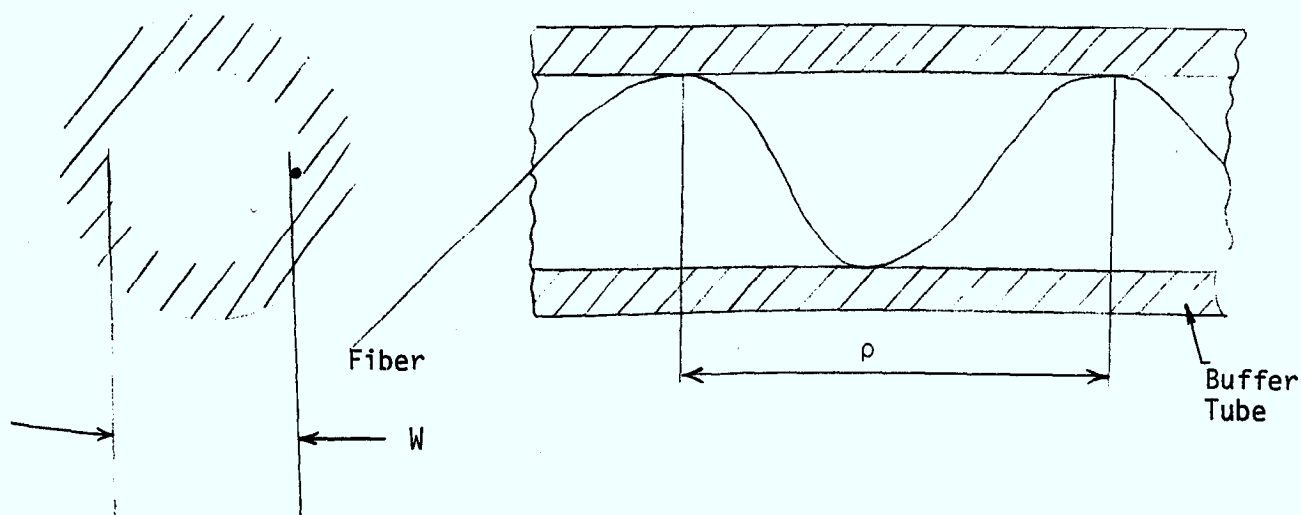
1.3.1 Cable Design

The individual fibres are placed inside hollow thermo plastic (buffer) tubes. This approach is commonly referred to as the loose buffer tube approach. The design approach allows the cable to elongate or contract due to external loads and/or temperature over a certain range without applying any stress to the fibres themselves.

The elongation/contraction range where the fibre remains stress free is determined by the parameters shown in Figure A below i.e. the inner fibre clearance W and the average helix period ρ .



1.3.1 Cable Design (cont'd)



The fibre excess length (N_T) over the buffer tube length is given by

$$N_T = \frac{\pi W^2}{2\rho^2}$$

For the cable design N_T is typically of the order of 0.1% so that the fibre in a 1000 m single fibre cable is approximately 1001 m long.

The value of N_T is tightly controlled during manufacturing. If N_T increases too much from the 0.1% value, the helix pitch becomes smaller resulting in more macro and micro-bending in the fibre.

A further consequence is that the fibre is under increased stress possibly resulting in early failure due to static fatigue.

If N_T decreases from the optimum value then the cable will have a lower performance in regard to imposed strain.



1.3.1 Cable Design (cont'd)

When the cable is subjected to low temperatures, the excess length (N_T) of fibre at any given temperature increases due to the difference in coefficients of linear expansion between fused silica and the thermoplastic materials.

Typical values for these materials are:

Fused Silica : $80 \times 10^{-7}/^{\circ}\text{C}$

Thermo Plastics : $600-700 \times 10^{-7}/^{\circ}\text{C}$

The loose buffer tubes are stranded around a steel strength member coated with plastic.

The elongation/ contraction window (N_S) in the stranded cable is also determined by the stranding lay length and pitch circle diameter (D).

Typical values of N_S in the stranded cable are in the range of 0.3% to 0.5%. The value of N_S and hence the allowable cable strain can be adjusted by judiciously selecting the cable parameters, such as buffer tube size, clearance W, pitch circle diameter D.

The amount of cable contraction with temperature in a stranded cable is primarily determined by the central element around which the buffered fibres are stranded.

The BCN cable has a steel strength member with a coefficient of expansion of $110 \times 10^{-7}/^{\circ}\text{C}$ and has an elastic modulus order of magnitude greater than the thermoplastics. The temperature range within which the fibre attenuation remains relatively constant is increased, since the temperature contraction of the cable is now primarily determined by the steel central member which has a coefficient of expansion ($110 \times 10^{-7}/^{\circ}\text{C}$) much closer to fused silica ($80 \times 10^{-7}/^{\circ}\text{C}$).



1.3.2 Fiber Dimensions and Characteristics

a) Number of Fibers	8
b) Diameter Over Fiber Core	62.5 μm nominal
c) Diameter Over Fiber Cladding	125 μm nominal
d) Fiber Material	Doped Silicate
e) Fiber Type	Graded Index, Multi Mode
f) Fiber NA	0.20 ± 0.03

1.3.3 Cable Construction and Dimensions

a) Cable Length (Standard shipping length)	1.0 km nominal
b) Cable Outer Diameter	13.08 mm
c) Cable Strength Member	Metallic-consists of solid steel wire located in the center.
d) Outer Jacket Material	Polyethylene
e) Fiber Identification	Brown buffer tube is #1 and is numbered using left hand rule in direction of print.
f) Sheath	Aluminum Shield Bonded

1.3.4 Mechanical Characteristics

a) Bending Radius	10D (D = diameter of cable)
b) Installation Pulling Tension	1500 Newtons max.



1.3.5 Electrical Characteristics

- | | |
|-------------------------------|-----------------------|
| a) Attenuation of Cable Fiber | 6.5 dB per km average |
| b) Bandwidth of Cabled Fiber | 550 MHz.km average |

1.3.6 Ambient

- | | |
|--|--|
| a) Attenuation Behaviour
vs Temperature | ± 1.5 dB over the temperature
range of -40°C to $+50^{\circ}\text{C}$ |
|--|--|

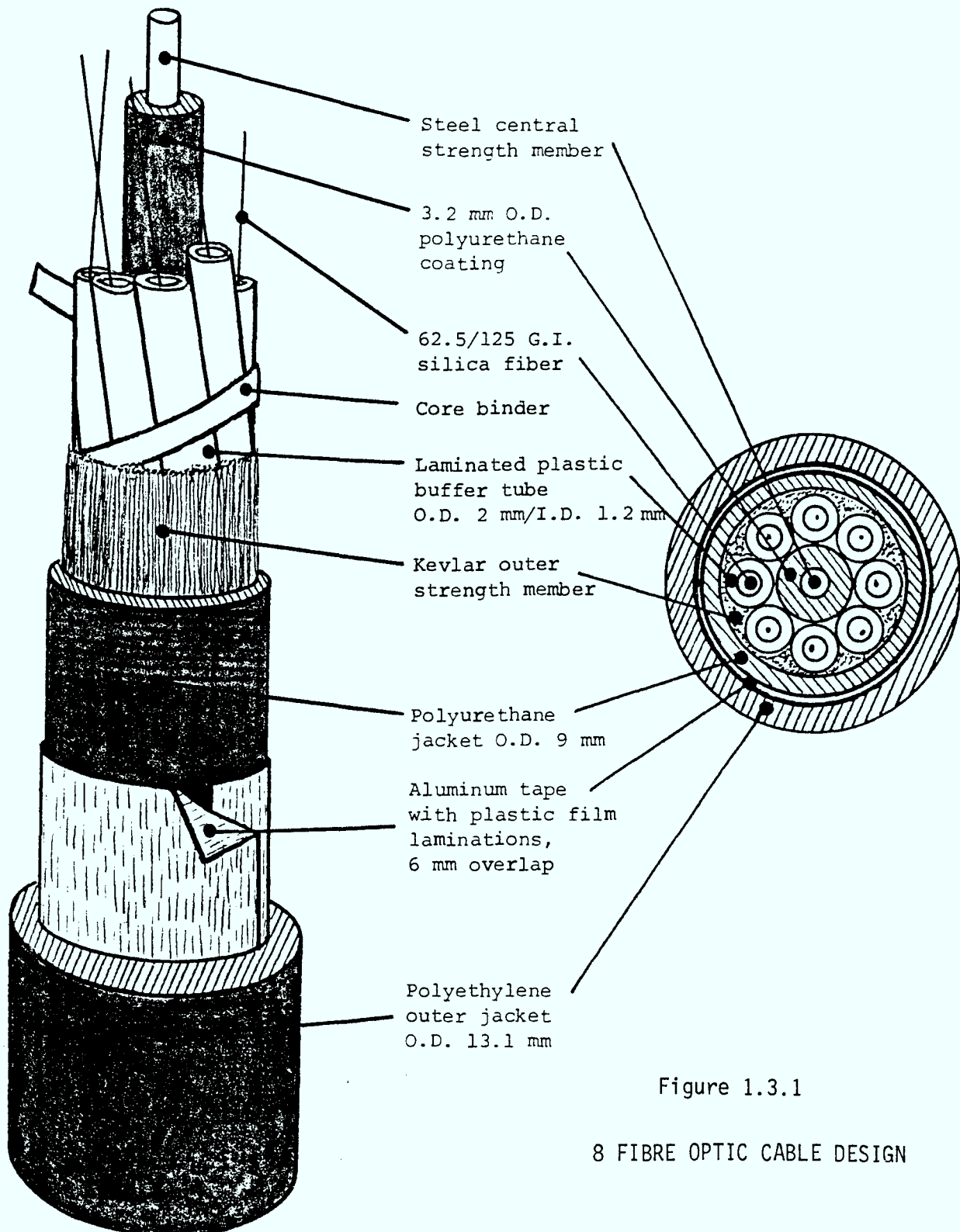
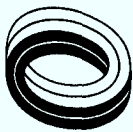


Figure 1.3.1

8 FIBRE OPTIC CABLE DESIGN



2.0 HISTORY OF MAJOR ACTIVITIES, PROBLEMS AND SOLUTIONS

2.1 General

What follows is a chronological sequence of events dating back to the pre-installation phase of the project. Those activities which have created technical controversy, problem areas and solutions shall be summarized.

The purpose behind this summary is to document the learning experiences which have materialized and make use of the knowledge developed.

Details regarding the proposal period of the BCN project are covered in the BCN proposal documents.

2.2 Pre-Installation Phase: September 1978 to November 1978

The major efforts during this period concentrated on fibre optic cable measurements as discussed below:

2.2.1 Attenuation Measurement

Results of factory attenuation measurements performed on 6 cable reels are documented in Attachment I of this section.

The losses measured were well within the 8.0 dB/km requirement.

The method used to measure the cable attenuation is described in Attachment II.



2.2.2 Bandwidth Measurement

Fiber bandwidth measurements were accomplished using "Pulse Dispersion" techniques. The 3 dB frequency bandwidth of the fiber response can be calculated from the temporal responses (pulse outputs) of the system with and without the fiber. If the pulse outputs are approximated by Gaussian shapes, the 3 dB frequency bandwidth can be expressed in a closed form as:

$$f \text{ (MHz)} = \frac{441}{\sqrt{(\Delta T_{s+f})^2 - (\Delta T_s)^2}}$$

where ΔT_{s+f} = width of the (system and fiber) pulse
at the half-power points

ΔT_s = width of the system pulse at the
half-power points

ΔT_{s+f} and ΔT_s are expressed in nanoseconds, and f is in MHz. However, real pulses may significantly depart from the Gaussian shape for any practical system. In some cases the departure of the pulseshapes from the Gaussian is considerable, and use of the above formula yields wrong results.

A computer program called FTRM has been written in Basic to calculate the bandwidth exactly using Fourier transform techniques.



2.2.2 (cont'd)

A summary of the exact calculations and comparison with the approximate Gaussian calculation are given below. It is obvious that the Gaussian method may be quite misleading in some cases.

Fibre No.	Exact B.W. (Program)	Approx. B.W. (Formula)
BCN186, #4	150 MHz	322 MHz
BCN186, #6	430 MHz	428 MHz
BCN187, #7	760 MHz	632 MHz
BCN187, #2	490 MHz	483 MHz
BCN191, #3	390 MHz	518 MHz

2.2.3 Temperature Testing

Temperature tests have been performed on the cable core provided by Siecor before extrusion of the outer jacket by Canada Wire and Cable. After extrusion temperature tests were repeated as described below. Results of these tests are documented in Attachment III.

2.2.3.1 Cable Core Temperature Measurement

Temperature cycling test has been performed on Cable No. 156A and Cable No. 182A.

One complete cycle, from -40°C to $+50^{\circ}\text{C}$, has been performed on both reels except for Cable No. 156A, where the initial reading was missed due to the system being disturbed during low temperature cycle.



2.2.3.1 (cont'd)

For both reels, fibres No. 1 to No. 4 were spliced to form a loop approximately 2 km in length. Three splices were used on each loop and the splices were not in the chamber during testing.

The procedure for the temperature cycling is as follows:

1. The complete cable, in reel, to be placed in chamber and record power level, (initial power level @ room temperature).
2. Lower chamber temperature to -40°C or raise temperature to $+50^{\circ}\text{C}$ and continue for 6 hours. Record power level at the end of the 6 hour period.
3. Raise or lower temperature to room temperature in about 12 hours. Record power level.
4. Raise chamber temperature to $+50^{\circ}\text{C}$ or lower to -40°C and maintain this temperature for 6 hours. Record power level at the end of the 6 hour period.
5. Return chamber temperature to room temperature in 12 hours or longer and record power level.
6. Cut fibre near transmitting end and record power level which is the input power to the fibre loop.

Cable No. 156A varied about 1.1 dB and Cable No. 182A varied about .12 dB throughout the complete temperature cycling.



2.2.3.2 Extruded Cable Temperature Measurements

After extrusion of the outer jacket by Winnipeg, Cable 182A was temperature cycled from September 9 to September 25.

Fiber No. 1 to No. 4 of the subject cable being spliced to one loop by using V-groove splices and at least five complete temperature cycling, from -40°C to $+50^{\circ}\text{C}$, has been done. As can be seen from the graph in Attachment III the attenuation variation, using initial attenuation at room temperature as reference, is less than 0.7 dB which may be contributed partly by the instability of the measuring equipment.

The time period for each temperature was maintained for approximately 12 hours. Due to environmental chamber problem the temperature was maintained at 0°C instead of -40°C for approximately 24 hours on September 13.

2.2.4 Strength Tests

Strength tests were performed on the Corning fibres after completion of the buffering and cabling. As a result of these tests two cable reels were rejected due to their high probability of failure.

The test method and results are documented in Attachment IV of this section.



2.2.5 Fusion Splice Experiment

AOI Sansho's Electric Fusion Splicer was used on Sept. 25 and Sept. 26, 1978 to perform in-house fusion splice experiments. A total of 29 readings were obtained and detail readings are tabulated in Attachment V. The average attenuation for the first day was 0.81 dB and 0.55 dB for the second day. 15 splices and 14 splices were made for the first day and second day respectively.

Air bubble(s) occurring at the joints after the fiber ends were fused together, indeed gave substantially higher loss as expected. This air bubble, if big enough, can usually be seen under the microscope during fusion process. Disregarding these splices the average attenuation for the second day became 0.36 dB.

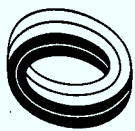
Again fiber end cut quality plays an important part in obtaining low loss splices by using this technique.

Northern Telecom's technique was also attempted but no improvement was determined over the "stroke length" technique when the existing adjustments or the AOI splicer was used.

2.3 Installation Phase: November 1978 to October 1979

2.3.1 General

Cable installation has been completed in November 1978.



2.3.1 (cont'd)

Splicing of the fibre optic cable went fairly routine and was completed by December 3, 1978.

For testing purposes Canstar has installed on their premises (aerially) two 500 meter cable sections.

Training of London Cable T.V. personnel in splicing and connectorization has taken place during the installation phase of this project.

Factory acceptance testing of the equipment was completed in June 1978.

Installation of equipment racks and repeater housings has been completed in December 1978. Equipment installation and line-up completed in February 1979.

2.3.2 Cable Installation

The main portion of the aerial fibre optic cable installation was begun October 17, 1978 and the splicing team started November 6, 1978. The cable installation and splicing was completed December 22, 1978.

Installation of the buried cable was completed May 23, 1978.

This section was approximately 1 km from CFPL-TV to Commissioners Road.

The aerial installation was generally lashed to the same strand as the one inch coaxial cable used in the existing London Cable system.



2.3.2 (cont'd)

The installation techniques used were the same as installing the standard one inch coaxial cable with the exception that the work procedure was such to avoid cutting the fibre optic cable. This was desirable to eliminate splices but it made it more difficult to get around obstacles such as trees, other cables crossing under the strand, or at the finish of the work day in order to return to the shop.

The fibre optic cable was installed on a separate strand from the end of the buried section on Commissioners Road to repeater 1 on Warncliffe Road. The remainder of the cable was installed on the strand supporting the 1" coaxial cable. The sharing of strand was necessary due to congestion of existing wires and cables on the utility poles.

The first complete aerial cable was pulled in about 400 meters, over pulleys attached to the strand. A rope was first fed through the pulley system then the cable was attached to the rope by means of a Kallem grip. The cable was pulled off the cable reel by one of the installation crew who visually monitored the tension. The pull-in rope was taken in by a power capstan. Hand-held transmitters provided communications between the feed reel location and the pull-in capstan.

Splice locations were chosen to allow access for the splicing platform but still allow optimum utilization of the cable on each reel.



2.3.2 (cont'd)

Seven meters of excess cable were left at each splice point.

The excess length allowed for a bow tie in case of re-splicing or fibre breakage. Figure 2.3.1 shows the derivation of this length and the specified splice housing mounting technique.

The cable was double lashed to the strand using .145" diameter stainless steel wire in the lashing machine. The lashing machine was pulled along the strand till the pole where lashing wire was tied off by a clamp near the pole.

The lasher was re-started again on the other side of the pole. Again the lashing wire was tied off by a clamp before starting the lasher. The lashing rate with one bucket truck and one truck pulling the cable trailer is approximately 1 km per day depending on obstructions.

The excess cable at the splice locations was rolled up into multiple 3 ft. diameter loops and fastened to the strand to be spliced later. The ends were protected by rubber boots attached by Pliobond glue. Subsequent installations should use plug and clamp assemblies.

Present coaxial cable installation techniques do not use expansion loops. However, as a test, expansion loops were used at each pole in the center link (between the old Repeater I and Repeater II section). The design of the expansion loop is shown in Figure 2.3.2.



2.3.2 (cont'd)

Where the cable path is down the pole to enter a duct, half shields were applied over the cable to protect it from damage.

Typical problems encountered during lashing were:

1. Cable to be lashed on field side of pole required the cable to be pulled in over rollers.
2. Some locations required the cable to be pulled through ducts requiring a rope to be fed through the duct and care not to exert too great a stress on the cable.
3. In one location trees were growing directly under the utility lines and trimmed with a "V" such that the full height of the tree existed on either side of the cable to be installed.

This required one of the installation crew to use a long pole to hold the cable. From the bucket truck he dropped the cable into the V-groove of the tree, the lasher rope was thrown through the opening and the lasher was pulled through.

4. The Bell cable crossed at right angles under the existing strand. At the same position utility lines also crossed above the strand and parallel to the Bell cable.

This required lifting the optical cable reel off the cable trailer and lifting it over the Bell cable but under the utility lines. This was done with a chain and the boom on the back of one of the installation trucks.



2.3.2. (cont'd)

5. Cable lashing over the railway tracks required a railway flagman and 72 hours notice.
6. Cable lashing through busy intersections was difficult but was generally co-ordinated with the traffic lights, resulting in little disruption to traffic.
7. Changing strands at an intersection required installation of clamping devices to retain the space relationship of one strand to the other.
8. Cable to be pulled through ducts in the middle of reel length required cutting the cable. In general the installation of the cable was such to eliminate this problem, however, in two cases this problem could not be overcome.

2.3.2.1 Splicing

All the fibre optic cable installed on the BCN project was field spliced using fusion splicing equipment and the splicing platform.

After cable installation the splicing platform was moved under the cable to be spliced. The platform was elevated and the cables were brought into each end of the splice platform housing. The cables were prepared and spliced. After this the top of the splice platform was lifted and the completed splice assembly was removed. The cables were made into a bow tie and the splice box was fastened to the stand. The cable was then lashed down with tie wraps. Figure 2.3.1 shows the configuration of the splice box and the cable.



2.3.2.1 (cont'd)

The splice box used was a modified Jerrold STH-7 line extender box with a modified Jerrold cable entrance connector.

The AOI fusion splicer was used but a few problems were encountered as follows:

- 1) The alignment jig has to be kept clean, especially the v-grooves, otherwise the fibre would not line-up.
- 2) The moveable alignment block does not travel freely at certain region.
- 3) Uncertainty still exists even if the fibre ends have been perfectly aligned or if there is enough of stroke length in some cases.

The cable problems experienced were as follows:

- 1) Cable O.D. varied. For the worst case the entrance connector had to be modified by local machine shop to fit the cable.
- 2) Brittle fibres were difficult to handle and difficult to obtain reasonable splice loss. (Cable 185 No. 2, 186 No. 1, 190 No. 7, 182A No. 1 and No. 5 are the particular ones).
- c) Fibre O.D. seems larger than others (Cable 184 No. 5 and Cable 186 No. 1).

2.3.2.2 Grounding

The cable contains two metallic elements to be grounded. These are the aluminum sheath and the steel center strength and were grounded at each splice and repeater location.



2.3.2.2 (cont'd)

The aluminum sheath of the cable is fused to the outer polyethylene jacket of the fibre optic cable and requires a different grounding procedure than coaxial cable.

A solid or braided metal strap is attached to this stud and the other end of the strap is connected to a convenient screw on the frame of the splice box or repeater. The steel strength member is attached to another screw in the housing. The housing is then attached to the strand which is connected to the utility ground.

2.3.2.3 Repeaters

The repeaters use a CATV repeater housing which is attached to the strand 2 to 4 m from the utility pole. As in the splice box the cable is in a bow tie (Figure 2.3.1) to allow a surplus of cable in the event of a problem requiring re-connectorization.

The D.C. regulators are mounted in a standard CATV repeater power supply housing. The A.C. input is fed from the utility 115 V supply. The power supply housing is fastened to the utility pole approximately 3 m from the ground. A flexible conduit houses a D.C. power cable from the power supply to the strand mounted repeater.

The repeater locations were first determined and then the cable was installed in each direction from the repeater. This was required as the repeater ends of the cable are pre-connectorized and cannot be cut.



2.3.2.3 (cont'd)

The power supply was checked and then the repeater modules installed. Future installation of repeaters where possible should be installed in less busy areas or located such as to be accessible without disrupting traffic.

2.3.2.4 Terminal Equipment

The terminal equipment was installed in the CATV terminal equipment room of London Cable at CFPL-TV. The equipment power supplies were checked, connectors were spliced on the fibre optic cable and the cable run into the equipment racks.

In addition to the airconditioning fans were required in order to maintain a workable environment. The fibre optic connectors were cleaned and connected to the equipment. During January 1979, the hub end equipment was installed in its own room at London Cable TV.

2.3.2.5 Connectorization

The BCN system uses a Harris connector which is a modified SMA connector.

The cables at the head end (CFPL-TV), hub end (London Cable TV) and at the two repeaters required connectorization. Four cables for the repeaters were factory connectorized prior to cable installation. The head end and hub end connectors were not connectorized directly on the cables but instead attached to two or two-and-one-half meter pigtails. These were later fusion spliced onto the cables on site.



2.3.2.5 (cont'd)

In the case of a fibre optic pigtail, a length (2 m) of wide bandwidth graded index fibre (125 μm diam.) is threaded into # 24 teflon tubing.

The connectorized pigtail is spliced to the prepared cable. After completion of the splices, heat shrinkable tubing is applied over the splices to become an integral part of the cable.

Prior to shipment the connectorized end of the cable was protected by placing in a 1" polyethylene tube with the ends sealed by a plug and clamp. This also protected the connectors in one case where the connectorized cable was pulled over rollers during installation.

2.3.2.6 Summary

Time required to complete one splice section is about 8 hours which includes the time for facility transportation, cable dressing, splicing and splice box lashing.

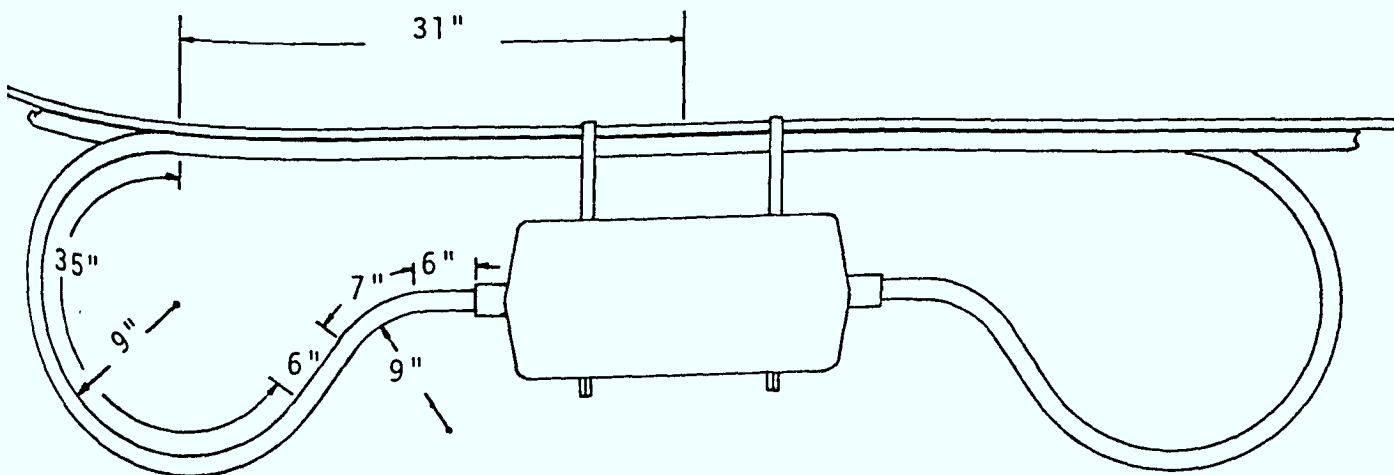
The Siecor TDR was used to check the link continuity and to detect particular high attenuation splices. The link attenuation and individual splice loss of the BCN cable cannot be measured by using this equipment as the equipment dynamic range is exceeded.

The Canstar AAM set did not provide meaningful measurement data either. The receiver showed input even though the transmitter had been turned off. It is suspected that signal was being picked up from surrounding area.



Figure 2.3.1

SPLICE BOX INSTALLATION AND
CABLE ALLOWANCE DERIVATION



Typical Splice on repeater housing installation showing the "bow tie" technique to allow extra cable in case of splice or connector re-work.

Cable Allowance

The following figures show the derivation of the cable allowance.

Cable "bow'tie" loops - 2 1/2 m.

Attenuation test - 2 m.

Splice allowance - 2 m.

Total cable allowance previous to splice = 6 1/2 m. minimum.

The measurement of the total allowance is from the center line of the splice box location to the cut end of the cable.



<u>Loop Dimensions</u>				
Cable Size	D	F	R1	L
750	8"	12"	12"	18"
500				
412	6"	12"	6"	33"

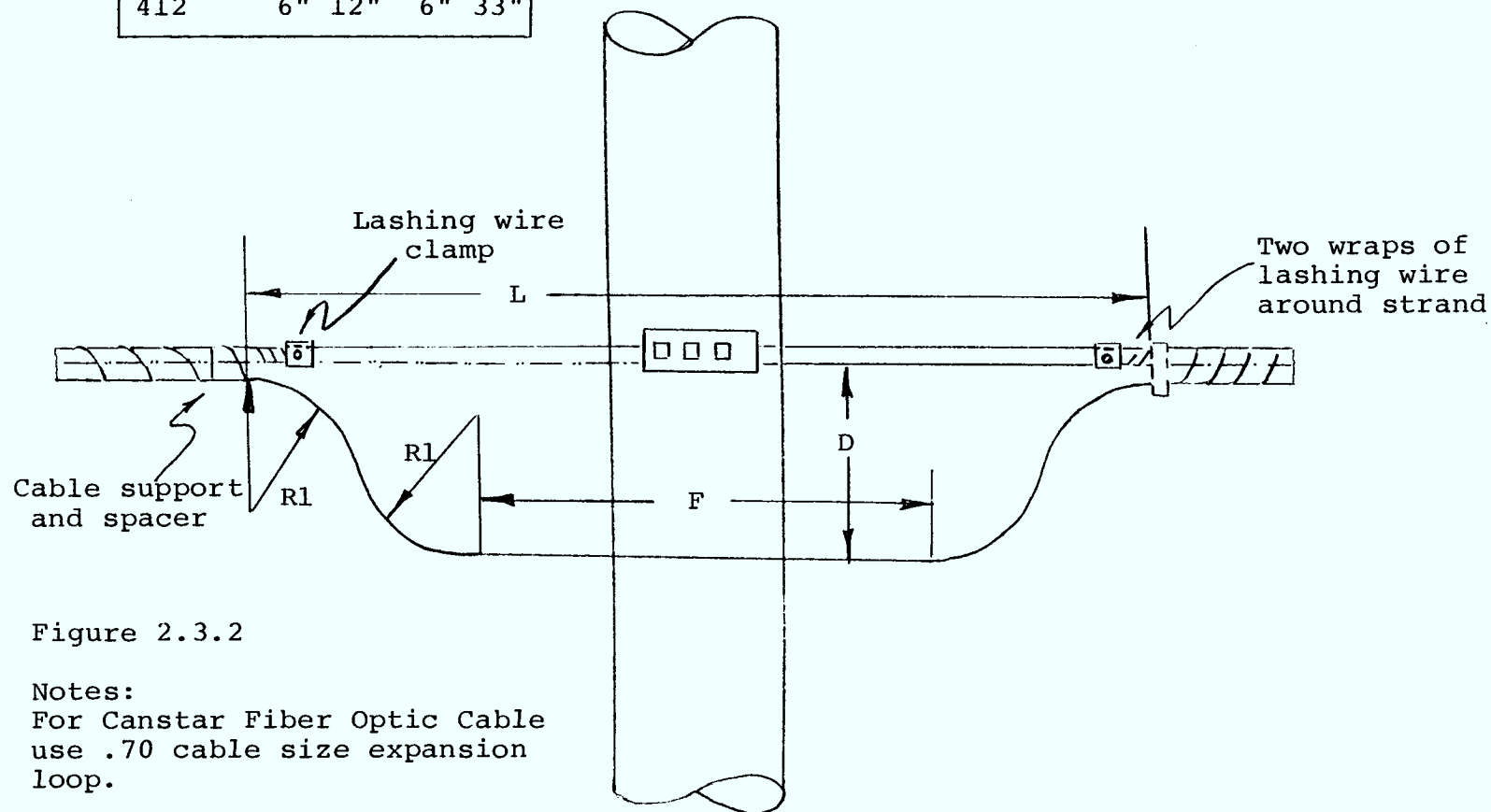


Figure 2.3.2

Notes:
For Canstar Fiber Optic Cable
use .70 cable size expansion
loop.



2.3.3 Cable Attenuation Measurement (CFPL to 1st Repeater -Jan.19,1979)

The attenuation of the completed links were not measured. In order to determine the link loss, the output of a Harris Encoder was connected to each fibre in turn and the output of the respective fibre measured at the repeater.

2.3.3.1 Source Power Measurement

A six foot fibre optic cable with Harris connectors at both ends was connected to the encoder drawer. The connector head was removed at the other end of the fibre optic cable exposing the ferrule. This was inserted in an adapter mounted on the photo electric head of the United Technology Detector. The light level was then read from the United Technology Detector photo meter.

The light level measured was 1.66 mw.

2.3.3.2 Received Power Measurement

The received power was measured by using the same fibre optic cable and optical power meter as employed in the source measurement.

The measurement was made using a bucket truck to gain access to the repeater. The optical meter was operated on its internal batteries.



2.3.3.2 (cont'd)

Levels	Headend Fibre #	Repeater Fibre #	Level	Attenuation
	1	1	1.83 uw	20 dB
	2	2	0.34 uw	37 dB
	3	5	1.3 uw	31 dB
	4	3	4.2 uw	26 dB
	5	4	0	
	6	8	0	
	7	6	1.0	32 dB
	8	7	0.26	38 dB

The following problems existed:

2.3.3.3 Problems

1. Too many parts to handle in bucket truck, i.e. meter, head, cable, fibre optic cable.
2. Batteries discharge fast and generator not always available.
3. Communications link from Head end to repeater virtually non existent.
Communication hand set will not transmit into head end room in basement.
4. Three cables not identified and markers fall off when applied due to cold and age.
5. Connectors and instruments must be operated without gloves limiting time for measurements in the cold.
6. Require a comprehensive tool and small parts equipment holder for use on bucket truck allowing ease of finding tools.



2.3.3.5 (cont'd)

7. Optical measuring device should be temperature stable held in one hand, easily attached to either male or female connectors.
8. Require small housing to work on repeater in bad weather as the repeater is exposed to the elements.
9. Access to utility A.C. supply at repeater power supply is highly recommended.
10. Optical measurements techniques should be improved.
11. Harris connectors are delicate and require more than special handling.
Cleaning of the female Harris connector requires disassembly, resulting in three loose, small parts.
Alcohol does not dry readily at low temperatures.
12. Splicing of pigtail results in a large length of pigtail which cannot be bent.
13. Communications could be improved by using a two way transmission system over one of the spare fibres.

2.3.3.4 General Repeater Problems

1. Insufficient space for connector mounting plate and mounting connectors without the possibility of damaging the pigtails.
2. PVC tubing covering on pigtail inflexible in cold.



2.3.3.4 (cont'd)

3. When connector mounting plate not used the organization of the pigtail is difficult due to quantity and lack of tie-down points.

Use of coloured tape to indicate upstream and downstream pigtails, and tie wraps used to bundle fibres requires improvement.

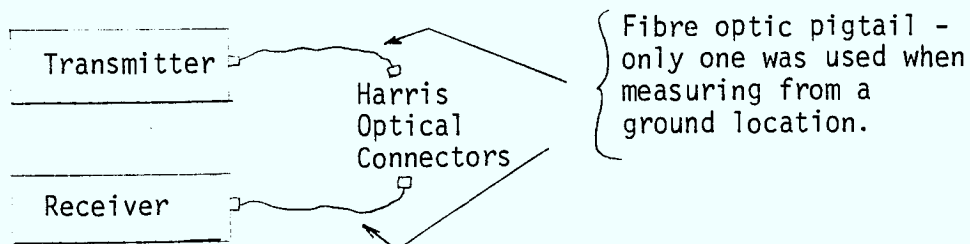
4. Power supply voltages difficult to check since it requires a jig plus an easily usable voltmeter. Adjustment of power supplies after installation difficult or nearly impossible. No provision for adjusting power supply in its housing.

2.3.3.5 Improved Fibre Optic Cable System Attenuation Measurements (January 22, 1979)

Each of the fibers of the three links of BCN system were measured to determine the attenuation.

For this measurement a Canstar AMS attenuation measuring set was modified to accept a Harris Connector without adjustment.

Attenuation Measurement





2.3.3.5 (cont'd)

The measuring equipment was calibrated by connecting the pigtails directly to each other using a metal female guide (part of a female Harris connector). Successive readings were taken by remaking the connection several times in order to reduce the connector error.

The transmitter and receiver were placed at their respective ends of the link. The attachment of the fiber optic pigtail to the link fiber under test was remade three times as in the calibration test. In the case of a ground location to the repeater, only one pigtail was employed, the other connection was made directly to the instruments. The calibration procedure was modified to reflect this change. The attenuation measurements for each link are tabulated below:

LINK ATTENUATION

Fiber No.	Link I Atten	Link II Atten	Link III Atten
1	32 dB	23 dB	22 dB
2	Note 1	19 dB	20 dB
3	24 dB	18 dB	18 dB
4	Note 1	18 dB	23 dB
5	31 dB	19 dB	Note 2
6	29 dB	23 dB	23 dB
7	28 dB	24 dB	20 dB
8	32 dB	17 dB	Note 2

Note 1: Connector defective at repeater 1.

Note 2: Connector defective at Hub End.



2.3.4 Degradation of Fibre Optic Cable Jacket

As a result of repair work carried out on a section of cable damaged by an excavating crew digging near the cable, fissures were discovered in the outer jacket of the armoured cable used. A report prepared by Canada Wire and Cable Engineering Services analyzing a sample cable utilized in the installation and a sample from a reel unutilized (storage) is provided in Attachment VII of this section.

2.3.5 Equipment Installation and Line-Up

2.3.5.1 General Summary and Status: February 15, 1979 to August, 1979

The status of the BCN project has been summarized by Canstar's Project Engineer as follows:

QUOTE:

The installation of all cable and equipment is completed. Two connectors are known to be faulty at the first repeater site. Since these two faults still allow for 6 optical paths (2 out of 8 fibres), this meets the minimum criteria of 6 optical channels required for customer acceptance. Our intent is to correct these faults in May when weather conditions allow for more efficient and effective working conditions. In connecting equipment to cable the first objective was simply to achieve correct signal transmission through the entire system path. When this could not be achieved, a detailed



2.3.5.1 (cont'd)

verification of signal levels in each of the links that comprise the complete channel revealed that the optical signal levels were above their specification. Attenuators from Harris were borrowed and one was made by Canstar to adjust receive signal levels to the correct value. In this manner, initially two channels were made operational. However, one channel failed shortly after and the second has since also failed for unknown reasons. At this point in time, additional attenuators were made by Canstar and installed in the field. A quick verification of the attenuators showed that they provided the desired attenuation, had no measurable dispersion and did not change characteristics with temperature shocks. However, no long term monitoring could be carried out. Field conditions at this time are almost impossible. Testing at repeater sites is further complicated by the lack of monitoring points. * Cable continuity and optical levels are correct but the channels exhibit interference.

END OF QUOTE.

* All repeater modules were later modified to include test points for monitoring the receive data. Since clock recovery was not available this test point provides only minor assistance.



2.3.5.2 Statement of the Problem

Major:

- a) Optical power levels exceed the dynamic range of the receiver (-20 to -40 dBm).
- b) Equipment module failures are frequent.
- c) Presence of Spurious Noise Phenomena i.e. primarily modal and delay noise creating heavy eye closure causing the receiver to remain out of lock.

Minor:

- a) Module extenders and troubleshooting information at component level not available.
- b) Adjustments of power supplies on rear apron of the module drawers difficult due to location of some potentiometers on the modular supplies.
- c) The electrical connector alignment between modules and rear connector board is problematic and poorly designed. Furthermore, once aligned, disconnection occurs with time due to vibration.
- d) Fibre optic connectors are poor. Connector loss can reach as much as 5 dB per connection. A report on the suitability of the BCN fibre optic connector is provided in Attachment VI of this section.

Since very little was known about "Spurious Noise" or "Laser Noise" this had become the major problem at hand. Briefly, laser noise generates an unwanted modulation of the optical signal which translates into timing jitter when an



2.3.5.2 (cont'd)

optical signal is regenerated without retiming at a repeater, and amplitude modulation of the optical signal at a receiver input.

The origin of laser noise is not fully understood but one theory suggests that backscattering of laser light into the laser chip from a joint or laser facet creates laser instability. Apparently the reflected light causes a dynamic shift in frequency of the optical power emitted from the laser.. an effect known as mode hopping.

The effect is more severe at high bit rates and with non-return to zero (NRZ) coding. NRZ coding causes a variable duty cycle of the modulated laser which affects the junction temperature of the source to an extent where mode hopping occurs.

From an experiment performed it was observed that:

1. Laser noise was very sensitive to flexing of the fibre at the Transmitter end but relatively insensitive at the Receiver end.
2. Changes in the temperature of the laser diode also caused laser noise.
3. Increasing the laser diode bias above threshold increased the laser noise. The occurrence of an ILD increases with increasing bias. Laser noise is prevalent with highly coherent sources.



4. When a 2 km cable length (used in the experiment) was replaced by an equivalent optical attenuator, laser noise effects were not observed.

Conclusions determined from the above experiment were:

1. Laser noise increases with fibre length.
2. Laser noise decreases with laser bias (above threshold).
3. Some laser diodes exhibit less inherent laser noise effects than others.
4. System BER can be improved in the presence of laser noise by lowering the decision threshold of the receiver to a level mid-way between the "0" level and the lower extreme of the "1" level upon which rides the amplitude modulated laser noise.

Regardless of the above, six fibre channels were made temporarily operational for the CCTA convention demonstration,

This was accomplished by:

- a) Butting connector ferrules through an alignment piece and index matching the butted joint by applying index matching gel.
- b) Securing the connections of several modules to its associated rear connector panel.



- c) Repair of power supply short circuit.
- d) Adjustment of 5 V power supply.
- e) Replacement of fiber section due to a slow rise time response.
- f) Hybrid configuration employed where several links operated with one repeater to maintain a receive level within the dynamic range of the receiver.

The above results made necessary an in-depth study of the problems whose outcome is summarized in what follows.



2.4 System Modification Proposal: November 1979 to January 1980

The period from October 1979 to January 1980 set the stage for complete system rework in an attempt to make the system operational, to commission the system, and to complete one year (reduced to six months) operation and maintenance program. A series of technical discussions and presentations proposing four options has led to the decision of implementing the 4th option.. a single repeater located mid-way between terminals. An analysis of each of the options is given below:

Option 1 was the contractual 2 x 2R repeater configuration.

The advantages associated with this option were:

- a) Met original contractual configuration.
- b) Did not require repeaters to be moved.
- c) Inexpensive for the short term.

The disadvantages associated with this option were:

- a) Required more testing, in the operating environment, to assess the probability of achieving avg BER = 10^{-7} with spurious noise present.
- b) General opinion, success is not likely.
- c) System may still experience overload problem on some channels (optical attenuators required).

In conclusion this approach is likely to involve extended experimentation/optimization and is still not likely to produce the desired results.



2.4 (cont'd)

Option 2 was the hybrid configuration i.e. 3 optical links using only 1 x 2R repeater at existing location and the remaining 3 optical links with no change (2 x 2R). The advantages associated with this option were:

- a) Enabled 2 x 2R "experimentation" and data collecting, which would allow final conclusion as to feasibility of 2 x 2R and 10^{-7} BER.
- b) Did not require repeaters to be moved.
- c) Fewer modules were to be modified as compared to Option 4.
- d) Provided 10^{-7} avg BER on 3 of 6 channels.

The disadvantages associated with this option were:

- a) Not regarded as an acceptable Final configuration.
- b) Created two different types of repeater and terminal transmitter modules.
- c) Interfered with "loop back" testing.

In conclusion Option 2 is unfavourable mainly due to the configuration being non-symmetric and uncertainty of success on 3 of the 6 links.

Option 3 was a single FOTS-type retiming repeater located at ≈ 4 km (mid-way) between terminal ends. The advantage associated with this option was that it provided the best possible performance results.



2.4 (cont'd)

The disadvantages associated with this option were:

- a) Very high cost.
- b) Long term delivery of new repeater equipment.
- c) Defeated some of the LTMU system features.
- d) Required repeaters to be removed and new one installed.

The conclusion of high cost and long delivery schedule made this option unacceptable.

Option 4 was a single 2R (non-retiming) repeater located \approx 4 km (mid-way) between terminal ends.

The advantages associated with this option were:

- a) No unique repeater or transmitter modules required.
- b) No overload problems existed.
- c) System performance will provide average 10^{-7} BER on all six channels.
- d) LTMU will work as designed.

The disadvantages associated with this option were:

- a) Required repeaters to be removed and one to be reinstalled.
- b) Required maximum equipment modification.

In conclusion this option was expected to be the least costly and the most expeditious approach to success on all six channels and therefore Option 4 has been implemented.

The link analysis detailed in Table 2.4.1 below shows a 1.0 dB link margin for an average cable loss of 6.5 dB per km for Option 4 configuration.

TABLE 2.4.1: LINK LOSS ANALYSIS WORKSHEET

SYSTEM DATA	1. LINK LENGTH	km	<u>4.0</u>
	2. REQUIRED BANDWIDTH OR BIT RATE.. <input checked="" type="checkbox"/> MHz <input type="checkbox"/> Mb/s		<u>150</u>
	3. REQUIRED SNR OR BER..... <input type="checkbox"/> dB <input checked="" type="checkbox"/> BER		<u>10^{-7}</u>
	4. UNIT CABLE LENGTH.....	km	<u>1.0</u>
	5. INSTALLATION: AERIAL <u>3.5</u> km ; DUCT <u>0.5</u> km ; BURIED	km	
	6. TEMPERATURE RANGE: AERIAL <u>-40 to +50</u> °C ; DUCT <u>-20 to 40</u> °C ; BURIED	°C	
SYSTEM DATA	7. FIBER TYPE	<u>Multi-mode graded index</u>	
	8. OPERATING WAVELENGTH	nm	<u>850</u>
	9. ATTENUATION	dB/km	<u>6.5</u>
	10. ACTUAL LINK BANDWIDTH AT <u>500</u> MHz.km ^γ (γ = <u>0.8</u>)	Mhz	<u>165</u>
	11. NO. OF CONNECTORS		<u>2</u>
	12. NO. OF SPLICES		<u>8</u>
	13. SOURCE TYPE		<u>ILD</u>
	14. DETECTOR TYPE		<u>APD</u>
SYSTEM GAIN	15. SOURCE AVERAGE OUTPUT POWER <input type="checkbox"/> RZ <input checked="" type="checkbox"/> NRZ	dBm	<u>- 1.0</u>
	16. RECEIVER SENSITIVITY	dBm	<u>-40.0</u>
	17. GAIN (15-16).....	dB	<u>39</u>
SYSTEM LOSSES	18. CABLE LOSS (1x9)	dB	<u>26.0</u>
	19. TOTAL CONNECTOR LOSS AT <u>1.5</u> dB/CONN (x11).....	dB	<u>3.0</u>
	20. TOTAL SPLICE LOSS AT <u>0.5</u> dB/SPLICE (x12).....	dB	<u>4.0</u>
	21. PENALTY FOR BANDWIDTH LIMITATION	dB	<u>N/A</u>
	22. ALLOWANCE FOR EQUIPMENT AGING & TEMPERATURE DEGRADATION	dB	<u>3.0</u>
	23. ALLOWANCE FOR CABLE TEMP. DEGRADATION AT <u>0.5</u> dB/km....	dB	<u>2.0</u>
	24. OTHER:	dB	<u>N/A</u>
	25. TOTAL LOSSES (SUM OF 18 THRU 24)	dB	<u>38.0</u>
MARGIN	26. UNALLOCATED LINK LOSS MARGIN	dB	<u>1.0</u>



2.4 (cont'd)

A connector loss analysis was performed at Canstar indicating losses as high as 5 dB however on the average a 1.5 dB loss is obtained. Histograms of the results are shown in Attachment VIII of this section.

The system configuration as of May 26, 1980 is illustrated in Figure 2.4.1 below.

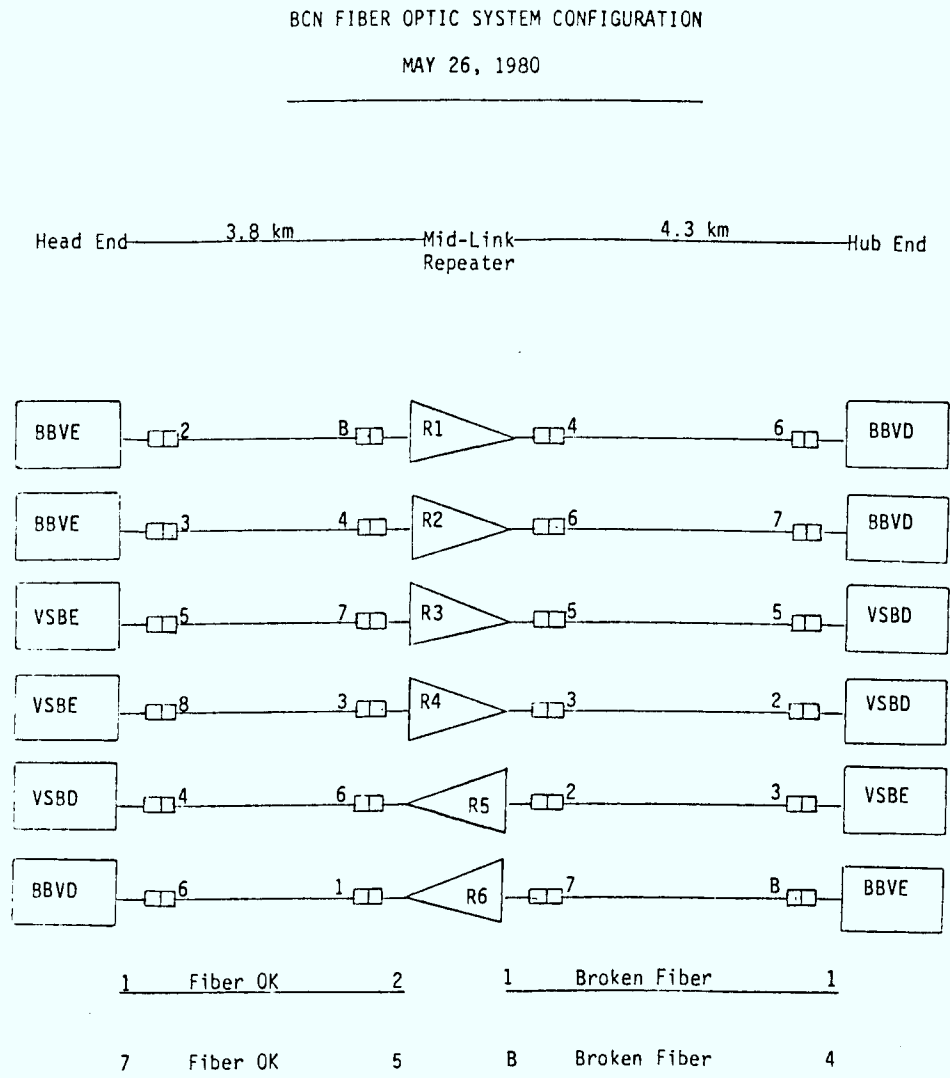


Figure 2.4.1



2.4 (cont'd)

It was expected that a long term bit error rate not worse than 10^{-7} would be achievable for the new configured link. Field Acceptance Testing was completed on June 10, 1980 witnessed by Leon Frank and Don Monteith (see Attachment IX). Field Acceptance Testing results are documented in Part II Section 3.1 of this report.

2.5 Pre-Commissioning Period: January 1980 to September 1980

The pre-commissioning activities consisted of the modification of the original system configuration and preparation of the modified system for final acceptance testing in the field. The activities associated with this period consisted of:

- a) The removal of the existing two repeater sites and the splicing together of their respective cable ends.
- b) The installation of a new repeater station mid-way between terminal ends which included the installation of repeater power supply, repeater housing, and the splicing of pigtail cords.
- c) The measuring of cable parameters on the new configuration.
- d) The manufacture and installation of a new set of optical pigtail cords.
- e) The repair of all faulty modules.



2.5 (cont'd)

f) The modification of all repeater and terminal transmitters consisting of:

- Rebias ILD for $-2.0 \text{ dBm} \leq P_o \leq 0.0 \text{ dBm}$.
- Reduce signal drive current to 13 ma p-p.
- Readjust PAM drive for $\approx 20\%$ p-p.
- Install external test points and pre-amp screen on the 13 repeater modules only.

g) The acceptance testing of the system.

2.6 Commissioning Period: October 1980 to November 1980

The Commissioning activity consisted of continuous monitoring of the frame sync status. The criteria of Commissioning acceptance was based on no significant frame sync losses for a period of 30 consecutive days. Frame sync loss was determined by recording the frame sync lamp condition on the front faceplate on each of the receiver drawers.

A report by Canstar's Project Engineer summarizes the events prior to resuming the Commissioning Period for a second attempt (which proved successful) on October 24, 1980.

QUOTE:

1. Background

After the acceptance testing of the BCN system on June 10, 1980 the 30 day Commissioning Period of the BCN system commenced. On June 16, 1980 all six fibre optic channels began experiencing continuous frame sync losses interrupting the countdown. An optical related phenomenon was considered then to be the cause of the frame sync losses.



2.6 (cont'd)

A Harris field trip in early August was therefore oriented toward measuring the optical pin lengths, cleaning the optical connectors and optimizing their coupling. In addition to the above activities, the equipment rack arrangement had been reconfigured to improve convection within the drawers.

The system continued to lose frame sync in spite of the above efforts and confused all as to the cause of the disturbance. Harris' immediate conclusion was optical feedback from the connector, i.e. backscattered light leading to spectral instability of the laser, disturbing its linearity, generating noise and errors. Their apparent solution was to observe performance of one link with optical connectors eliminated. At this point all parties split to allow Harris to analyze all the data accumulated and to formulate a plan of attack.

During this tranquil period Canstar requested Cablesystems Engineering to observe and monitor frame sync condition when physically shaking the repeater housing. A total system outage, i.e. frame sync loss, would be recorded on all channels each time the housing would be shaken. This information was immediately passed on to Harris. Harris requested that a repeater housing and several repeater modules be sent down to them for lab testing.



2.6 (cont'd)

The results of the lab tests showed that the repeater housing was functioning as should be, however the repeater and receiver modules individually showed frame sync hits whenever lightly banged or shaken. Harris proceeded to troubleshoot the modules and pinpointed the location of the disturbance. Eliminating a low frequency coupling capacitor apparently had solved the frame sync hits experienced in the lab.

2. Summary of Oct. 21 - Oct. 14, 1980 Field Trip

2.1 Harris team arrived on site and commenced operations on Oct. 21, 1980. The Harris team consisted of the following personnel:

Rich Patisaul - Lead Engineer

Don Alfred - Technical Assistant

Oli Fo - Optical Connector Assembler

2.2 Several activities were started up in parallel. Oli Fo was given the task of removing the metal screens wherever possible from modules to allow for additional air convection through the drawers. Receive power levels were measured for a comparison against level readings taken in their previous trip. An attempt was made to verify the behaviour of bit sync whenever a frame sync loss occurred. Lab tests indicated that bit sync was also obstructed for a very short time period, however not long enough to turn off the bit sync LED. Bit sync proved difficult to monitor because of inaccessability to bit sync circuitry.



2.3 Repeater and receiver modules at all locations were modified by removing a low frequency coupling capacitor between two line amplifiers. The system was reinstalled and powered up once more. Four optical channels were operational with no sign of frame sync hits. Baseband channel 2 was non-operational and baseband channel 1 experienced an excessively high error rate, approximately 10^{-5} with occasional frame sync losses which were purely related to high bursts of error (very clearly visible on the TV screen). Frame sync loss occurs at a bit error rate of 10^{-4} .

2.4 Second order problems were then attended to and included a bad power supply module, several video channels not operational, and thermal problems in one drawer. A blown fuse powering the fan and cleaning the air filters solved the thermal problem. A power supply from a spare encoder drawer replaced the faulty one. Inoperative video channels were linked to faulty equipment belonging to Cablesystems Engineering.

2.5 All optical connectors were cleaned and index matching gel was applied. This improved the error rate performance generally and cured the excessive error rate problem on baseband channel 1. Replacing a faulty repeater module and adjusting a bad electrical connection put baseband channel 2 back into service.



2.6 All channels were operational within specification. Frame sync hits had disappeared completely.

2.7 The following modules have been sent back to Harris Corporation for repair:

- a) Receiver module serial No. 007
- b) Repeater module serial No. 001
- c) Repeater module serial No. 010
- d) Repeater module serial No. 003
- e) 5V power supply unit.

3. Conclusions

No modal noise apparent on the eye diagrams; a relatively error free picture signal; and yet there existed instantaneous random frame sync hits on all optical fibre channels. These symptoms made it difficult to justify an optical or optical connector related problem. Normally frame sync losses would occur when channel error rate performance is operating around threshold. This obviously was not the case and finally the problem was eliminated by removing a low frequency coupling capacitor in all repeater and receiver modules. Presently there is no explanation for the interference caused by this capacitor. It may be, however related to a micro-sonic phenomena.

The past field trips have proven the Harris connector to be inferior and difficult to work with. To improve the system's error rate performance the connectors required optimization and



3. (cont'd)

the application of matching gel resulted in further improvement. However, in spite of their poor handling the Harris connector illusions have been somewhat stifled and perhaps now their operating performance understood and possibly tamed to provide acceptable performance.

END OF QUOTE.

Commissioning of the BCN Fibre Optic System was completed on November 24, 1980.

Removing the low frequency capacitor solved the problem of random frame sync losses occurring on the channels and allowed the system to pass the 30 day commissioning period. Although this capacitor was determined at the time to be unnecessary in the receiver card circuitry it's repercussion prevented the operation of the LTMU which was discovered only after completion of the 30 day commissioning run.

The low frequency capacitor is required in only one uplink channel which is a pre-selected channel to transmit the low speed data information of the LTMU by means of an asynchronous modulation/demodulation technique employing pulse amplitude modulation of the fibre optic bit stream. The LTMU information returned on the downlink path is multiplexed on the main bit stream using overhead bits and therefore the capacitor would not be required for these receivers since no low frequency information is being transmitted directly.



3. (cont'd)

Several attempts were made to make the channel operational with the LTMU by trying out different capacitor types however, to date a solution has not been found.

2.7 Post-Commissioning Period: December 1980 to May 1981

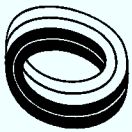
The Post-Commissioning activity consisted of a reduced one year period (6 months) of system operation and routine/periodic maintenance activities documented in Part III Sections 3 and 4 of this report.



ATTACHMENT I

(REFERENCE : PART II - SECTION 2.2.1)

FACTORY ATTENUATION
MEASUREMENT RESULTS

ATTENUATION MEASUREMENTSAFTER OUTER JACKET EXTRUDED BY CWC WINNIPEG

REEL #182B	FIBRE #	SIECOR CORE BEFORE SHEATHING (dB/km)	WITH OUTER JACKET EXTRUDED BY CWC (dB/km)
TEST # 6266 LENGTH: 1005m	1	N.T.	4.7
	2	N.T.	5.8
	3	N.T.	5.2
	4	N.T.	6.6
	5	N.T.	6.0
	6	N.T.	6.1
	7	N.T.	6.4
	8	N.T.	7.0
N.T.: NOT TESTED			
REEL #185 TEST #E6280 LENGTH: 1005m	1	6.6	6.5
	2	6.5	6.2
	3	6.0	6.2
	4	7.2	6.8
	5	6.4	6.4
	6	6.3	6.1
	7	5.9	6.2
	8	6.6	4.8
REEL #191 TEST #E6265 LENGTH: 1005m	1	6.4	DEFECTIVE FIBRE 5.72
	2	5.8	5.40
	3	5.4	5.45
	4	6.7	5.62
	5	5.5	6.49
	6	6.3	5.58
	7	5.3	6.32
	8	6.1	
REEL #184 TEST #E6278 LENGTH: 1005m	1	6.8	7.20
	2	6.8	6.65
	3	7.2	6.24
	4	5.8	5.89
	5	6.9	6.87
	6	6.6	6.22
	7	6.2	5.96
	8	6.5	6.53
REEL #187 TEST #E6281 LENGTH: 1005m	1	6.4	6.3
	2	6.1	6.0
	3	5.7	5.8
	4	6.5	6.4
	5	6.9	6.8
	6	6.2	6.4
	7	5.8	6.7
	8	6.2	6.5
REEL #186 TEST #E6279 LENGTH: 1038m	1	6.2	7.1
	2	6.3	5.7
	3	6.7	5.6
	4	7.8	7.5
	5	7.4	6.8
	6	6.4	6.1
	7	6.9	6.8
	8	6.6	6.3



ATTACHMENT II

(REFERENCE: PART II - SECTION 2.2.1)

FACTORY TEST METHOD:

CABLE ATTENUATION MEASUREMENTS



CANSTAR COMMUNICATIONS
FIBRE OPTICS ATTENUATION
MEASUREMENT SET
MODEL: CASD - AAM - 001
DESIGN AND OPERATION MANUAL



CONTENTS

Section 1	System Design
	. Design Goal
	. Design Considerations
	. System Configuration
	. Receiver Sensitivity
	. Noise calculation in pre-amplifier
	. Performance test
Section 2	Specifications
Section 3	Operation Instructions
	. Control Functions
	. Receiver Output
	. Measurement procedure
	. Precautions against measurement errors
	. Battery operation
	. Frequency tuning



Section 1

System Design



Design Goal

This equipment is designed to measure the absolute attenuation of optical fibres to a specified accuracy of $\pm 0.25\text{dB}$. The measurements range is to be greater than 30 dB. The measurement technique used is the reference fibre method in which the power coupled into the fibre under test and the power output from it are both measured. The attenuation is calculated by

$$A \text{ (dB)} = 10 \log \frac{P(\text{out})}{P(\text{in})}$$

This technique has the advantages of high accuracy and repeatability.



Design Considerations

The system consists of a transmitter and a receiver. The optical signal is amplitude modulated for the following advantages.

- . The received signal can be processed by high gain AC coupled amplifiers. Any DC offsets and drifts in the electronics will not cause significant measurement errors.
- . Spurious optical signals such as ambient light will not cause significant measurement error since only the modulated signal is selected and processed by the receiver.

The receiver will display the time average of the optical power received.

The optical coupling method used in the transmitter is a two-lens system and micromanipulator. The advantages are as follows:

- . The N.A. of the light launching into the fibre can be controlled. This is important in making accurate attenuation measurement with a defined launching condition.
- . Efficient coupling from the light source to the fibre can be achieved.

In the receiver, the light emitted from the fibre end is directly coupled to a large area photodetector (approximately 10^4 times larger than the area of the fibre core). An index matching liquid is used to reduce the Fresnel reflection at the fibre end.

A transimpedance amplifier is used as the pre-amplifier stage in the receiver because of its linearity and high gain.



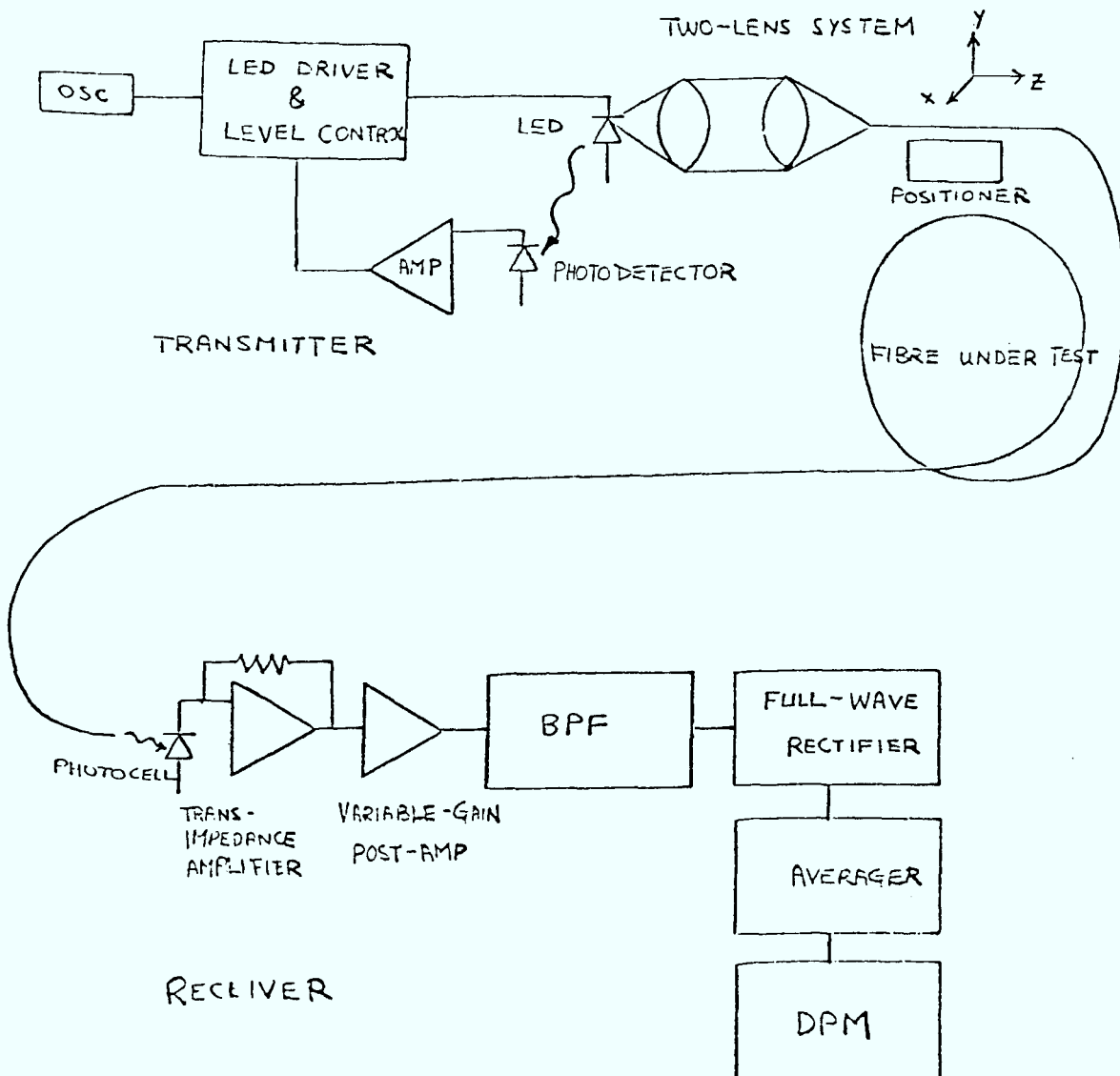
System Configuration

The system block diagram is shown below.

There is an optical feedback loop in the transmitter which maintains the optical output level at a constant level.

The receiver consists of a detector, pre-amplifier, variable gain post-amplifier, band-pass filter, full wave rectifier and an averager.

Fig. 1 System Configuration





Receiver Sensitivity

The required signal to noise ratio in the receiver is derived below:

$$P = \Delta 10 \log (Q + \Delta Q) - 10 \log Q$$

where ΔP = fluctuation in the measured power

Q = actual reading before conversion in dB reading

ΔQ = fluctuation in Q

$$\text{Hence } \frac{Q}{\Delta Q} = \frac{1}{10^{0.1 \Delta P} - 1}$$

$$\text{For } \Delta P = \pm 0.25 \text{ dB, } \frac{Q}{\Delta Q} = 16.8$$

This corresponds to a SNR of 24.5 dB. For the system, SNR degradations occur in the following areas.

<u>Sources</u>	<u>SNR degradation</u>
• Coupling loss to optical detector	1 dB
• Differentiation of responsivity on the active area of the detector	0.5
• Temperature induced fluctuation in the responsivity	0.8
• Frequency drift in the BPF	1.1
• Frequency drift in the transmitter	2.4
Total	5.8 dB

Hence the total required SNR is 30.3 dB.

Noise calculation in the pre-amplifier

The main source of noise in the receiver is the pre-amplifier stage which consists of a photodetector and an operational amplifier operating in the transimpedance mode.



The following model is used for the calculation of the noise at the output.

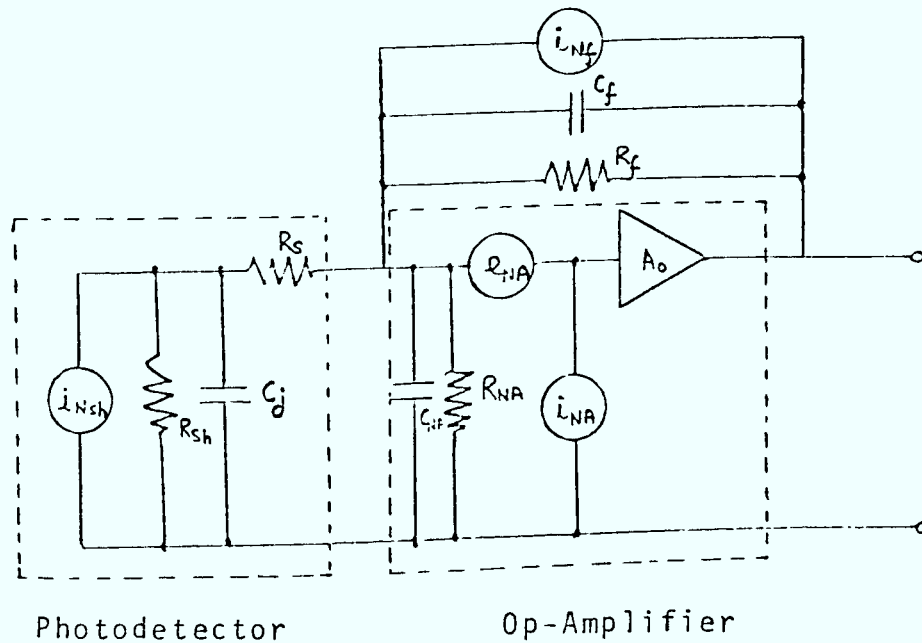


Fig. 2 Op-Amp/Photodiode - Electrical model

Total output noise voltage is given by:

$$e_{NT} = Z_f \{ (\underline{e_{na}})^2 B + (i_{NA})^2 B + i_{Nsh}^2 + i_{Nf}^2 \}^{\frac{1}{2}}$$

$$|Z_f| = R_f / (1 + \omega^2 C_f^2 R_f^2)^{\frac{1}{2}}$$

$$|Z_s| = R_{sh} / (1 + \omega^2 C_j^2 R_{sh}^2)^{\frac{1}{2}}$$

$$i_{Nsh} = (4kTB / R_{sh})^{\frac{1}{2}}$$

$$i_{Nf} = (4kTB / R_f)^{\frac{1}{2}}$$

B = bandwidth



Performance Test

The present operating system utilizes a low-noise J-FET OP-amplifier and a large area (0.187cm^2) photocell as the detector. The calculated noise voltage is $1.53\text{ }\mu\text{V}$. However, the total noise measured is $8.4\text{ }\mu\text{V}$ due to shielding problems.

To obtain a SNR of 30.3 dB, the minimum received power required is 111 pW or - 69.5 dBm assuming the responsivity of the photodetector is 0.5A/W average.

The equipment is used to measure the attenuation of a one kilometer sample of fibre with an attenuation of about 17dB.

Out of fifteen sample readings, the maximum deviation between the highest and the lowest readings is 0.2dB.

The performance of the equipment is summarized in next section.



Section 2

Specifications



Dated Nov. 22, 1978

Canstar Communications
Absolute Attenuation Measurement Set
Model CASD-AAM-001

Specifications:Transmitter:

Optical power output:	-20 dBm (maximum)
Power coupled into fibre (core dia. = 65µm, N.A. = 0.2, graded index)	-35 dBm (typical)
Launching mechanism:	two-lens system
N.A.	0.17
Focal length	16 mm
Fibre holder	X-Y-Z positioner
Light Source	LED
Wavelength (peak intensity)	820 nm
Bandwidth (50% points)	40 nm
Modulation frequency	150 ± 5 Hz
Optical output drift with temperature	± 0.0045 dB/°C
Long term stability (24 hours)	± 0.09 dB
Electrical power supply	115V, 60 Hz AC or built in 6V rechargeable battery
Dimensions	21.5 x 8.8 x 35 cm
Weight	2.8 kg

Receiver:

Dynamic Range	-34 dBm to -69 dBm
SNR	31 dB
Measurement Accuracy	± 0.25 dB
Detector	Silicon photocell
Fibre coupling method	Direct coupling and index matching fluid
Operating temperature	0°C to +40°C
Electrical power supply	115V, 60 Hz AC or built in ±12V rechargeable battery
Dimensions	8.8 x 21.5 x 32.1 cm
Weight	2.6 kg

(The above specifications are subject to change without prior notices.)



Section 3

Operating Instructions



Control Functions

The optical power output of the transmitter is adjustable from -35 dBm to -20 dBm by the potentiometer and the x1,x01 gain switch on the front panel of the transmitter. At the x0.1 setting, the output power is roughly one-tenth of that at the x1 setting.

The gain switch on the receiver determines the sensitivity of the receiver. There are four settings, x0.1, x1, x10 and x100. The fifth setting is for checking the voltage of the battery, which when fully charged, should read 10.5 or higher.

Receiver Output

The DPM is calibrated to read the average received power in nano-Watt. Calibration can be done by adjusting R₄₃ (layout diagram 3 B).

The decimal point shifts automatically with the gain setting.

To obtain a measurement accuracy of ± 0.25 dB, the minimum received power has to be over 0.126 nW (-69 dBm).



Measurement Procedures

1. Turn on power to the transmitter and set the power switch to x1 and the potentiometer dial to maximum reading.
 2. Remove the fibre holder from the X-Y-Z positioner by loosening the locking screw.
 3. Lift up the spring of the holder to about 1mm from the bottom of the groove.
 4. Cleave the fibre end of the fibre under test to obtain a flat and smooth end surface.
 5. Insert the fibre into the groove until the fibre is protruding for about 1 cm from the end of the holder.
 6. Press spring down until the fibre is clamped securely in the groove.
 7. Insert holder back into the X-Y-Z positioner until the fibre end is just inside the hole on the focal point marker.
 8. Tighten up the lock screw.
 9. Prepare the other end of the fibre.
 10. Turn on the power of the receiver and set the gain switch to x 100.
 11. Insert the fibre gently into the ferrule on top of the receiver until the insertion of the fibre is stopped.
 12. Make sure that the fibre is not sliding out of the ferrule. The fibre is normally retained in its position by the ferrule and the viscous index-matching liquid.
 13. Align the fibre end at the transmitting end using the X and Y adjustment.
- Switch to lower gains (x10, x1, 10-1) as necessary to prevent overloading of the DPM.

Overloading is indicated by the absence of the display digits.



14. Note the reading on the DPM (P out)
15. Without disturbing the transmitting end, cut the fibre at about 0.5m from this end. Prepare the fibre end and measure the power (P in) using the receiver as described in steps 11 and 12.
16. The attenuation of the fibre under test is calculated as follows:

$$A \text{ (dB/km)} = \frac{1}{L} 10 \log \frac{P_{\text{out}}}{P_{\text{in}}}$$

where L = length of the fibre in km.



Precautions against measurement errors

The following lists the most probable causes of measurement errors.

1. Fibre ends are poorly cleaved. This will result in either no transmission or excessively high coupling loss from the fibre end to the detector. Significant errors may be introduced when measuring either P in or P out.
2. Macro-bends or micro-bends on the fibre will lead to loss of transmission power. These bends are caused by mishandling of the fibre such as twisting, bending (less than 4" radius for most Corning GI fibres), or letting the fibre to rest on a rough surface or a sharp edge.
3. The fibre end at the transmitting end is not positioned inside the focal point of the launching light, or is not centred along the axis of the launching light. This will result in instability in the receiver reading.



Battery Operation

The batteries in the transmitter and receiver have capacities of 1.8A/hour at 6V and 1.5A/hour at $\pm 12V$ respectively and will last for 20 hours of continuous operation after fully charged. The charging time is about 24 hours. Charging can be done by connecting the transmitter/receiver to the 115V AC mains with the ON/OFF switch in the OFF position.



Frequency Tuning

The operating frequency of the system is designed to be 150 Hz. The modulation frequency in the transmitter and the band-pass filter in the receiver can be tuned according to the following procedure.

1. Connect a frequency counter which is capable of measuring 150 Hz across pin3 of IC4 and the circuit ground (point A) as shown in diagram 3A.
2. Adjust trimming potentiometer R_{23} until the counter reads 150 Hz.
3. Using a short piece of fibre, connect the transmitter optical output to the receiver input. Set gain switch to X0.1 and adjust R_{42} (receiver layout diagram 3B) until the DPM reading is maximum.

No further adjustment is necessary.

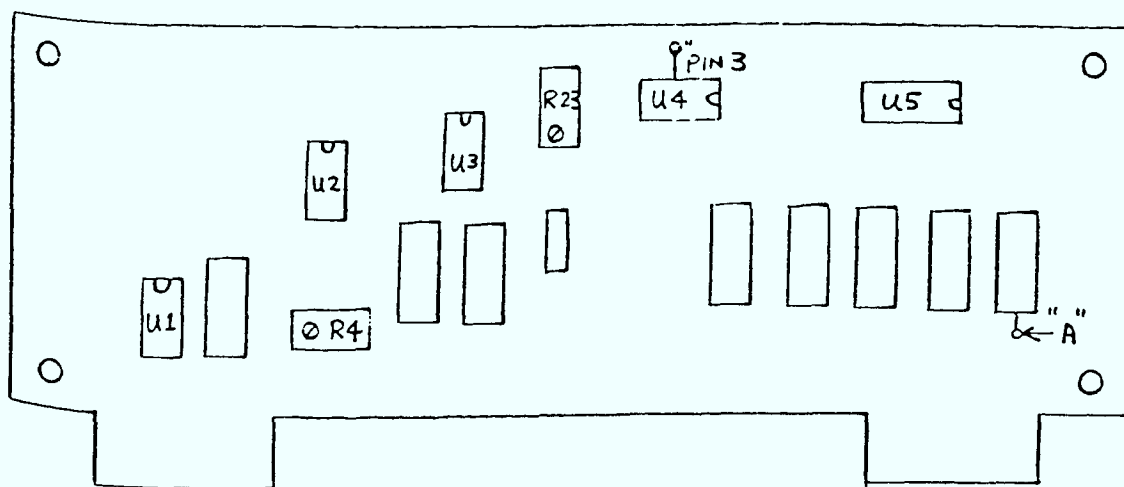


Fig. 3A Transmitter layout diagram

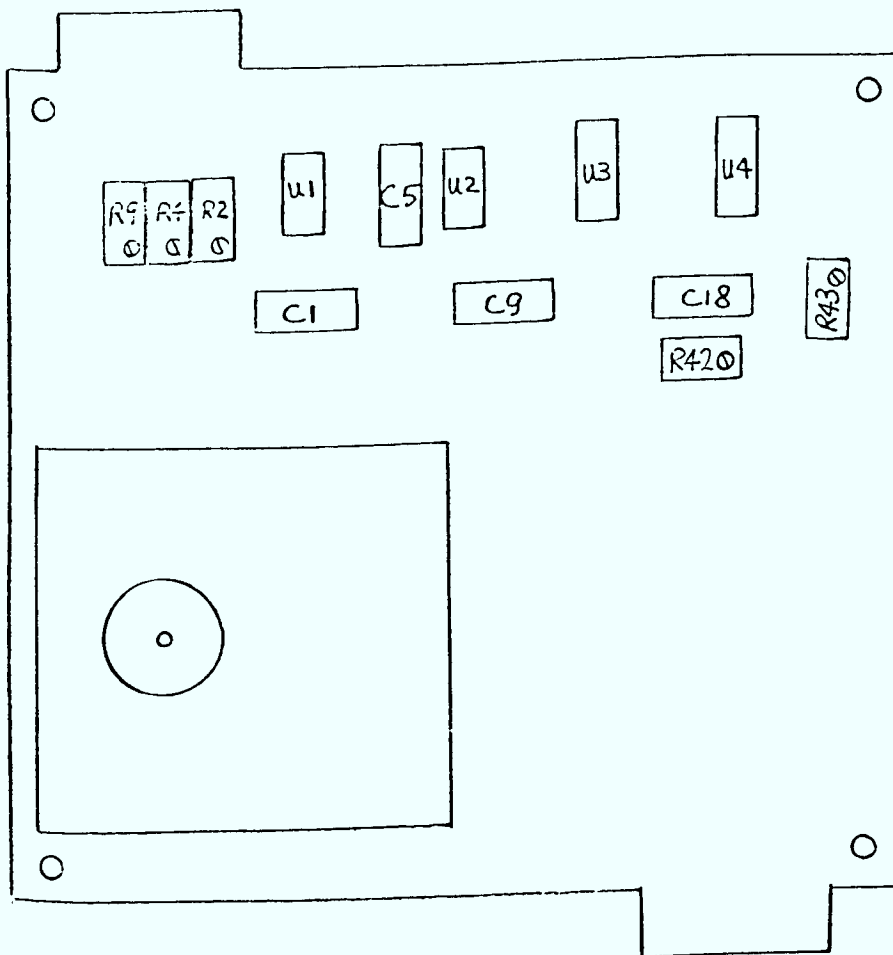


Fig 3B Receiver layout diagram



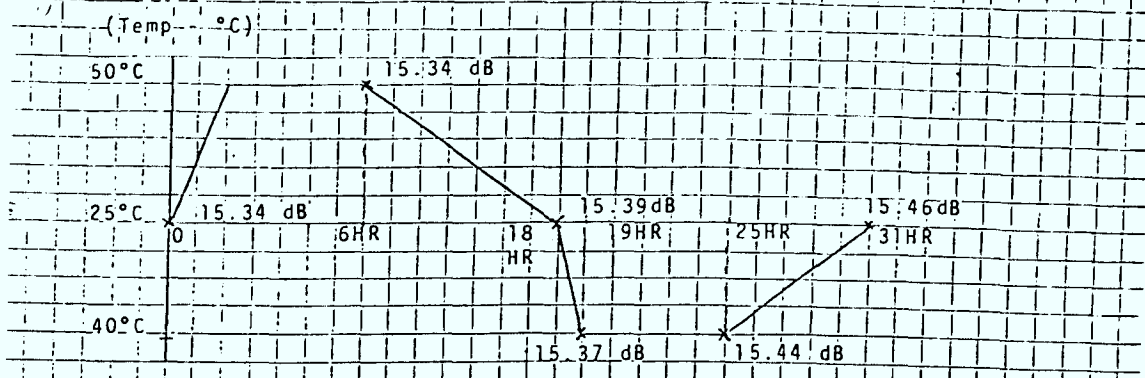
ATTACHMENT III

(REFERENCE: PART II - SECTION 2.2.3)

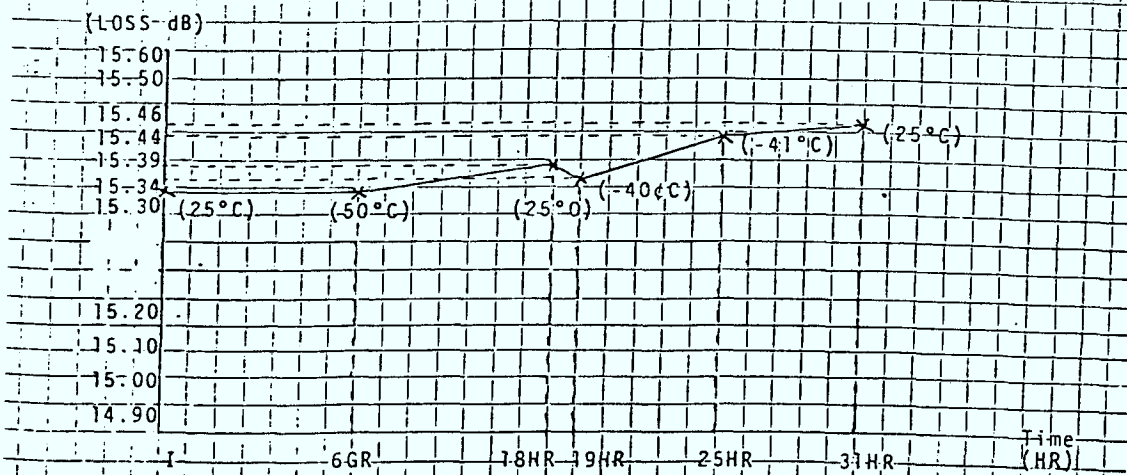
TEMPERATURE CYCLING CURVE



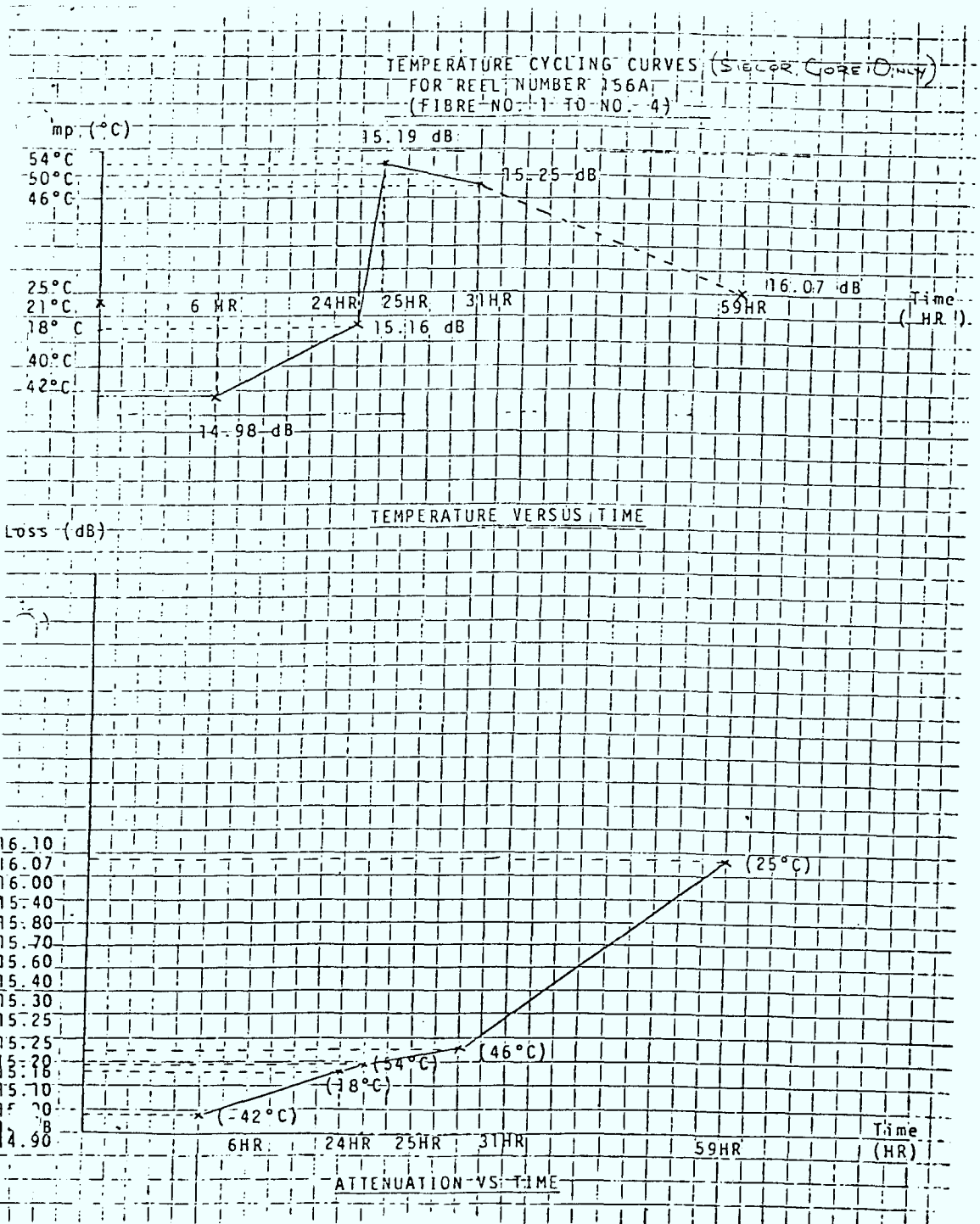
TEMPERATURE CYCLING CURVES (Steady State Data)
FOR REEL NUMBER 182A
(FIBRE NO. 1 TO NO. 4)

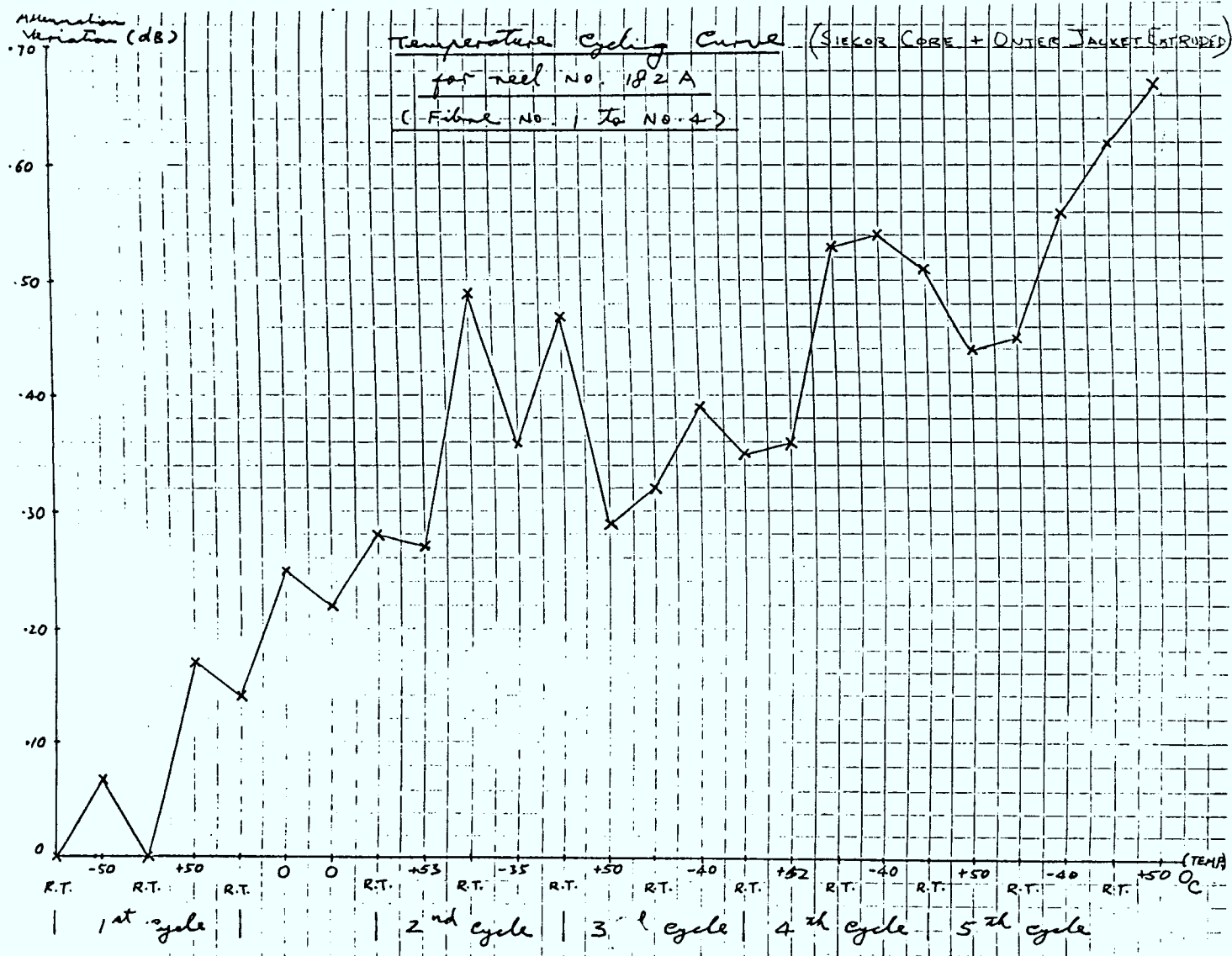


TEMPERATURE VS. TIME



ATTENUATION VS TIME







ATTACHMENT IV

(REFERENCE: PART II - SECTION 2.2.4)

STRENGTH TEST
METHOD AND RESULTS
ON
BCN FIBRES



STRENGTH TEST METHOD AND RESULTS ON BCN FIBRE

1.0 GENERAL

Each sample contained eight individually tubed fibres; one tube was colour coded (brown) for identification purposes. Each fibre was numbered sequentially starting with the brown tube and increasing in the clockwise direction, as viewed from the beginning of the cable (lowest meter marking).

2.0 PROCEDURE FOR REMOVING FIBRE

A circumferential cut through the outer sheath, and extending to, but not cutting the inner jacket, was made at intervals of 8 inches along the length of the cable. These short pieces of sheath were slipped from the cable core. The inner jacket was carefully slit with a sharp knife and peeled from the stranded core. The individual tubes were then uncoiled from the central strength member. By holding 1 meter of buffer tube straight, the fibre could easily be slipped from the tube.

3.0 OBSERVATIONS ON CABLE STRUCTURE

The buffer tubes were helically stranded with a pitch of approximately 8 cm. This stranding was very tight, causing



periodic collapse of the buffer tube. Many of the tubes have flat spots at 8 cm intervals over part of their length. Dissecting the tube shows that the hole is almost blocked at these points trapping the fibre.

STRENGTH TEST PROCEDURE

The test procedure consists of wrapping a 1 meter gauge length of fibre around a series of mandrels. The mandrel section is chosen to develop a maximum stress on the outer surface of the fibre according to the relationship $\sigma = \frac{E \cdot d}{D + 2c}$ where D is the mandrel diameter, c is the coating thickness, d is the fibre diameter, E is Young's modulus of the fibre material. Six mandrels were used giving stresses from 100 kpsi to 350 kpsi. The same length of fibre is wrapped successively on smaller mandrels, recording the number of breaks for each mandrel, until the number of breaks becomes excessive. Where possible, the test was repeated on a second 1-meter gauge length to demonstrate reproducibility.

TESTING CONDITIONS

Mandrel diameter (mm) 12.6 8.4 6.1 5.0 4.2 3.6
Approx. Applied stress (kpsi) 100 150 200 250 300 350

RESULTS

Cable no.	Fibre no.	Number of breaks at specified stress (kpsi)					
		100	150	200	250	300	350
6265	1 (brown)	0	0	38	N.T	N.T	N.T
	3	0	0	0	1	1	7
	3 repeat	0	0	0	4	6	N.T
	4	2	0	0	0	6	N.T
	4 repeat	0	1	4	6	N.T	N.T
	5	0	1	4	1	2	7
	8	0	0	1	0	4	8
	8 repeat	0	0	1	0	2	7
6281	1 (brown)	0	2	12	N.T	N.T	N.T
	1 repeat	0	0	15	N.T	N.T	N.T
	2	0	0	4	6	10	N.T
	2 repeat	0	1	7	N.T	N.T	N.T
	3	0	1	18	N.T	N.T	N.T
	3 repeat	0	2	>8	N.T	N.T	N.T
	4	0	0	18	N.T	N.T	N.T
	4 repeat	0	1	11	N.T	N.T	N.T
	5	0	0	12	N.T	N.T	N.T
	5 repeat	0	2	6	N.T	N.T	N.T
	6	0	2	>20	N.T	N.T	N.T
	6 repeat	0	1	12	N.T	N.T	N.T
	7	0	0	25	N.T	N.T	N.T
	7 repeat	0	0	10	N.T	N.T	N.T
	8	0	0	14	N.T	N.T	N.T
	8 repeat	0	0	6	N.T	N.T	N.T

N.T. : Not Tested



DISCUSSION

The fibres from cable E6265 exhibited varying strength, but fibre 1 with 38 breaks at 200 kpsi is very weak. Fibres 4 and 5 do not look good, but further samples would be needed to give conclusive results. By comparison, it is our experience with extensive tests on similar Corguide fibre that

at 150 kpsi-breaks	are very rare	1% of samples tested
200 kpsi-	1 - 2 breaks, about	25% of samples
250 kpsi-	1 - 2 breaks, about	50%
300 kpsi-	1 - 2 breaks, about	75%

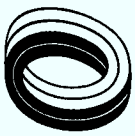
We have never observed more than 5 breaks on a sample below 250 kpsi.

All eight fibres in cable E6280 exhibited poor strength characteristics and their results were confirmed by a second test, which gave consistent results.

These fibres do not appear to have strength distribution consistent with Corning's data (Median strength 200 kpsi - or 3 mm bend radius). This could account for the difficulties experienced with connectorization. This may be aggravated by the flattened tubes which kink easily.

CONCLUSIONS

The high incidence of low strength defects in these fibres indicates that these cables are not suitable for field installation.



To guard against installing cable with a high failure probability, screen tests have been implemented on fibre strength.



ATTACHMENT V

(REFERENCE: PART II - SECTION 2.2.5)

FUSION SPLICE EXPERIMENT



A01 Fusion Splice Experiment in Montreal - September 25, 1978

Arc time: 2.5 sec.

Current: Minimum point at high range

Pressure: 10

Electro Distance: 2 mm

Input power $2.78 \pm .01 \mu\text{w}$

(1) $2.34 \pm .01$ Fused
 2.51 Tube on
 $2.63 \pm .01$ 10 min. later

(2) 2.53 Fused
 Fiber broken when moving tube.

(3) Input disturbed

Re-adjust input to $2.21 \pm .01 \mu\text{w}$

(4) 1.89 Fused
 1.98 U-connector on
 (very bad ends)

(5) 1.85 Fused
 1.86 Tube on

(6) 1.71 Fused
 Fiber broken

(7) 1.62 Air bubble in joint

(8) 1.17 Fused (very bad ends)
 1.17 Tube on

(9) $1.65 \pm .01$ Fused
 1.73 Tube on

(10) $2.06 \pm .01$ Fused
 $1.95 \pm .01$ Tube on



Re-adjust input to $2.43 \pm .01 \mu\text{w}$

- (11) $2.08 \pm .01$ Fused (air bubble)
 $2.08 \pm .01$ Tube on
- (12) $2.16 \pm .01$ Fused
 $2.16 \pm .01$ Tube on
- (13) $2.14 \pm .01$ Fused
 $2.19 \pm .01$ Tube on
- (14) $2.15 \pm .01$ Fused (air bubble)
Fiber broken
- (15) $2.19 \pm .01$ Fused
 $2.12 \pm .01$ Tube on
- (16) 2.14 Fused
 2.01 Tube on

September 26, 1978

Pressure: 8

Others the same as Sept. 25.

Input $2.64 \pm .02 \mu\text{w}$

- (17) $1.95 \pm .01$ Fused
Bad end and air bubble in joint
Deutsch cutter being used.
 $2.30 \pm .02$ 3 min. later
 $2.26 \pm .01$ Tube on
- (18) Input disturbed, but splice measured
by using other system the loss is 0.6dB.
- (19) 2.40 Fused
 $2.58 \pm .01$ Tube on
- (20) $2.31 \pm .01$ Fused (N.T.)
 $2.47 \pm .01$ Tube on
- (21) $2.24 \pm .01$ Fused (N.T.)
 $2.37 \pm .01$ Tube on
- (22) 2.56 Fused (N.T.)
Fiber broken
- (23) $2.64 \pm .01$ Fused (CWC)
 $2.50 \pm .01$ Tube on



Re-adjust input to $3.16 \pm .01 \mu w$

- | | | |
|------|----------------|-------------------------|
| (24) | 2.62 | Fused (CWC) |
| | $2.77 \pm .01$ | Tube on |
| (25) | $2.50 \pm .01$ | Fused (air bubble) |
| | $2.63 \pm .01$ | Tube on |
| (26) | $2.25 \pm .01$ | Fused (air bubble) |
| | $2.25 \pm .01$ | Tube on |
| (27) | $2.70 \pm .01$ | Fused |
| | 2.70 | Tube on |
| (28) | $2.79 \pm .01$ | Fused (air bubble) |
| | $2.80 \pm .01$ | Tube on |
| (29) | $2.49 \pm .01$ | Fused (air bubble) |
| | $2.52 \pm .01$ | Tube on |
| (30) | $3.03 \pm .01$ | Fused (very good joint) |
| | $3.04 \pm .01$ | Tube on |



ATTACHMENT VI

(REFERENCE: PART II - SECTION 2.3.4)

BCN OPTICAL CONNECTOR REPORT



B.C.N. OPTICAL CONNECTOR
REPORT

REAL POMERLEAU & DON MONTEITH



B.C.N. OPTICAL CONNECTOR

July 24, 1979

ABSTRACT:

An experiment was performed on the B.C.N. link to determine the suitability of the optical connectors presently in use. The experiment consisted of conducting a predetermined sequence of attenuation measurements on successive fibre/connector configurations with a common laser source. A high degree of unrepeatability in the experimental results indicates that the reliability of the link's optical connectors is suspect.

PROCEDURE:

In the experiment, two laser modules were used in each of the two repeater stations as reference optical sources. The received optical power was then measured using an optical power meter (Photodyne model 22XL) at the receiving stations. Figure II illustrates the experimental set-up.



Pre-experimental preparation included the cleaning of all optical connectors. The following describes the cleaning procedure.

The ferrule end of each male connector was cleaned with a cotton swab moistened with lens cleaning fluid, and subsequently dried with another cotton swab. Both male and female connectors were then blown with compressed air, to remove any dust or cotton fiber present.

Subsequently laser #1 was connected to fibers 1 through 8 and the received power measured at each corresponding end in the appropriate receiving station. This sequence was repeated three times and each time before interconnecting the laser with the fiber, the connectors were blown with compressed air. After the three runs, the above was repeated with laser #2.

Figure 3 shows the experimental set up in detail:

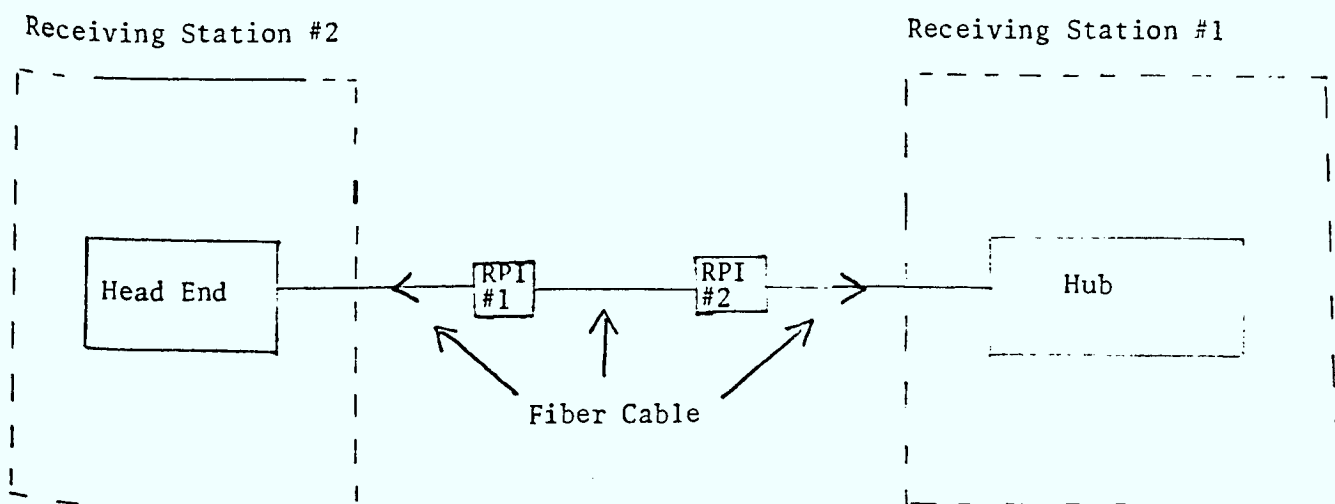


FIGURE II

DISCUSSION:

This experiment was conceived and conducted subsequent to two unsuccessful attempts in correlating link attenuation readings. Since no correlation could be obtained, it was considered necessary to investigate the dependence of received optical power on:

- 1) fibre attenuation
- 2) optical connector loss.

On July 11th, an analog chart recorder was interfaced to the optical power meter to provide a continuous record of received optical power. To date, no long-term fluctuations in the received optical level greater than .4db/hr and 1 db/24 hrs. has been observed. These results indicate that the large short-term fluctuation in optical received power is not highly dependent on fibre attenuation changes.

An analysis of optical connector losses, however, reveals that large link attenuation fluctuations can easily be introduced. Figures 4 and 5 show a typical fiber to fiber connection (i.e., male, female respectively).

Defining dA to be the most probable error in the connection,

$A \dots \text{attenuation of the connector} = f(x, y, z),$

then dA is given by the following formula,

$$dA^2 = \sum_i \left(dci \frac{\partial A}{\partial ci} \right)^2$$

Where C_i are the various parts of the connectors as shown in figure 4,5:

$$i = 1 \dots n \quad n=12$$

Here dci represents the mechanical tolerances of each part of the connector and $\frac{\partial A}{\partial Ci}$ is the partial derivative of the function A with respect to C_i .



In this particular case, a detailed analysis of the above can become extremely complex. A much simpler approach is to perform physical measurements on the link, and with the use of maximum likelihood analysis of the data, a figure for dA can be obtained. See appendix 1 for detail. A simple conclusion can be arrived at on the above analysis by simply noting that the most probable error will increase proportional to the number of parts used in a connector. Therefore to minimize dA, one should use a minimum number of individual parts. Notice that the above analysis does not make any compensation for the fact that the fiber core might have lateral, longitudinal, and angular displacement, since this is a function of the fiber itself and not of the connector.

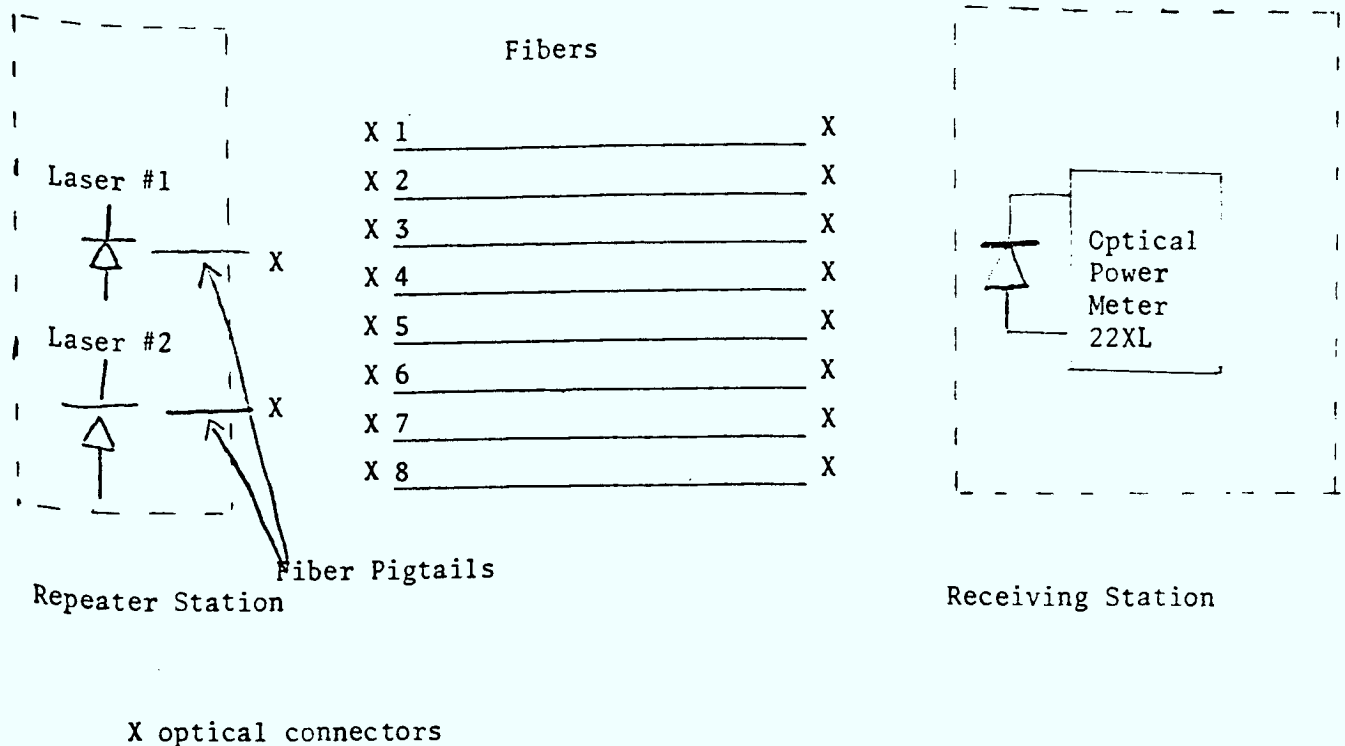


FIGURE III



CONCLUSION

An experiment was conducted in the BCN link to determine a "mismatch" and/or "most probable" error in mating optical connectors.

A figure up to 6.3dB was obtained for such error. Included is a plot of the interconnector distribution for both repeaters. Ideally both of the curves should have a narrow peak at zero. Proper link operation would require the two curves to be close to ideal.

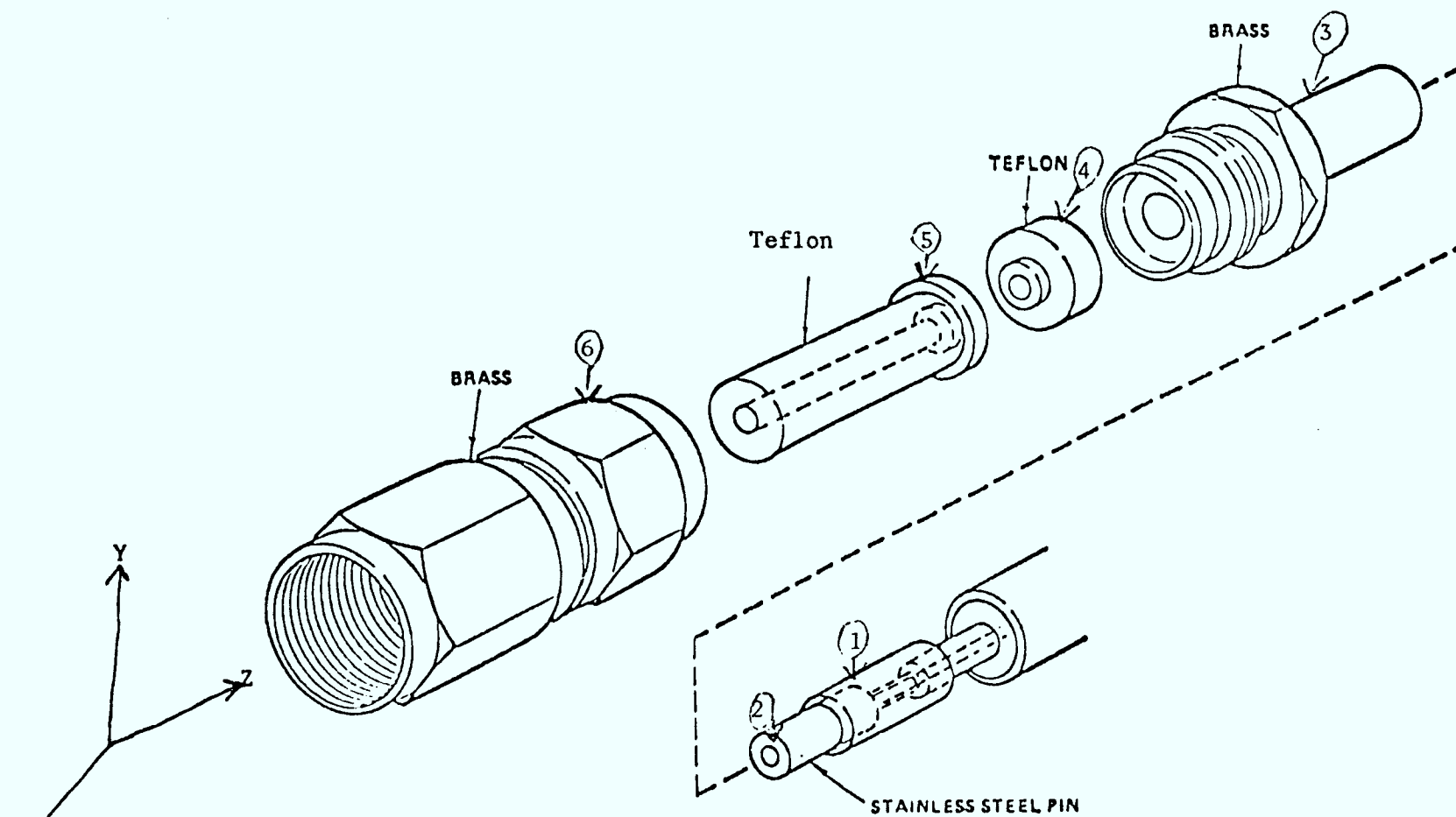


Fig. 4

HARRIS FIBER OPTIC CONNECTOR

EXPLODED VIEW (MALE)

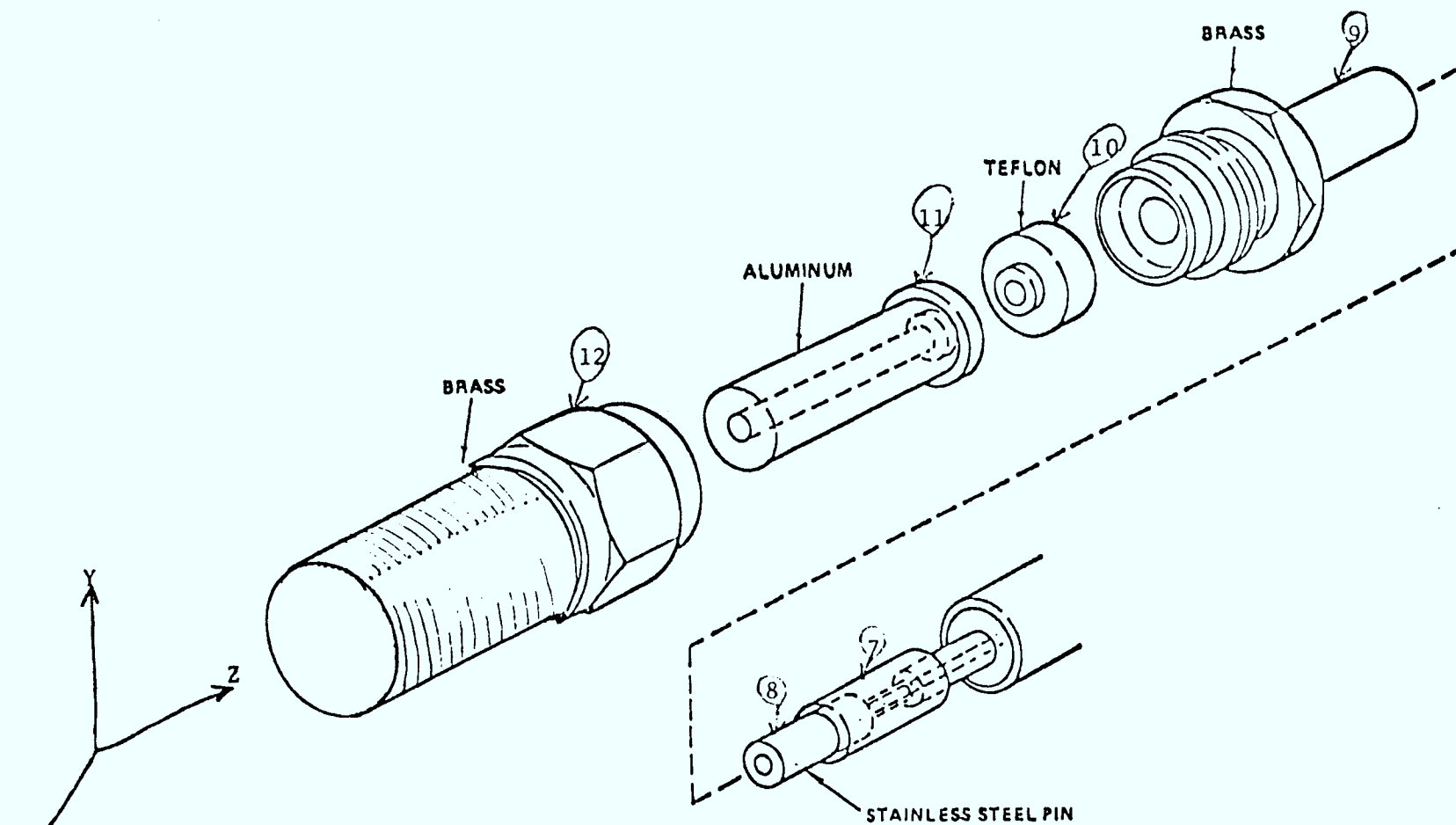
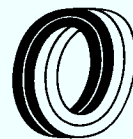


Fig. 5

HARRIS FIBER OPTIC CONNECTOR

EXPLODED VIEW (FEMALE)



APPENDIX 1

This appendix outlines the maximum likelihood method for estimation of parameters in a stochastic model.

Let X_i represent the loss of each fiber measured respectively.

Let the measure power level and its uncertainty be represented by Y_i and σ_i $i = 1, M$ $m = 3 \times N$

N ... number of fiber measured. In the case of the photodyne model 22XL, the uncertainty is 1% of the reference level.

X_i and Y_i can be related in a matrix equation.

$$AX = Y \quad \dots \text{Eg. 1}$$

Where X and Y are column matrix,

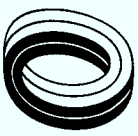
A is a, M by N matrix, M being the number of readings taken.

	1	2	3	4	5	6	7	8
Y_1	1	0	0	0	0	0	0	0
Y_2	0	1	0	0	0	0	0	0
Y_3	0	0	1	0	0	0	0	0

$A =$

A_{ij} is either 1 or 0 depending on whether the particular fiber is being measured or not.

Now since there are more equations than unknowns, one must resort to least square estimates to find a solution for X .



Assuming that the measured result Y_i is Gaussian, then the likelihood function is proportional to:

$$L(X_1, X_2, X_3, \dots, X_n) = \prod_{i=1}^M \frac{1}{\sqrt{2\pi}\sigma_i} \exp \left[-\frac{(Y_i - \xi_i)^2}{2\sigma_i^2} \right] \quad \text{eg. 2}$$

$\xi_i = \xi_i(X_1, X_2, \dots, X_n)$ The theoretical value of Y_i .

To find the best fit, we must maximize the likelihood function. Maximizing the function is equivalent to minimizing the exponent.

$$\sum_{i=1}^M \frac{(Y_i - \xi_i)^2}{2\sigma_i^2}$$

Which leads to the condition of least square fit, namely:

$$\sum_{i=1}^M \frac{(Y_i - \xi_i)}{\sigma_i^2} \frac{\partial \xi_i}{\partial X_j} = 0 \quad j = 1, 2, \dots, N \quad \text{eg. 3}$$

$$\text{Since } \xi_i = \sum_{j=1}^N A_{ij} X_j \quad i = 1, 2, \dots, M$$

and from eg. 1, the maximum likelihood condition of eg. 3 becomes

$$\sum_{i=1}^M \frac{A_{ij} Y_i}{\sigma_i^2} = \sum_{i_l=1}^M \frac{A_{ij} A_{i_l} X_{i_l}}{\sigma_i^2} \quad \text{eg. 4}$$



In matrix form eg 4 becomes:

$$Y = MX \quad \text{eg. 5}$$

$$\text{Where } Y_j = \sum_{i=1}^M \frac{A_{ij} Y_i}{\sigma_i^2} \quad j=1, 2 \dots N$$

is simply a modified data vector and

$$M_{jL} = \sum_{i=1}^M \frac{A_{ij} A_{iL}}{\sigma_i^2} = M_{Lj} \quad j, L = 1, 2 \dots N$$

is a symetrix square matrix.

The solution of 5 is:

$$X = M^{-1}Y$$

and the standard error in Y_j is

$$AX_j = (M_{jj}^{-1})^{1/2} \quad j = 1, 2 \dots N$$

The expected measured power is then given by:

$$\xi_i = \sum_{j=1}^N A_{ij} X_j \quad i = 1, 2 \dots M$$

and the expected measured uncertainty

$$\eta_i = \left[\sum_{j=1}^N A_{ij} AX_j^2 \right]^{1/2} \quad i = 1, 2 \dots M$$

A computer print-out Appendix 2, 3 gives "True Value" as ξ_i ,
calculated standard error as η_i .

APPENDIX 2

LIHOOD 11:30 AM

24-Jul-79

REPEATER 2 TO HUB

ENTER BASE USED ? 1E-6

ENTER THE NUMBER OF FIBER MEASURED ? 7

FILENAME ? FILE3.DAT

TRUE VALUE		USING MODULE #1 MEASURED VALUE	(DB _μ W)	FIBER #
17.9667	18.8	17.8	15.6	8-8
15.2333	14.6	17.8	15.7	4-1
15.1	13.9	14.6	17.3	7-4
15.9667	16.6	17	16.5	3-5
14.8667	14.2	15.4	14.4	2-2
13.6333	11.4	16.1	15.9	5-7
16.4667	17.8	15.6	14.3	1-6

CALCULATED STANDARD
ERRORERROR IN
MEASUREMENTS

.252002E-1

.436481E-1

ATTENUATION

UNCERTAINTY FIBER #

14.2833	.688483E-1	8-8
17.0167	.688483E-1	4-1
17.15	.688483E-1	7-4
16.2833	.688483E-1	3-5
17.3833	.688483E-1	2-2
18.6167	.688483E-1	5-7
15.7833	.688483E-1	1-6



FILENAME ? FILE4.DAT

		USING MODULE #2		
TRUE VALUE		MEASURED VALUE	(DBUW)	FIBER #
-6.23333	-6.6	-6.3	-8.4	8-8
-6.2	-6.3	-6	-7.1	4-1
-7.16667	-7.3	-6.2	-6.1	7-4
-9.66667	-9.3	-7.3	-6.1	3-5
-6.46667	-6.5	-9.9	-6.9	2-2
-8.53333	-8.8	-6.2	-9.8	5-7
-6.7	-6.3	-8.4	-6.7	1-6

CALCULATED STANDARD
ERROR

.252002E-1

ERROR IN
MEASUREMENTS

.436481E-1

ATTENUATION

19.1333
19.1
20.0667
22.5667
19.3667
21.4333
19.6

UNCERTAINTY

.688483E-1
.688483E-1
.688483E-1
.688483E-1
.688483E-1
.688483E-1
.688483E-1

FIBER #

8-8
4-1
7-4
3-5
2-2
5-7
1-6

EXTRA ATTENUATION DUE
TO CONNECTORS MISMATCH

UNCERTAINTY

4.85
2.08333
2.91667
6.28333
1.98333
2.81667
3.81667

.137697
.137697
.137697
.137697
.137697
.137697
.137697

Ready



RUN LIHOOD.BAS

REPEATER 1 TO HEAD-END

ENTER BASE USED ? 1E-6

ENTER THE NUMBER OF FIBER MEASURED ? 6

FILENAME ? FILE1.DAT

TRUE VALUE		USING MODULE #1 MEASURED VALUE		(DBμW)	FIBER #
2.4	1.9	3	2.3	1-1	
-4.9	-4.5	-5	-5.2	6-8	
6.5	6.5	6.4	6.6	7-6	
8.2	8.4	8.2	8	8-7	
6.73333	6.3	7.3	6.6	3-5	
7.43333	7.3	7.6	7.4	4-3	

CALCULATED STANDARD
ERROR

.252002E-1

ERROR IN
MEASUREMENTS

.436481E-1

ATTENUATION

29.35
36.65
25.25
23.55
25.0167
24.3167

UNCERTAINTY

.688483E-1
.688483E-1
.688483E-1
.688483E-1
.688483E-1
.688483E-1

FIBER #

1-1
6-8
7-6
8-7
3-5
4-3



FILENAME ? FILE2.DAT

TRUE VALUE		USING MODULE #3 MEASURED VALUE		(DBUW)	FIBER #
5.43333	6.4	4.5	5.4		1-1
-4.63333	-5	-4.4	-4.5		6-8
7.76667	7.9	6.9	8.5		7-6
7.13333	7.3	5.9	8.2		8-7
8.6	7.9	8.9	9		3-5
8	10.3	7.1	6.6		4-3

CALCULATED STANDARD
ERRORERROR IN
MEASUREMENTS.252002E-1.436481E-1

ATTENUATION

UNCERTAINTY

FIBER #

26.6767
36.7433
24.3433
24.9767
23.51
24.11

.688483E-1
.688483E-1
.688483E-1
.688483E-1
.688483E-1
.688483E-1

1-1
6-8
7-6
8-7
3-5
4-3

EXTRA ATTENUATION DUE
TO CONNECTORS MISMATCH

UNCERTAINTY

2.67333
.933333E-1
.906667
1.42667
1.50667
.206667

.137697
.137697
.137697
.137697
.137697
.137697

Ready

EXPLANATION OF COMPUTER PRINT-OUT

Base used	dBmW or dB μ W on 22XL meter
Measured value	Experimental results
True value	Likelihood estimate of experimental results
Calculated standard error	Estimate error on true value
Error in measurements	Error in experimental results
Attenuation	Tx optical power - true value
Uncertainty	Error in attenuation figure Calculated standard error + error in Tx power measurement
Extra attenuation due to connectors mismatch	Attenuation using module #1 Attenuation using the other module
Uncertainty	The addition of both attenuation uncertainty figure.

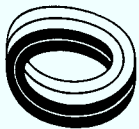


ATTACHMENT VII

(REFERENCE: PART II - SECTION 2.3.4)

REPORT ON

DEGRADATION OF FIBRE OPTIC CABLE JACKET



Canada Wire and Cable Limited

Central Engineering Services Report

NO. CES-79-17

FILE: MP-5.1; CL-1501

DATE: June 11, 1979

TITLE: Degradation of Fibre Optic Cable Jacket

SYNOPSIS

A sample of a Siecor fibre optic cable, dug up from an installation in London, Ontario, was submitted for determining the cause of cracks in the outer polyurethane jacket.

It appears that the cracks are a result of physical deterioration of the jacket due to the flooding compound under the jacket.

Reported by

Checked by

Checked by

Distribution

S. M. Jaczek
G. Reesor - Canstar
D. Vineberg - Canstar
File



1. Background

A fibre optic cable of German manufacture obtained through Siecor in the U.S. was installed by Canstar. It was buried directly in a trench, in sand, to a depth of about six feet, in London, Ontario. A portion of the cable was dug up about eight months later, and cracks in the outer jacket were observed. A sample of the cable was submitted to this laboratory for evaluation of the cause of this cracking and the suitability of this cable for further service. A sample of the same cable, which was not installed and which was still on a reel, was also examined along with this sample for comparison.

2. Description of sample

The cable has a central strength member surrounded by eight glass fibres in tubes, laid up with Kevlar fibres. The assembly has an inner jacket of black polyurethane. The armouring consists of a single, helically applied, steel tape, longitudinally layed steel wires, another single, helically applied (in opposite direction to the inner tape) steel tape. The steel armour is flooded with a waxy grease. The cable has an overall black polyurethane jacket.

3. Analysis of samples

The outer jacket was identified, by infrared analysis, as a thermoplastic, polyester type, polyurethane. The flooding compound on the steel armour was an amber coloured greasy material and was determined to be a petrolatum-based compound with a polyethylene wax additive.

The unaffected portions of the polyurethane jacket had good physical properties. On a sample of jacket taken from an uninstalled length of cable, the tensile strength was 5100 psi with an elongation of 530%. The jacket (from both samples) had good flexibility at low temperatures (-25°C).

In order to assess compatibility with the flooding compound, a sample taken from the jacket of the damaged cable was smeared with the flooding compound, stressed and aged at 160°F for 72 hours. Another sample, immersed fully in petroleum jelly telephone filling compound (Dussek's Insojell C-2852) was aged under identical conditions. Both samples did not show any further cracks or fresh cracks as a result of this accelerated aging test.

Examination of the jacket inner surface and the flooding compound on the steel armour of the damaged cable reveals that there was an excess of this flooding compound in many areas (not uniform), especially at the edges of the steel tape armour. It was also apparent that a majority of the cracks on the jacket were at these areas or have initiated at these areas. The compound had dried and was turning to powder in places where the jacket had cracked.



The jacket was very tight and has probably been pressure extruded, and it is believed that some non-homogeneity has occurred due to penetration of the flooding compound (at areas of excess) while the jacket was being extruded, causing physically weak spots in these areas. In a cable construction such as this, tubing type extrusion is more common.

Examination of the sample of cable taken from the reel in stock shows that there was excess of flooding compound in some areas, and the inside of the jacket showed signs of cracking. In Appendix I attached to this report, are photographs (1) showing cracks on the inner surface of jacket from cable in service and (2) showing damage on the inner surface of jacket from cable in storage.

4. Discussions

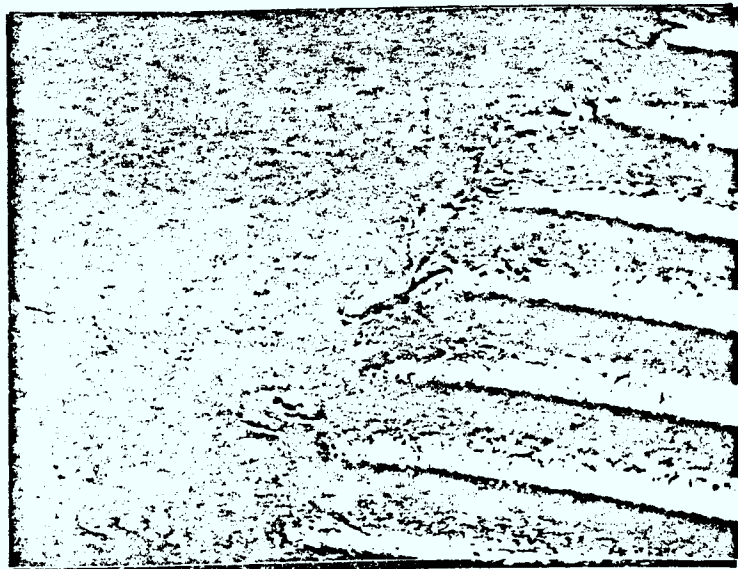
1. The polyurethane jacket from its physical characteristics appeared to be sound in areas that show no cracks. No chemical deterioration has taken place.
2. The jacket was physically weakened due to absorption of the flooding compound in some areas (of excess compound) making it incapable of withstanding normal environmental conditions.
3. The damage was due to faulty product and not due to mechanical abuse during installation.

5. Conclusions

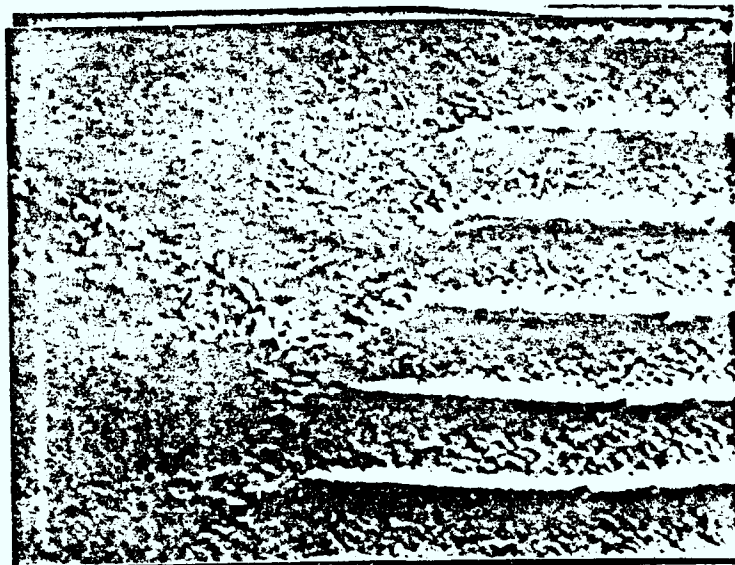
1. The failure (cracking) of the jacket was due to its physical deterioration as a result of non-homogeneity caused by excess flooding compound. Water will get under the jacket, and although the flooding compound is meant to protect the steel from corrosion, it is not possible to judge the effectiveness of this protection.
2. Analysis of these samples has shown that the cable jacket was faulty, and to the best of our knowledge, the cable jacket is not suitable for this application.



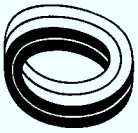
APPENDIX I



Cracked inner surface of cable
in service for 8 months. 10x



Damaged inner surface of cable
from stock. 10x



ATTACHMENT VIII

(REFERENCE: PART II - SECTION 2.3.4)

CONNECTOR LOSS HISTOGRAM DRAWINGS



FIGURE 1

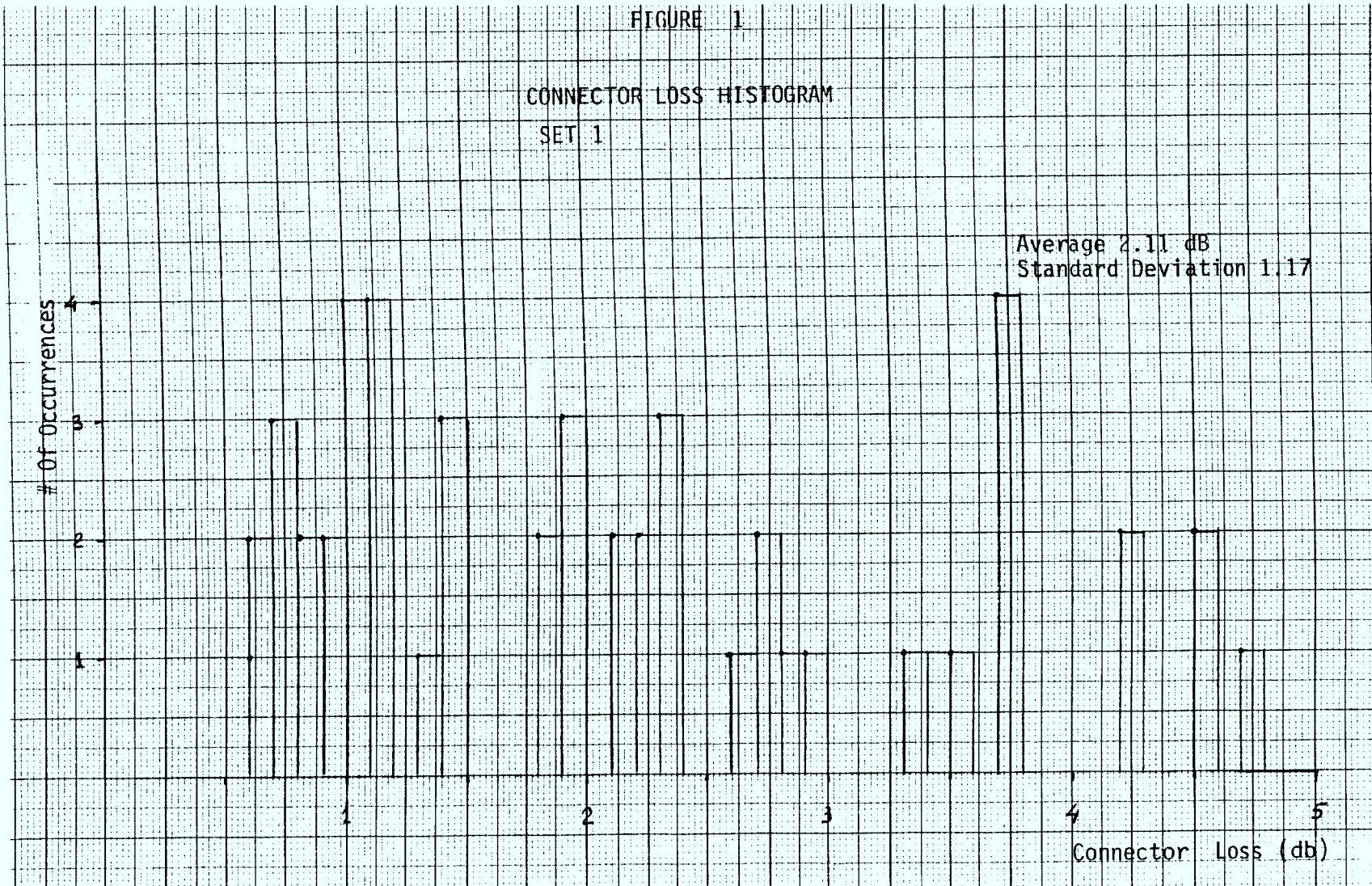
CONNECTOR LOSS HISTOGRAM

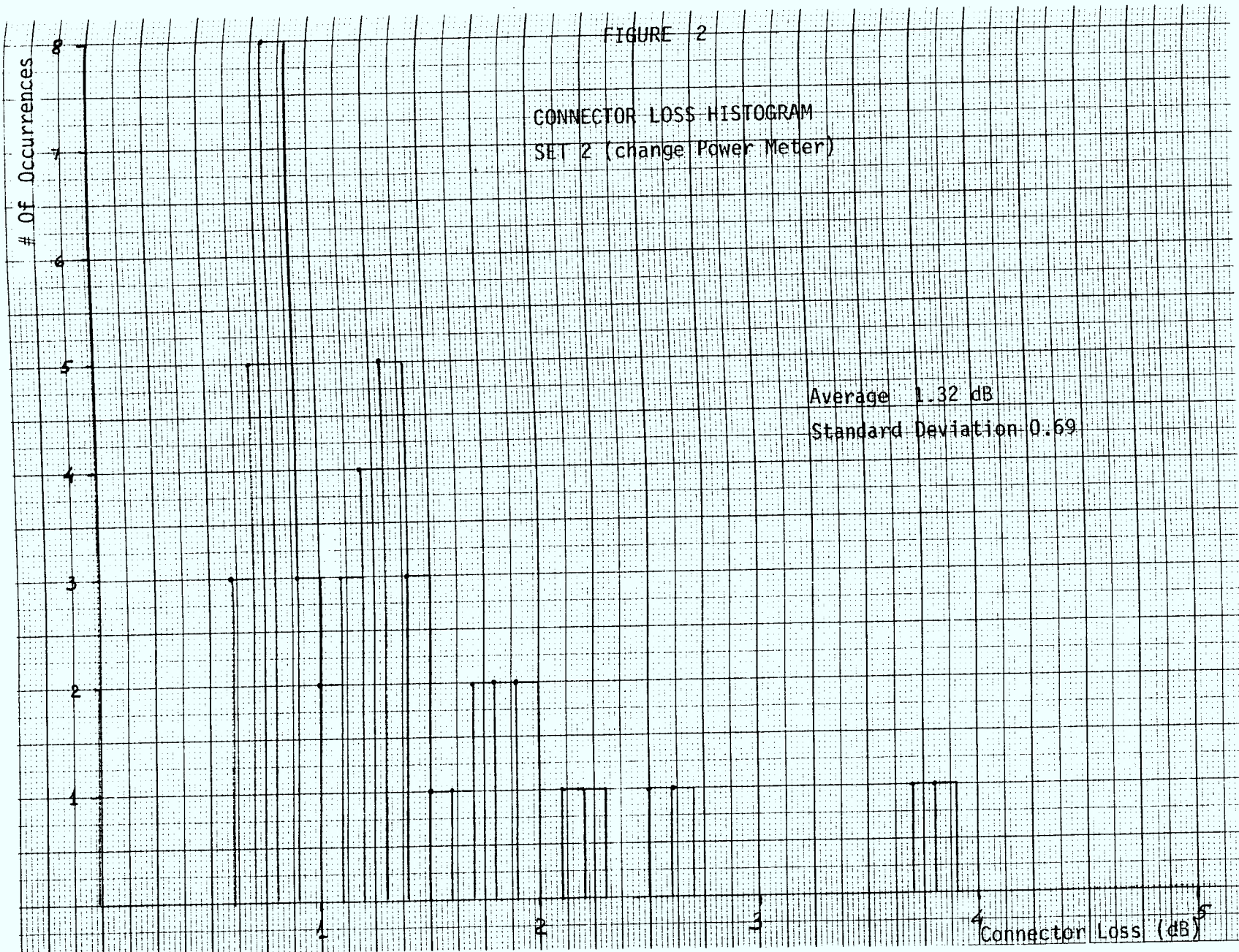
SET 1

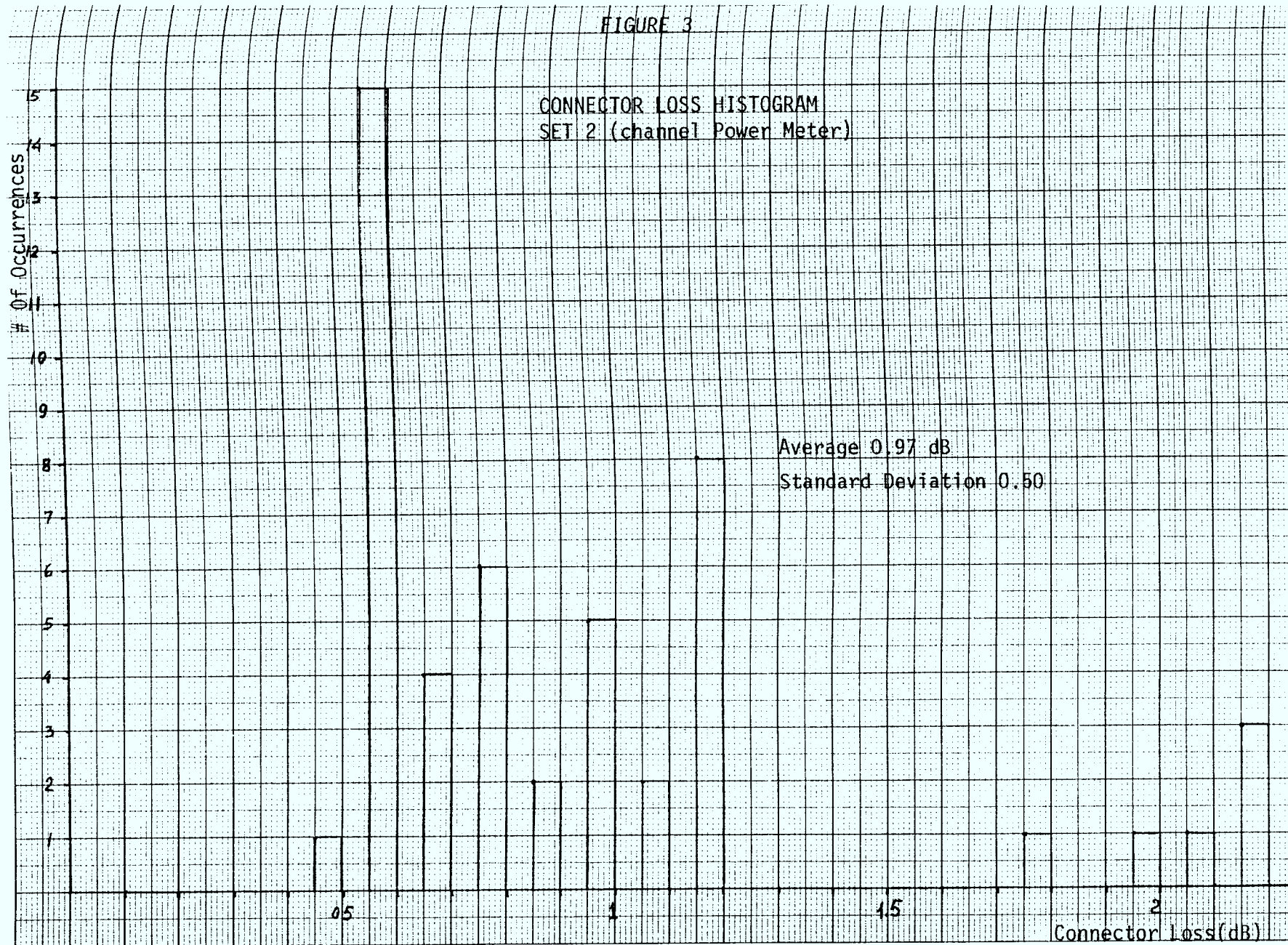
Average 2.11 dB
Standard Deviation 1.17

Of Occurrences

Connector Loss (db)







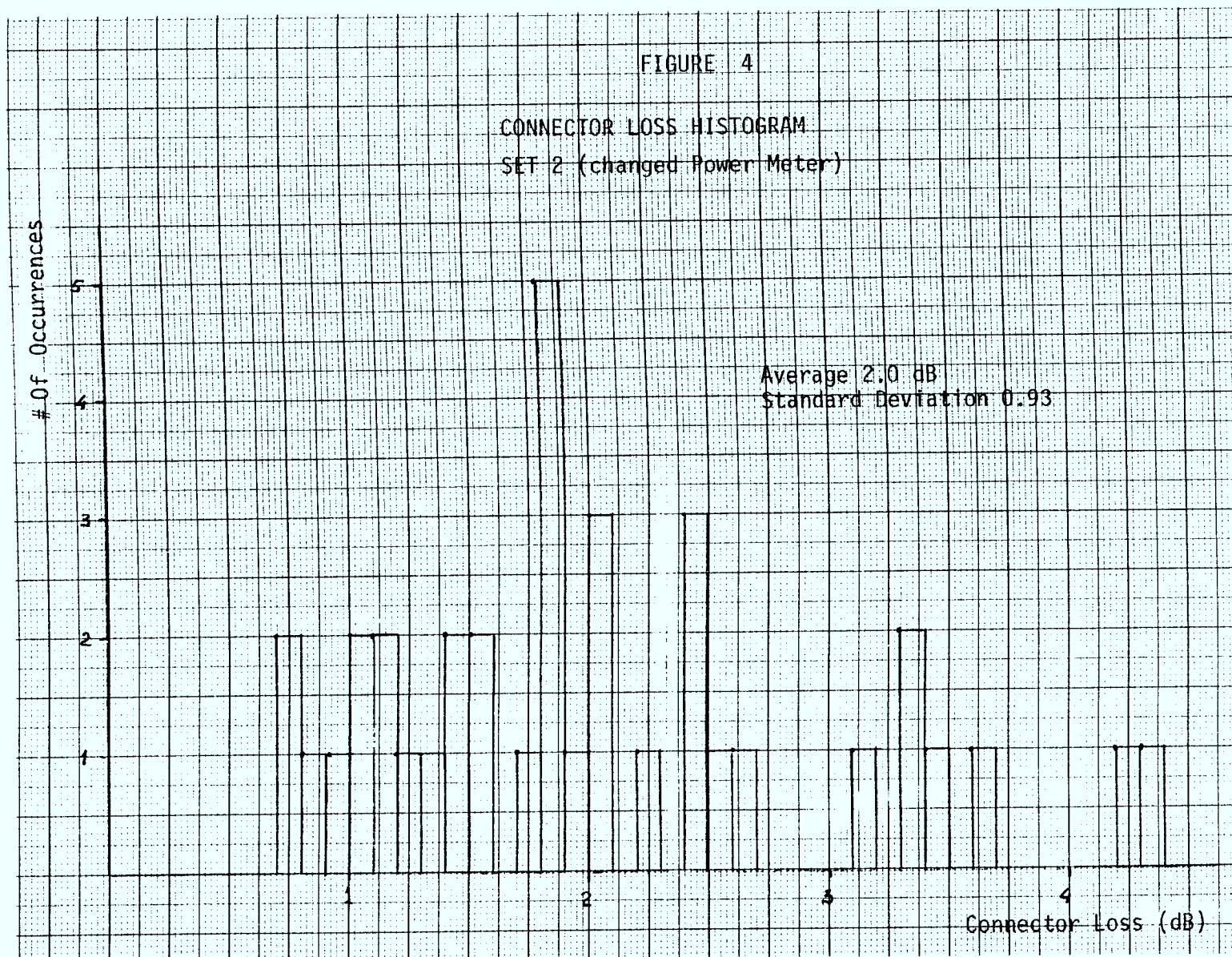
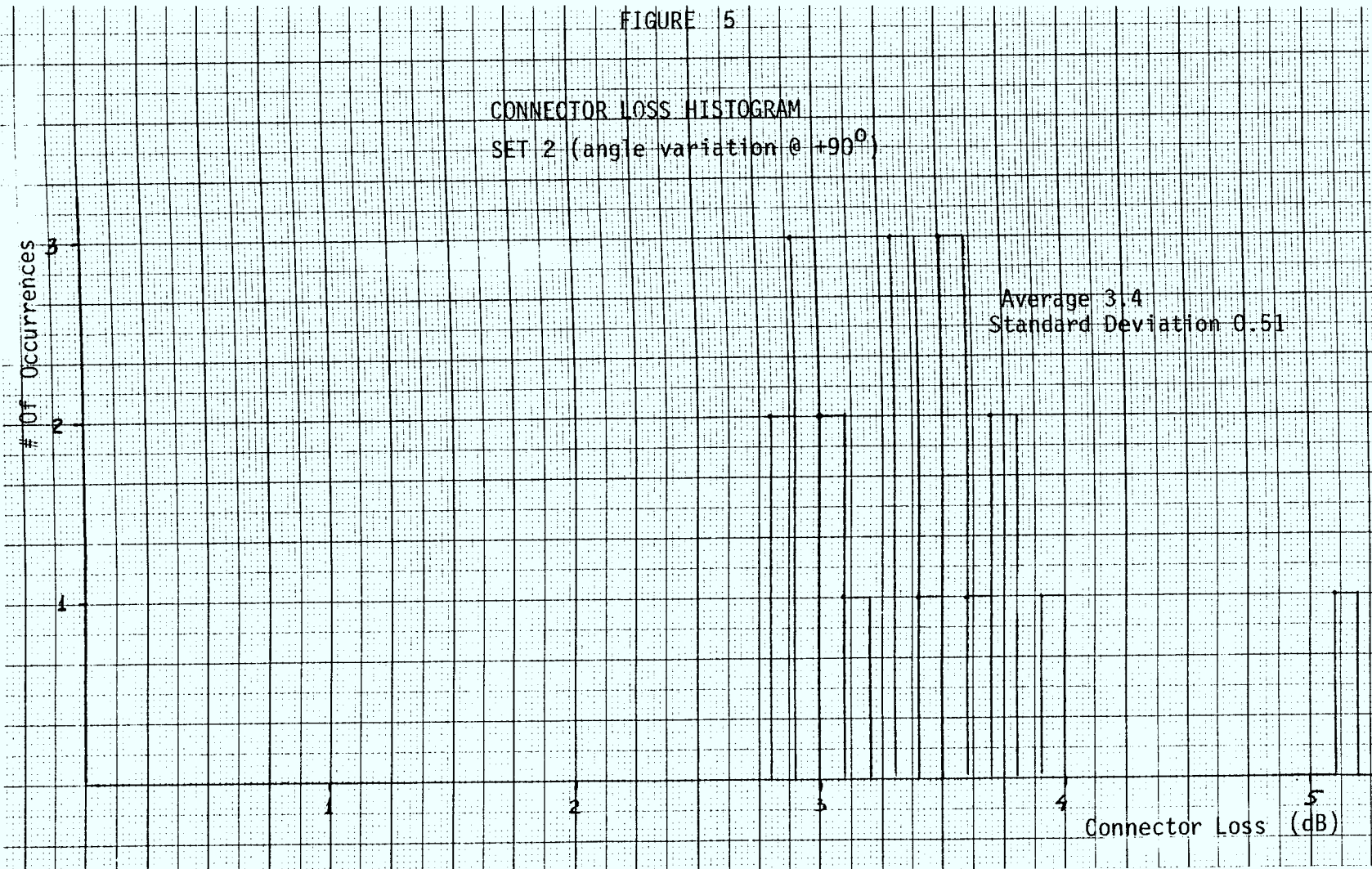
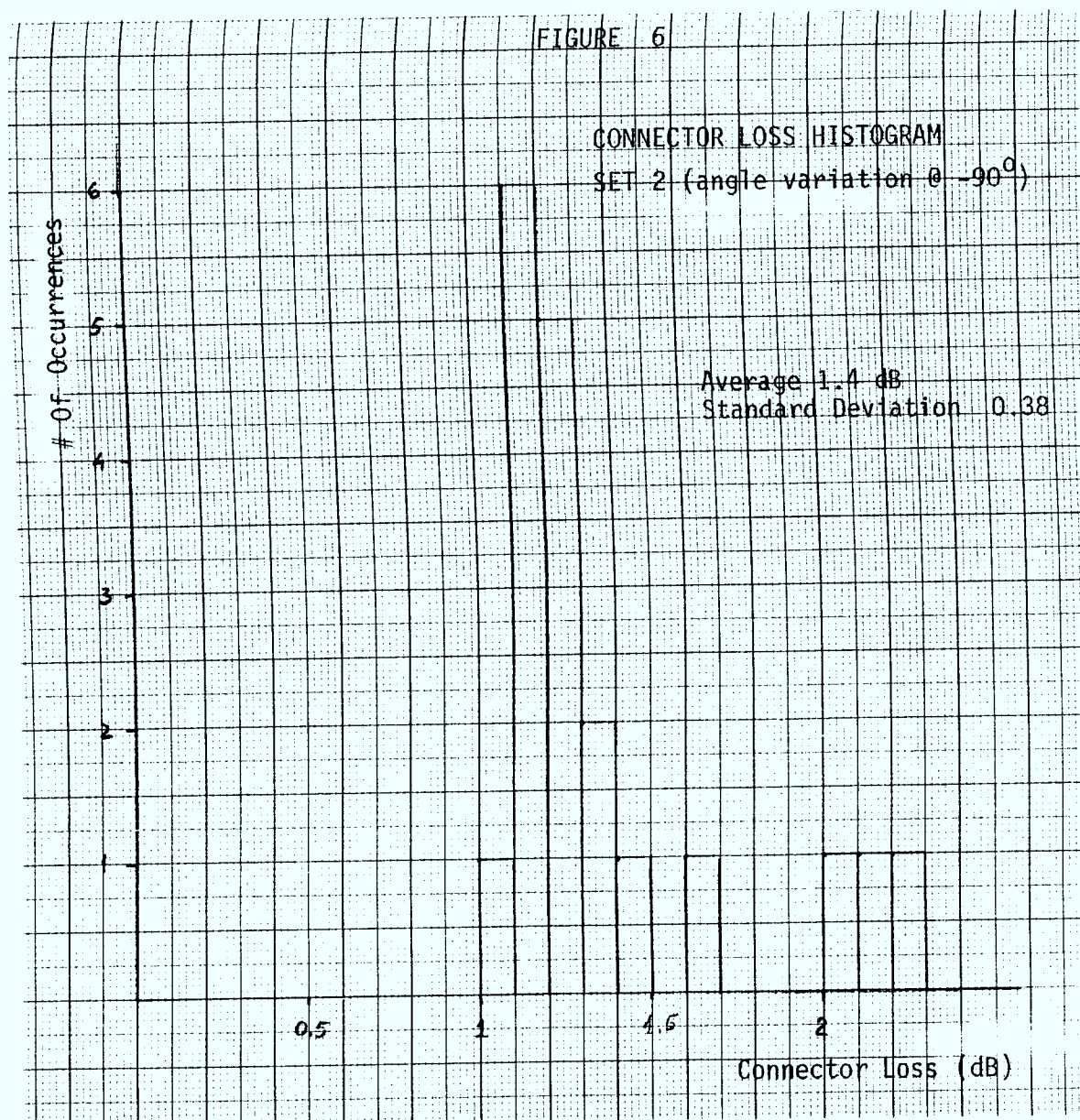




FIGURE 5





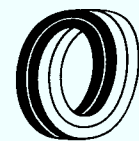
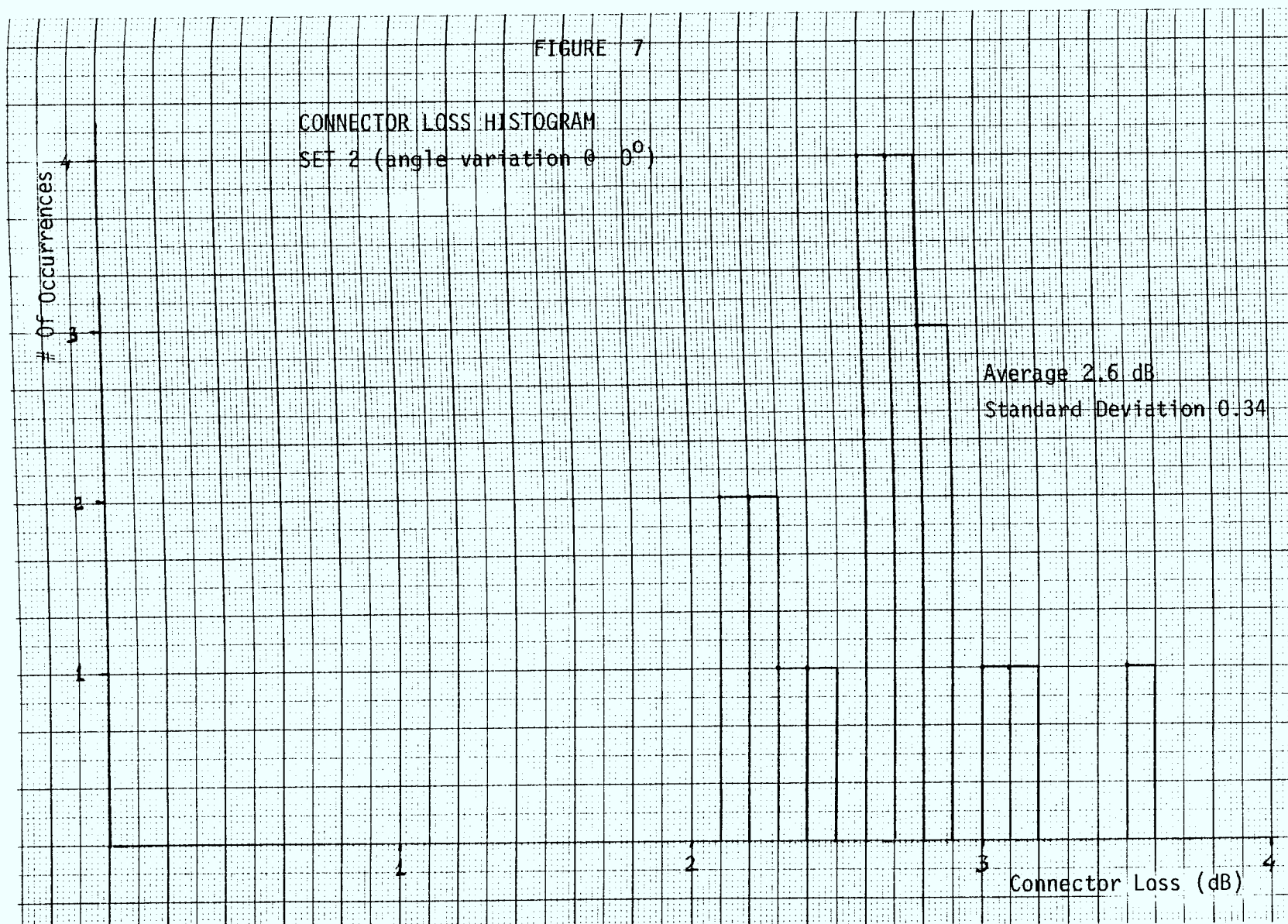
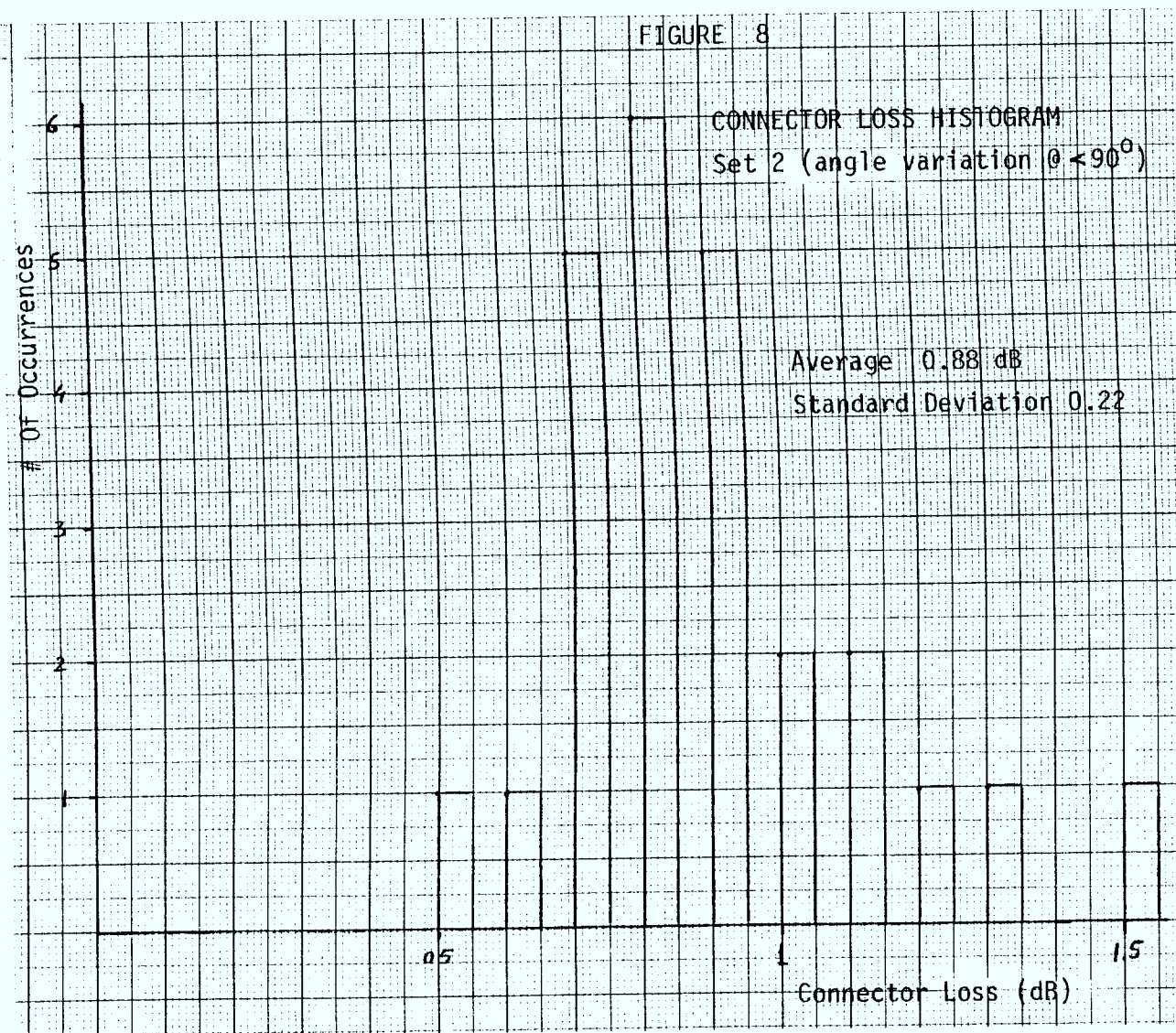
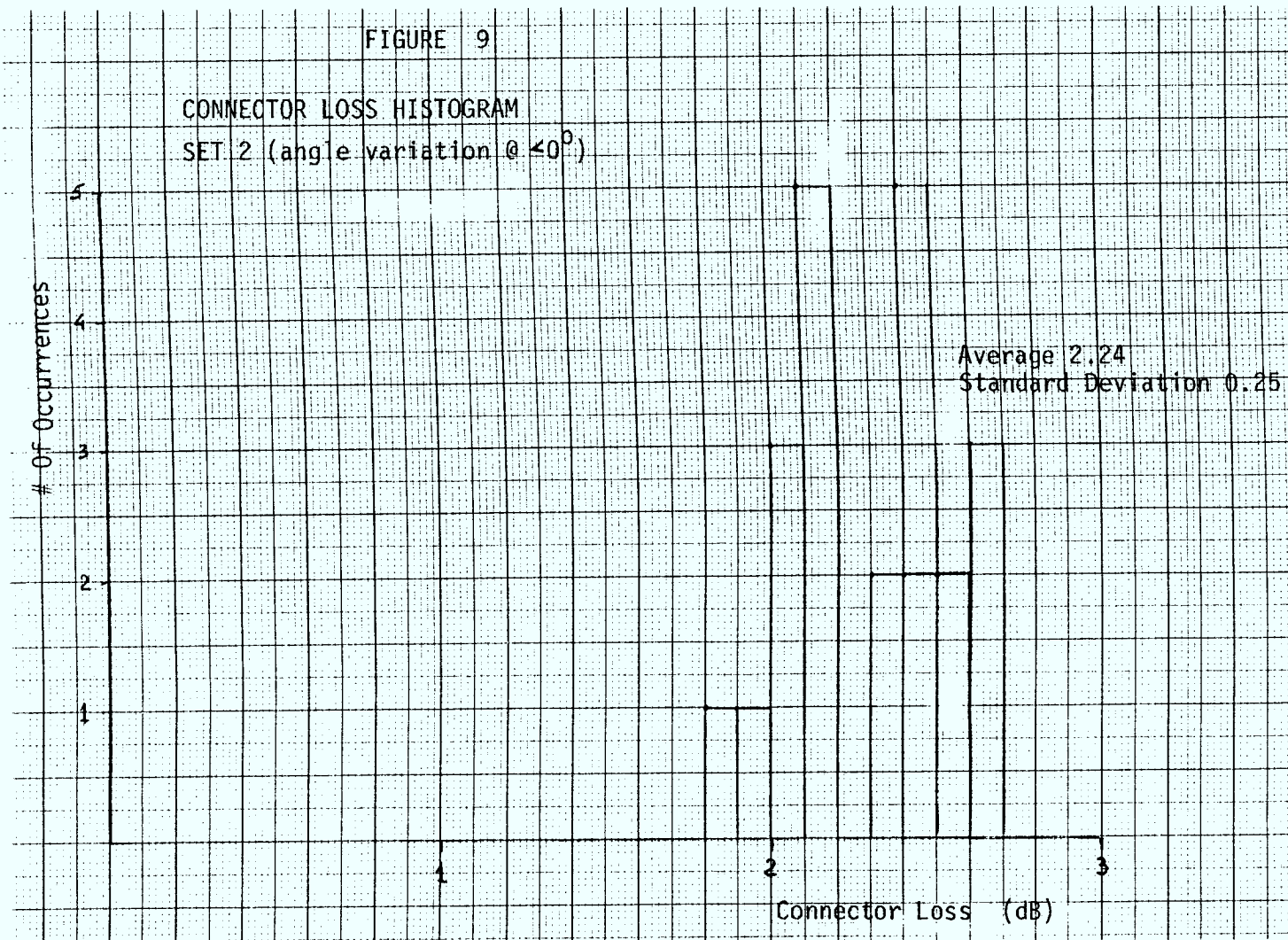


FIGURE 7









ATTACHMENT IX

(REFERENCE: PART II - SECTION 2.4.1)

BCN FIBRE OPTIC FIELD ACCEPTANCE
TESTING ACKNOWLEDGEMENT



BCN FIBER OPTIC FIELD ACCEPTANCE TESTING

PERFORMED BY: HARRIS CORPORATION OF BEHALF OF CANADA WIRE
AND CABLE

HELD ON: May 26 to June 5 1980

COMPLETED ON: June 10 1980

THIS IS TO ACKNOWLEDGE THAT THE FIELD ACCEPTANCE TESTING, AS PER
ATP-HFO-TP-4130001, AMENDED FOR FIELD ACCEPTANCE MAY 7, 1980 HAS
BEEN COMPLETED SATISFACTORILY AND THE COMMISSIONING PERIOD OF THE
BCN FIBER OPTIC SUPERTRUNK IS UNDERWAY AS OF THE ABOVE COMPLETION
DATE.

Donald L. Montello

BROADBAND COMMUNICATIONS NETWORK
(BCN)

DEPARTMENT OF SUPPLY AND SERVICES
DEPARTMENT OF COMMUNICATIONS
(DOC/DSS)

Ken Frank

CANSTAR COMMUNICATIONS



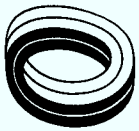
3.0 TEST RESULTS

Test result comparisons of the system performance are based on results obtained in London during field acceptance testing completed on June 10, 1980.

The system level tests performed consisted of the functional capability of the fibre optic system to transmit baseband, vestigial sideband and FM stereo signals as well as meet the specifications described below as the performance targets.

The functional capability of the system was a qualitative judgement verifying subjectively video and audio transmission quality and that all intended features of the system such as the LTMU are operative.

The functional capability of each of the six fibre optic links was determined acceptable. The equipment test results meeting the specification parameters are described in Section 3.1. Cable performances are described in Section 3.2. Simulation of long haul transmission by looping through the receiver-transmitter at the terminal ends was only superficially evaluated.



3.1 PERFORMANCE TARGETS vs PERFORMANCE RESULTS

The performance targets vs the actual results obtained during acceptance testing is compared in Table 3.1.1. It should be noted, however that the transmit test signal originated at the Hub End and was looped back at baseband level at the Head End for retransmission over a return fibre optic channel for measurement recording back at the Hub. VSB measurements were performed under identical circumstances. This is illustrated in Figure 3.1.1.

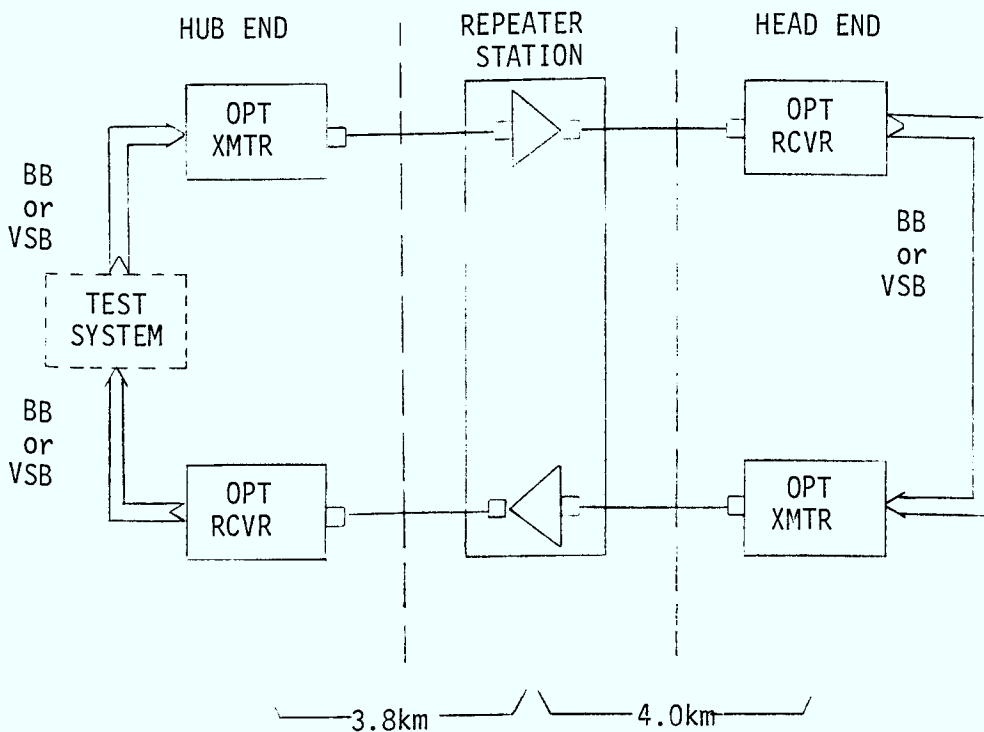


Figure 3.1.1 TEST CONFIGURATION



TABLE 3.1.1: PERFORMANCE TARGETS vs PERFORMANCE RESULTS

Test #	Parameter	Performance Target	Performance Results
<u>A. Video System</u>			
1	B.B. Video: S/N (unweighted peak white-to-blanking to RMS noise)	46 dB	52 dB
2	B.B. Video: Channel Intermodulation Products	61 dB	70 dB or better
3	B.B. Video: Spurious Signal	57 dB	70 dB
4	B.B. Video: HUM (Signal to Hum p-p)	45 dB	unobservable due to so little hum.
5	B.B. Video: Differential Gain	± 1 dB	9% or 0.74 dB
6	B.B. Video: Differential Phase	$\pm 3^\circ$	$\pm 3^\circ$
7	B.B. Video: Far End Cross View Ratio	63 dB	Not Tested
8	B.B. Video: Chrominance Delay (flat)	50 nS	Not Tested
9	B.B. Video: Echo Distortion (0-5 μ S)	32 dB	Not Tested
10	B.B. Video: Echo Distortion 10 μ S)	39 dB	Not Tested
11	B.B. Audio: S/N (Peak audio to RMS noise in 15 khz)	52 dB	54 dB
12	B.B. Audio: Channel Intermodulation & Spurious Signals	50 dB	Better than 65 dB
13	B.B. Audio: Frequency Response (≤ 50 Hz- ≥ 15 khz)	± 3 dB	≤ 1 dB (60 Hz to ≈ 19 khz) External tmfr problem obstructed results down to 50 Hz.
14	B.B. Audio: Two-Tone Intermod	52 dB	66 dB
15	VSF Video: C/N (Carrier to noise ratio- 100 khz B.W.)	45 dB (modified from 52 dB)	48 dB
16	VSF Video: Spurious Signals (30 khz B.W.)	50 dB	52 dB



TABLE 3.1.1 (cont'd)

Test #	Parameter	Performance Target	Performance Results
A. <u>Video System</u> (cont'd)			
17	VSBS Video: Channel Intermodulation Products	45 dB (modified from 50dB)	52 dB
18	VSBS Video: Three Tone Intermod Test	Within W-Curve from B.P.-23	Within W-Curve from B.P.-23
19	VSBS Video: Return Loss	Input: 20 dB Output: 20 dB	Input: 20 dB Output: 24 dB
20	FM Stereo over VSBS Channel: C/N (RMS carrier to RMS Noise in 200 khz)	52 dB	52 dB
21	FM Stereo over VSBS Channel: Channel Intermod and Spurious Noise Signal	50dB @ 10.7Mhz ± 0.5 Mhz 40dB @ 5-100 Mhz	44 dB worst case
B. <u>Optical System</u>			
1	Optical Transmit Output Power	0 dBm average	Adjusted between -2 dBm -0 dBm to reduce modal noise influence
2	Unallocated Link Margin	6-10 dB	1 dB (due to change in configuration- one fiber channel is marginless)
3	Reliability (all channels fail-MTBF)	8800 hours	Unacceptable
4	Mean Time to Repair (travel not included)	0.5 hours	Inconclusive
5	Reliability (per channel - MTBF)	17000 hours	Unacceptable
6	Mean Time To Repair (travel not included)	1 hours	45-90 minutes
7	Bit Error Rate	10 ⁻⁹	Varied between 10 ⁻⁴ and 10 ⁻⁷



TABLE 3.1.1 (cont'd)

Test #	Parameter	Performance Target	Performance Results
<u>C. Cable</u>			
1	Number of Fibers	8	8
2	Number of Channels	6 (minimum)	6
3	Cable Attenuation	8 dB/km	6.5 dB/km average
4	Cable Bandwidth	600 Mhz-km	500 Mhz-km average
5	Max. Cable Tensile Load	2900 Kg(self-supporting)	Not Tested
		230 kg (lashed)	Not Tested
6	Operating Temperature Range	-40°C to +50°C	refer to Section 3.2
7	Driving Rain with 80km/hour wind	30 mm/hour	{ To date installed fibre optic cable is withstanding London, Ontario's climatic environment.
8	Freezing Rain at 80/km hour wind	30 mm radial ice	
9	Maximum Wind at 10 meters above ground	150 km/hour	

Chart recordings of several of the tests performed are illustrated in Figures 3.1.2 to 3.1.16.

To summarize, baseband performance results met performance targets with the exception of reliability. VSB met performance targets as well, again with the exception of reliability and of the carrier to noise ratio which was marginally acceptable. An 8-bit encoder was used for the VSB system. A 9-bit encoder is required to meet the C/N performance target.



TABLE 3.1.1 (cont'd)

Discrete third order performance was originally compliant with the specification. A change in the down converter/up converter local oscillator frequency would be required to meet this specification.

FM performance results met the required targets.

The system bit error rate did not perform to the 10^{-9} requirement but fluctuated between $< 10^{-4}$ and 10^{-7} .

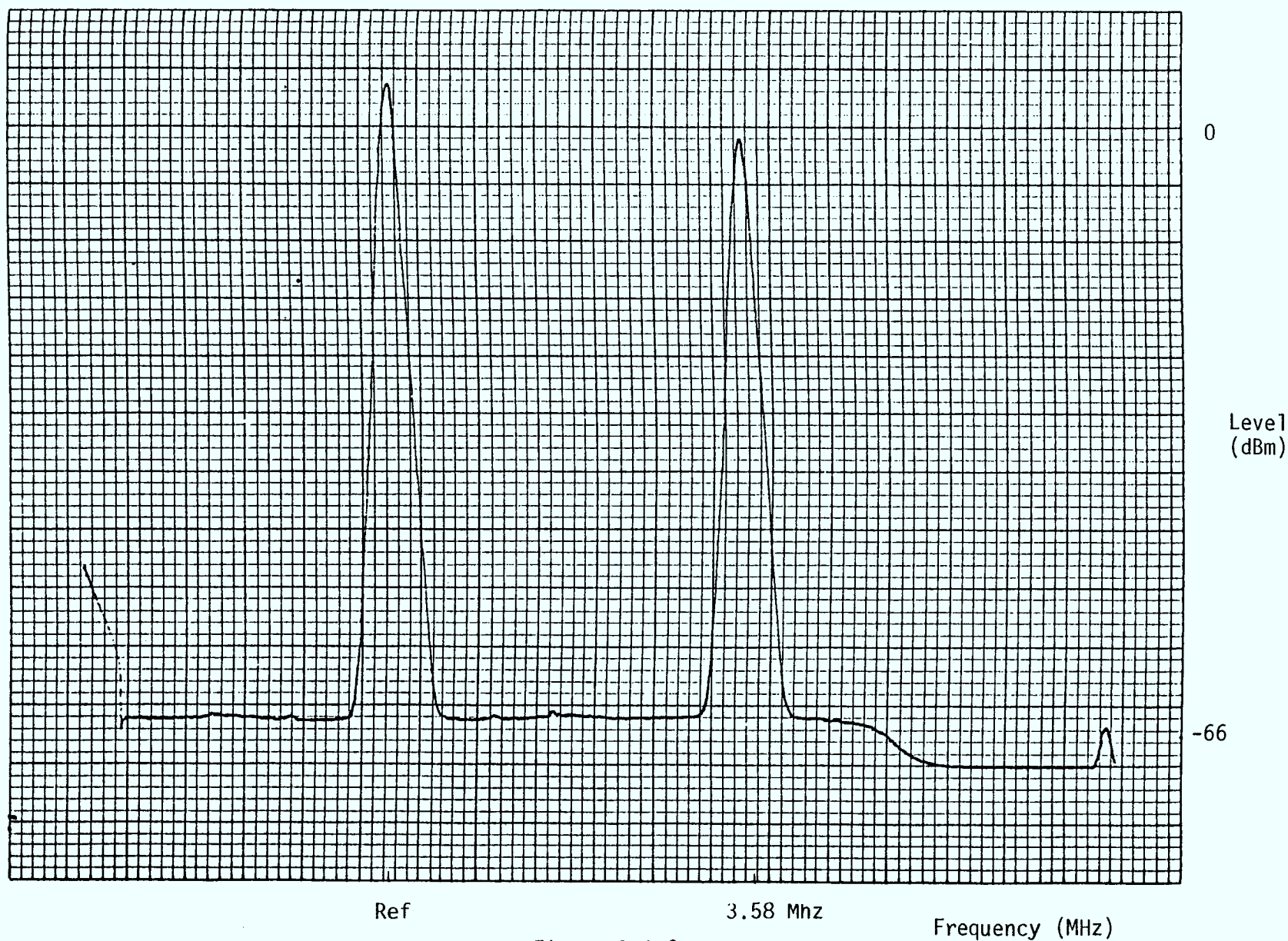
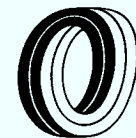


Figure 3.1.2
BASEBAND S/N ON FIBRE # 1 CHANNEL C

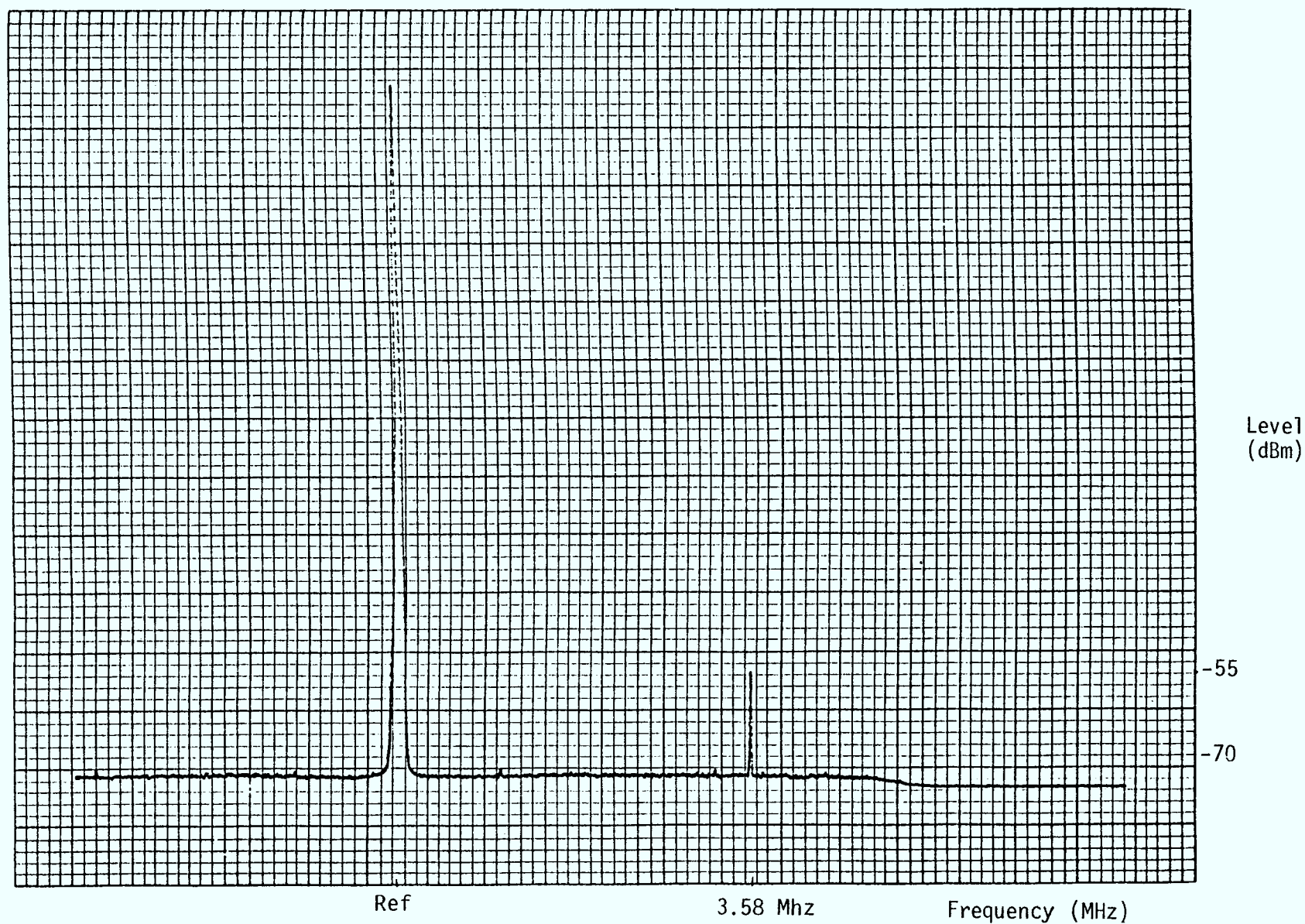


Figure 3.1.3
BASEBAND SPURIOUS NOISE ON FIBRE #1 CHANNEL C

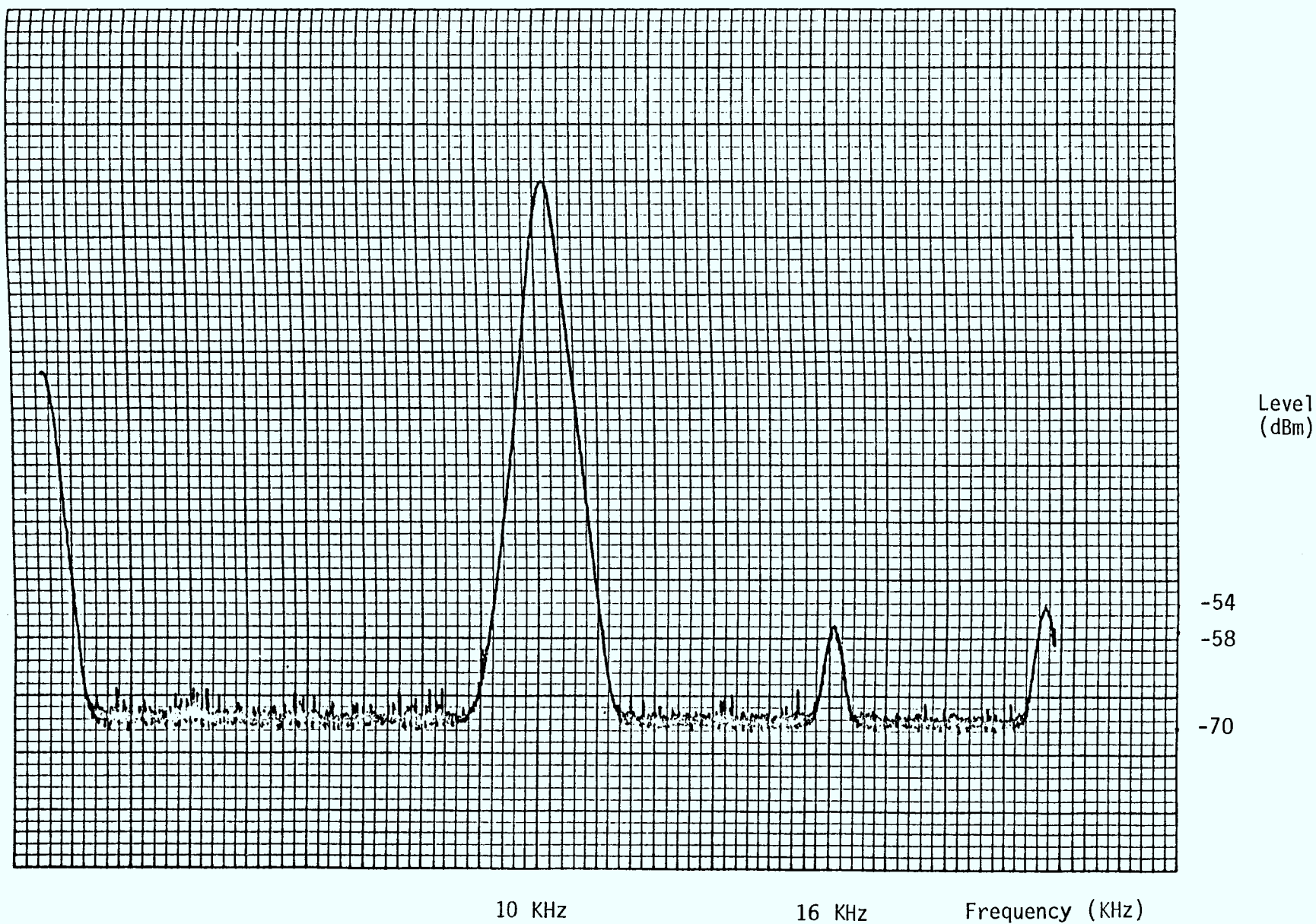
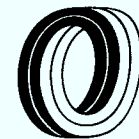


Figure 3.1.4
BASEBAND AUDIO S/N

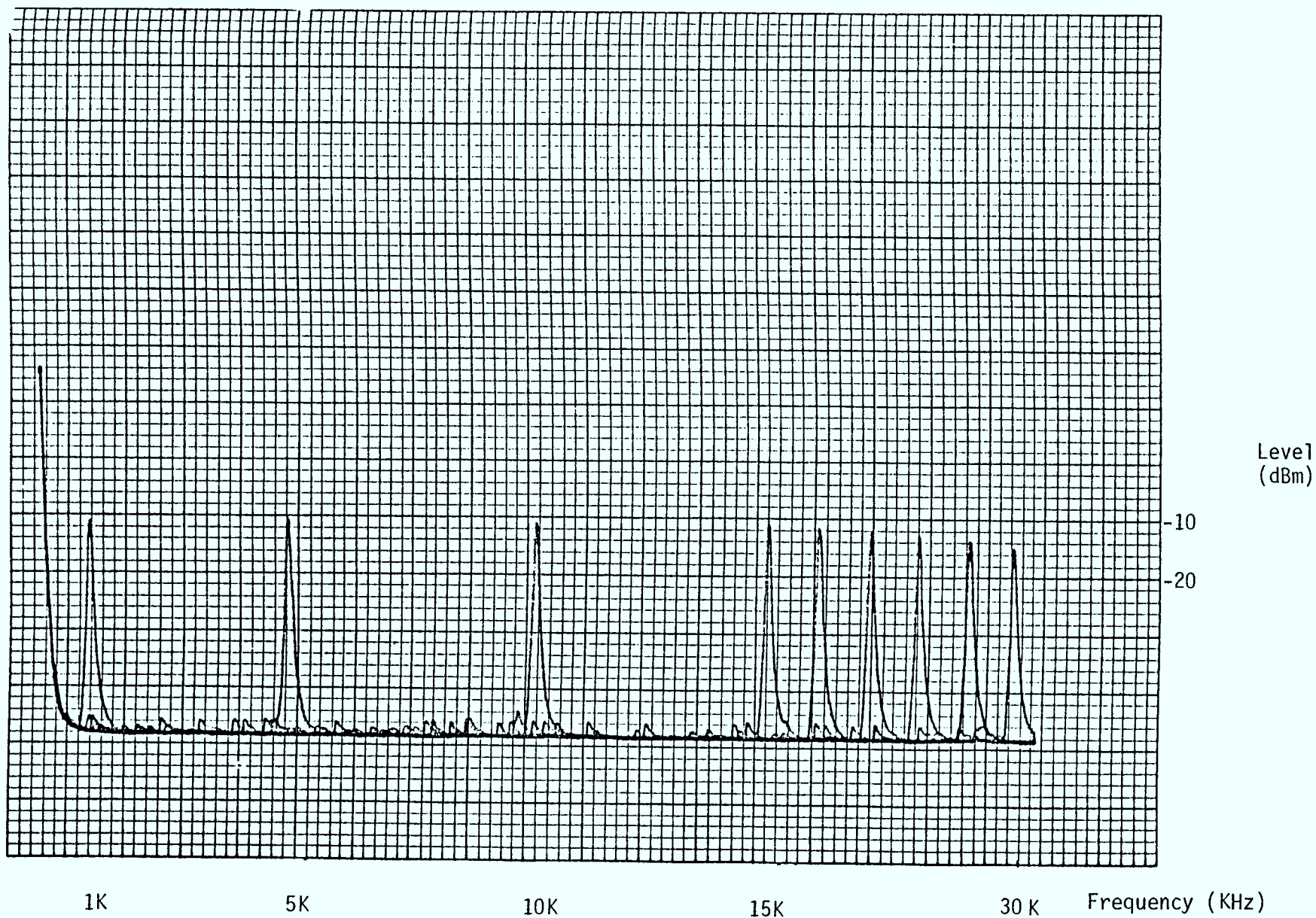
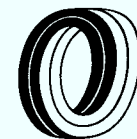


Figure 3.1.5
BASEBAND AUDIO FREQUENCY RESPONSE

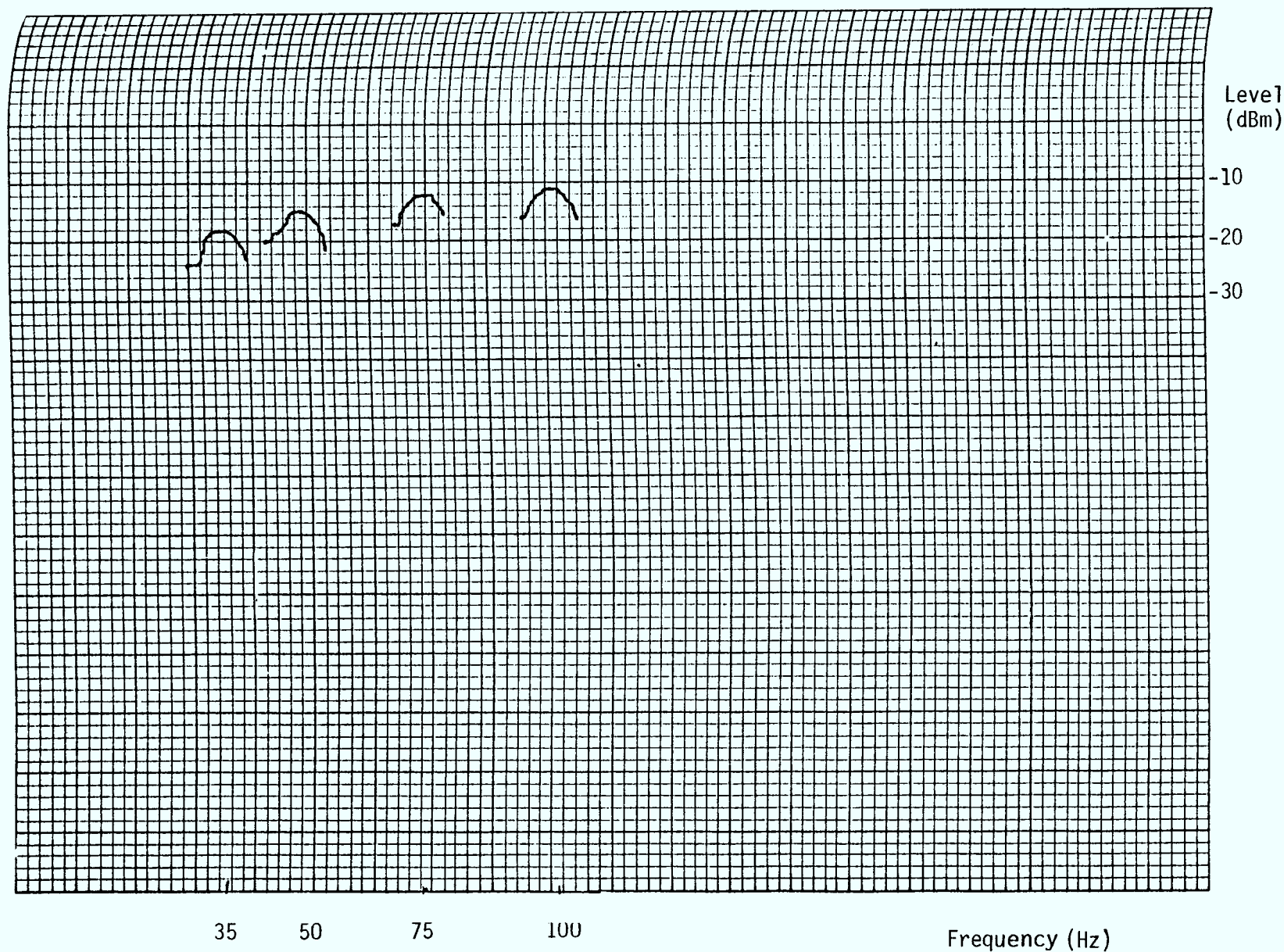
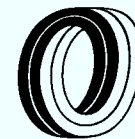


Figure 3.1.6
BASEBAND AUDIO FREQUENCY RESPONSE BELOW 1 KC

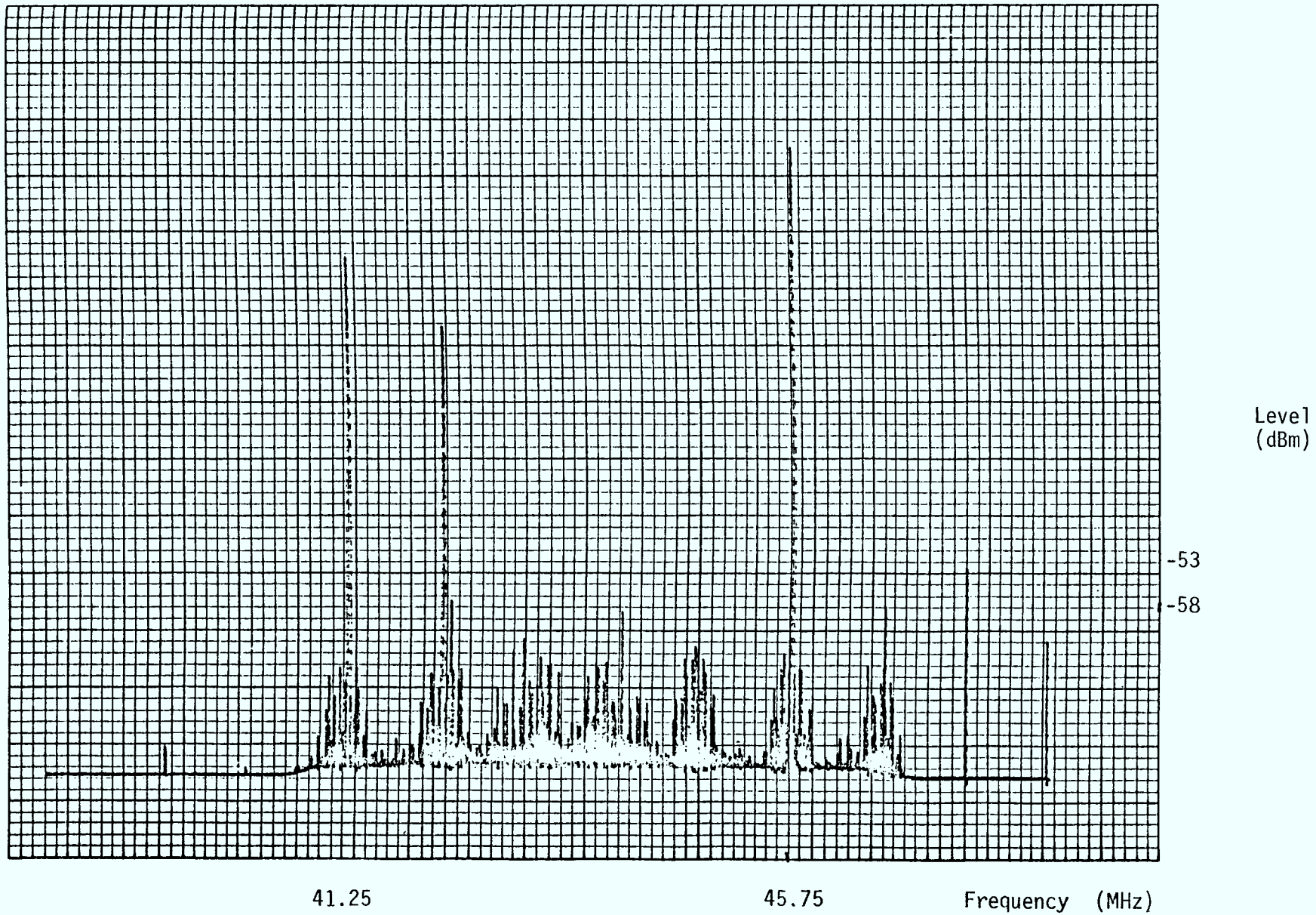


Figure 3.1.7
VSB SPURIOUS NOISE AND INTERMODULATION PRODUCTS : FIBRE #3A

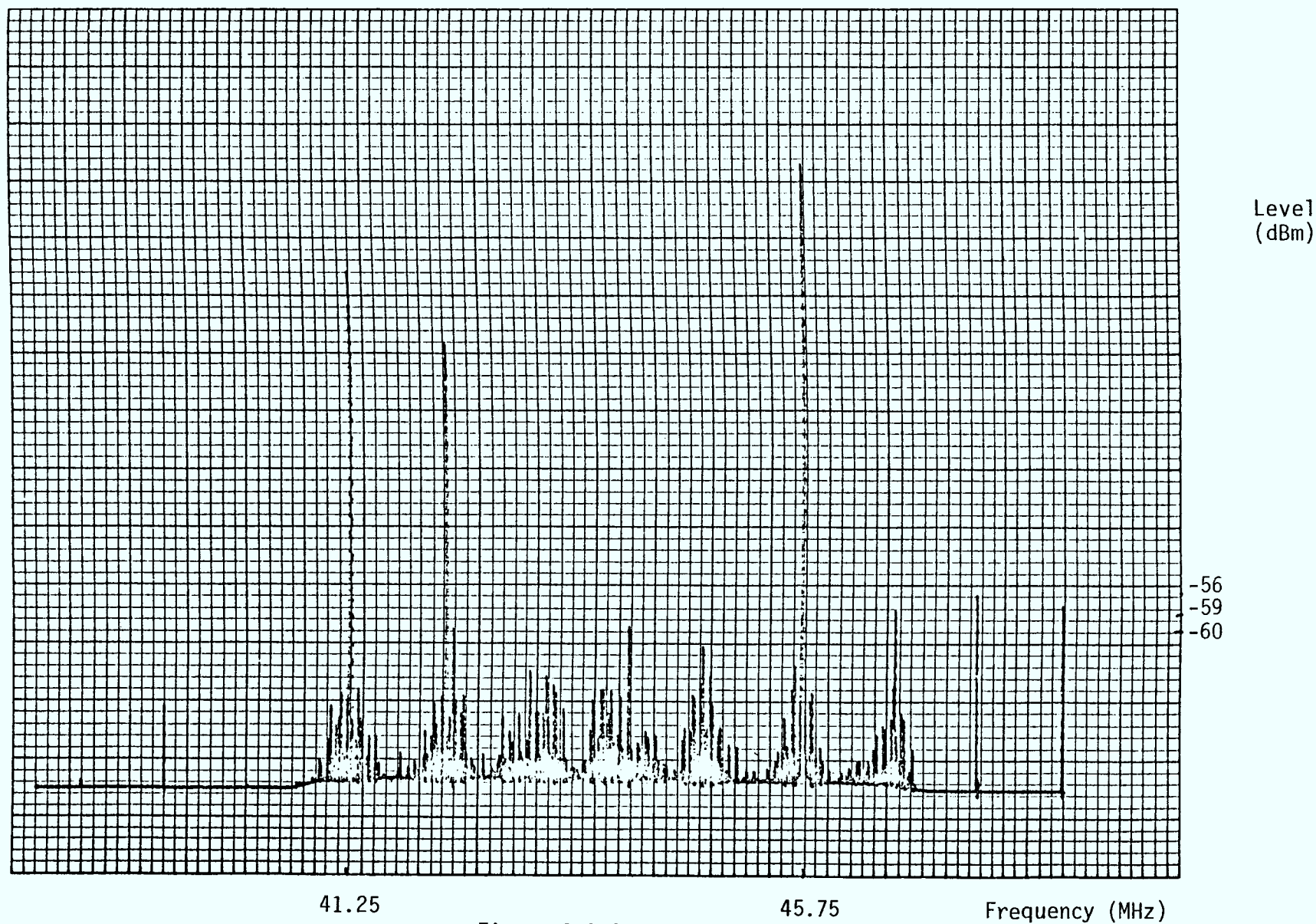
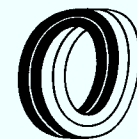


Figure 3.1.8
VSB SPURIOUS NOISE AND INTERMODULATION PRODUCTS : FIBRE #4A

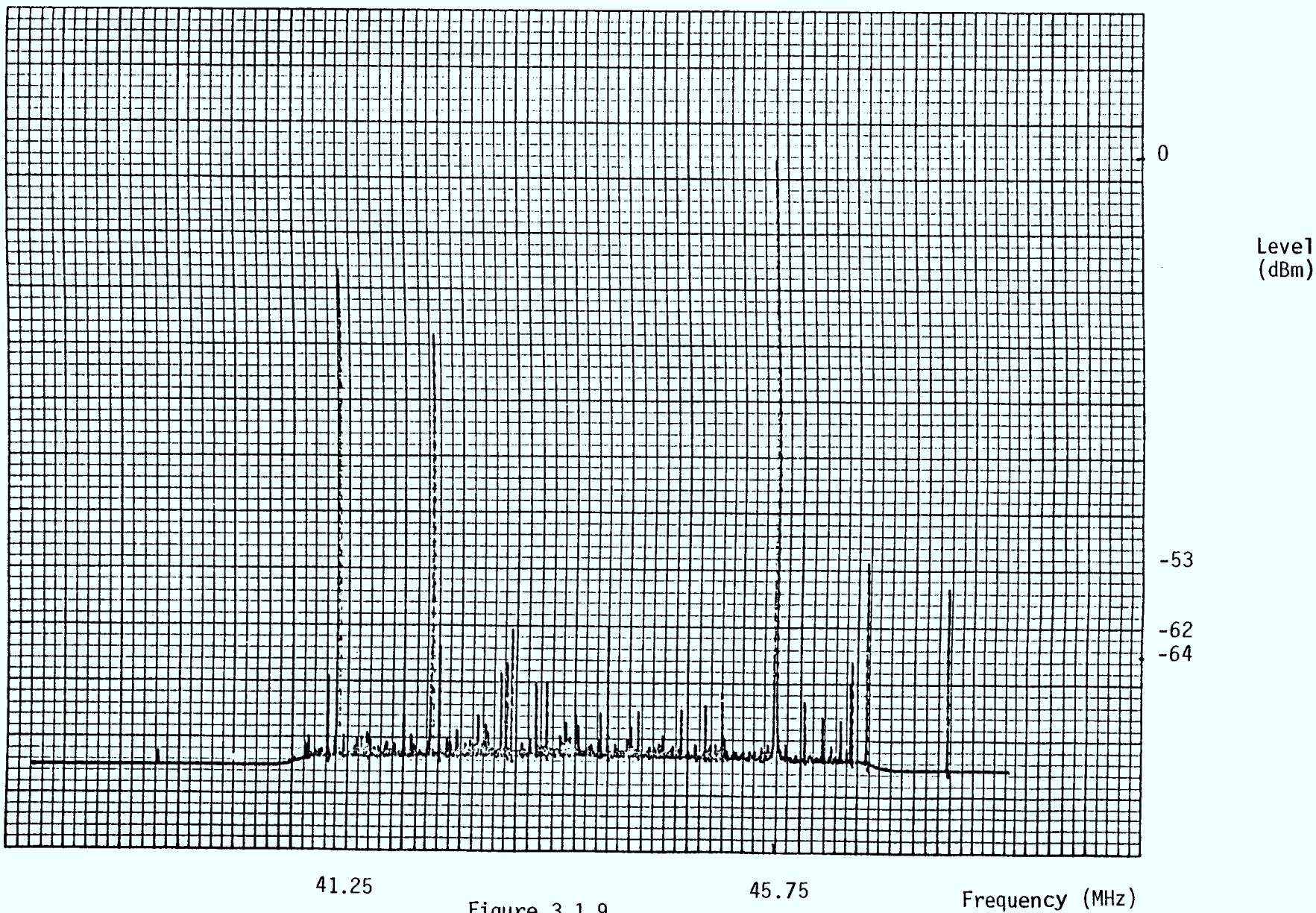
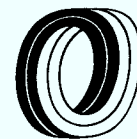


Figure 3.1.9
VSB SPURIOUS NOISE AND INTERMODULATION PRODUCTS : FIBRE #4B

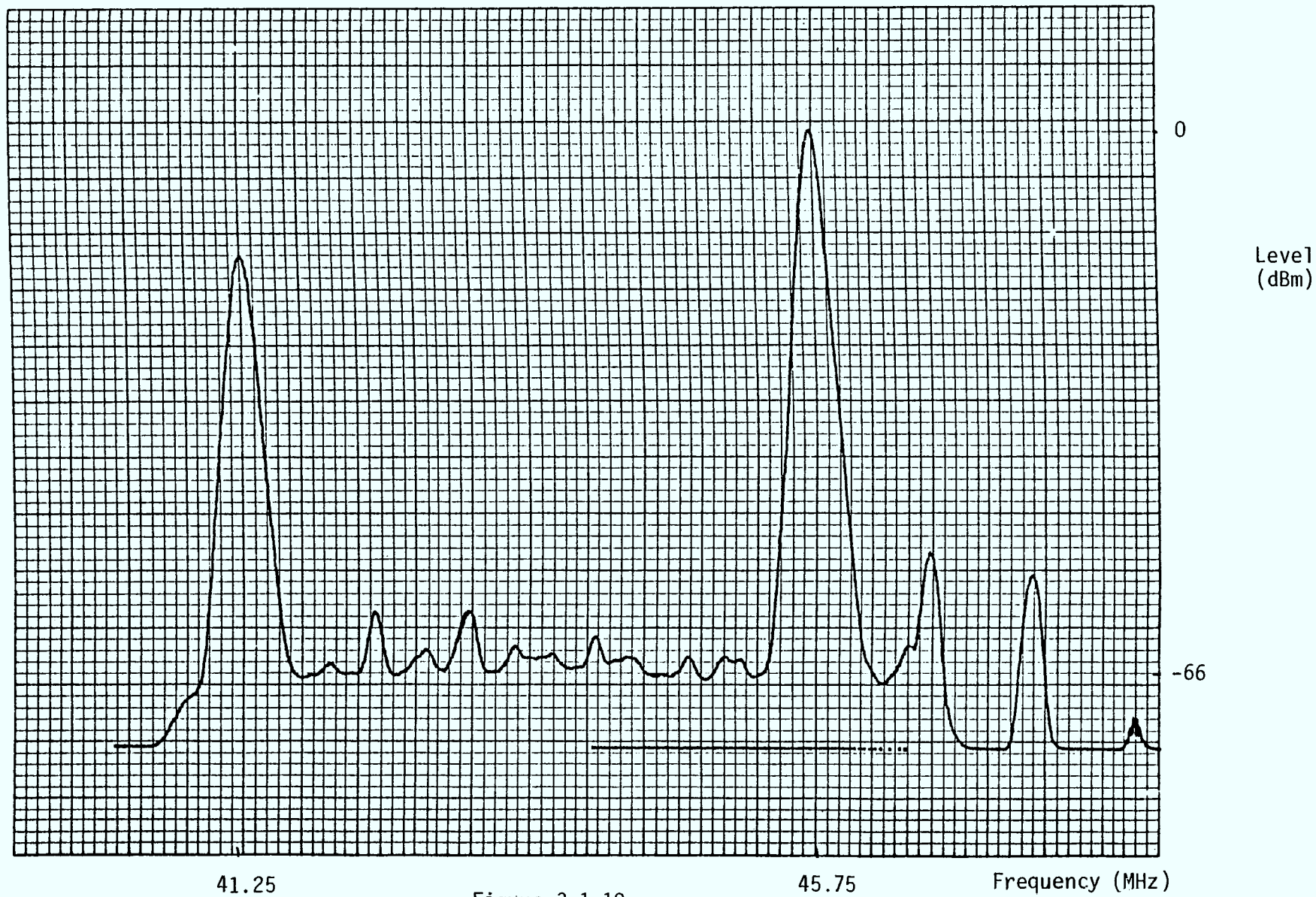


Figure 3.1.10
VSB S/N RATIO

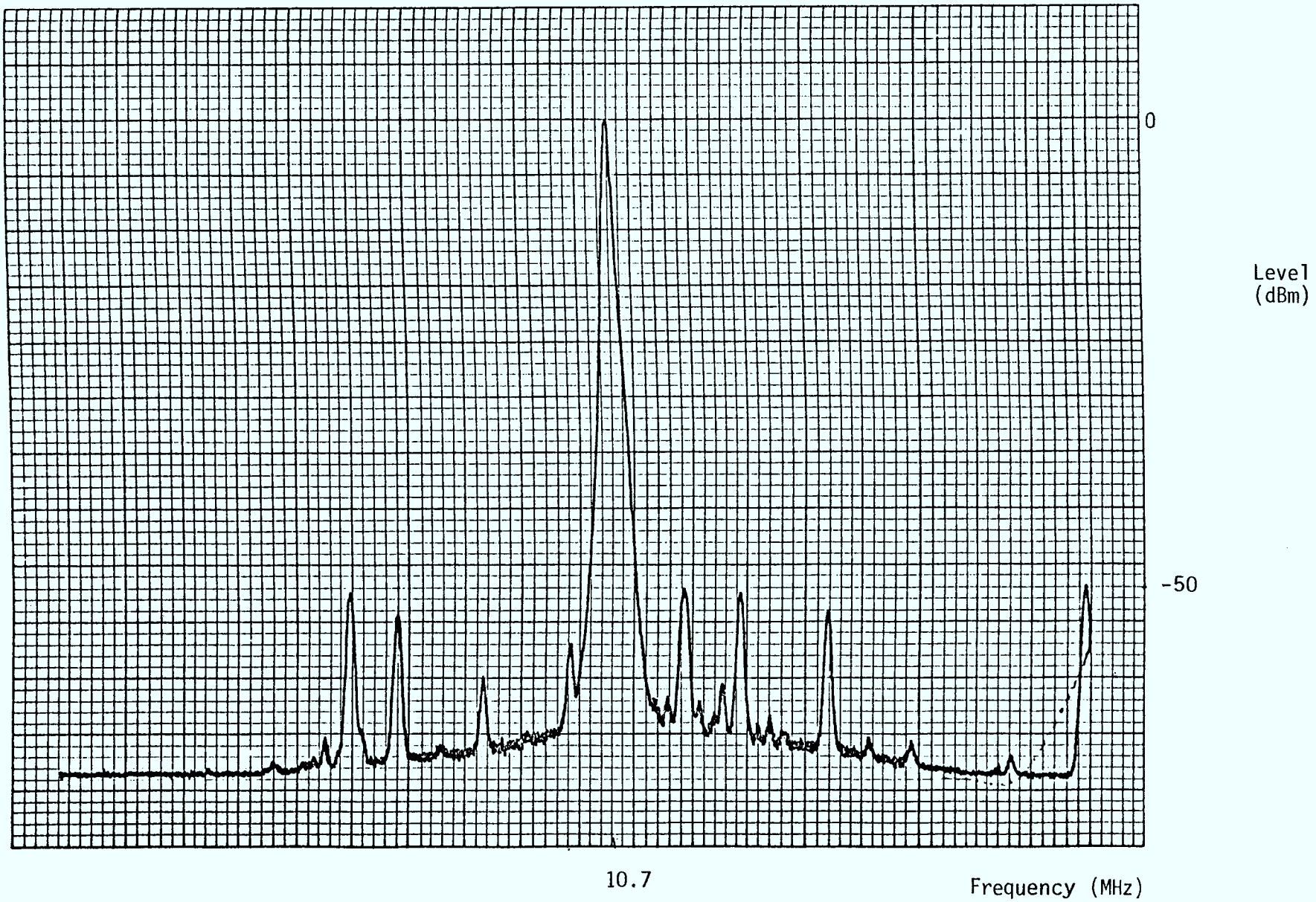


Figure 3.1.11
FM CHANNEL C/N RATIO (OVER BB #1)

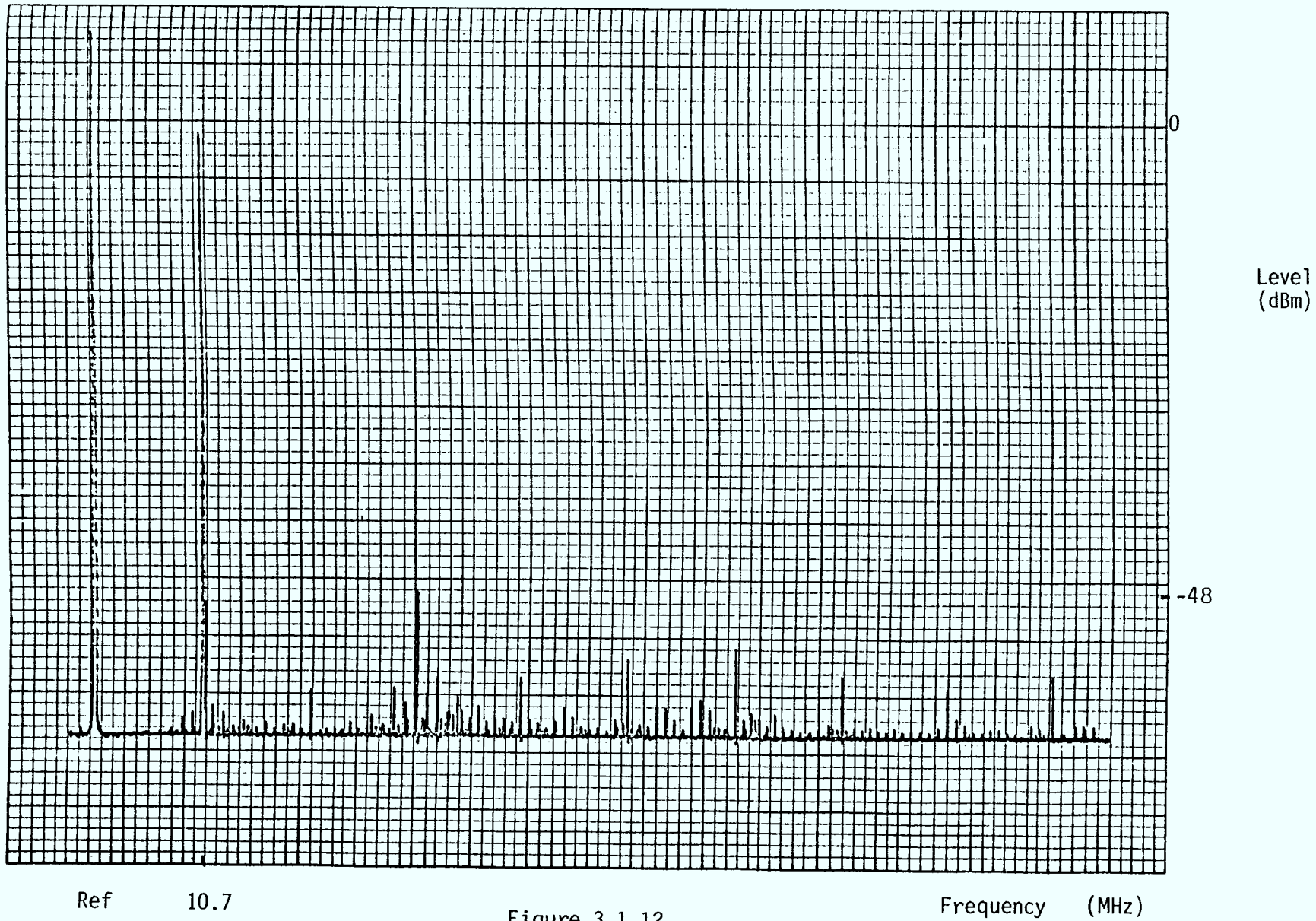


Figure 3.1.12
FM CHANNEL INTERMODULATION AND SPURIOUS SIGNALS (OVER BB #2)

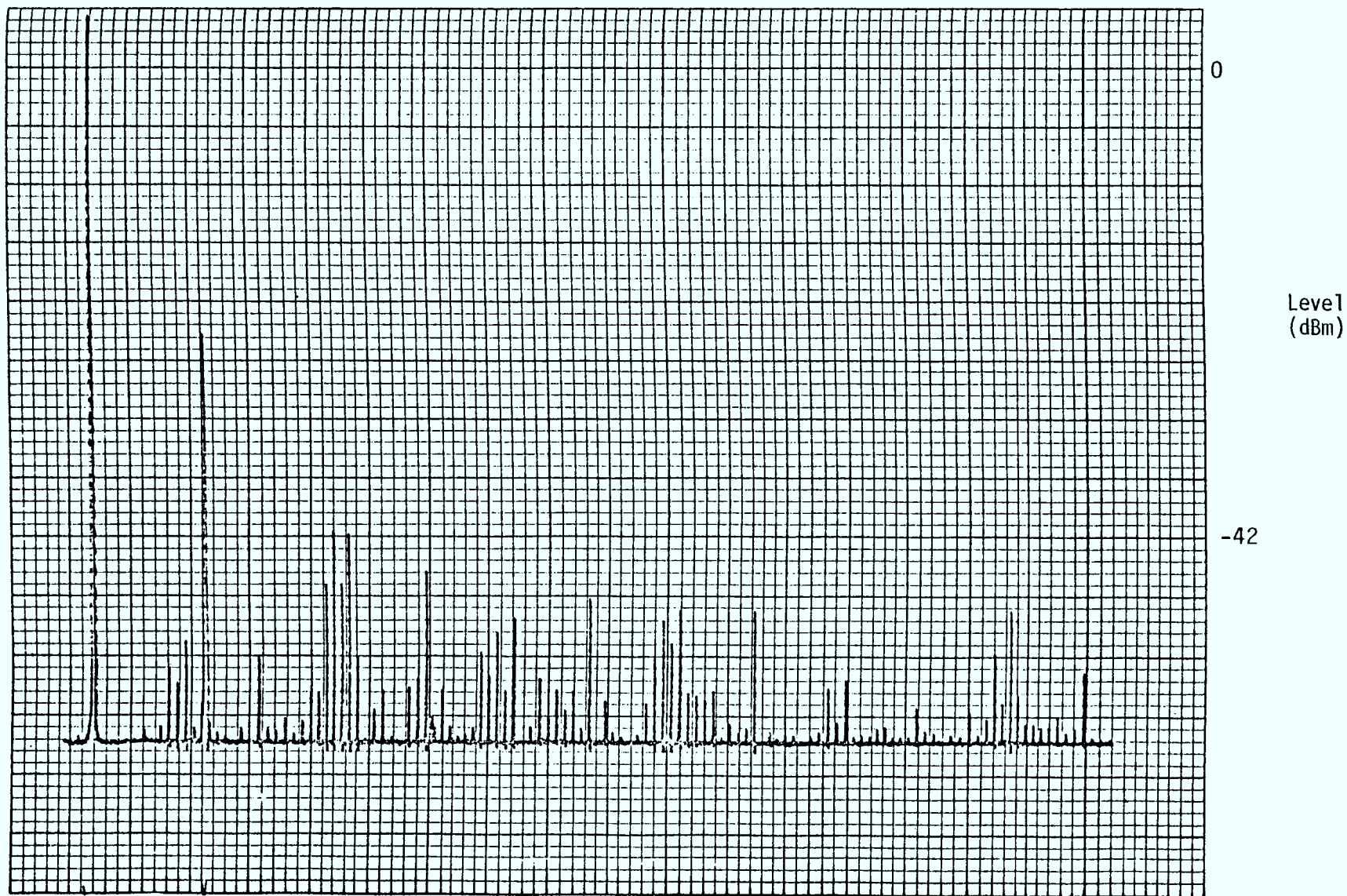


Figure 3.1.13

10.7

Frequency (MHz)

FM CHANNEL C/N RATIO (VSB #2)



Ref 10.7

Frequency (MHz)

Figure 3.1.14

FM CHANNEL INTERMODULATION AND SPURIOUS SIGNALS (OVER VSB #2)

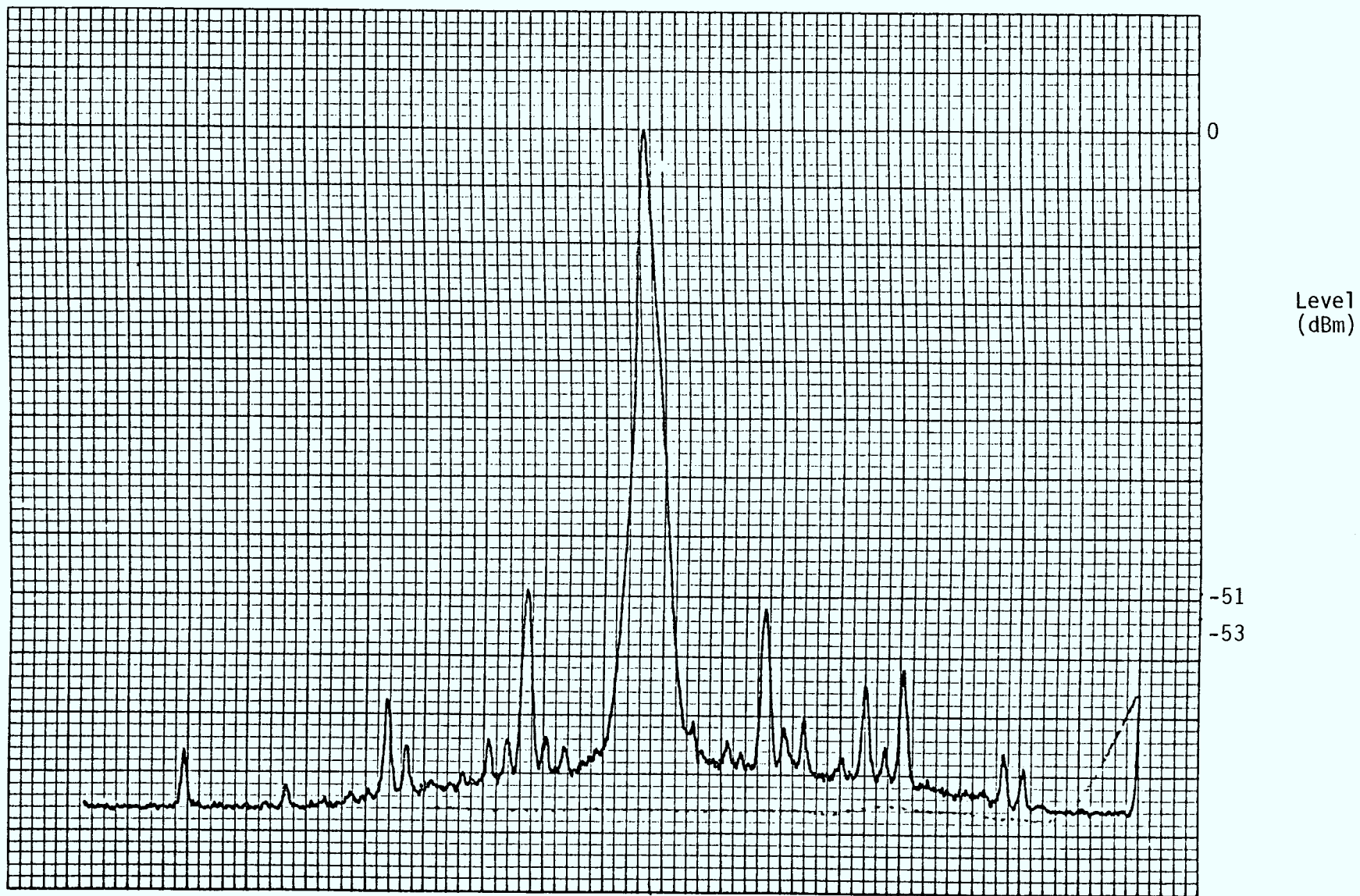


Figure 3.1.15
FM CHANNEL C/N RATIO (OVER VSB #1)

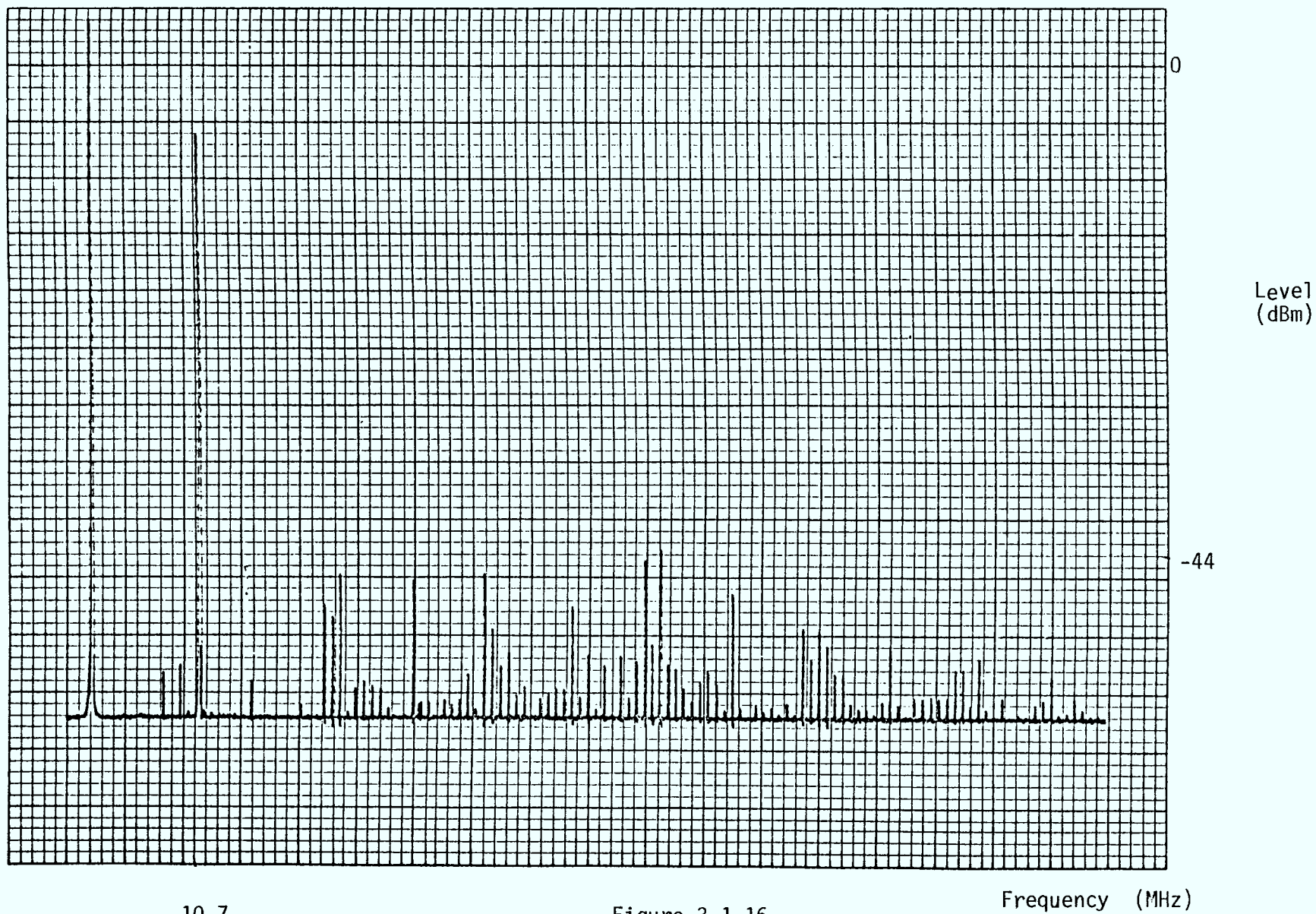
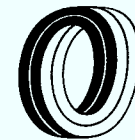


Figure 3.1.16
FM CHANNEL INTERMODULATION AND SPURIOUS SIGNALS (OVER VSB #1)



3.2 FIBRE OPTIC CABLE TRANSMISSION CHARACTERISTICS

3.2.1 Cable Attenuation

Cable attenuation measurements were performed three times to comparing environmental effects on cable performance.

The obtained results are tabulated in Table 3.2.1.

It is recommended that system design calculations include as a maximum 0.5 dB per kilometer for temperature degradation.

The test equipment used to measure the cable attenuation consisted of:

- a) Harris Optical Transmitter
- b) Optikon Photo-dyne Meter

The reference output power of the Harris Transmitter was first determined. Each fibre, in turn, was then interfaced with the transmitter and the output power at the end of the fibre was recorded, the difference between the two resulting in the cable attenuation. The interface of cable and transmitter was accomplished by means of a connector. The connector bulkheads were removed and the ferrules of each connector end fed through an alignment piece to optimize the associated connector loss.

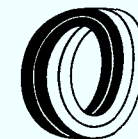


TABLE 3.2.1 CABLE ATTENUATION MEASUREMENTS

TIME/CLIMATIC LOG	FIBER ATTENUATION HUB END - REPEATER STATION								FIBER ATTENUATION HEAD END - REPEATER STATION								*
	6-4	7-6	5-5	2-3	3-2	8-7	4-8	1-1	2-8	3-4	5-7	8-3	4-6	7-5	1-2	6-1	
FEB. 11, 1980																	
TEMP HI: -5°C LO: -9°C																	
WIND SPEED: 30 KM/HR NO PEAK GUST	25.9	25.6	26.2	25.6	26.3	24.3	α	28.4	27.6	28.6	25.4	27.5	25.4	27.7	30.2	30.1	
APRIL 14, 1980																	
TEMP HI: +6°C LO: -0.1°C																	
WIND SPEED: 33.9 KM/HR with PEAK GUST AT 54 KM/HR	26.4	24.5	25.7	24.6	23.9	22.7	α	29.9	29.1	30.6	25.3	30.6	28.4	27.5	α	30.2	
RAIN: 28.1 mm																	
SNOW: 32.9 mm																	
AUG. 15, 1980																	
TEMP HI: 23.4°C LO: 12.7°C																	
WIND SPEED: 19 KM/HR NO PEAK GUST	28.9	29.8	26.1	27.7	26.5	27.5	α	α	28.7	29.2	26.4	30.6	27.3	33.3	32.3	35.0	
* numbers identify fibre ends																	



3.2.2 Change In Attenuation vs Temperature

A 1 km length of 8 fibre cable manufactured for the BCN project as a spare length was coiled onto a 'SWIFT' and subjected to step-temperature cycles in a temperature chamber.

Changes of less than 2.0 dB/km were observed from +20 to -40 to +20°C and six fibres showed no change up to +50°C but the attenuation of fibres 5 and 7, sharply increased to approximately 7.5 and 15 dB/km respectively as the temperature was increased to +50°C. All fibres recovered to their initial values at the end of the cycle.

Only one set of figures is provided in Table 3.2.2 for the three cycles performed since the attenuation change for each of the cycles were within 0.1 dB. However, the change was documented for fibres 5 and 7 since the spread above 20°C was much greater for the same three cycles as shown in the Table.

3.2.3 Cable Bandwidth Measurements

Cable bandwidth measurements were performed in the field on the BCN cable using the discrete frequency response method on April 24, 1980.

A spare BCN fibre pigtail was butted to a Hitachi laser operating at 830 nm and the connectorized side of the pigtail was connected to the fibre under test. At the receive end the connector bulkhead was removed and the ferrule was butted to an APD.



3.2.3 (cont'd)

Back to back frequency response of the equipment between 5 Mhz and 500 Mhz was flat within 1 dB. Neutral density filters were used to simulate the cable loss.

At the repeater end the APD receiver and spectrum analyzer were prepared and a fibre was accessed for transmission of the signal from the Hub end. At the Hub end the transmit generator was adjusted at discrete frequencies between 5 Mhz and 500 Mhz in 50 Mhz steps and the amplitude was recorded. Four fibres were measured whose results are shown in Figures 3.2.1 to 3.2.5.

TABLE 3.2.2 CHANGE IN ATTENUATION vs TEMPERATURE

Start of Test: March 28, 1980
 Length: \approx 950 m
 Attenuation Change: dB/km

FIBER No.	<u>1</u>	<u>2</u>	<u>3</u>	<u>4</u>	<u>5</u>	<u>6</u>	<u>7</u>	<u>8</u>
TEMP °C								
20	0	0	0	0	0	0	0	0
10	0	0	0	0	0	0	-1.2	0.1
0	0.1	0.1	0.2	0	0	0.2	-1.7	0.3
-10	0.2	0.2	0.3	0.1	0	0.4	-1.9	0.5
-20	0.5	0.3	0.5	0.1	0	0.2	-1.9	0.6
-30	0.8	0.5	0.7	0.2	0	1.1	-1.8	1.0
-40	1.3	1.0	1.0	0.3	0	1.8	-1.8	1.5
-30	0.4	0.3	0.4	0.1	0	0.5	-1.8	0.4
-20	0.2	0.1	0.3	0.1	0	0.3	-1.9	0.3
-10	0.1	0	0.1	0	0	0.2	-1.9	0.1
0	0	0	0	0	0	0.1	-1.8	0.1
+10	0	0	0	0	0	0.1	1.1	0
20	-0.1	-0.1	-0.1	0	1.0 0.7 0.2	0	2.3 1.4 0.1	0
30	-0.1	-0.1	-0.1	0	2.6 2.0 1.2	0	6.3 4.9 3.0	0
40	-0.1	-0.1	-0.1	0	6.1 5.6 3.5	0	12.7 11.3 7.7	0
50	-0.1	-0.1	-0.1	0.2	7.0 6.9 6.5	0	14.6 14.2 13.7	0
40	-0.1	-0.1	-0.1	0	3.0 2.8 3.0	0	7.8 7.2 7.8	0
30	0	0	0	0	0.5 0.4 0.9	0	2.3 1.9 3.4	0
20	0	0	0	0	0	0	0 -0.2 -0.4	0

REF:

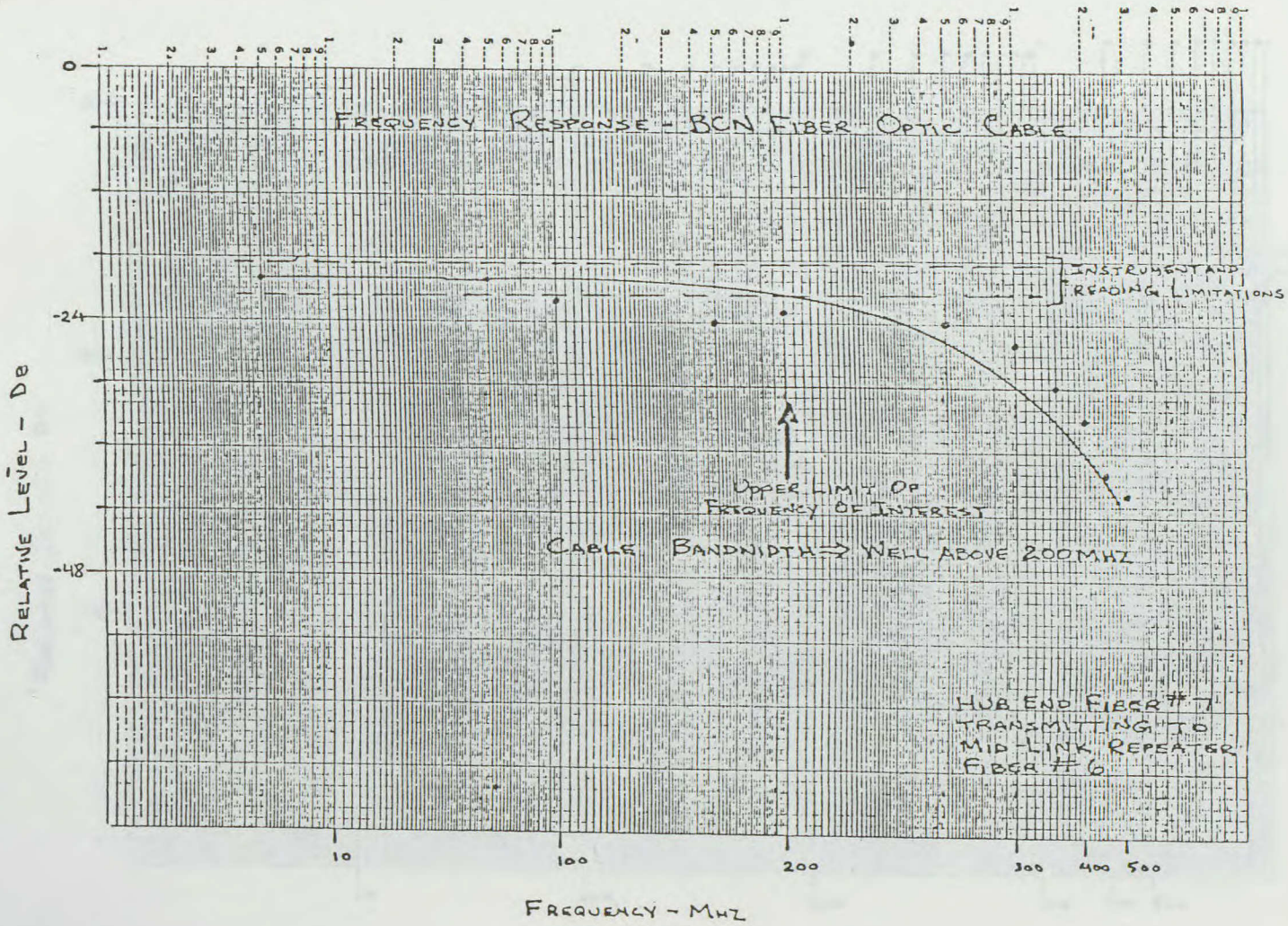


Figure 3.2.1

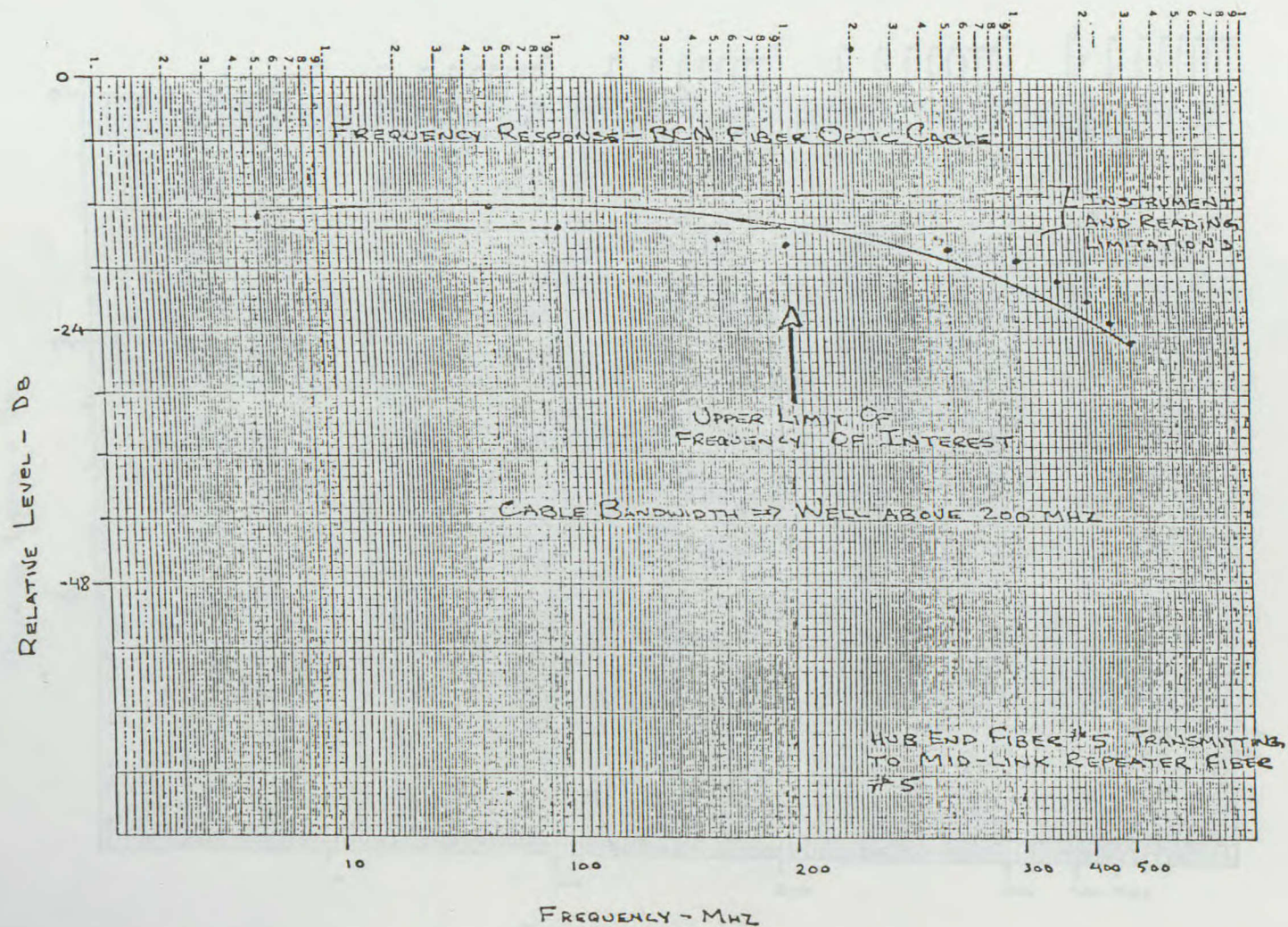


Figure 3.2.3

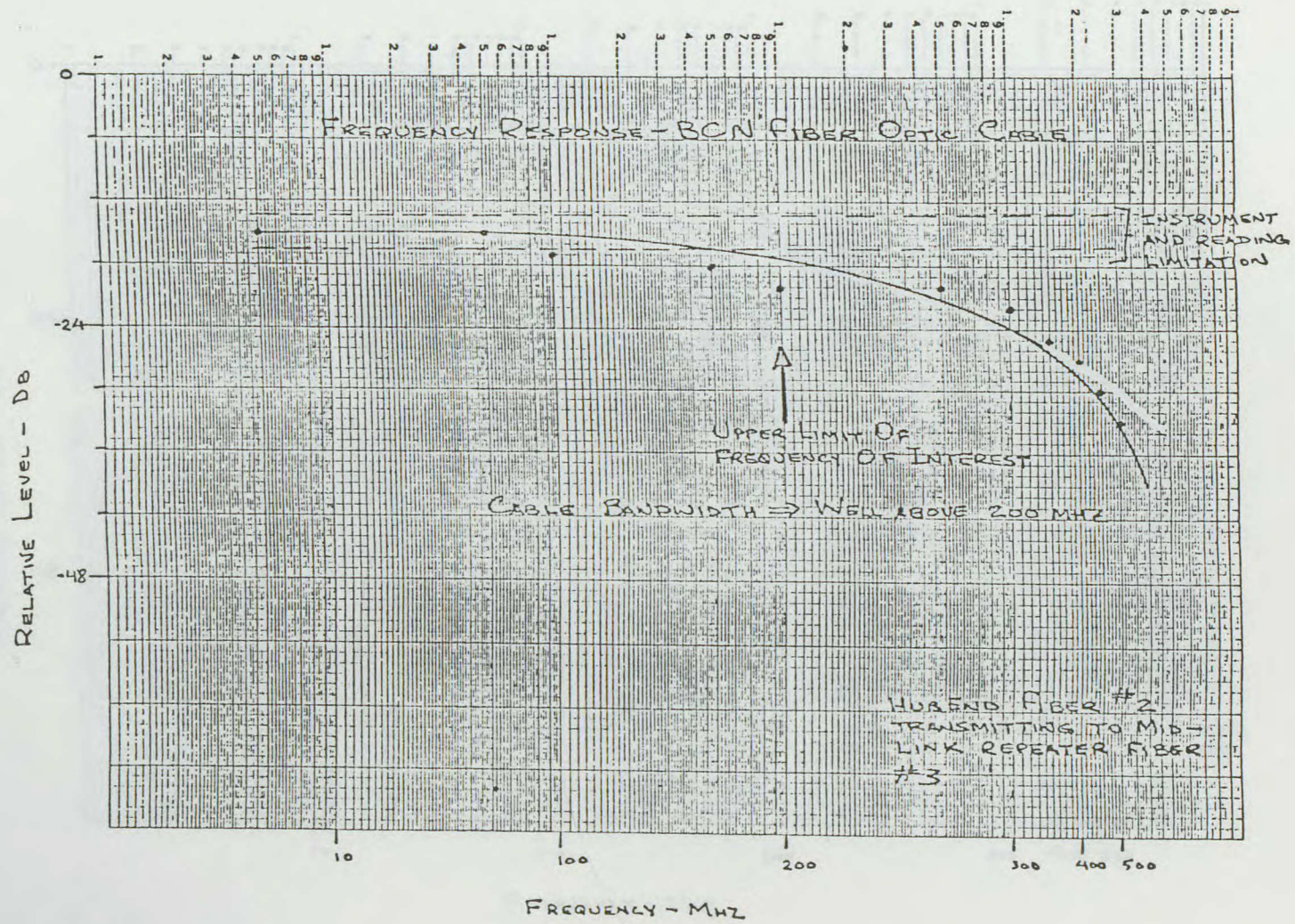


Figure 3.2.2

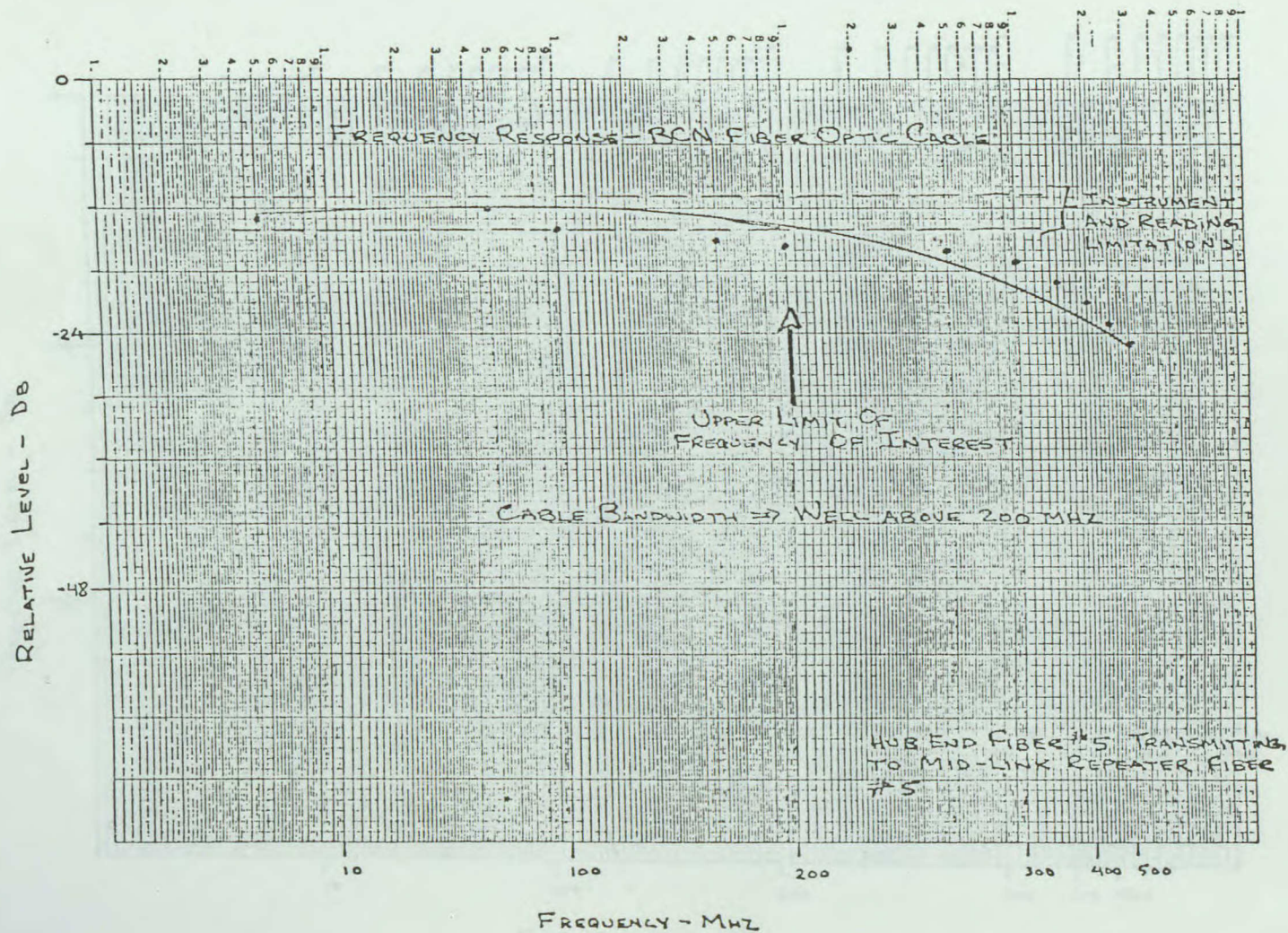


Figure 3.2.3

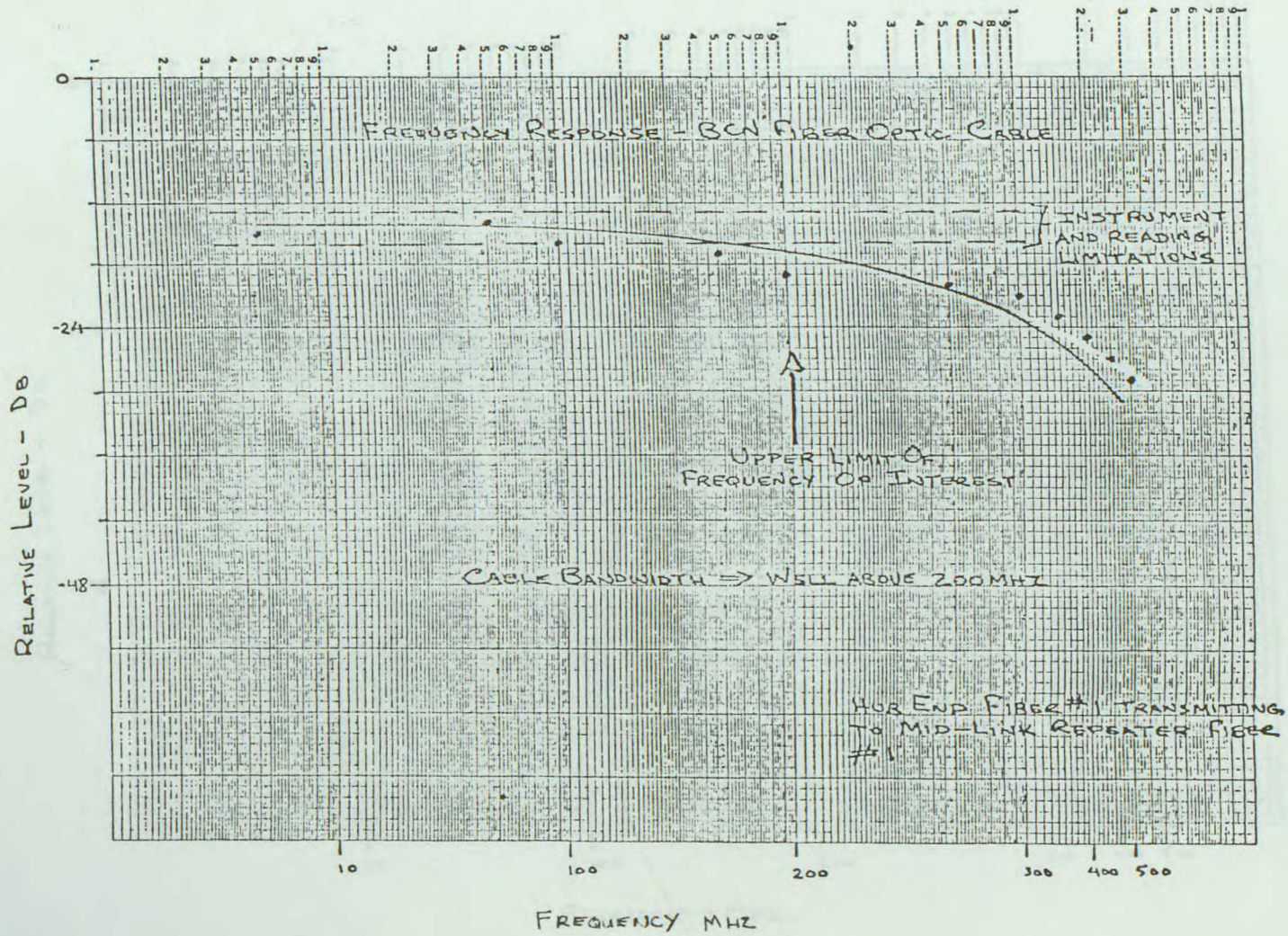


Figure 3.2.4

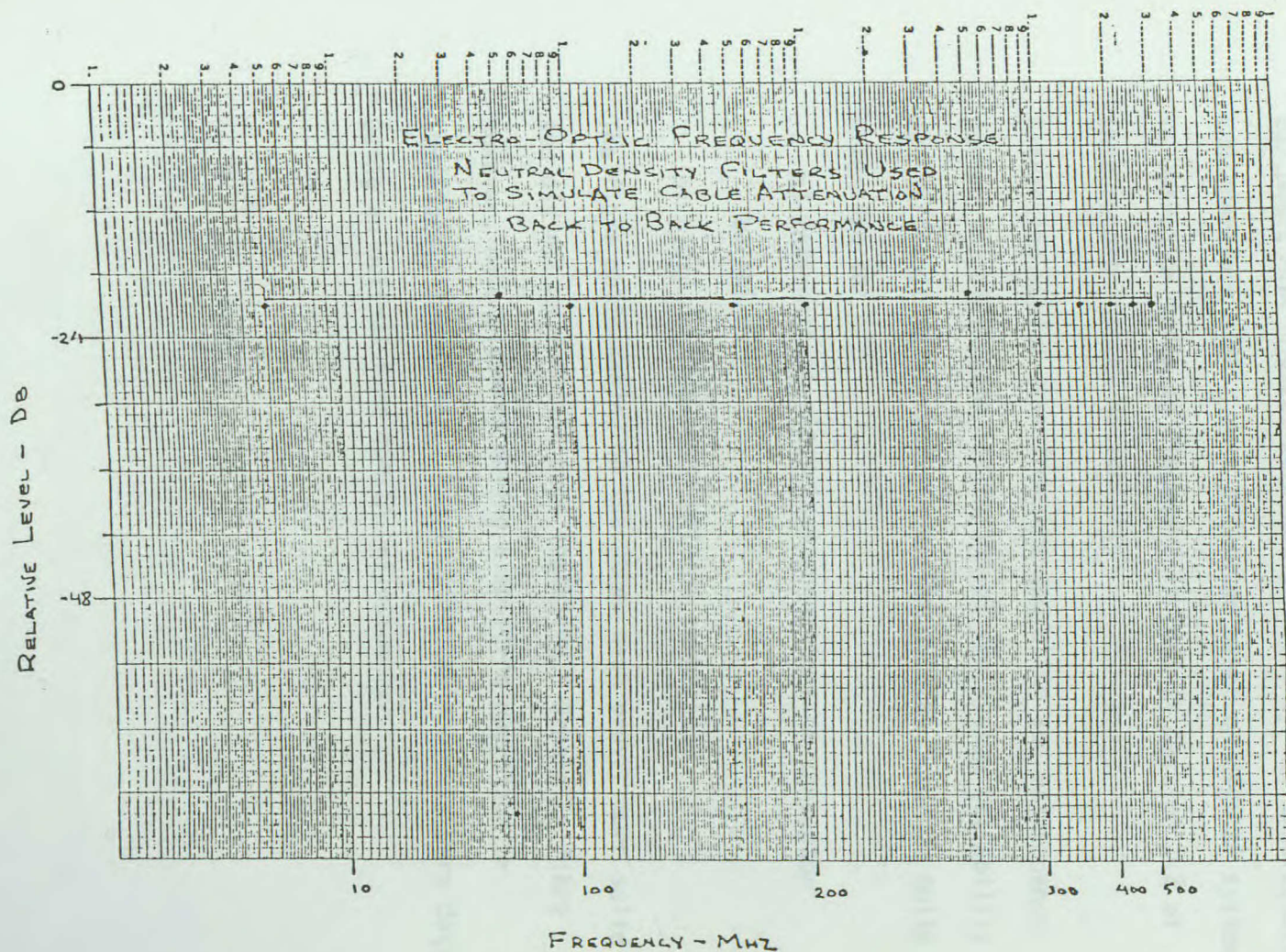
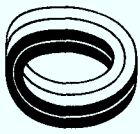


Figure 3.2.5



3.3 MEAN TIME BETWEEN FAILURES

Equipment MTBF figures were not provided by the manufacturer and therefore MTBF's were estimated based on digital systems in operation today as discussed in Part IV Section 1.2 of this report "System Reliability".

Extracting useful data from the operating and maintenance period to obtain some indication of the system reliability was difficult mainly because system outages occurred quite often due to:

- a) intermittent electrical connectors on connector backplane
- b) dirty or misaligned optical connectors

The fibre optic cable, on the other hand proved more solid and did not malfunction once installed. Breaks in fibre however, have occurred during a splicing operation or immediately thereafter. Fibre optic cable breaks were determined using an optical time domain reflectometer.



3.4 MEAN TIME TO REPAIR

Repairing a fault in an optical channel link requires two categories of troubleshooting:

- a) Step I : Detecting location of the fault
- b) Step II : Repairing the fault

The LTMU assists in reducing the MTTR of Step 1 by a least half the time since it has the capability of remotely reporting repeater and far end transmitter-receiver status. This is true, even more so, if the number of repeater stations increases beyond one.

For reasons discussed earlier the LTMU has been inhibited therefore each site needs to be interrogated separately by a maintenance crew until the location of the fault is determined, naturally increasing repair time of Step I.

A repair at a repeater station would take approximately 45 minutes. The repair constitutes:

- i) entry into the repeater housing
- ii) disconnecting connectors to allow for measuring receive and transmit levels

assuming the receive level is in order i.e. cable and far end transmitter are functional whereas the transmit output has dropped then the repair continues by:

- iii) unscrewing repeater module from repeater frame
- iv) plug-in and secure spare repeater module into position



3.4 (cont'd)

- v) measure output power of repeater module to insure its operation
- vi) clean connectors at both cable pigtails and module ends
- vii) reconnect the repeater module pigtails to the cable pigtails
- viii) re-seal the repeater housing

The repair time at a repeater site does not include the handling of the bucket truck or ladder to gain access to the repeater housing.

The repair of a transmit or receive terminal end would take close to 90 minutes. This is mainly due to the transmit and receive modules not being of the plug-in type. In order to replace such a module the drawer must be removed from the rack. A transmit or receive drawer is easily determined faulty by back to back tests using equipment drawers known to be in good working order. Once a terminal drawer is determined faulty, a module by module substitution may place the drawer back into service. If this is not the case the drawer is shipped to the factory for repair.



3.5 SYSTEM PERFORMANCE AS A FUNCTION OF ENVIRONMENT

Cable attenuation as a function of temperature has been illustrated. Bit Error Rate as a function of temperature is documented in Part III Section 3.0.

From the cable attenuation results we observe several spans whose receive level are close to the optical receiver sensitivity level at a bit error rate of 10^{-7} . Temperature effect on the cable or at the repeater equipment can easily create a degradation in bit error rate or cause loss of frame sync. Dirty or poorly matched connectors (optimization of connectors are not possible in the field) further degrades the system bit error rate performance resulting quite often in a link outage.

System performance degradation due to snow, rain, ice and wind loading were not observed.



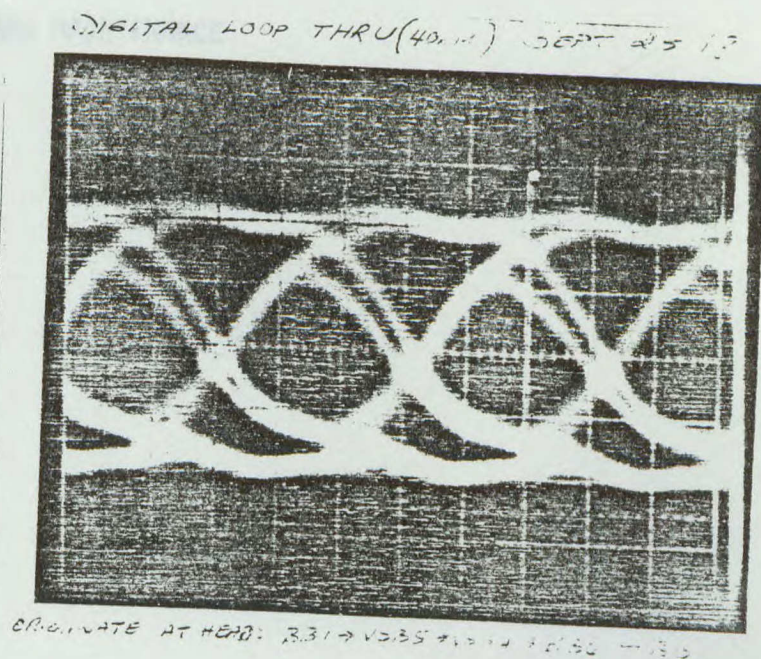
3.6 DIGITAL LOOP THRU TEST

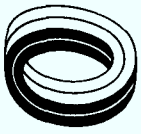
Digital loop thru operation was performed creating a 24 km and 40 km link.

The 24 km digital loop thru set-up showed subjectively a deterioration of BER by approximately 2 decades. The 40 km test caused the link to go in and out of frame sync at a rate of approximately 1 sec. While in lock (40 km simulation) the BER, again subjectively showed a deterioration of an additional 2 decades. Further measurements were not possible at the time and therefore locating the source of this BER disturbance could not be determined.

Eye diagrams taken at the receiver detected data are displayed in Figure 3.6.1. The eye diagrams taken at the far end receiver for the 24 km and 40 km loop show no distortion relative to the 8 km link before the loop thru was initiated. The eye diagrams therefore relate only noise which occurred on the last 8 km section of the loop thru with errors from the previous sections simply being regenerated.

However, sufficient errors are present to prevent the channel from receiving the correct frame information.





PART III

TRAINING AND MAINTENANCE



1.0 CABLE PREPARATION AND SPLICING PROCEDURE

The cable preparation and splicing procedure used in the BCN installation is provided in Attachment I of this section.

An updated version of a splice enclosure is shown in Attachment II.



2.0 CONNECTORIZATION

The detailed procedure for the assembly of the the Harris connector is provided in Attachment II of this section.



3.0 ROUTINE MAINTENANCE

Routine maintenance of the link was difficult to perform due to the prototype nature of the link. Furthermore a great deal of time was spent troubleshooting and maintaining the system operational.

The LTMU equipment which was designed to monitor link BER and optical parameters of both the transmitter and receiver at the hub, head-end and repeater was functional during the six month trial at the expense of baseband link No. 1.

This made routine diagnostics more difficult.

A chart recorder was installed to monitor each link's loss of frame synchronization. This record provided the best available data to monitor link performance. Generally, an increased frequency of frame sync loss was traced to either a fault in the repeater module, misaligned or dirty connectors or intermittent electrical connectors on the connector backplane of a drawer at the head-end or hub. When frame sync losses increased, the general troubleshooting process involved:

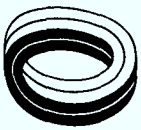
- 1) Optical power readings were taken to determine if either an optical connector had become misaligned or an optical transmitter had become marginal.



3.0 (cont'd)

- 2) If the optical connector was at fault, the connector was cleared and realigned.
- 3) If the optical transmitter was at fault, it was replaced at the module level.
- 4) If the optical system appeared intact then electrical connectors on the connector backplane of a drawer were checked for intermittancy. This was achieved by module inter-change and ensuring a proper connection.

Other routine maintenace operations included cleaning the air intake on the racks for air cooling. Frame sync losses increased in frequency if there was insufficient air circulation to keep the equipment cool. On a daily basis, fibre status and subjective picture performance was noted.



4.0 PERIODIC MAINTENANCE - SYSTEM MEASUREMENTS

Periodic maintenance was performed during the operation and maintenance phase of this project. A major effort during this period included troubleshooting equipment faults diagnosed frequently to either faulty repeater modules or receiver drawers.

Other than maintaining the system operational (limited to spare module availability) system performance tests were carried out similar to those tests undertaken during acceptance testing. No evidence of degradation was observed. Bit error rate, on the other hand, has degraded appreciably. Cleaning connectors and replacing the repeater module improved BER performance in the majority of occurrences.

4.1 Eye Diagram Recording

Eye diagrams taken at the end of the commissioning period and at the end of the operation and maintenance period are illustrated in Figures 4.1.1 to 4.1.3. Generally good eye openings are observed however, an increase in noise is visible on the readings taken in May of 81.

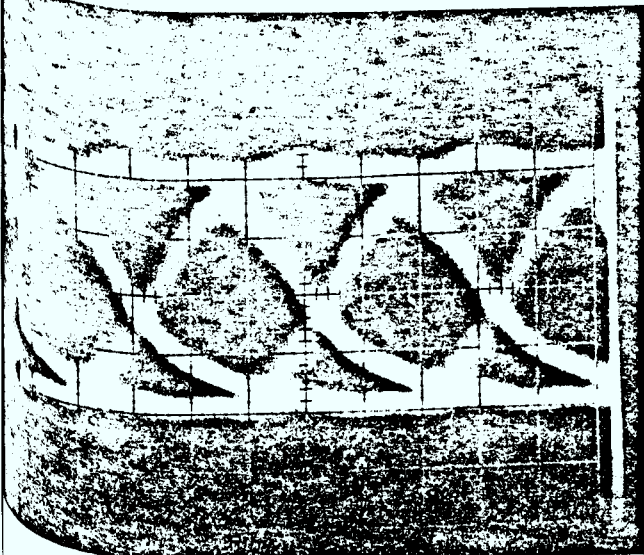
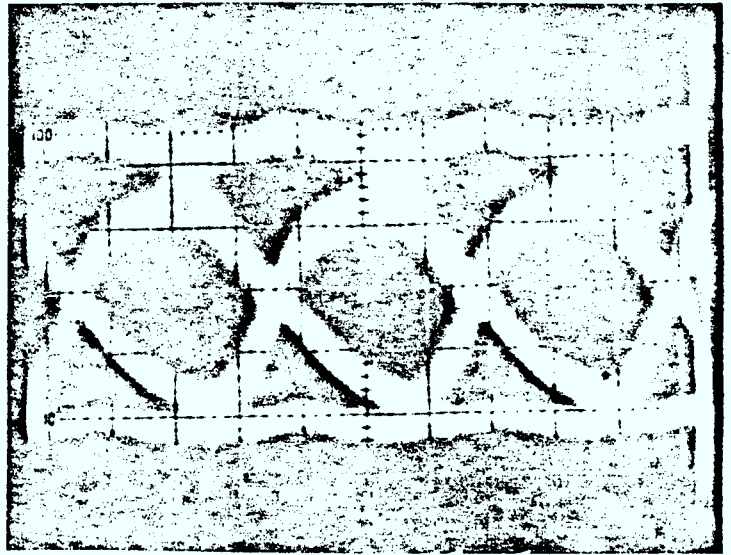
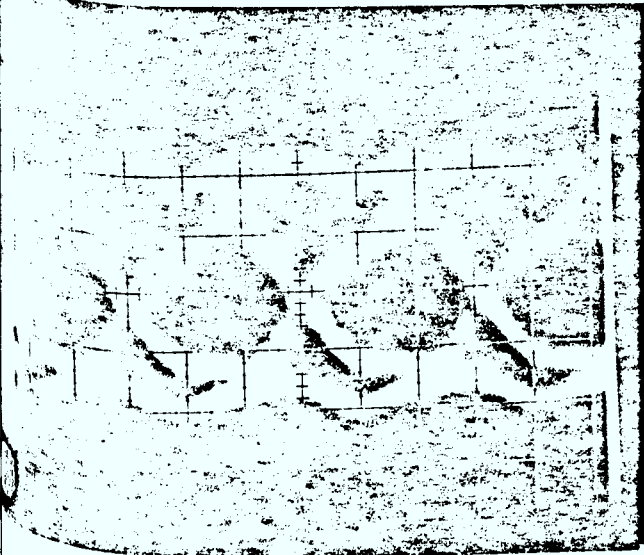


November 28, 1980

May 28, 1981

(Measured at Hub End)

(Measured at Hub End)



0.5 mV/DIV
1 nS/DIV

0.5 mV/DIV
1 nS/DIV

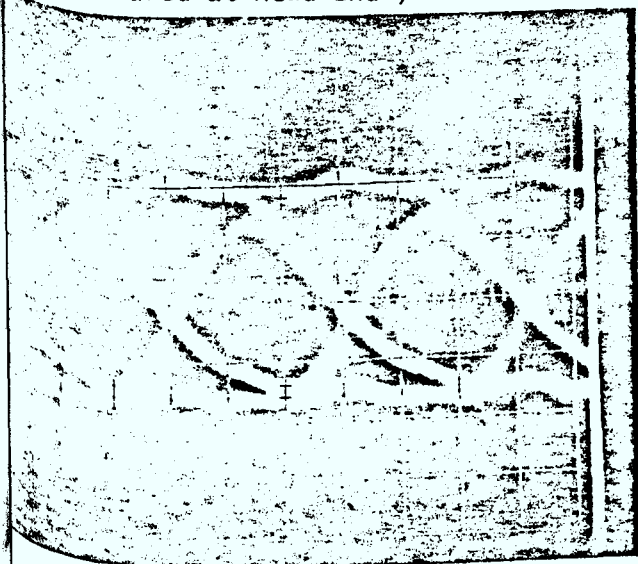
EYE DIAGRAM MEASUREMENTS

Figure 4.1.1



November 28, 1980

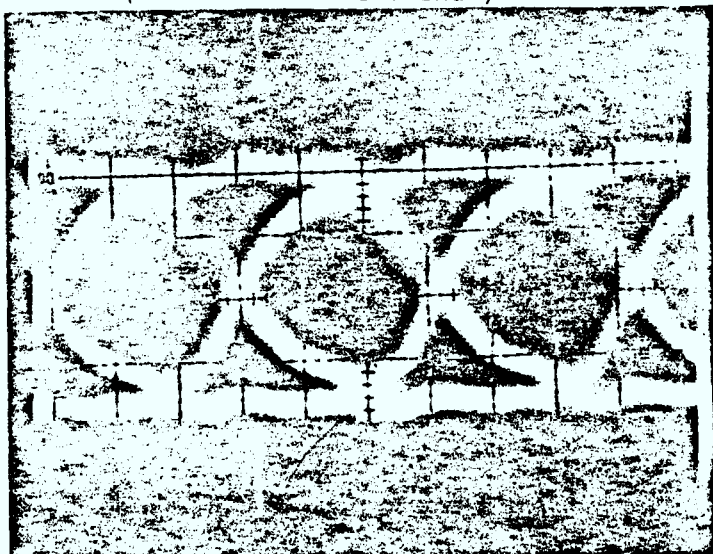
(Measured at Head End)



0.5 mV/DIV
1 nS/DIV

May 28, 1981

(Measured at Head End)



0.5 mV/DIV
1 nS/DIV

EYE DIAGRAM MEASUREMENTS

Figure 4.1.2



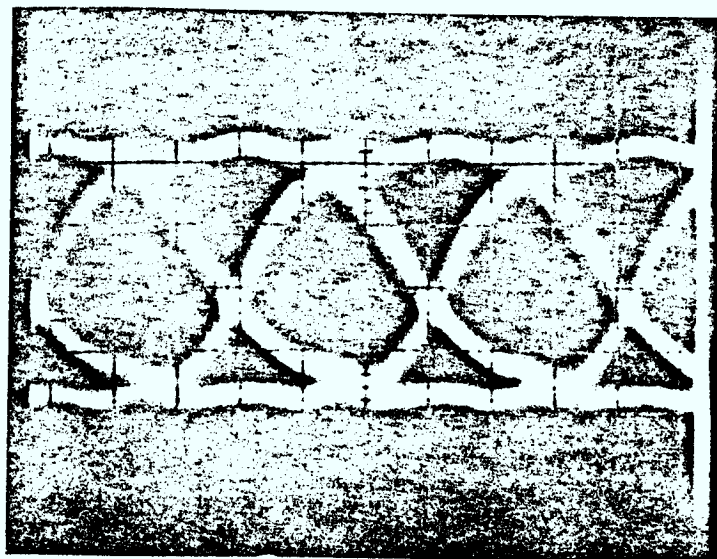
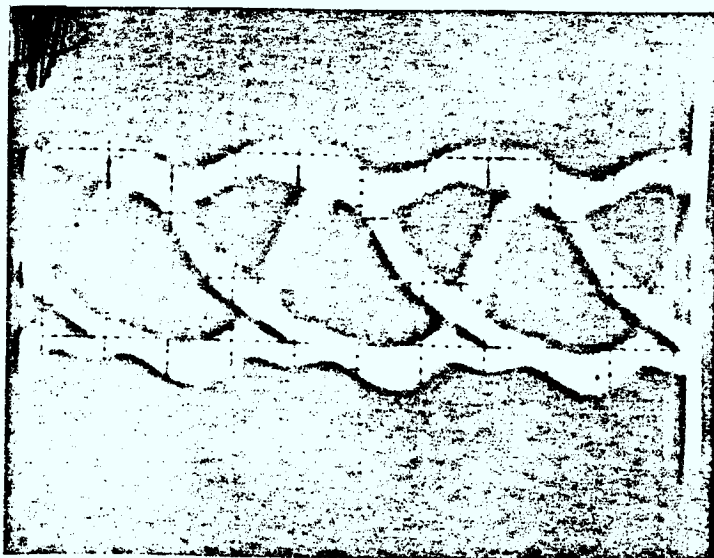
November 28, 1980

(Measured at Hub End)



May 28, 1981

(Measured at Hub End)



0.5 mV/DIV
1 nS/DIV

0.5 mV/DIV
1 nS/DIV



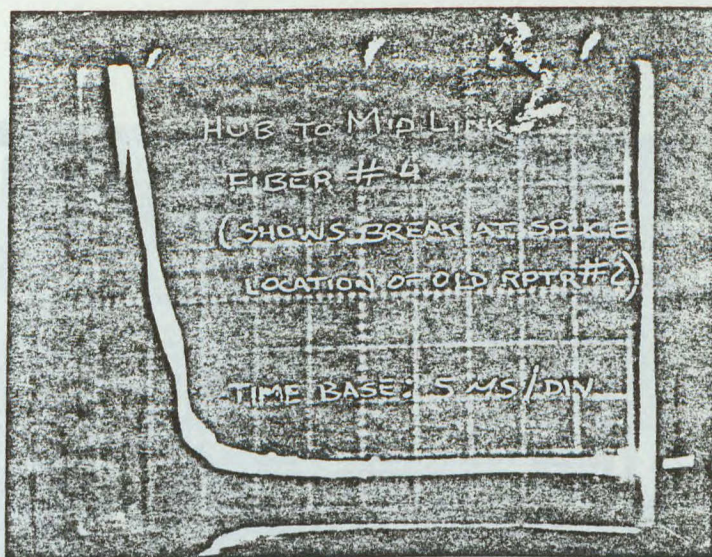
4.2 Optical Time Domain Reflectometer (O-TDR)

The O-TDR was used to evaluate the quality of splices during the cable installation period as well as determine the location of breaks in the fibre optic cable.

Figure 4.2.1 illustrates the response obtained from broken fibre #4 between the Hub and repeater site showing the reflection at 2.6 km away. Originally this was the location of repeater #2 site which was spliced through during reconfiguration.

Figure 4.2.2 illustrates the response obtained from a good fibre showing the end of the fibre correctly at 4.3 km away.

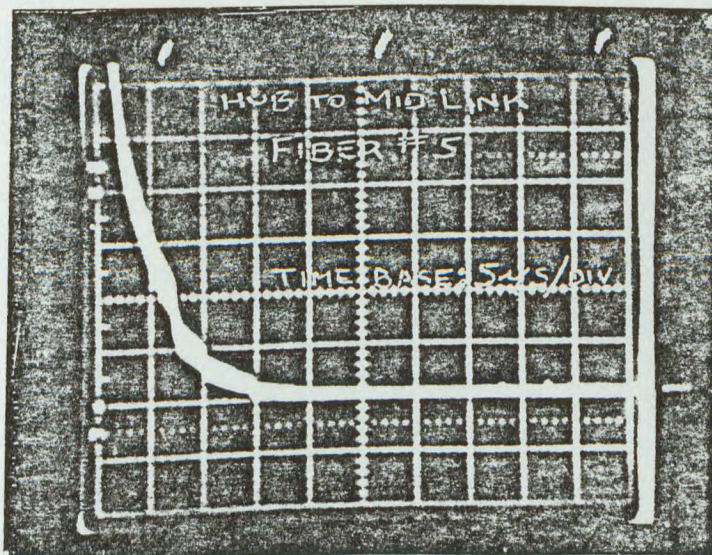
Figure 4.2.3 illustrates the response obtained from broken fibre #1 between the Hub and repeater site showing no reflection. Testing the fibre with the O-TDR from the other end should locate the break. The application note on the O-TDR is provided in Attachment IV of this section.



Link length 4.3 km.
Response of a non-continuous fibre.
Break shown 2.6 km away.

O-TDR RESPONSE

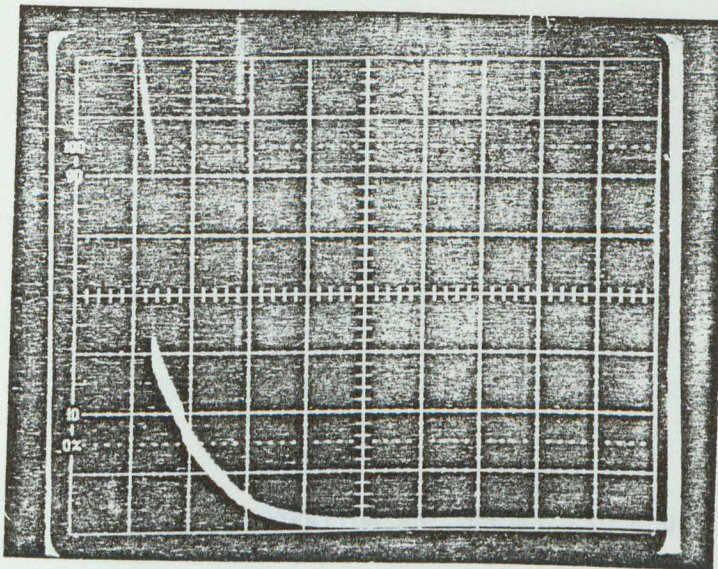
Figure 4.2.1



Link length 4.3km.
Response of a continuous fibre.

O-TDR RESPONSE

Figure 4.2.2



Link length 4.3km.
Response of non-continuous
fibre.
Break (or reflection)
not visible.

O-TDR RESPONSE

Figure 4.2.3



ATTACHMENT I

(REF: PART III, SECTION 1.0)

CABLE PREPARATION AND SPLICE PROCEDURE



CABLE PREPARATION AND SPLICE PROCEDURE

1. Introduction

This procedure describes fibre optic cable splicing with particular attention to fibre splicing aspects.

The fibre optic cable installation is not within the scope of this procedure and conventional telephone cable/CATV cable installation methods and equipment can be employed for fibre cable installation.

It is assumed that all relevant tests on the cable have been performed before installation and fibre connections.

Continuity of each fibre should be tested before actually dressing the cable for splicing due to the possibility of fibre breakage during cable installation operations. If pigtails were employed at the cable ends, continuity of all pigtails should also be tested prior to the splicing operation.

The time required for one eight-fibre cable splice, which includes equipment, set-up, cable dressing, splicing enclosing and lashing if it is aerial cable, is about six to eight hours for a trained person.

Due to equipment limitations the splice loss can not be monitored during splicing operations in the field at present. Therefore, the splice quality will rely greatly on the experience of the splicer. Even though the actual splice loss can not be monitored in the field, the quality of the splice can be judged under the microscope during fusion operations.



If there is any doubt about the splice quality the operation should be repeated until a good quality splice is obtained.

2. Tools/Equipment Required:

- Tent and platform (or scissors platform and booth for aerial cable splicing)
- Work bench and chair
- Portable generator and extension cord
- Lighting
- Fusion Splicer
- Heat Gun
- Pipe Cutter
- Wire stripper
- Fibre cleaving tool (NEC or others)
- Utility knife
- Cable jacket stripper
- Cable cutter
- Adjustable wrench
- Long-nose pliers
- Heater if required
- Hole puncher



3. Splicing/Grounding Material:

- Splice enclosure
- Acetone or other suitable solvent for fibre cleaning as recommended by fibre manufacturer
- Rubbing Alcohol
- Paper Tissue
- .118" O.D. .065" I.D. brass tube
- 3/32" dia. clear polyolefin shrinkable tube
- 3/8" dia. black shrinkable tube
- Grounding kit
- Silicon contact cement

4. Cable Dressing:

- (1) Strip outer jacket for approximately one meter by using pipe cutter to cut around outer jacket but be sure not to cut inner jacket or apply excessive pressure on the cable core.
- (2) Use jacket stripper to strip inner jacket and leave about 2 to 3 cm from the outer jacket.
- (3) Cut Kevlar
- (4) Identify and number fibres.
- (5) Cut buffer tubes to the length leaving approximately 3 to 4 cm of buffer tube measured from the inner jacket.
- (6) Replace the cut buffer tube with size 24 Teflon tubes. The Teflon tube should go into the buffer tube for about $\frac{1}{2}$ to 1 cm.



- (7) Slide a piece, approximately 4 cm, of size 3/32" clear Polyolefin shrinkable tube overlap the joint of Teflon tube and buffer tube and shrink it by using a heat gun.
- (8) Slide a piece of size 3/8" Black Polyolefin Shrinkable tube overlap the inner jacket and all the clear shrinkable tubes which cover the joints of Teflon tubes and buffer tubes.
- (9) Slide entrance connector over the cable and slide cable into splice box.
- (10) Split outer jacket into two halves for about 3 to 4 cm in length. Punch hole on one of the halves and put grounding clip on.
- (11) Ground the Alpeth sheath to the splice box.
- (12) Cut centre strength member, steel wire, to approximate length and ground to the splice box.

5. Splicing:

- A. The following splicing process applies to fusion splicers FX302 manufactured by A01 Sansho Company Ltd.
- (1) Slide a piece, approximately 4 to 5 cm in length, of size 3/32" clear Polyolefin shrinkable tube onto each end of the fibre to be spliced and one piece of size .118" O.D. .065" I.D. brass tube in length of approximately 5 ½ cm to one end.
- (2) Strip Teflon tube to protrude bare fibre for about 4 to 5 cm in length.



- (3) Dip fibre end into Acetone for about one minute and wipe with wet tissue to clean off lacquer coating on fibre.
- (4) Cut fibre by using NEC fibre cutter or equivalent.
- (5) Put both fibre ends into v-grooves of AOI fusion splicer and clamp both fibre and Teflon tube down.
- (6) Observe fibre end cut quality through microscope. Re-cut if necessary.
- (7) Align fibre ends.
- (8) Provide sufficient stroke length.
- (9) Align electrodes.
- (10) Set welding time to 2.5 seconds.
- (11) Welding current set at minimum point of high range.
- (12) Fuse fibres.
- (13) Observe splice quality through microscope. Re-cut and re-splice if necessary.
- (14) Release all clamps which clamp the fibre and Teflon tube and lift them away from the v-groove blocks.
- (15) Slide brass tube over the fibre. The Teflon tubes should stay inside the brass tubes and there should be no tension.
- (16) Slide and shrink the size 3/32" clear shrinkable tubes overlap the brass tubing and the Teflon tube.
- (17) After all the splices complete, loop the fibre into the splice box in Figure 8 pattern and to avoid any sharp bends on the fibre.
- (18) Tighten fibres securely by using small cable tie.
- (19) Tighten entrance connectors and close splice box.



-
- (20) Apply Silicone cement to seal entrance connector.
 - (21) Lash splice box onto Messenger Wire.



ATTACHMENT II

(REF: PART III, SECTION 1.0)

DETAILED PROCEDURE FOR ASSEMBLY OF HARRIS CONNECTOR



DETAILED PROCEDURE FOR ASSEMBLY OF HARRIS CONNECTOR

1. Dress cable end; it may be necessary to replace the buffer tubes with spaghetti tubing small enough to allow insertion of buffer tube with shrink tube over it into the back of the connector body. Use 24 ga. Teflon, TFT-200-24.
2. Strip back buffer tube to allow about one inch of fibre to protrude.
3. Clean all coating off fibre back up to the tube, being careful to avoid solvent wicking up into the tube and weakening the fibre.
4. Run cleaning wire through ferrule, it should run freely.
5. Wash ferrule in alcohol.
6. Put ferrule onto fibre, from the countersunk end, sliding it up to the buffer tube; alcohol may help lubricate the fibre. The fibre should extend beyond the end of the ferrule. Remove the ferrule again.
7. Dip the end of the fibre in the epoxy and slide it into position in the ferrule. When it is in place, make sure there is a small drop of epoxy where the fibre exits the ferrule and also in the countersunk entry. Be careful to keep the adhesive from getting into the buffer tube or forming large lumps on the fibre or the outside of the ferrule.



8. Heat the assembly gently. The epoxy will decrease in viscosity and wick up into the ferrule. As it curves, it will turn brown. Epoxies other than the one supplied will turn other colors or none at all. Heat may be applied both for cure and for tube shrink with a small heating coil.
9. Put a piece of 1/16" shrink tubing in place to bridge the gap between the buffer tube and the ferrule. It should extend no more than 0.2 inches on the ferrule.
10. Carefully scrape off any epoxy which may have slopped over onto the outside of the ferrule so that it will slide easily into a #66 hole.
11. Polish the end of the ferrule, first with a fine abrasive, then with the polishing compound on the pad. This can be done by hand using first crocus cloth and the polish, or it can be done on a wheel turning 200-300 RPM using a wet carbide paper and then the polishing felt. In the latter case, make a small fixture to hold the ferrule perpendicular to the wheel; a piece of metal about 1/4" thick with a hole through it (No. 66) is perfectly adequate.
12. When it is polished to perfrection, wash it well in water and then in alcohol. If, when examing the end under the microscope, you can see the core brightly illuminated, it probably means the fibre is broken in the shrink tube.
13. Make sure a No. 36 drill will pass through the outer brass shell of the connector.



14. Put some RTV on the ferrule where it meets the shrink tube and push ferrule assembly into connector base from the small end with the small teflon piece removed.
15. Dab RTV around the ferrule where it exits, filling the cup in which the removed teflon piece sits.
16. Push the teflon piece back down over the ferrule into the cup so that the RTV is forced back down the barrel.
17. Put the appropriate gauge piece over the ferrule and move the ferrule in or out so that its end is just flush. Use P/N 312864-004 with the American P/N 1031-7188 cable end; use the shorter P/N 312864-003 with American's 1034-7188 Bulkhead fitting. Note that the assembly is likely to shift due to hydraulic pressure built up when the RTV was forced down. It may be helpful to put on the outer shells. Turn only the floating screw on the connector base to avoid strain on the fibre.
18. Let the RTV cure, at least overnight, preferably longer. Curing may be accelerated by drilling a small hole in the shank of the base to expose the RTV to the air.
19. Remove and save the gauge. In the case of the cable end 1031, install the teflon piece supplied by the manufacturer; on the bulkhead connector, install instead the brass piece supplied by Harris. Screw on the outer shells, gently wrench tight, again turning only the connector base.



-
20. Deal with whatever outer jacketing has been used by gluing and/or heat shrinking it to the connector base. A vinyl-covered fibre glass braid tube may provide enough protection and does not stretch along its length.

N.B. Harris has modified the procedure to overcome problems within temperature cycling. It is now necessary to bore out the connector base to .076". They also recommend two sets of holes at 90° in the shank.

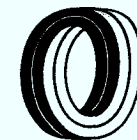
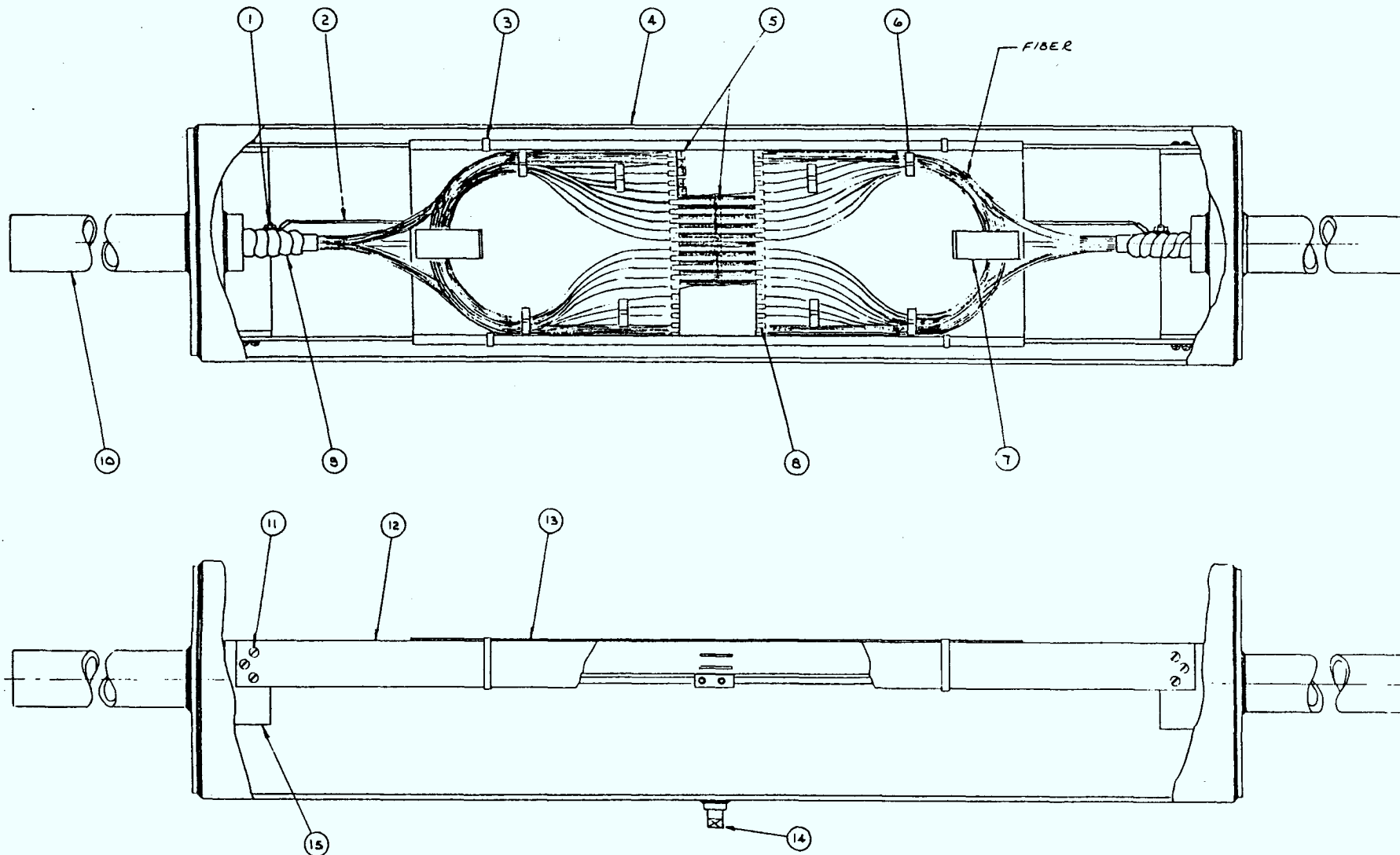


ATTACHMENT III

(REF: PART III, SECTION 1.0)

TYPICAL SPLICE ORGANIZER AND ENCLOSURE

1. BOND STUD COIN
 2. GROUNDING HARNESS
 3. CABLE TIE
 4. MAIN SLEEVE ASS'y
 5. WIRE MARKERS
 6. WIRE CLIP
 7. FLAT WIRE CLIP
 8. SUMITOMO SPLICE
 9. VINYL TAPE
 10. END DISC ASS'y, 1 1/4 AUX.
 11. #10-32 x 3/8 SCREW, BRASS, NI. PLTD. & SPRING L' WASHER
 12. TIE BAR
 13. TRAY
 14. 'C' PLUG
 15. TIE BAR END PLATE
- PROTECTION PACKAGE



Canstar Communications

MA-200-000240



ATTACHMENT IV

(REF: PART III, SECTION 4.2)

APPLICATIONS AND USE OF THE OPTICAL
TIME DOMAIN REFLECTOMETER FOR FIELD
MEASUREMENT

A ·		RELEASED		27/7/81		1/1	
REV. NO.		REVISION		DATE		APPR. BY	
DRAWN BY		DATE		CHECKED BY		DWG. NO.	
HI		27/7/81		1/1		TD - 140-000289	
						SIZE A	



CANSTAR COMMUNICATIONS
DIVISION OF CANADA WIRE AND CABLE LTD.

TITLE Applications and use of the
Optical Time Domain Reflectometer for
Field Measurement

APPLICATIONS AND USE OF THE OPTICAL TIME DOMAIN REFLECTOMETER FOR FIELD MEASUREMENT

Introduction

The Optical Time Domain Reflectometer (OTDR) is an important diagnostic tool used for monitoring, maintenance testing or troubleshooting an optical transmission link. It operates on a principle analogous to conventional cable TDR instrumentation but uses an optical rather than electrical interface to the line under test. A simplified block diagram of an OTDR is given in Figure 1. A high-power, short-period optical pulse is launched into one end of the fiber. Some optical energy is scattered or reflected back toward the source end as the light pulse travels down the optical waveguide.

A high-speed, high-gain photo-detector converts the backscattered optical signal into an electrical signal which is then displayed as a function of time on a conventional oscilloscope. Signal processing is often implemented to increase the signal-to-noise ratio of the backscatter signal thereby extending the resolution and range of the OTDR.

Through analysis of the backscatter signal it is possible to determine various properties of the fiber link under test.

The slope of the backscatter curve gives an indication of the attenuation along the length of the fiber. As the optical pulse travels down the fiber, perturbations, bubbles, other small defects, or a break (glass-air interface) can cause a varying amount of light to be reflected back. By analyzing these reflected pulses and by knowing the velocity of light in the waveguide it is possible to determine the distance to the fault or break as well as obtain a qualitative measure of any change in attenuation that resulted.

NOTE ON SAFETY

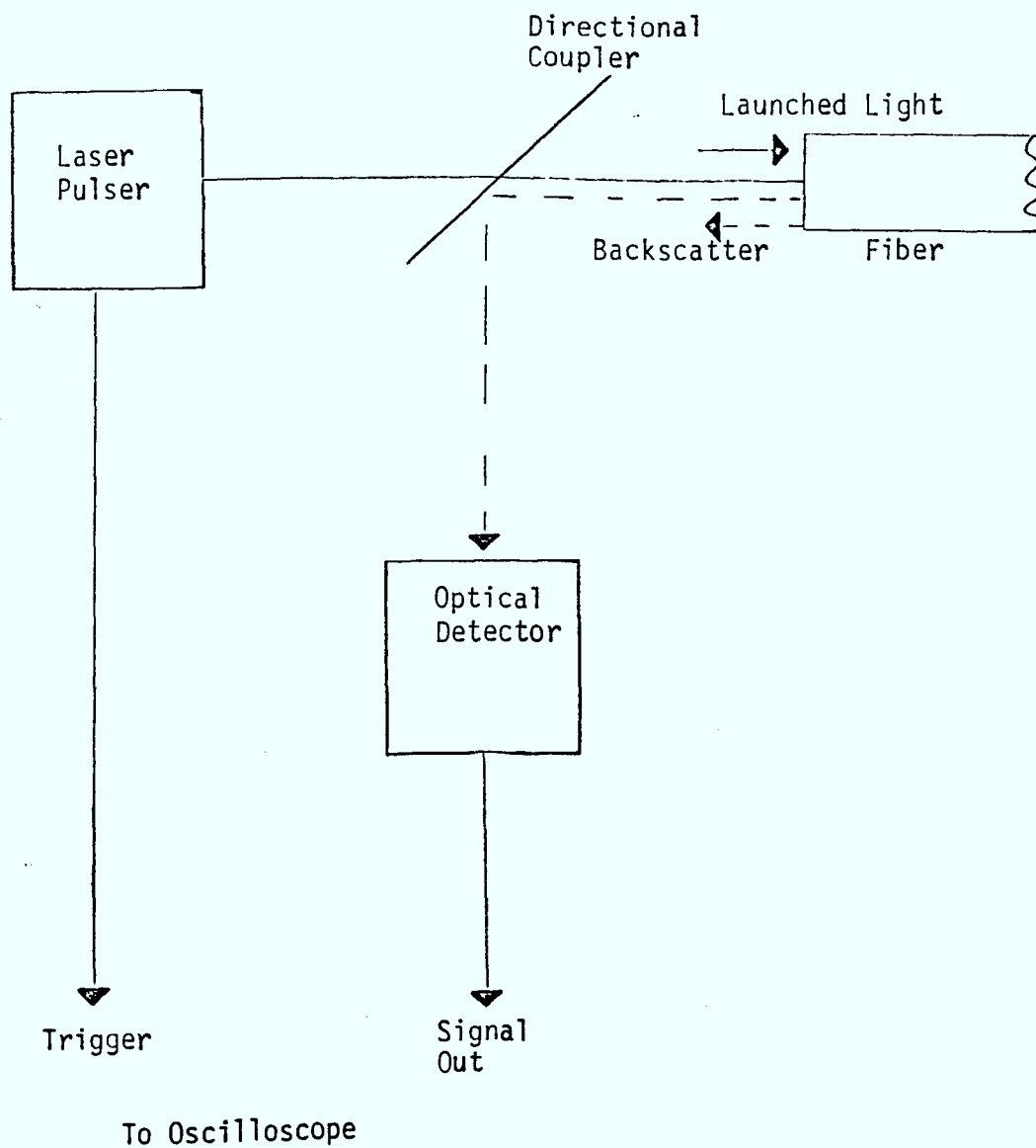
The OTDR outputs a high-power optical pulse at wavelengths invisible yet potentially harmful to the human eye.

Never look directly at the output of the OTDR along the optical axis.

The far end of the fiber under test should not be viewed directly.

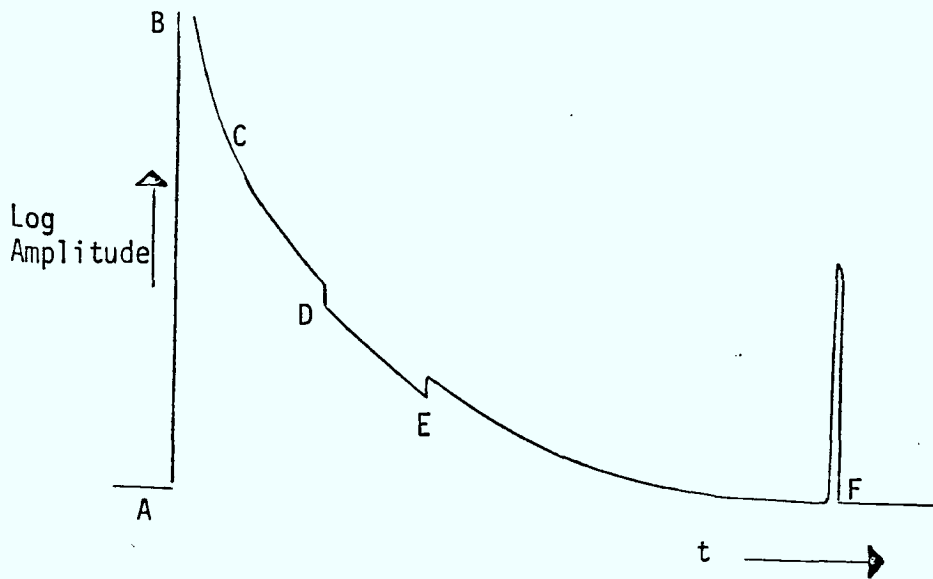
Interpretation of OTDR Display

A typical OTDR display is shown in Figure 2.



Block Diagram OTDR

Figure 1



OTDR Display

Figure 2

Point A is the start of the sweep and shows the leading edge of the initial pulse launched into the fiber. Because of the high power of this pulse, a strong initial reflection is usually seen at point B.

The backscatter signal seen as portion C of the curve decays at a rate proportional to attenuation of the fiber along its length. Eventually the trace disappears into the noise thereby setting a limit on the ability of the OTDR to measure attenuation properties past a certain point down the fiber.

Point D represents a fault or imperfection which has caused a step change (down) in the backscatter signal. This is typical of what one expects to see at a splice location.

Point E shows a step change (up) or increase in signal level. This is not to be interpreted as a splice having gain but is due to the fiber following the splice having a higher amount of backscatter than the fiber preceding the splice. This can occur because of different intrinsic properties (N.A., index of refraction, core diameter, etc) in the two fibers. Point F represents the reflection from the far end (glass-air interface).

A reasonably accurate measure of the true splice loss can usually be made by taking OTDR measurements from both sides of the splice and taking the average of the two. In this way, the effect of unequal backscattering of the two fibers cancel.

Cracks, bubbles or other imperfections in the fiber may show up as a combination of reflection (spikes) and loss characteristics (step or slope changes) depending on the exact nature of the anomaly. The signature at a total break or far end of the link will typically show up as a large reflection which drops abruptly to the baseline.

The OTDR recommended for field use is the Siemcor Model 38 which in our experience has shown to be reliable, rugged instrument. The following procedures are written around this instrument, but may apply to other OTDR's as well.

Apparatus

- 1) Siemcor Model 38 OTDR.
- 2) Oscilloscope with 100 MHz B.W. minimum and delay time base (Tektronix 475 or equivalent).
- 3) RG58 coaxial cables, 1 to 2 meters long, fitted with BNC connectors.
- 4) Fiber end preparation material, cleaving tool, acetone, etc.

OTDR Setup

- 1) Remove the outer protective cover exposing the controls and micro-positioners.
- 2) Set both the power switch and the laser switch to off.
- 3) Completely loosen the micropositioner hold-down screw. There is a retaining clip that will keep it from falling out.
- 4) Connect the 3-wire line cord to the instrument, and plug into a 110V, grounded, 60 Hz A-C source.
- 5) Loosen the stage cover screw to allow the cover to be raised.
- 6) Connect the OTDR trigger output to the oscilloscope's external trigger input.
- 7) Set the oscilloscope's trigger mode to external, positive.
- 8) Connect the OTDR signal output to the oscilloscope's vertical input.
- 9) Set the vertical input to A-C coupled, 0.5V/div.
- 10) Set the oscilloscope's time base to 1 μ sec/div (which gives a display which corresponds to approximately 100 meter/div). Use 0.5 μ sec/div or 2 μ sec/div if it seems appropriate in consideration of the expected fiber length.

- 11) Set the OTDR's optical power control (if equipped) to the full clockwise position.
- 12) Set the OTDR's photodiode amplification control to the 3:00 o'clock position.

Take care at all times to keep the instrument, especially the output lens and the micropositioners, clean. Keep the outer cover in place when the instrument is not in use.

Operating Procedure

- 1) Prepare a good end on the optical fiber to be tested.
- 2) Lift the stage cover.
- 3) Clamp the fiber into the appropriate V-groove. The end of the fiber should lie in the plane of the front of the smaller (upper) ledge.
- 4) Adjust the X,Y and Z micropositioners to the initial setting values given on the stage label.
 - 4.1 Replace the cover over the positioner stage. (This cover activates the safety interlock switch.)
 - 4.2 Turn the line power switch on. (Wait 15 seconds.) Turn on the laser power switch.
- 5) Turn the photodiode amplification control clockwise slowly until noise starts to appear on the trace. Then turn it back counterclockwise slightly. Do not maintain the photodiode amplification beyond this value where noise is evident; doing so may damage the photodiode.
- 6) A front end reflection should immediately be evident, as in Figure 3. Depending on the alignment of the fiber's end, a far end reflection of noticeable height should also be seen.

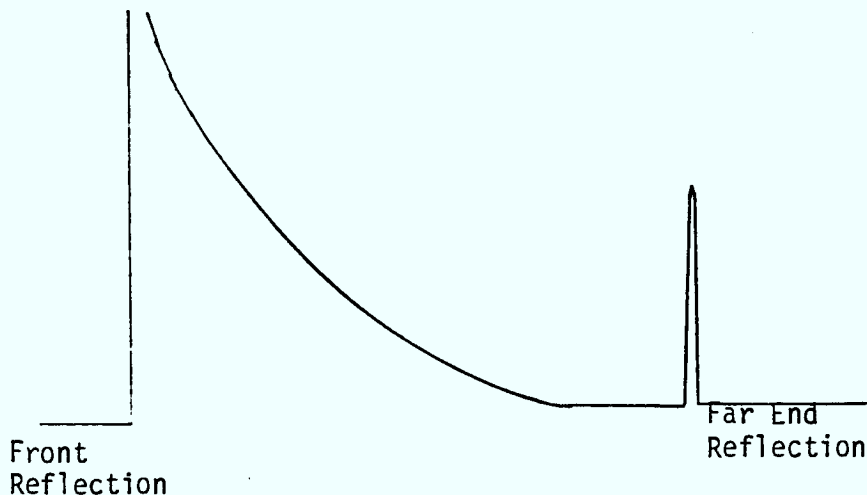


Figure 3

- 6 -

TD-140-000289
Rev. AMeasurement of Fiber Length

Length may be determined by measuring the time difference Δt between the initial pulse from the front reflection and the delayed reflection pulse from the far end or a fault.

Length is calculated using the formula

$$L = \frac{c}{n} \frac{\Delta t}{2}$$

where c = velocity of light in free space

$$= 3 \times 10^8 \text{ meters/second}$$

n = effective refractive index of the optical waveguide core, typically 1.49 for graded index, fused silica.

The factor 2 in the denominator is due to the round trip of the pulse which has been reflected back. For fused silica with a graded index core, the factor $c/2n$ typically has the value 100.7 meters/microsecond.

Length may be determined by a direct readout from the display as shown in Figure 4.

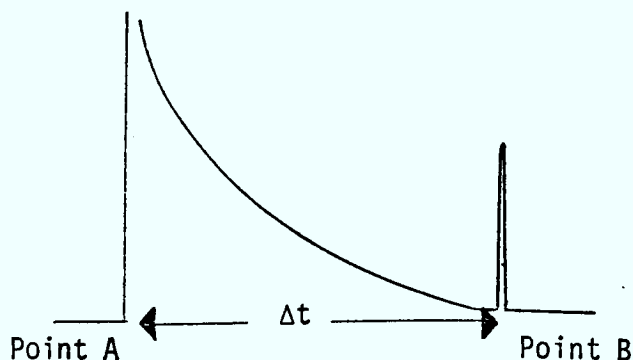


Figure 4

For example, if $\Delta t = 5.5 \text{ usec}$

$$L = 100.7 \times 5.5 = 554 \text{ meters}$$

A more accurate determination of the distance to a fault may be obtained by using the delay time base of the oscilloscope. By superimposing the far-end pulse on the initial pulse in delay mode, the time difference can be read directly from the setting of the delay position knob. Some oscilloscopes can provide a direct digital readout of delay time between two pulses.

- 7 -

TD-140-000289
Rev. A

Best results are obtained when the 50% points of the leading edges of the two pulses are aligned.

The same procedure may be used for determining distance to a localized fault or splice rather than to the end break.

Sources of Error

There are several possible sources of error when making length measurements including:

- 1) Index of Refraction - unless accurately specified is assumed to be 1.49
- 2) Cable Layout - The OTDR measures fiber length not cable length. The fiber typically follows a spiral path within the cable, cable layouts are not necessarily perfectly straight and some extra cable length occurs at splice enclosure points making it difficult to pinpoint the exact location of the fault within the cable.
- 3) Operator Error - Accurate readout of the oscilloscope trace may be difficult because of the noise on the signal or limited graticule resolution.
- 4) Timebase Error - The oscilloscope time base typically has an accuracy of $\pm 1\%$.
- 5) Pulse Distortion - When the total one-way loss between OTDR and the far ends of the cable is greater than 15 or 20 dB, the determined length may be greater than the actual due to pulse distortion resulting from the high APD gain needed.

Overall, the total expected error should be held to better than 5%.

This is usually not a problem since there are most likely reference points (splice locations) along the length of the fiber which can assist in accurately determining fault locations.

Measurement of Attenuation

The slope of the backscatter trace gives the fiber attenuation. In Figure 5, the loss between points X and Y is

$$\text{Loss} = -5 \text{ LOG } \frac{A_2}{A_1}$$

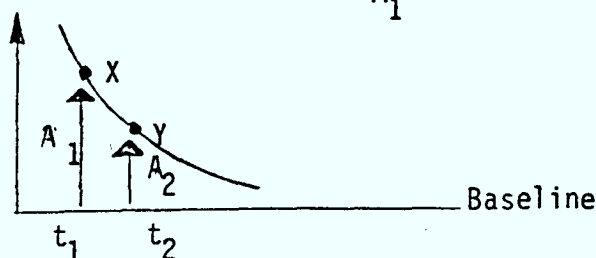


Figure 5

- 8 -

TD-140-000289
Rev. A

If one wishes to normalize this to 1 km

$$L \text{ (dB/km)} = -5 \text{ LOG } \frac{A_2}{A_1} \frac{1}{(t_2 - t_1) \times (.1007)}$$

$(t_2 - t_1)$ difference in μsec between points Y and X.

.1007 $c/2n$ factor $\text{km}/\mu\text{sec}$

For example, if $A_2 = 0.3$, $A_1 = 0.5$, $(t_2 - t_1) = 3 \mu\text{sec}$

$$L = 3.7 \text{ dB/km}$$

Measurement of Splice or Interconnection Loss

A splice or interconnection will typically appear as a localized drop in the backscatter signal amplitude. No change in amplitude or even a slight step increase in amplitude are possible. This can occur if the backscatter of the fiber past the splice point is higher than the backscatter of the fiber before the splice. In any case the splice loss is calculated by:

$$L = -5 \text{ LOG } \frac{A_2}{A_1}$$

As shown in Figure 6, the loss of the splice is calculated to be:

$$L = -5 \text{ LOG } \frac{.5}{.6} = 0.4 \text{ dB}$$

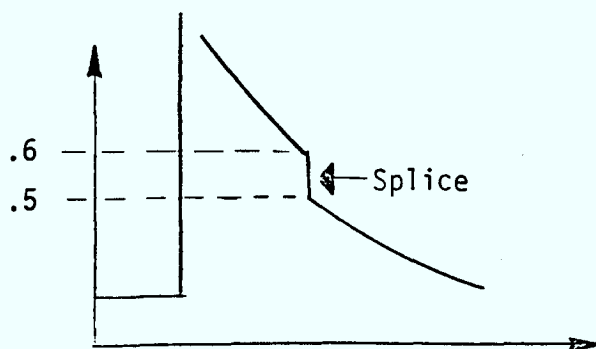


Figure 6

An accurate measurement may be difficult because of the noise level on the display especially when measuring in the "tail" of the backscatter signal.

Measurement on Short Lengths of Fiber

If the distance to a fault or break is less than about 50 meters from either end, the OTDR must be equipped with an additional length of fiber which serves as a delay line. This is necessary because the OTDR is unable to resolve closely spaced faults.

The pulse width of the Siecor Model 38 is 100 nsec nominal which, at best, can resolve down to 10 meters between two reflections. Since the initial front reflection typically overloads the detector for which some recovery time must be allowed for, the practical minimum distance to the first measureable reflection or loss is 50 meters.

The OTDR is set up with a fiber delay line of known length (minimum 50 meters) as shown in Figure 7.

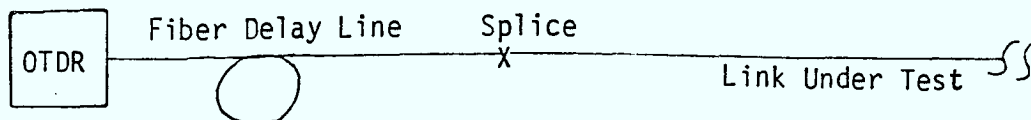


Figure 7

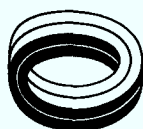
If distance/length measurements are being made, the known length of the fiber delay line must be subtracted from the total measured distance.

If measuring localized attenuation or splice loss in the link the delay line serves no purpose other than to position the splice point on the measurable part of the backscatter curve.



PART IV

CONCLUSIONS

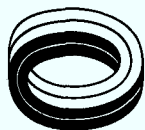


1.0 GENERAL CONCLUSIONS

This report has outlined the main objectives of this project and has detailed the method used to fulfill these objectives and the results obtained. It is fair to say that a large percentage of the specified objectives were completed and the success lies in the learning experience obtained by the manufacturers and CATV user which places into perspective how fibre optics meets the requirements of the CATV environment and no doubt has influenced the evolvement of more practical and improved systems.

In addition, the performance quality of the BCN system has been clearly demonstrated and the transfer of technology to a CATV environment proven.

The observations, which follow, pertain to the BCN system as reconfigured with one repeater mid-way between terminals and are based on the perspective as observed by the author.



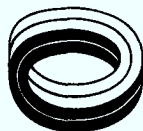
1.1 OBSERVATIONS

The observations derived from this report can be summarized as follows:

- a) The initial analysis that a 2R repeater is a cost effective solution has been proven ineffective. A 3R repeater, although more expensive initially, would in the long run reduce the maintenance effort and increase the performance quality of the system. Improved performance would mainly come about by the reduction in pulse width distortion and jitter causing inter symbol interference.
- b) Link feasibility is generally based on the results of link analysis determining the unallocated or safety margin available which accounts for breaks in the cable and other unforeseeable circumstances. Variations with temperature aging, etc., have been included in the calculation. It is quite reasonable to assume therefore that the analysis described in Part II Section 2.4 of this report requires improvement and may easily be the cause of bit error rate degradation.
- c) The successful completion of the acceptance testing has demonstrated that studio quality video can be transmitted over fibre optics. The design however, being state-of-the-art was plagued by unexpected spurious noise and as a result further research is required to nullify this interference.



-
- d) Handling and maintenance of the fibre optic system can be considerably improved by:
- i) mechanically designing the optical transmitter, receiver and repeater modules to be of the plug-in type.
 - ii) mechanically designing the splice enclosures as a fibre organizer and as a support for each of the splice packages providing a higher degree of protection upon re-entry during maintenance.
 - iii) utilizing fibre optic connectors manufactured with higher precision and which conform better to a field environment.



1.2 SYSTEM RELIABILITY

1.2.1 General

One can appreciate from the results of the equipment performance that it has been practically impossible to perform a proper reliability evaluation however, some estimate can be obtained in the form of predicted percent availability and yearly outage time for a one way video channel based on commercially available equipment.

This calculation uses individual equipment reliability figures which are Canstar's best estimate derived from other proven manufactured equipment. The estimated MTBF's of the key equipment are:

- a) Optical Transmitter - 25,000 hours
- b) Optical Receiver - 35,000 hours
- c) Optical 2-R Repeater - 70,000 hours
- d) Fibre Optic Cable - negligible relative to the above
(see discussion below)

Unavailabilities have been calculated uniformly with an MTTR of 3 hours taking into consideration automatic alarm reporting.

1.2.2 Reliability Models

The availability analysis of a fibre optic channel is straight forward using the model described by the equations given in the following paragraphs.



1.2.2 (cont'd)

It should be mentioned that these equations do not include the fibre unavailability which has been considered negligible compared to the unavailability of other elements of the model.

A large elongation of glass fibre during installation increases the probability of failure of fibre optic cables. Furthermore, a small residual elongation of fibre after installation accelerates the static fatigue of glass fibre and finally results in fibre failure. By measuring the change in modulation signal $\Delta\theta$, the elongation of glass fibre ΔL is obtained by equation (A)* below:

$$\Delta L = \frac{C \cdot \Delta\theta}{2\pi f N} \left\{ 1 - \frac{N^2}{2} \left[P_{12} - \nu (P_{11} + P_{12}) \right] \right\}^{-1} \quad (A)$$

where: f is the modulation frequency

N is the group refractive index of the fibre ($=n - \lambda \frac{dn}{d\lambda}$)

P_{11} is the element of strain-optic tensor ($=0.121$)

P_{12} is the element of strain-optic tensor ($=0.270$)

ν is Poisson's Ratio ($=0.17$)

C is the velocity of light

In order to prevent the fibre failure during the installation and obtain the long term reliability based on static fatigue due to residual elongation a smaller fibre elongation is desirable. The maximum strain within the cable is able to



1.2.2 (cont'd)

be estimated from the measured fibre strain when the sinusoidal distribution for the excess strain is assumed:

$$E(Z) = E_0 + \frac{\Delta E}{2} \left[1 + \sin \frac{2\pi Z}{P} \right] \quad (B)^*$$

where:

E_0 is the fibre strain under a static tension

ΔE is the maximum excess strain

P is the stranding pitch in the cable

Z is the coordinate along the fibre length

Based on this the maximum strain $E_{\max} = E_0 + \Delta E$ and is estimated to be 0.07% based on test data results $E_0 = 0.05\%$ and $\Delta E = 0.02\%$ during squeezing of the cable at a tension of 3000 Newtons. The maximum residual strain is also estimated about 0.2% after squeezing the cable six times at a tension of 8000 N.

In actual field installations cables are installed with a tension smaller than 3000 N and with fewer curved sections or bends per km than six (more than 2 bends is generally not exceeded). Therefore, a much smaller residual strain of optical fibre than the above value is expected in the actual application. Sufficient long term reliability can be expected when the installation conditions and the proof testing of optical fibres are appropriately designed.



1.2.2 (cont'd)

The estimated fibre lifetime without failure as a function of proof test strain is >30 years. The probability of failure for a fibre optic cable having a lifetime of 30 years is:

$$U \approx \frac{\text{MTTR}}{\text{MTBF}} \approx \frac{3}{262800} = 1.1 (10^{-5}) \text{ or } 1.1\% \text{ in } 1000 \text{ hours}$$

(refer to section 1.2.3 for definition)

Therefore, the fibre contribution to the total system unavailability has been judged non essential and neglected in the reliability models.

- * Reference: "Study on Mechanical and Transmission Characteristics of Optical Fibre Cable During Installation" by NTT & SEI.



1.2.3 Formulas

The availability of a one channel system is given by:

$$A = 1 - U_S \quad (1)$$

where U_S is the unavailability (failure rate) of the total system modelled as a chain of equipments whose failure determines the system failure.

In the case of a one-way fibre optic channel:

$$U_S = U_P + U_T + U_R + m U_{REP} \quad (2)$$

where:

U_S is the one-way channel unavailability

U_T is the unavailability of an optical transmitter

U_R is the unavailability of an optical receiver

U_{REP} is the unavailability of an optical repeater

m is the number of repeaters in the section

U_P is the unavailability of the fibre optic cable

The unavailability (failure rate) U of any equipment with:

mean time between failures = MTBF

mean time to repair = MTTR

is given by:

$$U = \frac{MTTR}{MTTR + MTBF} \approx \frac{MTTR^*}{MTBF}$$

* Reference: ITT-Reference Data for Radio Engineer, Section 43-27



Since the unavailability of the fibre optic cable is negligible and the number of repeaters is equal to one, therefore equation (2) becomes,

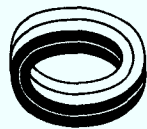
$$\begin{aligned} U_s &= U_T + U_R + U_{REP} \\ &= \frac{3}{25000} + \frac{3}{35000} + \frac{3}{70000} \\ &= 2.486 \times 10^{-4} \end{aligned} \quad (3)$$

Substituting in equation (1) the availability of one fibre optic channel is 99.975%.

The outage time t in minutes per year of a fibre optic channel is given by:

$$t = 525600 \times U = 130 \frac{\text{Minutes}}{\text{Year}}$$

Hence, the availability of 6 fibre optic channels becomes 99.85% with an outage time of 784 minutes per year.



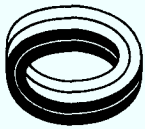
2.0 ECONOMICS OF FIBRE OPTIC SYSTEMS

The demand for fibre optic systems is rapidly increasing especially in the telecommunication market segment. In this area, fibre optic is extremely attractive when system planning is based on 10 year growth periods. As a result volume production is created and encourages further cost reduction for optic systems.

This progression will certainly affect favourably the economics of CATV fibre optic broadband applications.* However, beyond economic features, fibre optics offers advantages in performance and capacity. As technological advances overcome the limitations of transmitting CATV signals over fibre optics further cost reductions are expected.

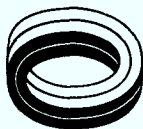
Regardless of this steady decline in cost of fibre optic systems the requirement of studio quality video performance for CATV applications depends on high resolution video codec equipment which dramatically elevates the terminal equipment

* Baseband (as apposed to broadband) systems are more economical for applications involving low aggregate data rates, about 3 Mb/s or less, over short cable lengths, 1 to 2 km or less, since no data modulation onto RF carriers are required.



2.0 (cont'd)

costs making systems of this nature presently non-competitive
with regard to a coaxial alternative.



2.1 FIBRE OPTIC COST PROJECTION

Market surveys indicate that world wide fibre optic systems for video applications was \$15 million dollars for the year 1981 and its projected growth is to \$116 million dollars (in present day dollars at time of analysis) by 1986. As a percentage of the total market it will increase from 10 to 12 percent. Figure 2.1.1 illustrates the world wide fibre optic market forecast segmentation by various facilities.

Most CATV applications remain confined to transmission between company facilities while widespread interface to subscriber equipment is still not feasible. Future applications include using fibre optic technology in home information services, picture telephones, etc., wherever high data transmission becomes unsuitable via copper cables.

Projected costs analysis shows a steep decline in fibre, cable and optical components. This is illustrated in Figure 2.1.2 to 2.1.5 below.

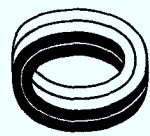


Figure 2.1.1
FIBER OPTIC MARKET FORECAST
CUMULATIVE BY END USER(Worldwide, All Product Types)

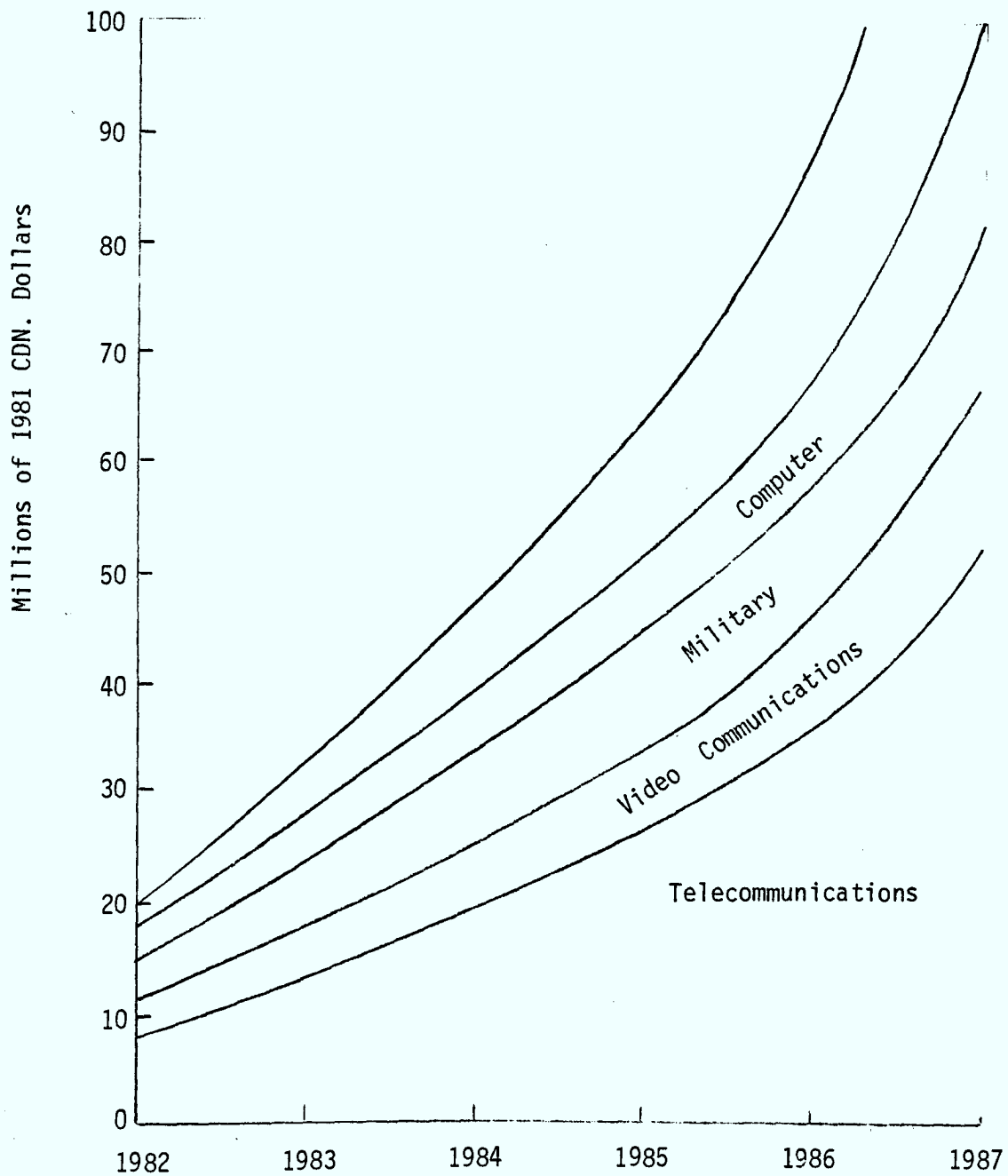
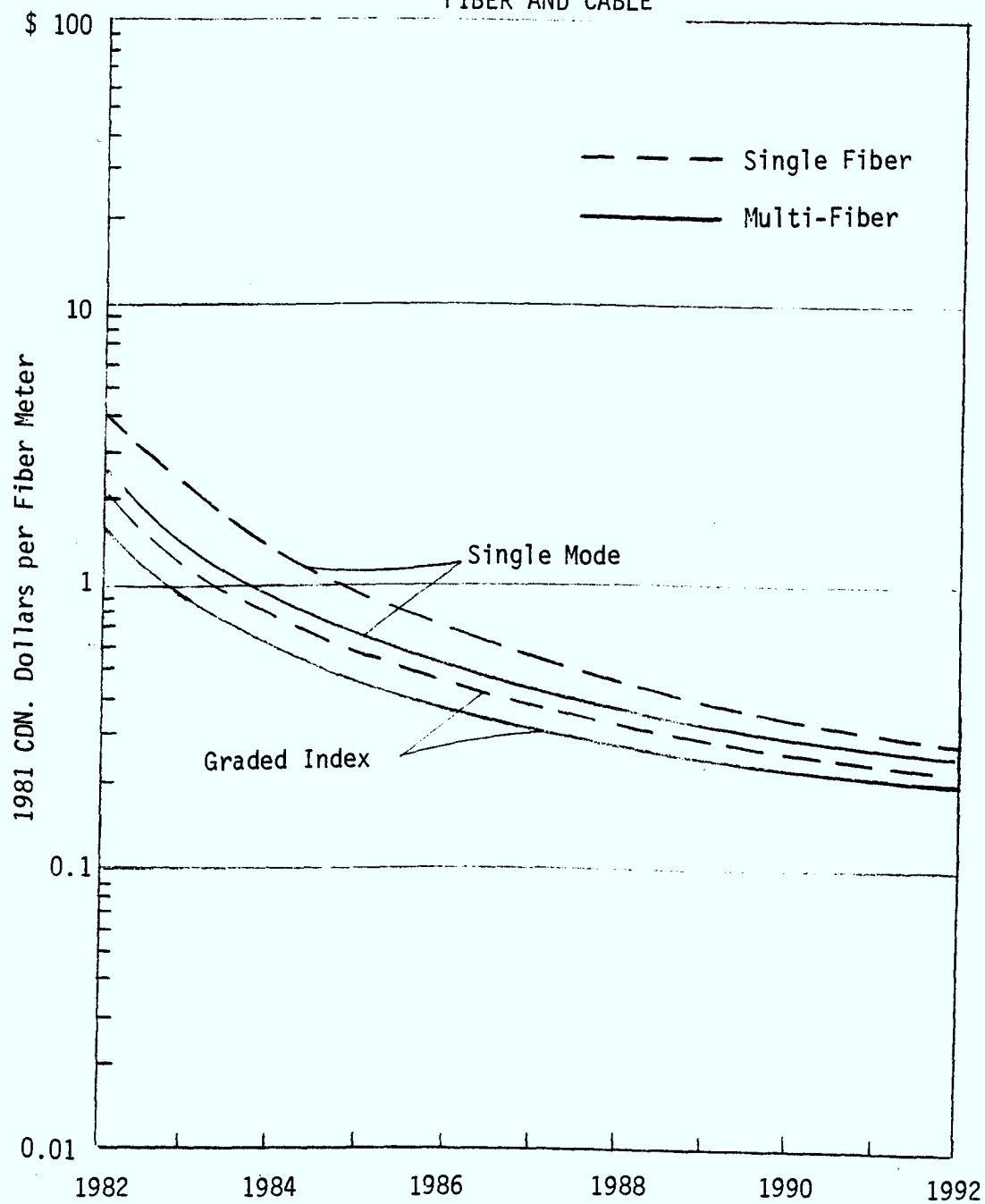




Figure 2.1.2
AVERAGE SELLING PRICES
FIBER AND CABLE



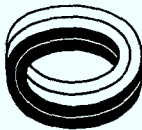


Figure 2.1.3
AVERAGE SELLING PRICES
EMITTERS

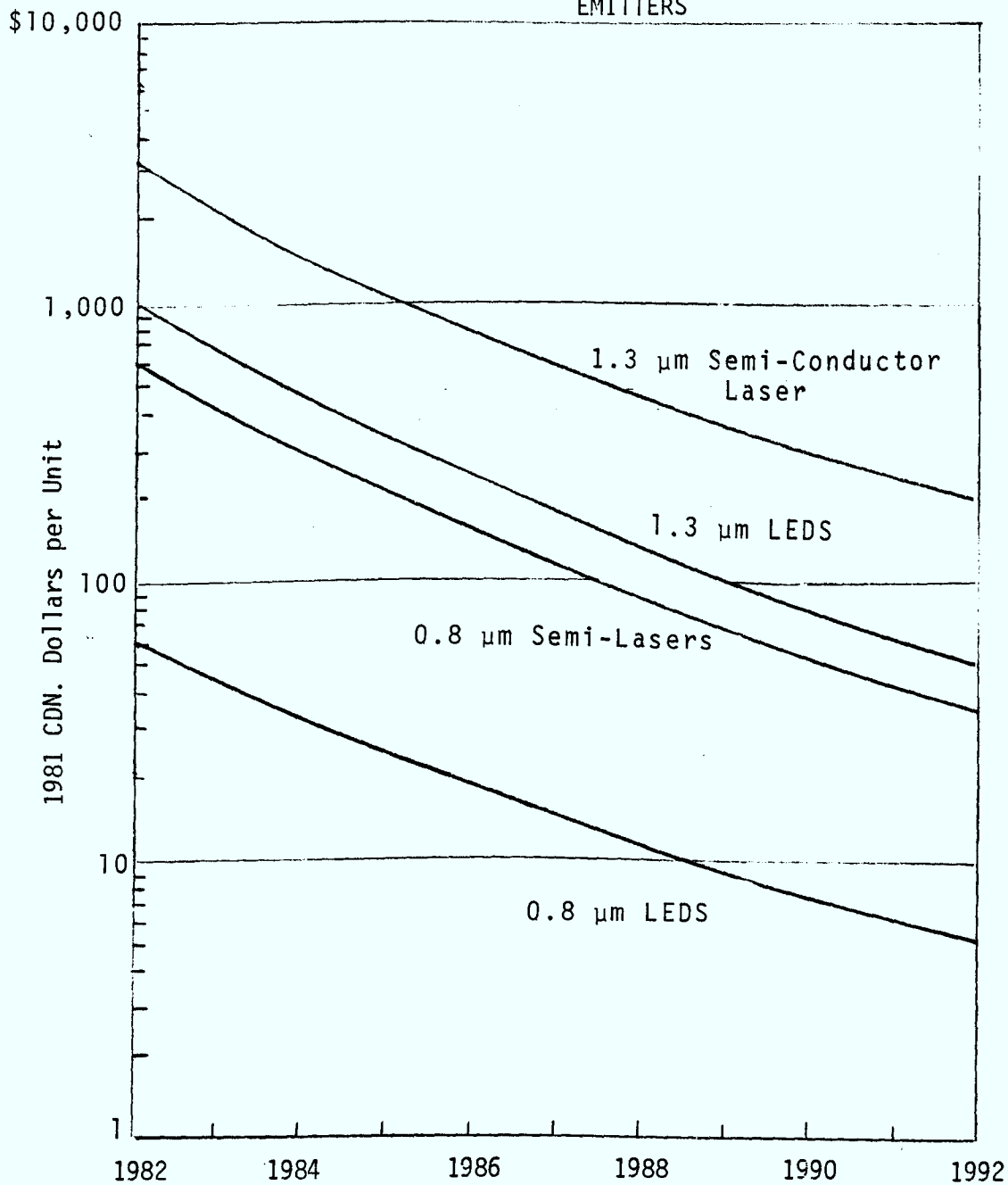




Figure 2.1.4
AVERAGE SELLING PRICE
DETECTORS

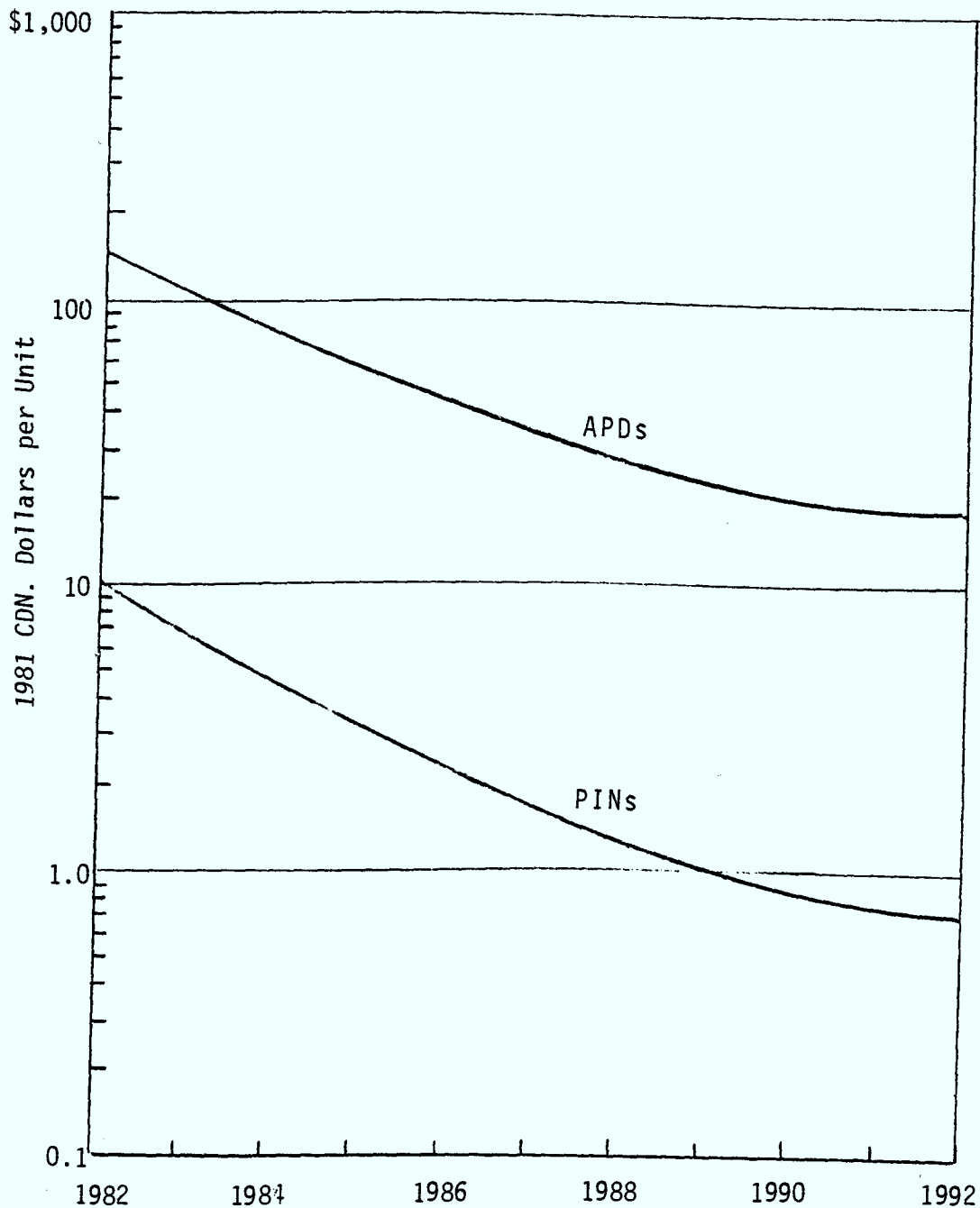
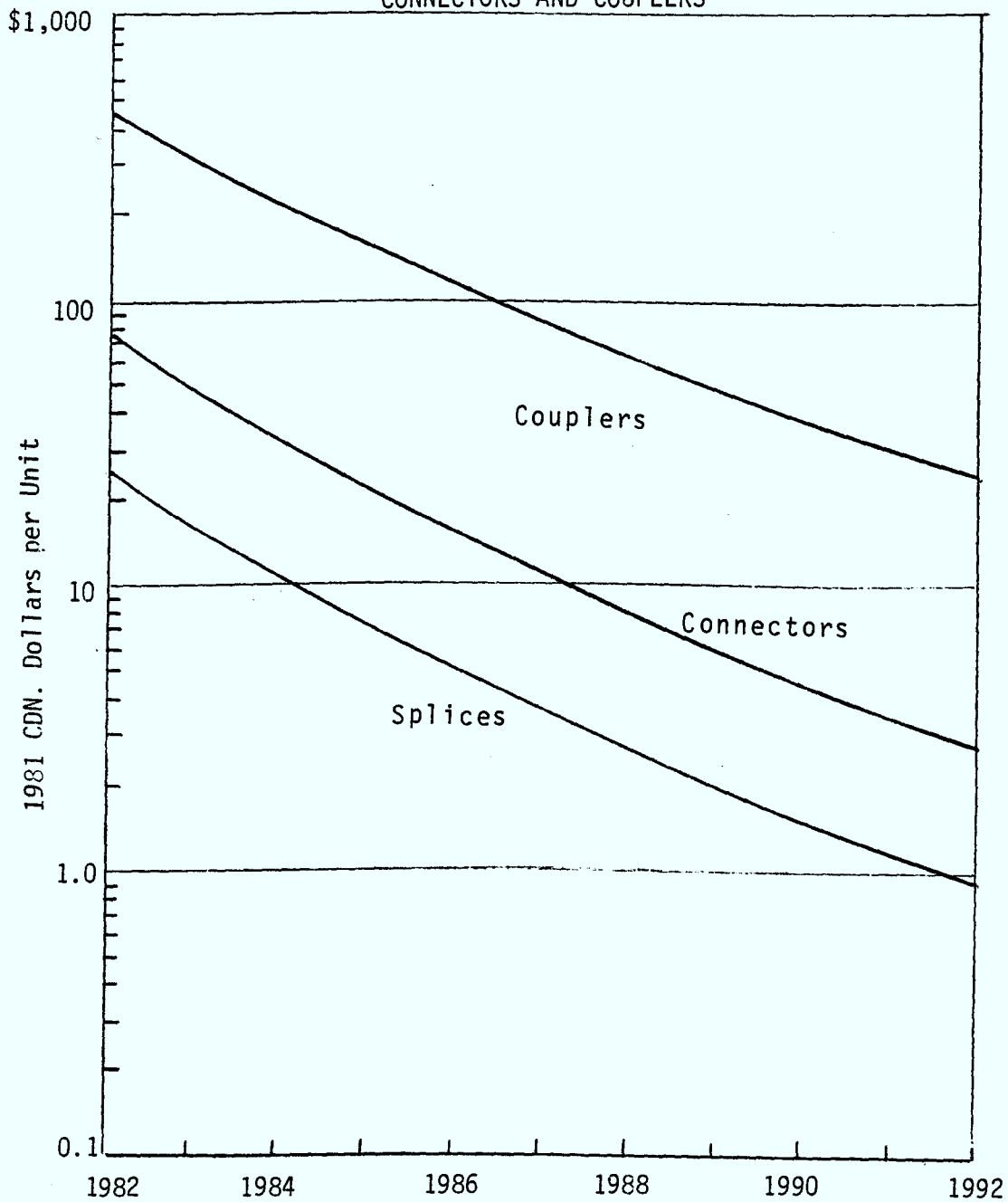




Figure 2.1.5
AVERAGE SELLING PRICES
CONNECTORS AND COUPLERS



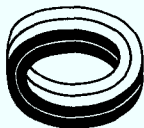


2.2 ALTERNATIVE FIBRE OPTIC SYSTEM DESIGN

Alternative fibre optic system designs are discussed in this section. The main impact of the designs chosen is the utilization of equipment which operate at standard digital transmission rates and maintain studio quality video performance. A single mode transmission scheme has been suggested since it is expected to be the near future solution to long-haul high bandwidth requirements and is considered as a useful development for a field trial system.

2.2.1 System Description

The block diagrams below illustrate three possible alternatives for transmission of broadband video signals. Figure 2.2.1 represents a point-to-point link of up to 16.5 km using single mode components and digital codecs for CATV transmission quality. Figure 2.2.2 is identical however, the digital codecs shown are for broadcast quality transmission standards. In both cases the digital multiplexers operate in the standard North American digital hierarchy T3 to T4 with an optical terminal interface at T4. Receiver sensitivity shown in the link feasibility is for 10^{-9} operation. Figure 2.2.3 is an example of how wavelength division multiplexing is implemented using optical filters. Because of the broad spectral response of available optical fibers several optical wavelengths, each representing a separate communication signal can be transmitted simultaneously over a single fibre. Thus through the use of WDM expansion of the capacity of optical fibre transmission systems does not



2.2.1 (cont'd)

necessarily require additional cable capacity. The WDM key components consist of:

- a) fiber
- b) laser/APD
- c) WDM filter

Fibres with large spectral response covering the range from 800 to 1500 nm can be used. A typical spectral response curve of the fibre is illustrated in Figure 2.2.4. For keeping as low as possible the attenuation of the cable, wavelengths such as 1.3, 1.5 and 1.55 μm may be considered.

Long wavelength Injection Laser Diodes (ILD) can be manufactured with a variety of emission wavelengths. By changing the relative concentration of the two constituents of a InGaAsP/InP device, peak emissions in the whole range from 1100 to 1500 nm are obtained. The same is true for optical detectors. Germanium avalanche photo diodes are available for the 1100 to 1500 nm region offering fair sensitivity in the wavelength region that corresponds to the available emission wavelength of optical sources.

Present basic types of wavelength division multiplexers-demultiplexers are:

- a) prism
- b) diffraction grating
- c) multiple reflection and interference filter

The multiple reflection and interference filter offers low insertion loss and good stability relative to temperature variation, mechanical vibration and aging.

Figure 2.2.5 illustrates the FM stereo FOTS configuration.



HEAD END

HUB END

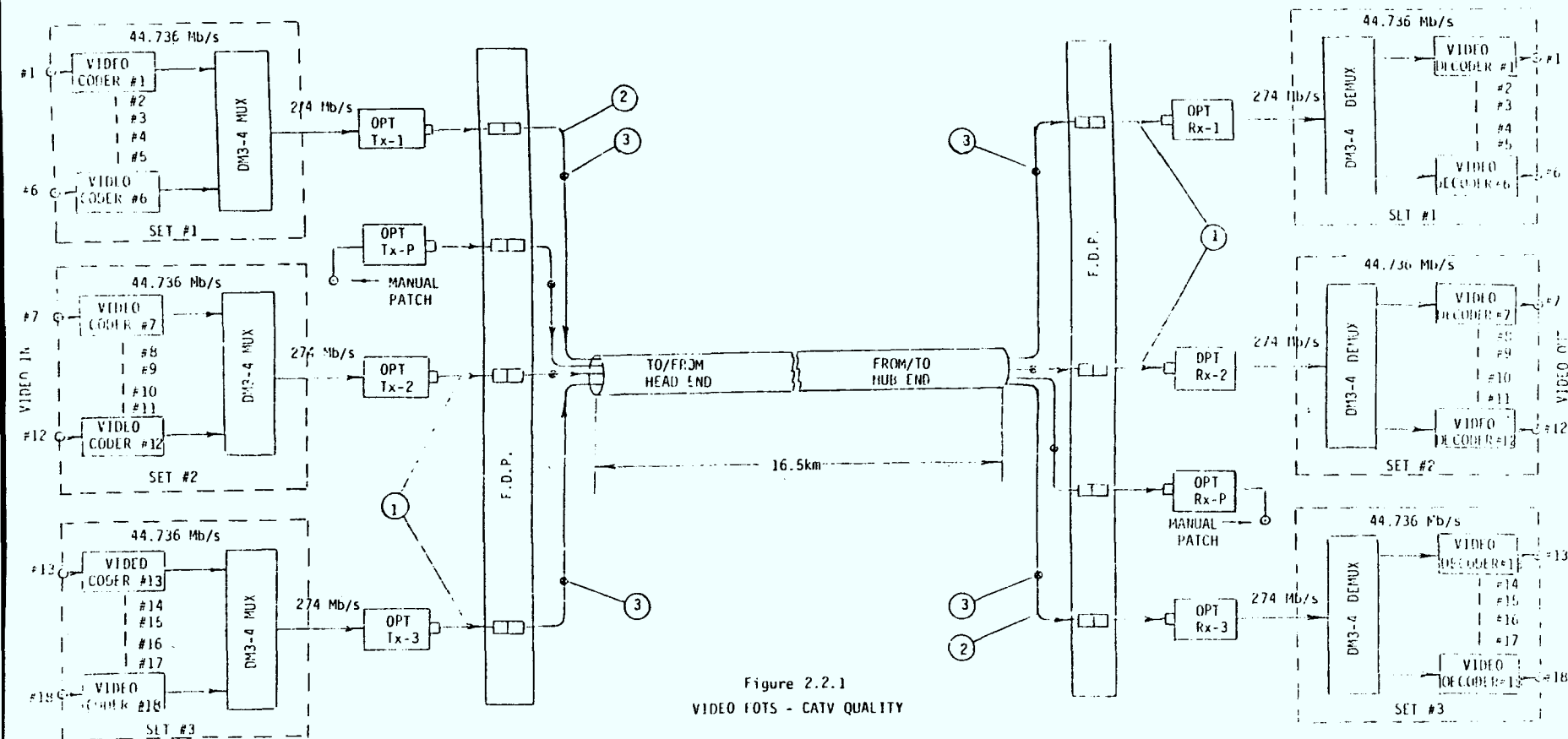


Figure 2.2.1
VIDEO FOTS - CATV QUALITY

Notes:

1. FIBER PATCH CORD
2. FIBER PIGTAIL CORD
3. SPLICE

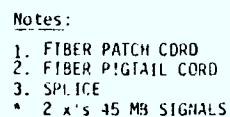
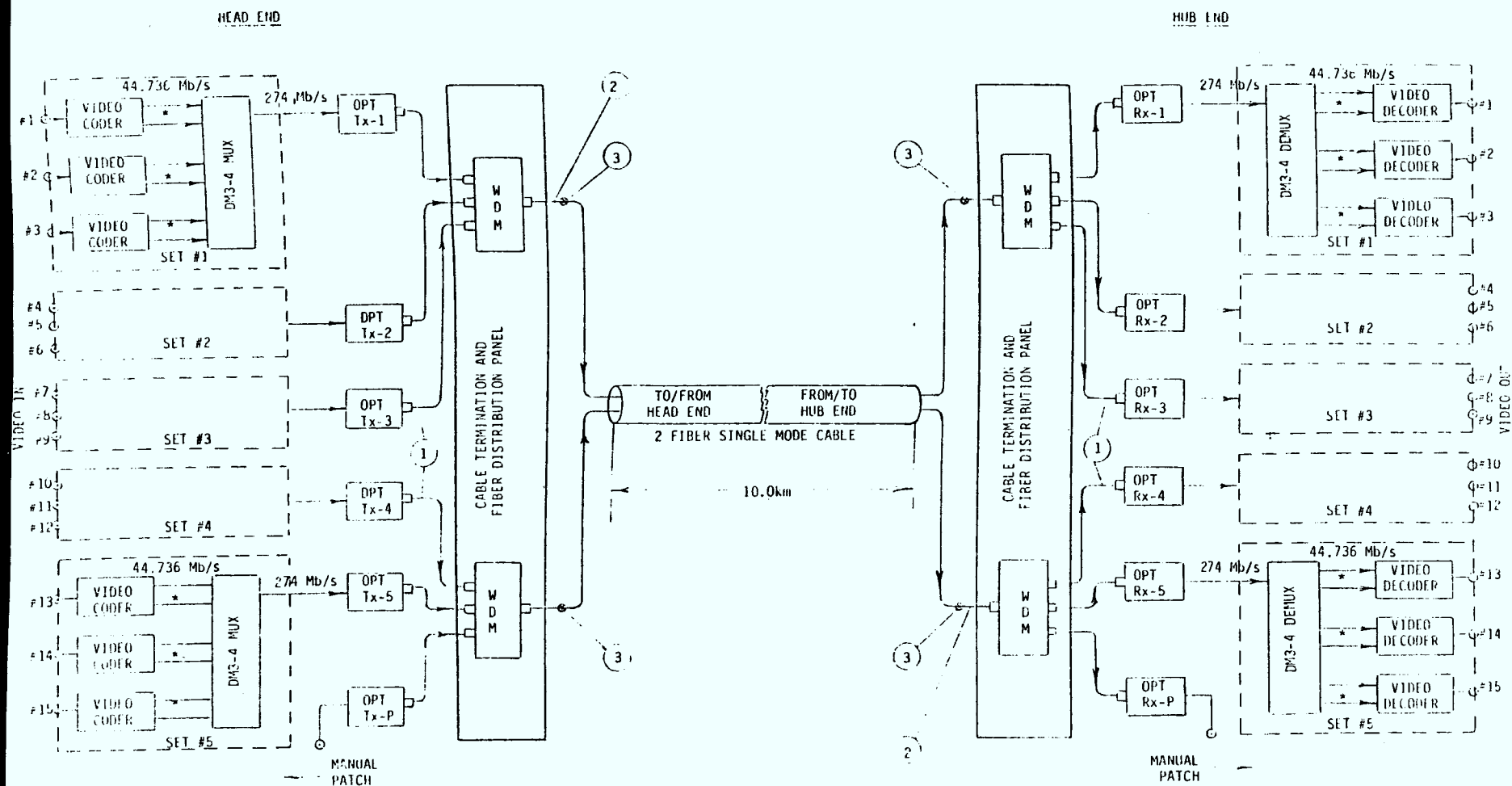


Figure 2.2.2
VIDEO FOTS - BROADBAND QUALITY



Notes:

1. FIBER PATCH CORD
2. FIBER PIGTAIL CORD
3. SPLICE
- * 2 x's 45 MB SIGNALS

Figure 2.2.3
VIDEO FOTS WDM

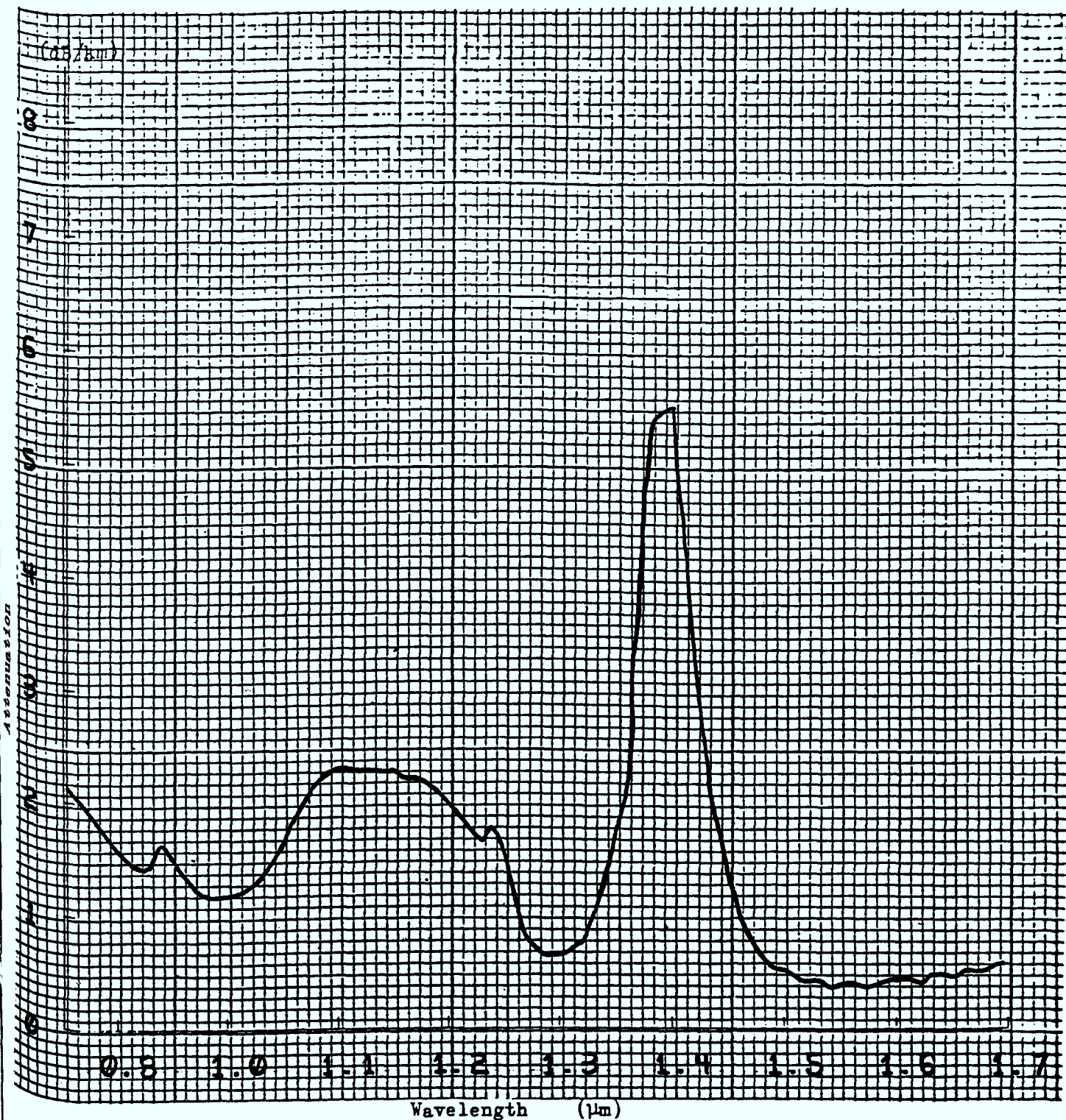


FIGURE 2.2.4 Typical Attenuation Curve Of Monomode Fibre With Wavelength (0.85 - 1.6 μm)

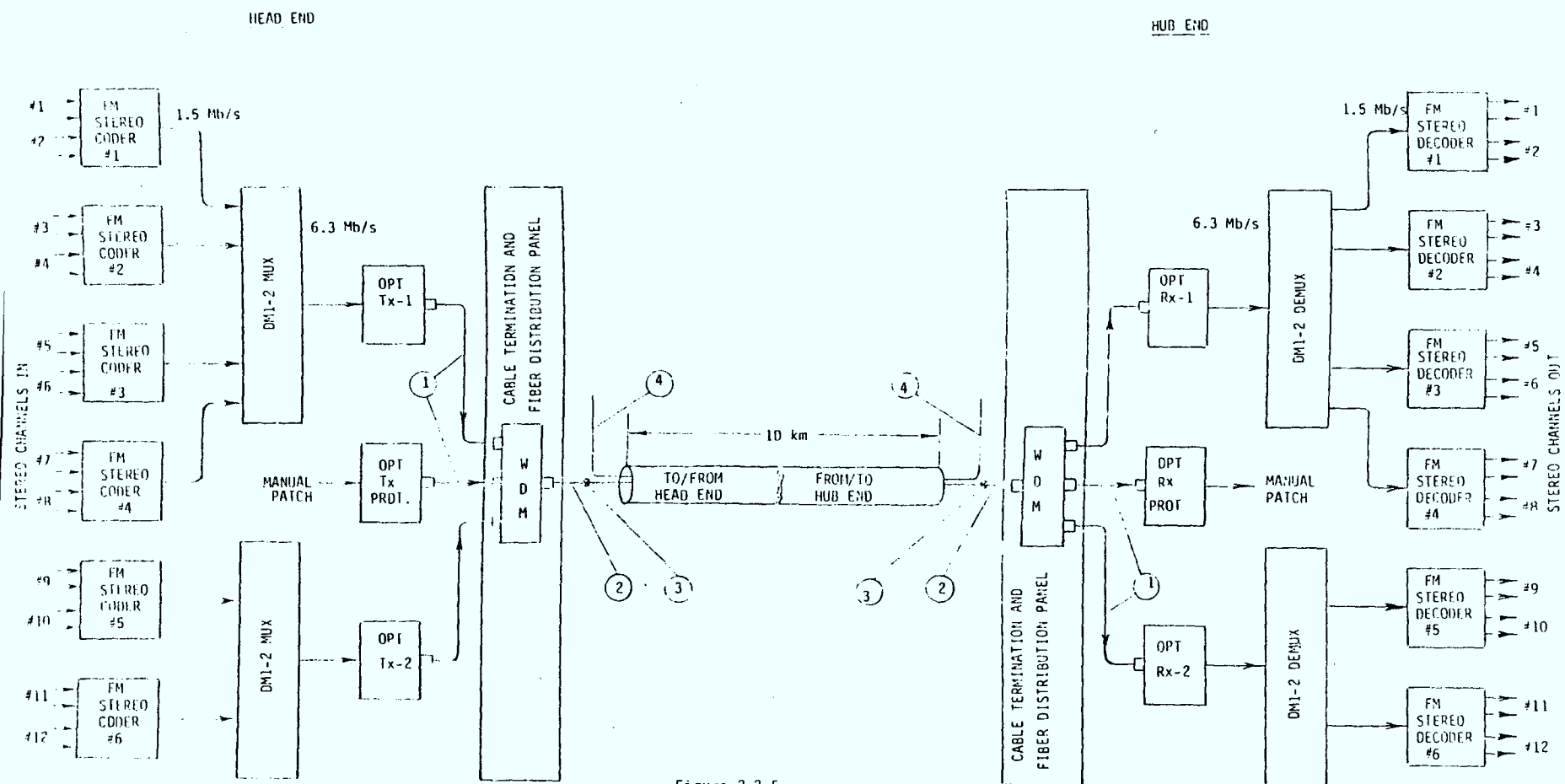
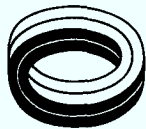


Figure 2.2.5
FM STEREO FOTS WDM

- Notes:
1. FIBER PATCH CORD
 2. FIBER PIGTAIL CORD
 3. SPLICE
 4. SPARE FIBER

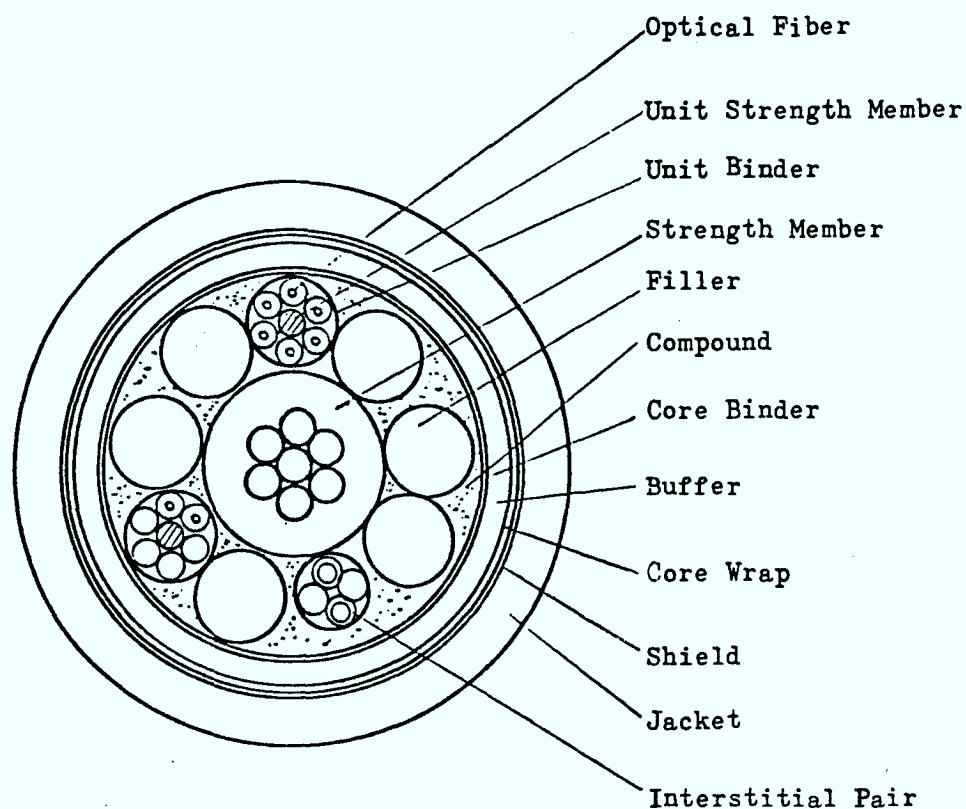


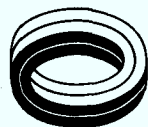
2.2.2 Fibre and Cable Structure

The structure of the monomode fibre is described in the table below:

GLASS FIBER	CORE	MATERIAL	DOPED SILICA GLASS
		NA	NOM. 0.09 ± 0.01
		DIAMETER	NOM. $8 \pm 2 \mu\text{m}$
	CLADDING	MATERIAL	SILICA GLASS
DIAMETER		NOM. $125 \pm 3 \mu\text{m}$	
COATING	PRIMARY (BUFFER)	MATERIAL	SILICONE RESIN
		OUTER DIAMETER	APPROX. 0.4 mm
	SECONDARY (JACKET)	MATERIAL	NYLON
		OUTER DIAMETER	$0.9 \pm 0.1 \text{ mm}$

The typical cross-sectional cable design using monomode fibre is illustrated below:





2.2.3 Video Codec Parameters

A. CATV Quality

1. Video Encoding

Video Input/output	Standard NTSC color/monochrome television signal: 1 Vp-p (75 Ω , unbalanced)
Sampling Frequency	9 MHz
Coding Algorithm	High-order predictive coding
S/N Ratio	55 dB (CCIR weighted)
Field Time Waveform Distortion	4 IRE
Line Time Waveform Distortion	3 IRE
Short Time Waveform Distortion	10 IRE
Chrominance Luminance Gain Inequality	5 IRE
Chrominance Luminance Delay Inequality	33 ns
Differential Gain	4 %
Differential Phase	1.5 %

2. Line Interface

Bit Rate	44.736 Mb/s \pm 20 ppm
Impedance	75 Ω unbalanced
Code Format	B3ZS
T3 Framing Bit	Optional

3. Power Requirements

AC 117V \pm 10%
Current 2A, max.

4. Environmental Specifications

Temperature	5 $^{\circ}$ to 40 $^{\circ}$ C (40 $^{\circ}$ to 100 $^{\circ}$ F)
Humidity	Up to 80%



2.2.3 (cont'd)

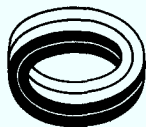
B. Broadcast Quality1. Video Encoding

Video Input/Output	Standard NTSC color/monochrome television signal, 1 Vp-p/75 Ω
Sampling Frequency	10.7 MHz (3 FSC)
Coding Algorithm	Higher order predictive coding
S/N Ratio	56 dB (non-weighted)
Field Time Wave Form Distortion	2 IRE
Line Time Wave Form Distortion	1.5 IRE
Short Time Wave Form Distortion	4 IRE
Chrominance Luminance Gain Inequality	4 IRE
Chrominance Luminance Delay Inequality	\pm 30 ns
Differential Gain	2 %
Differential Phase	1 Degree

2. Line Interface

Bit Rate	44.736 Mb/s x 2 (DS3 x 2)
Code Format	B3 ZS
Impedance	75 Ω Unbalanced

3. Power RequirementsAC 117V \pm 10%



2.2.3 (B) (Cont'd)

4. Environmental Specifications

Temperature	5° to 40°C (40° to 100°F)
Humidity	Up to 80%

2.2.4 DM3-4 Digital Multiplexer1. Signal Characteristics

Bit Rate	274.176 Mb/s
Line Code	B3 ZS
Stability	± 10 ppm
Nominal Level at X-Connect	5.7 dBm (all ones signal)

2. Multiplexing Characteristics

No. of DS-3 Channels	6
Multiplexing Efficiency	97.9%
Jitter (max B-B output jitter)	21 degrees
Max Transmitter Input Jitter	106 degrees
Max Receiver Input Jitter	493 degrees
Max Receiver Output Jitter	116 degrees
Forward Guard Time	13 µSec max
Reframing Time	102 µSec max



2.2.5 Optical Terminal

2.2.5.1 Optical Source

Type	InGaAsP [™] double-heterostructure
Wavelength	Approximately 1.3 μm
Spectrum Width	< 5 nm
Output Power (peak)*	-0.5 dBm
Threshold Current	\approx 80 mA
Operating Speed	> 600 MHz

* Measured with 10 μ -core single mode optical fibre

2.2.5.2 Optical Detector

Type	GE-APD
Quantum Efficiency	> 0.6 ($\lambda = 1.3 \mu\text{m}$)
Excess Noise Factor (*)	< 1.0
Coupling Loss (with fibre)	< 0.3 dB

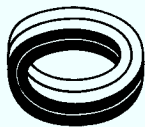
2.2.5.3 DSX-4 Interface

Line Rate	274.176 Mb/s \pm 10 ppm
Line Code	B3ZS

2.2.5.4 Line Interface

Optical Wavelength	1.3 μm (nominal)
Bit Rate	276.352 Mb/s
Line Code	Scrambled unipolar with 50% duty cycle (optical pulse)
Average Output Power*	-4.5 dBm
Receiver Sensitivity (BER @ 10^{-9})	-30.7 dBm

* Measured with 10 μ -core single mode optical fibre



2.2.5.5 Power Requirement

Source	- 48 Vdc \pm 25%
Consumption	300 W max

2.2.5.6 Environment

Operating Temperature Range	5°C to 40°C
Relative Humidity	Maximum 95% at 40°C

2.2.6 Link Feasibility

A. No WDM

Data

1. Link Length	X km
2. Unit Cable Length	1.7 km
3. Cable Loss	0.6 dB/km
4. No. of Connectors	2

System Gain

5. Average Source Power Output	-4.5
6. Receiver Sensitivity @ BER 10^{-9}	-30.7
Total gains	26.2

System Losses

7. Total Cable Loss @ 0.6 dB/km	0.6(x)dB
8. Total Connector Loss @ 1.0 dB/km	2.0 dB
9. Total Splice Loss @ 2.0dB/km	0.2(x)dB
10. Cable Temp. Degradation @ 0.1dB/km	0.1(x)dB

A. System Losses (cont'd)

11. Equipment Aging & Temperature Degradation	3.0dB
<hr/>	
Total Losses	$5 + 0.9x$
Unallocated (safety) margin	5dB

therefore,

$$26.2 - 5 + .9x = 5$$

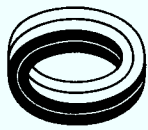
$$x = 18.0 \text{ km}$$

B. With WDMData

1. Link Length	X km
2. Unit Cable Length	1.7 km
3. Cable Loss	0.6 dB/km
4. No. of Connectors	2

System Gain

5. Average Source Power Output	-4.5
6. Receiver Sensitivity @ BER 10^{-9}	-30.7
<hr/>	
Total Gains	26.2



B. System Losses (cont'd)

8. Total Cable Loss @ 0.6 dB/km	0.6 (x) dB
9. Total Connector Loss @ 1.0 dB/km	2.0 dB
10. Total Splice Loss @ 0.2 dB/km	0.2 (x) dB
11. Cable Temperature Degradation @ 0.1 dB/km	0.1 (x) dB
12. Equipment Aging & Temperature Degradation	3.0 dB
13. WDM Coupling Loss	7.0 dB
<hr/>	
Total Losses	12 + 0.9 x
Unallocated (safety) margin	5 dB

therefore,

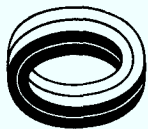
$$26.2 - 12 + 0.9 x = 5$$

$$x = 10.2 \text{ km}$$



PART V

APPENDIXES



APPENDIX 1

The Phenomenon of Modal Noise in Analog And
Digital Optical Fibre Systems by: R.E. Epworth

THE PHENOMENON OF MODAL NOISE IN ANALOGUE AND DIGITAL OPTICAL FIBRE SYSTEMS

R.E. Epworth
Standard Telecommunication Laboratories Limited, Harlow, Essex

Summary

The signal-to-noise ratio obtainable at the receiver of a multimode optical fibre system may in some circumstances be dominated by an effect called 'modal noise'. It appears as unwanted amplitude modulation of the received signal and is extremely sensitive to physical distortion of the fibre. From observations it appears that conditions giving rise to modal noise are, (1) narrow source spectral width, (2) variable spatial or modal filtering. The performance impairment due to a misaligned joint may be far greater than that due to the loss of received power alone, thus rendering large operating margins ineffective as a means of overcoming such defects. The paper describes how to avoid modal noise.

1. Observed Phenomena

We have observed noise in both analogue and digital optical fibre transmission systems which is not related to shot or thermal noise. This noise occurs when 'good' narrow spectrum injection lasers (20 μm) stripe [1] are used as the source, and it is a function of the characteristics of the fibre, joints and the source. It appears as unwanted amplitude modulation of the received signal, the depth of this modulation being extremely sensitive to slight mechanical distortion of the fibre. We call this phenomenon 'modal noise'.

Fig. 1 shows an 'eye' diagram of a 140 Mbit/s system in which one fibre-to-fibre joint has been deliberately misaligned. This misalignment is sufficient to produce about 10 dB of loss, yet the system margin is so large that the error rate should be negligible. However, modal noise is causing considerable 'eye' closure, resulting in a poor error rate. It is worth noting that it is modulation of the amplitude rather than the addition of noise, the effect being dominantly in the 'one' level (c.f. shot noise). The sensitivity to mechanical distortion may be seen in Fig. 2, which clearly shows the fluctuations in amplitude over a period of one second, caused by slight bending of the fibre before the misaligned joint. (The apparent modulation of the 'zero' level is due solely to the lack of d.c. response of the receiver.)

The effects of modal noise can be conveniently demonstrated by modulating the laser with a low frequency (250 kHz) square wave as in Fig. 3, simulating a sequence of successive 'ones' in an NRZ (non-return-to-zero) code. This process was found to produce much more distinct repetitive waveforms. The top trace is a monitor of the total power out of a short fibre tail connected to the laser. The middle and lower traces are the output from a receiver which is connected via a second fibre to the first and in both cases the fibre-to-fibre connection is misaligned to give a significant and identical loss. To emphasise the effects, the zero level power was set one-half the one level power. The middle trace shows gross distortion of the waveform even to the extent of a temporary reversal of polarity on the positive-going edge. By slight manipulation of the fibre before the misaligned connector or adjustment of the connector itself (without decreasing the mean attenuation), it was possible to produce the lower trace or an almost infinite variety of waveforms similar to the middle trace.

When the laser modulation was adjusted to give a more realistic extinction ratio, i.e. biased just below threshold and the

modulation frequency reduced even further, then waveforms were produced such as Fig. 4. This waveform was obtained with the laser launching into 1 kilometre of graded-index fibre, the far end of which was joined to a 1 metre fibre tail by an adjustable connector, which was deliberately seriously misaligned to give 10 dB excess loss (as will be evident later, very much smaller values of excess loss can still be a problem). This short tail was coupled to the receiver photodetector. Observe that the pattern appears to be bunched up at the leading edge of the pulse; this will be discussed in more detail later. The peak-to-peak amplitude deviation during the 'one' level, x , is in this case approximately equal to the mean amplitude, y , of the pulse itself. It is possible to manipulate any part of the fibre before the misaligned connector in order to minimise or maximise the amplitude modulation. If we measure the worst (i.e. highest) ratio $x:y$ obtained for increasing levels of misalignment loss, then we obtain a curve as in Fig. 5. It is clear that relatively low misaligned connector losses cannot be tolerated even for a binary code, unless modal noise can be prevented from occurring.

Analogue optical transmission systems generally have a higher capacity per transmission bandwidth, but require high received power levels when compared with digital systems. For this reason the greater source power available from lasers compared with LEDs makes them quite attractive (providing that the linearity and other problems can be overcome). If we consider the implications of modal noise on analogue systems then it will be quite clear from Figs. 3, 4 and 5 that a simple intensity modulation system would be impractical with these lasers (generally, non-linearity already precludes this for 20 μm stripe lasers). Fig. 4 already looks like video! The various pulsed analogue modulation systems (e.g. PPM, PPM, PIM) seem more practical for non-linear lasers so we performed measurements of the signal-to-noise ratio obtained with 70 MHz 50% duty cycle modulation, biased above threshold (to minimise non-linearities resulting from turn-on delay which is dependent on the interpulse period). Fig. 6(a)(b) shows the results which, as with the previous experiments, are extremely dependent on the precise physical position of the fibre before the connector and the connector itself. In general, only the measurement of the lowest C/N is satisfactory for system design, but it is interesting to note the range of values obtained. These curves show clearly that there would be very large C/N penalties produced by modal noise in such a system, particularly with misaligned connectors.

It is clear that if modal noise is to be eliminated then the mechanism by which it is generated must be understood.

2. The Effect Of Interference Patterns On Fibre Joint Loss

When light from a monochromatic source such as a HeNe laser is launched into one end of a length of multimode fibre, then the light emerging from the far end will have near and far field intensity distributions of which Fig. 7 and Fig. 8 are typical (the fibre was 50 μm core, graded index). These 'speckle' patterns are produced by interference between the various modes, each of which is subjected to slightly different delays through the fibre ('mode dispersion'). Readers interested in the mathematics of these patterns are recommended to study the work of Crosignani, Daino and DiPorto [2] who have measured modal dispersion from the near field speckle patterns of fibres. The position of the individual speckles is extremely sensitive to physical distortion of the fibre, due to changes in the local refractive index, and this effect has been studied and made use of in an optical fibre data collection highway by Davis & Kingsley [3].

Fig. 9(a) and (b) shows respectively the effect variations in near and far field patterns produced by slightly different physical bending at one place in the fibre. Similar pattern changes may be caused by very small changes in source wavelength. It is interesting to note the similarity of the near and far field patterns. The number of speckles in either of these patterns is proportional to the number of modes propagating in the fibre. Therefore, a large core will have more speckles than a small core; step index fibre will have more than graded index fibre, and high N.A. fibre will have more than low N.A. fibre if the numerical aperture is filled. Compare Fig. 10(a), (b), which are near and far field patterns for 350 μm 0.4 N.A. step index fibre, with Fig. 9(a), (b), which are for 50 μm core 0.2 N.A. graded index fibres: these patterns scale with λ .

If a fibre is joined to another similar fibre but with axial misalignment and monochromatic light is launched, then only the speckles within the circle drawn on Fig. 7 will be coupled to the second fibre. Alternatively, if there is a longitudinal alignment error then only the speckles within the circle drawn on Fig. 8 will be coupled (the size of the pattern with respect to the fibre end will be proportional to the separation and the numerical aperture). In practice there may be a combination of near and far field effects.

It can be seen from Figs. 7 and 8 that a linear displacement of one fibre will not produce a smooth change in coupled power (as would occur with white light illumination), but instead an irregular one depending precisely on what the pattern is at the time of the experiment. Thus a joint with fixed misalignment will have a loss which will vary with changes in source wavelength and with physical distortion of the fibre before that misaligned joint.

The foregoing discussion of interference effects assumes a monochromatic source

such as a HeNe laser, but injection lasers can be far from monochromatic when directly modulated. To help understand the effects of the source spectra, consider the near field images of the fibre ends whilst illuminated by a monochromatic source. Under these conditions a near field speckle pattern with very large grain structure is produced. However, if the fibre is physically distorted, it is possible to produce an average of a number of superimposed speckle patterns. Fig. 11(a) is an individual speckle pattern of a 350 μm core plastic clad silica fibre under static conditions showing little evidence of surface damage. Fig. 11(b) is the average of six successive exposures, each with different physical distortion of the fibre, and it should be noted that some surface damage is now apparent. Similar results would be obtained by simultaneous illumination with six monochromatic sources (or one source with six narrow lines in its spectrum). Fig. 11(c) was a long exposure of the continuously varying speckle pattern produced when the fibre was subjected to a slowly varying distortion. Nearly all trace of the speckle pattern has disappeared, leaving a fairly reasonable image of the fibre end and the damage can now be seen more clearly. Similar results can be obtained by increasing the spectral width, either by sweeping the source wavelength during the measurement interval or by phase modulating the light, which is what occurs when the fibre is flexed [3].

Fig. 12(a) and (b) show the results for a 50 μm core vapour-deposited, graded-index fibre with light deliberately launched into the core-cladding interface to make both core and cladding visible (consequently the speckle pattern in the core is not representative of normal launch conditions, c.f. Fig. 7). The speckles at the centre of the core are smaller than at the edge due to the variation of N.A. across the core. It is interesting to note that in Fig. 12(b) a chip in the cladding surface debris and the deposited ring structure in the core are all evident.

3. Coherence Time and Coherence Length

The finite spectral width of practical lasers may conveniently be expressed as a 'coherence time'. This is the time up to which the wave may be delayed, but yet still correlate with the undelayed wave. Fig. 13 is a gross simplification, the actual shape of the auto-correlation function being determined by the nature of the incoherence. For simplification we will consider that there is no significant correlation after time τ_c . The important concept to grasp is that there can be no interference between two rays with a difference in delays greater than the coherence time τ_c , even though they are from the same source. (The coherence length L_c is simply the coherence time multiplied by the propagation velocity, but as the velocity is a function of the refractive index then the medium must be specified.)

When light is launched into a multimode fibre exhibiting mode dispersion, the power is split between the various modes, each propagating at slightly different velocities along the fibres: thus when we measure dispersion in the time domain, a narrow launched pulse is seen to increase in width due to the spread in arrival times. Fig. 14 shows a fibre system in

which there are two misaligned fibre-to-fibre joints. If we consider the action of two modes only, it will help us to understand the interaction of dispersion and coherence length.

At the launch end of its fibre the two propagating modes, 1 & 2, are completely coherent, i.e. no differential delay has occurred because there is no delay. The light propagates along the fibre to the first misaligned joint with a total delay of τ_{m1} and τ_{m2} for modes 1 and 2

respectively. There is a difference $\Delta\tau$ between the arrival times and at the m first joint in the figure this is shown to be less than the coherence time τ_c of the laser. Near and far interference patterns will therefore exist at this joint and any misalignment will result in an uncertainty in the attenuation; furthermore, any change in the relative phase of these two modes will change the interference patterns and hence change the loss. Large phase changes will occur for small changes in source frequency due to the very large number of wavelengths traversed in the fibre and large changes of differential phase occur for very little physical distortion of the fibre, due to localised changes in refractive index [3]. Either of these will result in a change of joint attenuation and a variation of these with time will produce amplitude modulation of the signal received at the photodetector, i.e. 'modal noise'.

Let us now consider what effect a misaligned joint will have if the path length and dispersion are sufficient for the differential delay $\Delta\tau_m$ to be greater than the coherence time τ_c , as is illustrated at the second misaligned joint in Fig. 14. There can no longer be any interference as the light waves in the two modes are now incoherent with each other and hence no modal noise can be introduced at this joint. Consequently if there are no misalignment joints for $\Delta\tau_m > \tau_c$ (i.e. if the

first joint in Fig. 14 is perfectly aligned) there will be no modal noise. Any technique which reduces the effective modal dispersion (e.g. using successive joined lengths of under and over compensated profile fibre to optimise the mean profile) could lead to increased modal noise from a distant misaligned connector relative to a near one. This is, of course, a gross simplification: a practical fibre might have a hundred modes, each capable of interfering with any other modes provided that their differential delay is less than the coherence length. Clearly at any point along the fibre some pairs of mode will be capable of interfering, others will not, so we can consider the near and far field patterns to be the superposition of an interference pattern, Fig. 11(a), on a smooth illumination pattern, Fig. 11(c). As the light travels further along the fibre the ratio of power in the interference pattern to power in the smooth pattern will decrease. Therefore, there will be no sudden disappearance of modal noise after a given length, but rather a reduction in the effect with increased length. For analogue systems modal noise will still be significant at a greater length due to the higher S/N requirement. This discussion does not take into account mode conversion in the fibre or at misaligned joints.

4. Conditions Giving Rise to Modal Noise Generation

Before looking at means of prevention, let us reappraise the necessary conditions for modal noise generation.

1. Narrow source spectral width (long coherence time).
2. Modal or spatial filtering.
3. Time variation of either modal or spatial filtering.

All three conditions must be present for 'modal noise' (a system carrying information at d.c. might be troubled by conditions 1 and 2 alone, e.g. joint attenuation measurement).

Narrow spectral width is obtained with single longitudinal mode injection lasers [1]. Modal or spatial filtering can occur when splices or connectors are longitudinally or axially misaligned, or by dirt on either of the fibre ends. It can also occur at the coupling from fibre to detector, but this is unlikely with practical detector sizes. Variations of filtering are caused by physical distortion of the fibre preceding the 'filter' or by changes in source wavelength. Such changes may be induced by changes in laser temperature (due to the low-frequency content in the modulating signal current) and may be influenced by variations in reflections from adjacent external optical cavities.

We have used a laser package which utilises a very short fibre tail (2.5 cm) as a package window and as one-half of a demountable connector. It was found that this short fibre acted as a Fabry-Perot resonator, and by feedback caused the laser to perform very small abrupt jumps in wavelength as the temperature varied. This effect was fortuitous as it enabled us to see more clearly what happens during long pulses. Fig. 15 shows a 'modal noise' waveform which is produced by a misaligned connector distant 1 metre of fibre from this laser. Notice the abrupt jumps, and that the pattern is compressed towards the leading edge of the pulse. Compare this with Fig. 4 which was for the same configuration but without the initial 2.5 cm window. The time between jumps is found to increase exponentially during the pulse and the total number of jumps during a long pulse is approximately proportional to the amplitude of the modulating current, which suggests a simple thermal time-constant. See Fig. 16. These patterns helped us greatly in our initial understanding of modal noise. When laser temperature was increased, the pattern moved and bunched up towards the leading edge, as can be seen in Fig. 17 which is three superimposed waveforms at very slightly differing laser temperatures.

The most significant observation is that, when the fibre is manipulated preceding the misaligned joint, or if the joint itself is disturbed, the position of transitions stays the same, but the levels to which the waveform jumps vary. This can be understood if we think of jumps as jumps from one speckle pattern to another and so on (see Fig. 9). The pattern is held stable between jumps by the external resonant cavity (2.5 cm fibre), unlike Fig. 4 in which the pattern is continuously varying. All modal noise patterns are determined by the conditions before and at the connector. They are

generally unaffected (ignoring fibre bandwidth limitations) by the conditions following the joint, each successive joint adding its own amplitude modulation of the signal. These stable regions between jumps are only produced close to the laser. If the light from the same laser is passed through 1 km of 2 ns/km fibre before the misaligned joint then the waveform looks like Fig. 4 again. This is because the laser, although appearing stable between jumps, is in fact changing wavelength slightly. The frequency of the amplitude modulation is proportional to the rate of change of wavelength and to the intermodal dispersion [2] and after 1 km the interference pattern is rapidly fluctuating.

Figs. 5 and 6 were of course for lasers without the short (2.5 cm) tail, but it is worth noting that in Fig. 5(b) the noise produced after 1 km is significantly less than after 1 m. This may be because the large changes in wavelength (produced by the low frequency content of the modulating signal, below the thermal time-constant) make the effective coherence time (when measured with 20 MHz receiver bandwidth) shorter than much of the intermodal delay. Fig. 6, however, shows the maximum high frequency noise to be the same despite the initial 1 km length of fibre, but shows that the noise can no longer be minimised by manipulation of the fibre. This is because the interference patterns are quite stable close to the laser but highly unstable after 2 ns of mode dispersion. The 70 MHz modulation is well within the thermal time-constant of the laser so no large wavelength variations occurred. (No deviation was applied to the 70 MHz signal at the time of the experiment.) The different results of these two experiments highlight the need to consider carefully the modulation conditions before predicting the presence or absence of modal noise.

5. Means of Prevention of Modal Noise

As all three of the conditions are necessary for modal noise, prevention of any one will solve the problem.

(i) Source considerations

If we can use a broad spectrum source then we can avoid modal noise: but how broad a spectrum? The simple answer is that it must be sufficiently broad to eliminate interference effects at any modal or spatial filter. There are two ways in which the spectrum can be usefully broadened. The first is simply by increasing the width of the single longitudinal mode, i.e. decreasing its coherence time. The second is by increasing the number of lines (longitudinal modes) without necessarily decreasing the coherence time of the individual lines. (In practice multiple longitudinal mode lasers will usually exhibit short coherence times for each mode or line.)

For single longitudinal mode operation, the coherence time should be shorter than the intermode dispersion time at the point of the first modal or spatial filter, i.e. the lower the dispersion then the shorter the coherence time must be. When the source has several longitudinal modes, then the effect is rather different. In this case we have a superposition of several interference patterns and these will tend to average out (see Fig. 11(b)). Therefore,

the greater the number of lines, the less modal noise. We have found that the use of narrow stripe lasers (3-5 μm) exhibiting multiple longitudinal modes (and broader line width/shorter coherence length) almost completely eliminates modal noise.

One advantage of using the coherence time rather than the line width to describe the spectrum is that the relevant linewidth must be the instantaneous linewidth measured by time-resolved spectroscopy. To illustrate this point, consider a single longitudinal mode laser with long coherence length whose wavelength is slightly modulated by the small temperature changes induced by the modulating signal. The spectral width when measured as a time average will appear broader than it really is instantaneously. In a PCM system, the photodetector/receiver averages the received photons over a bit period so if we can sweep the frequency during each bit period, we can effectively broaden the spectrum.

When injection lasers are modulated from below threshold the spectrum is initially broad, consisting of a number of longitudinal modes and over a period of several nanoseconds the number of lines reduces until with a 'good' laser there may be just a single longitudinal mode [4]. At the same time the mean frequency and the frequencies of each of the lines are moving as the laser temperature changes with the increased current. When such a laser is modulated from above threshold, it operates continuously in a single mode (Fig. 18(a)) and therefore this has previously been considered the ideal modulation condition as material dispersion is minimised [5]. Also with this method there is no turn-on delay. However, the occurrence of modal noise (as well as reduced extinction ratio and increased laser noise close to threshold) now makes modulation from slightly below threshold more attractive. It is vital that a return-to-zero (RZ) code is used to ensure that the spectrum broadening occurs for successive logic 'ones' and, of course, the pulse duration must not be long enough for the laser to settle back into single longitudinal mode operation.

Fig. 18(b) shows the spectrum broadening induced by this method of modulation at 140 Mbit/s. Note both the increase in number of lines and in the individual line width (Fig. 18(a) is monochromator, resolution limited). For connectors close to the laser, the increased number of lines is probably much more useful than the increased linewidth in overcoming modal noise, relative delay between modes being still relatively small. Fig. 19 shows the improvement in the 'eye diagram' produced by this spectrum broadening. The top trace shows the 'eye' when normal NRZ modulation is used and the laser biased to threshold during the zero level. The modal noise appears as gross 'eye' closure. The middle trace shows the effect of changing the modulation to RZ whilst keeping the bias the same. The 'eye' is still severely degraded. The lower trace shows the effect of modulating RZ from below the threshold by increasing the modulation current. A good clean 'eye' diagram is evident despite the presence of a deliberately misaligned joint. If the same 140 MHz RZ modulation is applied to the low frequency square wave used in the tests recorded in Fig. 5, then the improvement can be clearly seen.

Furthermore, the improvement is greater after 1 km (Fig. 5(b)) than 1 metre (Fig. 5(a)) due to the much greater dispersed length than coherence length.

It is, of course, possible to reduce artificially the coherence length simply by passing the laser light through an initial length of highly dispersive fibre. This is equivalent to ensuring that the first misaligned connector can never be too close to the laser.

It remains to be seen whether any of these broad spectrum solutions will be satisfactory for future very high bandwidth analogue systems where there will be a compromise between modal noise and material dispersion. Perhaps single mode fibre will be necessary.

(ii) Prevention of modal and spatial filtering

There should be no problem provided lossless connectors and splices are used! However, if a misaligned joint should occur, a large system power margin may be ineffective in overcoming the increased loss because of the generation of 'modal noise' at that joint. The high S/N required in analogue systems make them extremely sensitive to small joint misalignments.

It is worth reminding ourselves that the number of speckles in the interference pattern is proportional to the number of modes which are propagating in the fibre. Therefore, any increase in the number of modes will reduce the modal noise for the same relative misalignment. Also, if the increase in modes is achieved by use of a larger core diameter then the same alignment error will result in smaller relative misalignment. Further, high N.A. will be an advantage if only axial misalignment occurs.

As can be seen from Figs. 5 and 6, greater modal noise may be produced by longitudinal misalignment than by axial misalignment, especially for high attenuation. This is most easily understood if we consider separating the two fibre ends until only one speckle of the far field pattern falls on the core of the second fibre (see Fig. 8). Clearly a small change in the interference pattern can now cause a dark region to be coincident with the fibre core, resulting in 100% amplitude modulation of the signal. For the axial misalignment, however, the effect is of two overlapping circles so even at the extreme misalignment case several speckles may be coupled. Lastly, all the dimensions scale with wavelength so there will be a greater penalty with longer wavelength sources.

(iii) Prevention of time variation of 'filtering'

It does not seem practical to prevent the slight physical distortion of the fibre which facilitates modal noise, especially when one considers the fibre as a distributed microphone. Even if this was possible, it would still be necessary to prevent any variations in source frequency and this would not be possible with direct modulation of the injection laser.

6. Conclusions

We have encountered and investigated a phenomenon which we call 'modal noise'. It is 'generated' at misaligned fibre-to-fibre joints when the source coherence time is longer than the inter-mode delay preceding the joint in question (mode dispersion). Digital systems are only seriously degraded by modal noise when both very narrow spectral width sources are used and when splices or connectors become misaligned. Some multimode analogue systems, however, may be quite impractical with narrow spectral width sources, even with relatively low loss joints.

The best solution to the problem of modal noise appears to be to use as broad a spectral width source as is practical for each system without introducing significant material dispersion. It is also important to use as high dispersion as is practical. Lastly, low loss connectors with little chance of accidental gross misalignment will help considerably.

Modal noise is a fascinating phenomena as it involves and requires the understanding of so many of the components in an optical system. This paper is an attempt to communicate the concept without getting into the mathematics of the problem. Much of the detailed analysis required of the fibre has been published previously [2, 3]. Further work is now required to extend this to the analysis of modal noise in practical optical fibre systems.

Acknowledgement

I wish to thank the many colleagues whose valuable discussions have contributed to this paper, particularly those in our laser group. I would also like to thank the management of STL for their permission to publish this paper.

References

- [1] P.R. Selway, Proc. IEE, Vol. 123, No. 6, pp 609-618, 1976
P.R. Selway, A.R. Goodwin, Electronics Letters, 1976, Vol. 12, No. 1, pp 25, 26
- [2] B. Crosignani, P. DiPorto, SPIE Vol. 77 (1976) Fibres and Integrated Optics, 49-56
B. Crosignani, B. Daino, P. DiPorto, Appl. Phys. Letters, Vol. 27, No. 4, pp 237-239, 1975
B. Crosignani, B. Daino, P. DiPorto, Proc. 2nd European Conference on Optical Fibre Communication, Sept. 1975
- [3] D.E.N. Davies, S.A. Kingsley, Proc. 1st European Conference on Optical Fibre Communication, Sept. 1976
D.E.N. Davies, S.A. Kingsley, Proc. Electro-Optics/Laser International '76 UK, March 1976
B. Culshaw, D.E.N. Davies, S.A. Kingsley, Electronics Letters, 1977, Vol. 13, No. 25, pp 760, 761
- [4] P.R. Selway, Private Communication
- [5] M.M. Ramsay, A.W. Horsley, R.E. Epworth, Proc. IEE, Vol. 123, No. 6, pp 633-641, 1976.

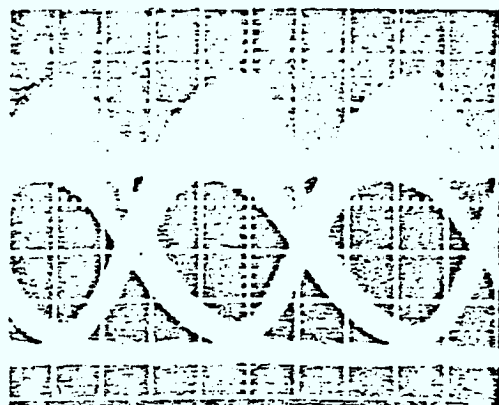


Fig. 1 : 140 Mbit/s NRZ 'eye diagram' showing modal noise (2 ns/div)

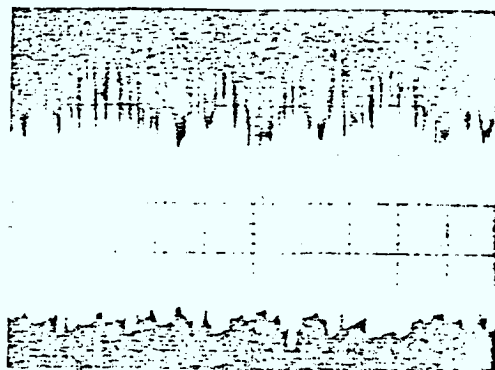


Fig. 2 : Slow scan of Fig. 1, showing amplitude fluctuations during 1 second (100 ms/div)

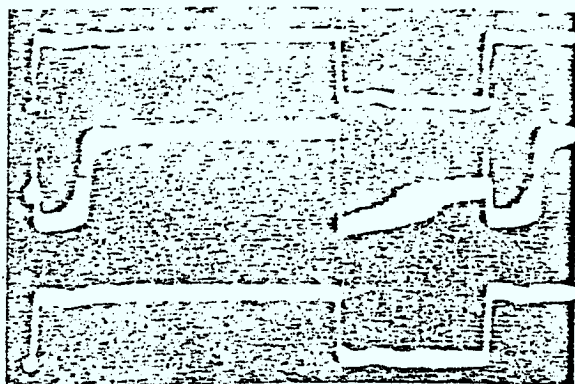


Fig. 3 : Top trace: total output from fibre. Middle trace: signal received via misaligned connector. Lower trace: as middle trace but with fibre bent to produce best looking trace

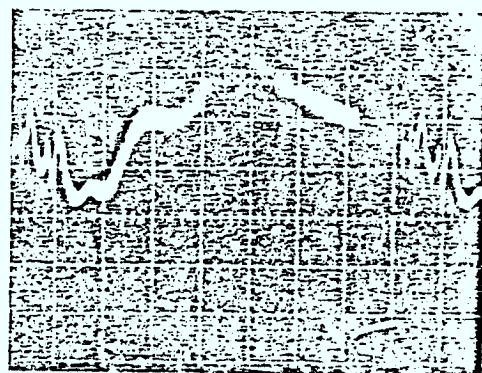


Fig. 4 : Repeating modal noise pattern appearing on 60 kHz square wave (2 μs/div)

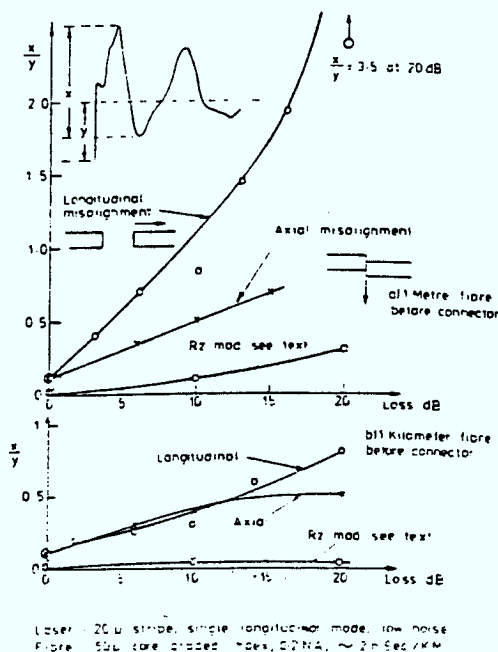


Fig. 5 : Maximum unwanted amplitude modulation vs connector loss. Measured for longitude (O) and axial (X) misalignment

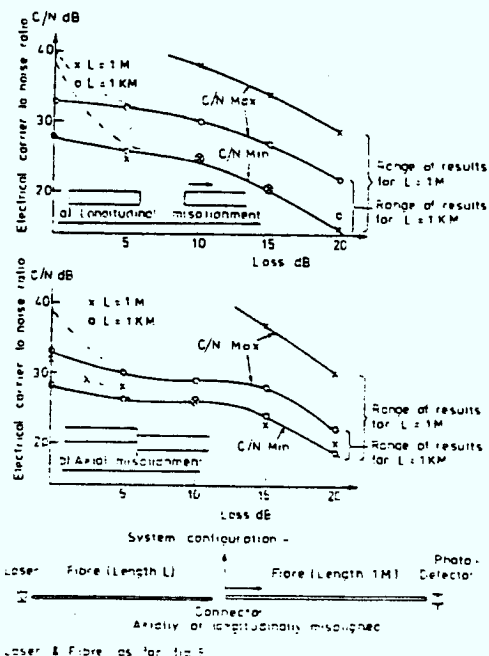


Fig. 6 : Measured r.m.s. carrier/noise ratio vs connector loss for 70 MHz modulation and 40 MHz BW

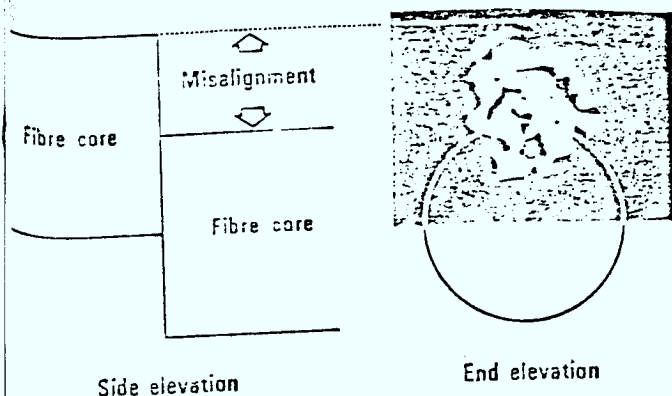


Fig. 7 : Diagram showing near-field interference pattern and effect of axial misalignment

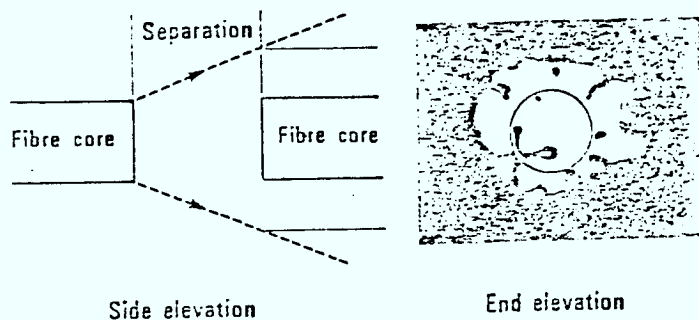


Fig. 8 : Diagram showing far-field interference pattern and effect of separation of fibre ends

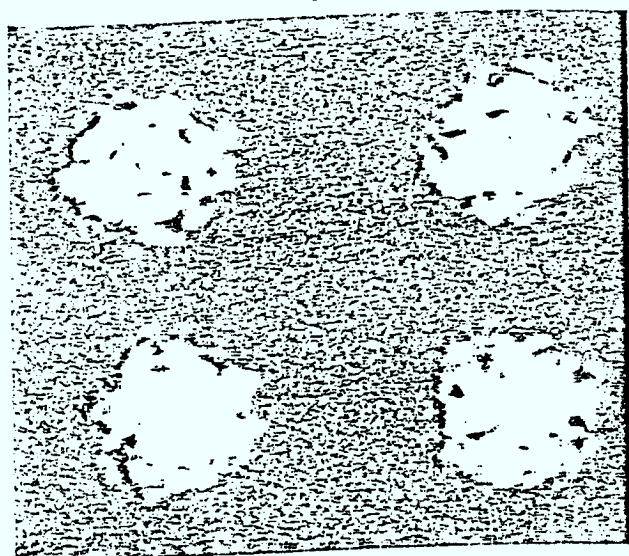


Fig. 9(a) : Near-field patterns

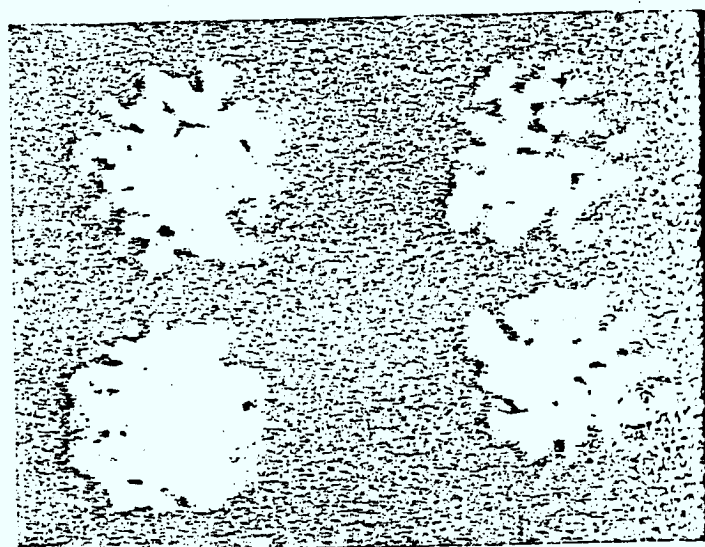


Fig. 9(b) : Far-field patterns

Fig. 9 : Some of the patterns produced by different bending of a 50 μm core graded index fibre with monochromatic illumination

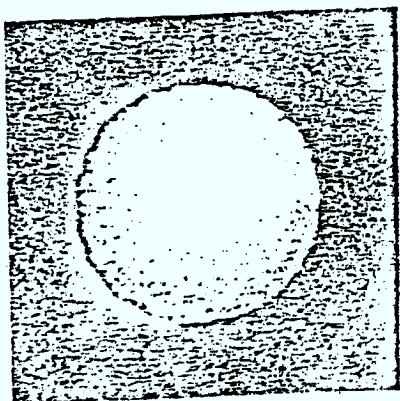


Fig. 10(a) : Near-field

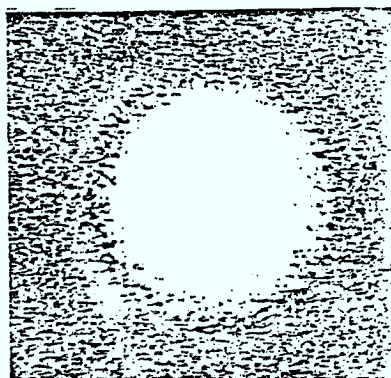


Fig. 10(b) : Far-field

Fig. 10 : Near-field and far-field interference patterns from 350 μm core, 0.4 N.A. plastic clad silica fibre

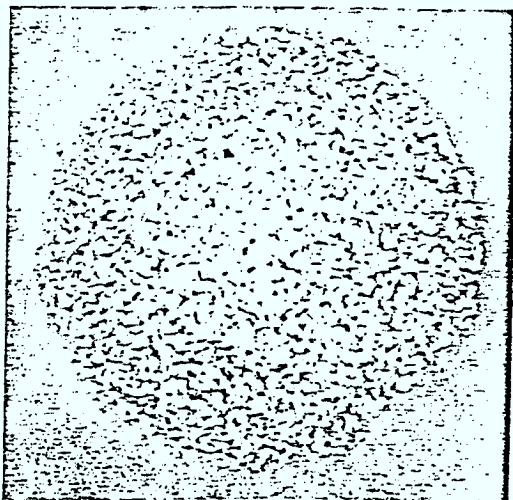


Fig. 11(a)

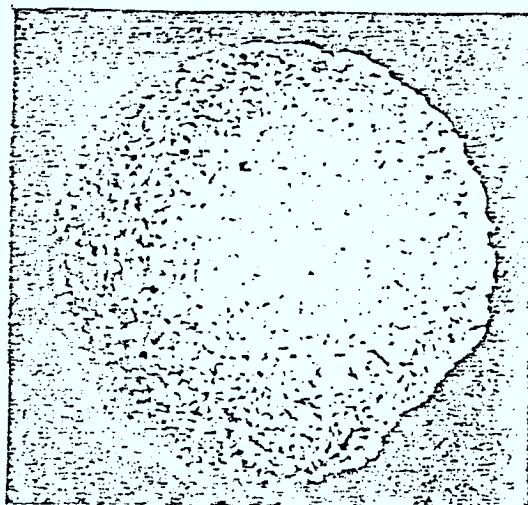


Fig. 11(b)

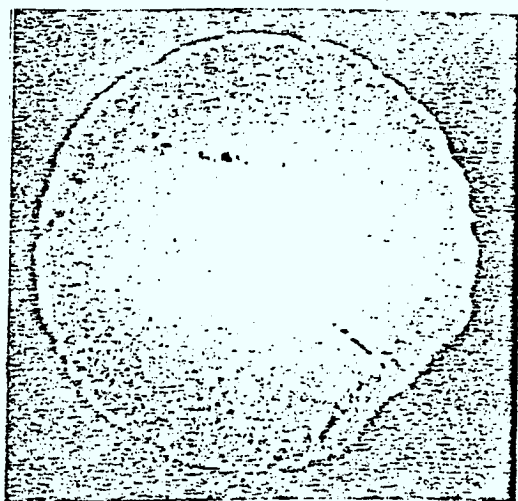


Fig. 11(c)

Fig. 11 : Fibre as for Fig. 10 -
Near-field images for:

- (a) single speckle pattern
- (b) 6 superimposed speckle patterns
- (c) long exposure with varying speckle pattern

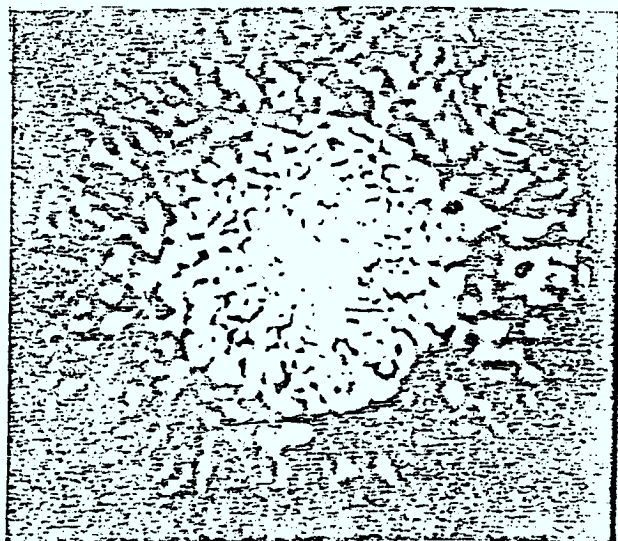


Fig. 12(a)

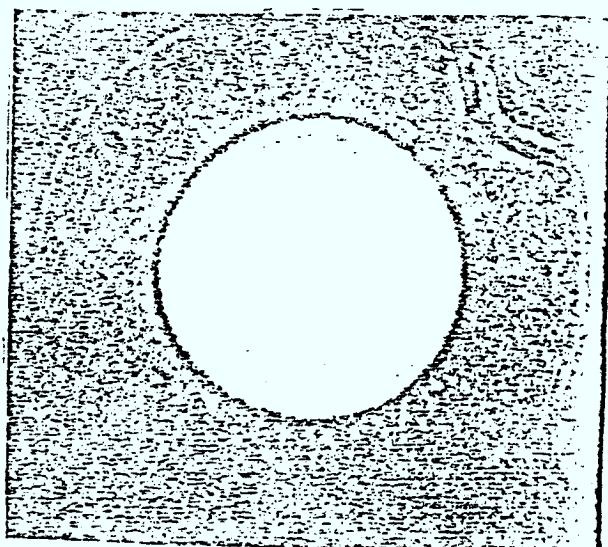


Fig. 12(b)

Fig. 12 : 50 μ m core, CVD, graded index fibre. Light launched at core/cladding interface: (a) single speckle pattern
(b) long exposure with varying speckle pattern

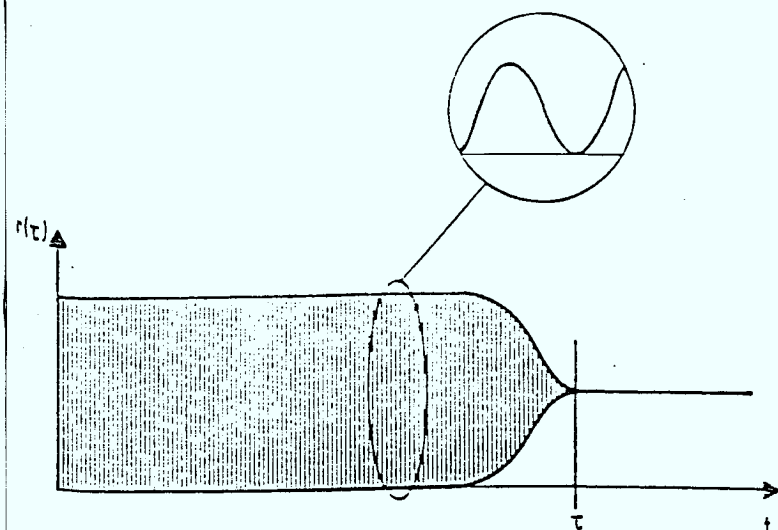


Fig. 13 : Simplified autocorrelation function of laser emission showing significance of coherence time τ_c

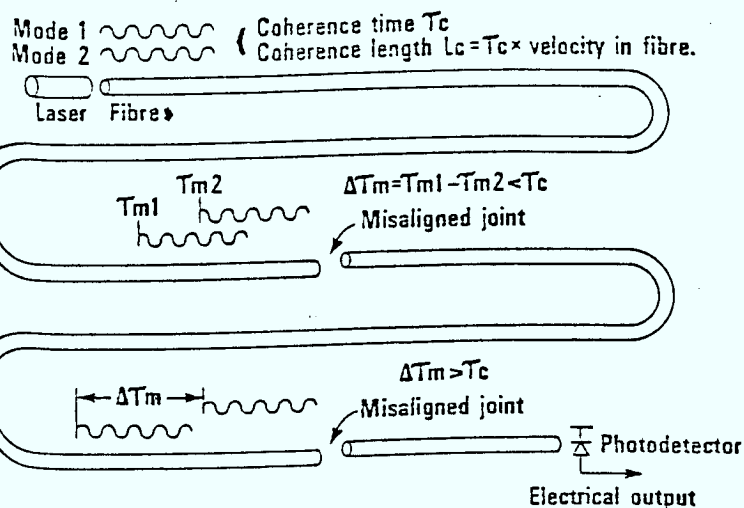


Fig. 14 : Simplified explanation of dependence of modal noise on source coherence time, mode dispersion and position of joint. Two modes only illustrated

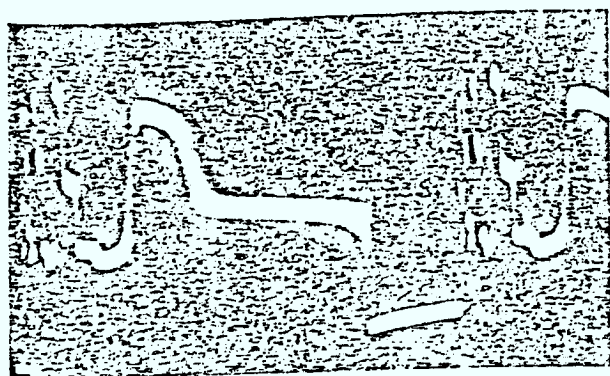


Fig. 15 : Modal noise waveform produced by laser feed-back effects showing jumps in level

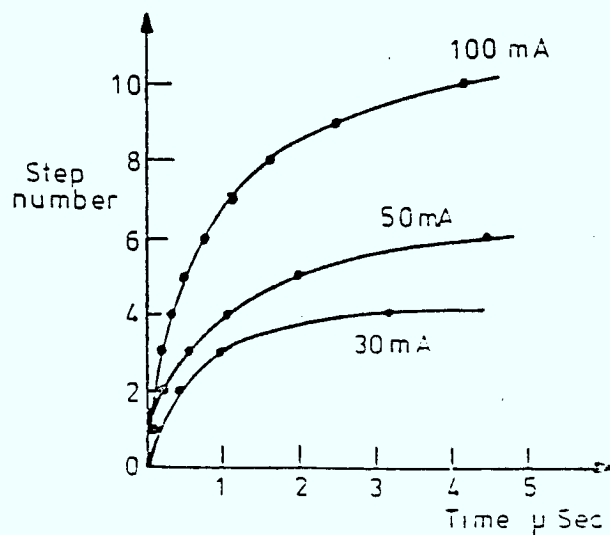


Fig. 16 : Graph of jump (step) number vs time in microseconds

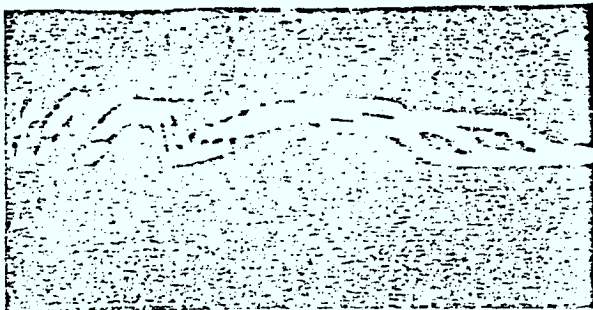


Fig. 17 : As Fig. 15 but for three slightly different temperatures

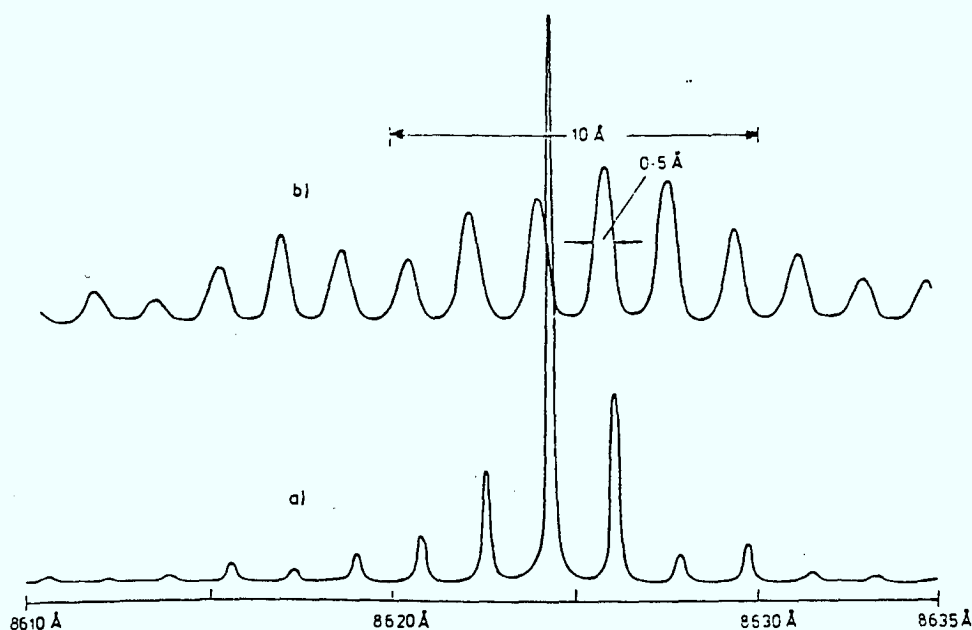


Fig. 18 : Laser spectra : a) normal, b) with spectrum broadening; with identical launched mean power

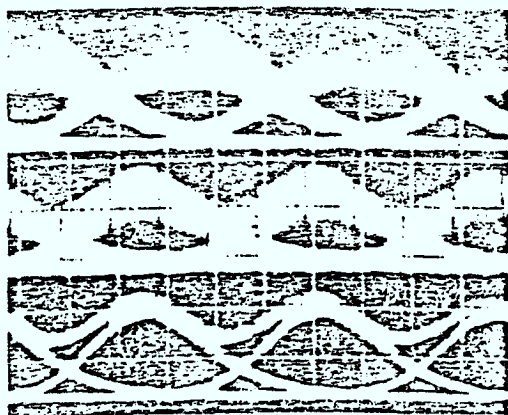


Fig. 19 :

140 Mbit/s 'eye diagram' -
 Top trace: NRZ with modal noise
 Middle trace: RZ still with
 'modal noise'
 Lower trace: RZ from below
 threshold,
 no 'modal noise'

Presented at the Topical Meeting on
optical fibre communication,
Washington D.C., March 1979.

THE PHENOMENON OF MODAL NOISE IN FIBRE SYSTEMS

R. E. Edworth

Standard Telecommunication Laboratories Ltd.,
London Road, Harlow, Essex.

When coherent sources are used in multimode fibre systems with mode selective loss, a hitherto unconsidered source of noise occurs. This we call "modal noise" (1). It appears as unwanted amplitude modulation of the received signal and is very sensitive to physical distortion of the fibre. The noise can be minimised or maximised simply by bending the fibre, and in practice may seriously degrade digital systems and completely disable analogue systems.

Speckle Patterns

The key to modal noise lies in the near field and far field speckle patterns that are observed at the end of a multimode fibre through which coherent light is propagating. These speckles are produced by interference between the various propagating modes, each of which is subjected to slightly different delays through the fibre caused by mode dispersion. The number of speckles in these patterns is approximately proportional to the number of propagating modes. A wide variety of speckle patterns can be produced simply by bending the fibre (the resulting changes in local refractive index cause small changes in the intermode delay) and similar pattern variations result from very small changes in wavelength (2, 3).

Now consider the effect of mode selective loss or mode filtering, such as would occur at a misaligned fibre-to-fibre joint. The number of speckles coupled to the second fibre will vary as the speckle pattern varies, thus a joint with fixed misalignment will have a loss uncertainty. The loss will vary both with changes in wavelength and with bending of the fibre before that misaligned joint.

Coherence

If we consider the source coherence time (i.e. the time by which the light may be delayed and yet still correlate or interfere with the undelayed light), it will be clear that there can be no interference between any two modes in a fibre when the difference in their delays (i.e. intermode dispersion) is greater than the source coherence time, even though they are from the same source.

To help understand the interaction of dispersion and coherence time, consider the action of just two modes and the effect of a misaligned joint at some point along a length of fibre. If the mode dispersion up to this point is less than the coherence time, then both near field and far field interference patterns are produced and there will be an uncertainty in the attenuation. Furthermore, any change in the relative phase of these two modes will change the interference patterns and hence change the loss. Large phase changes will occur for small changes in source wavelength, caused by the large difference in the number of wavelengths traversed by the two modes in the fibre and large changes in differential phase occur with physical distortion of the fibre as a result of localised changes in refractive index. Either of these will result in a change of joint attenuation and a variation of these with time will result in amplitude modulation of the propagating power, i.e. modal noise. The frequency of this amplitude modulation will be proportional to the product of the rate of change of wavelength and the intermode delay.

In practical systems small changes in laser wavelength are produced by fluctuations in the chip temperature resulting from direct modulation, and local refractive index changes in the fibre are caused by such things as vehicle traffic vibration.

If the mode dispersion before the misaligned joint is greater than the coherence time then there can be no interference as the two modes are mutually incoherent and hence no modal noise will be generated. Both the two mode case and the assumption of a single value of coherence are gross oversimplifications. In practice with increased fibre length from the source there will be a gradual fall in the fraction of the propagating power that is capable of intermode interference so misaligned joints close to the source tend to generate more modal noise than distant ones.

Implications for Practical Systems

The conditions that together give rise to modal noise are source coherence and time varying mode selective loss. The factors leading to increased levels of modal noise are as follows:-

1. High source coherence (i.e. narrow spectral width). LEDs give lower modal noise, not just because of their broader spectrum, but as a result of their low spatial coherence.
2. Mode selective loss. This occurs in misaligned joints, in mode selective splitters or taps and even in unjointed fibre as a result of microbending loss.
3. Small number of propagating modes, i.e. low NA, small core size, graded as opposed to step index, and underfilling of the fibre.
4. Low mode dispersion.

Reduction of Modal Noise

The use of low loss joints may be sufficient to prevent modal noise problems in digital systems, but the problems for future high capacity analogue multimode systems may be enormous. The best solution appears to be the use of as low coherence source as is possible without introducing a significant material dispersion penalty because of the broader spectrum (long wavelength will be advantageous, but remember that there will be fewer modes for the same core diameter), and to use a high number of modes. It is highly advantageous to increase the number of modes by increasing the core diameter as this will give reduced joint losses for a given misalignment as well as providing a finer speckle pattern. It is ironic that the development of "good" lasers (e.g. single longitudinal mode) and low dispersion fibre can lead to higher modal noise. It is tempting to say that single mode will be the complete solution, but as the two mode case is the worst case, the second mode must be highly suppressed.

Conclusions

The phenomenon of modal noise is a "multipath" problem which is fundamental to multimode fibre systems with mode selective loss and it involves and requires an understanding of so many of the components in an optical system. It is "generated" at the point of mode selective loss (e.g. a misaligned joint) when the source coherence time is longer than the intermode delay preceding that point. Digital systems are only seriously degraded by modal noise when very narrow spectral width sources are used together with misaligned joints. However, many multimode analogue systems may be quite impractical with narrow spectral width sources, even with low loss joints. Much detailed work now needs to be done before quantitative prediction of modal noise levels is practical and before the full implications of modal noise are apparent.

I would like to thank the management of STL for their permission to present this paper.

References

1. R. E. Epworth, "The Phenomenon of Modal Noise in Analogue and Digital Optical Fibre Systems", 4th European Conference on Optical Fibre Communication, 1978.
2. B. Crosignani, P. Di Porto, "Propagation of Coherence and Very High Resolution Measurements in Optical Fibres", *Fibres and Integrated Optics*, Vol 77, pp. 49-56.
3. D. Davies, S. Kingsley, "A Novel Optical Fibre Telemetry Highway", 1st European Conference on Optical Fibre Communication, 1974.

Fig. 1 Diagram showing near-field speckle pattern and effect of axially misaligned fibre joint

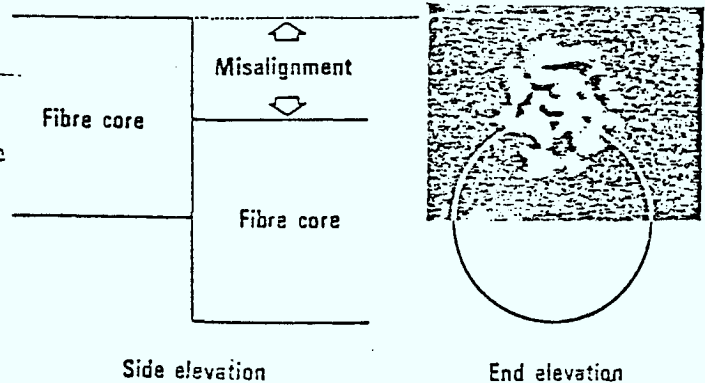


Fig. 2 Diagram showing far-field speckle pattern and effect of longitudinally misaligned fibre joint

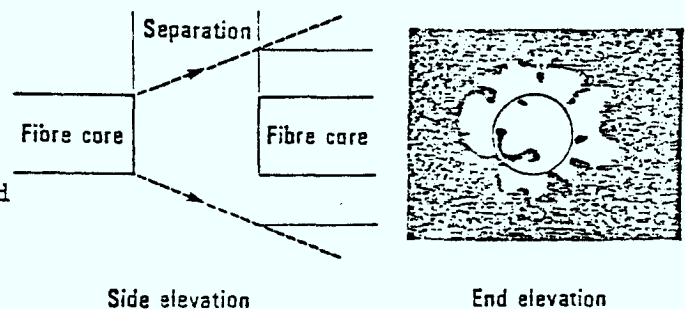


Fig. 3 Fibre power splitter showing presence of speckle pattern at the point where the power is divided

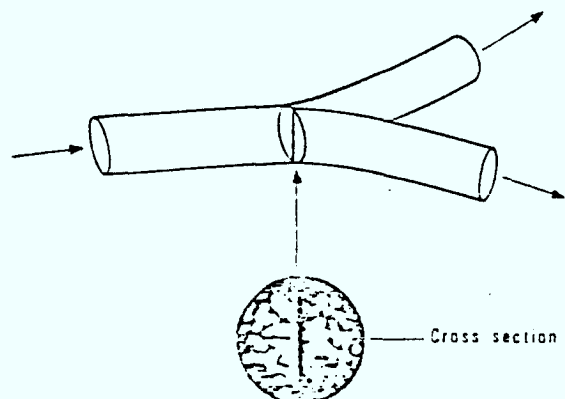


Fig. 4 Simplified coherence function of laser emission showing significance of coherence time τ_c

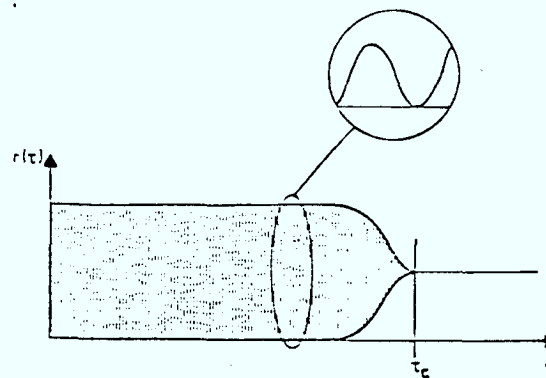
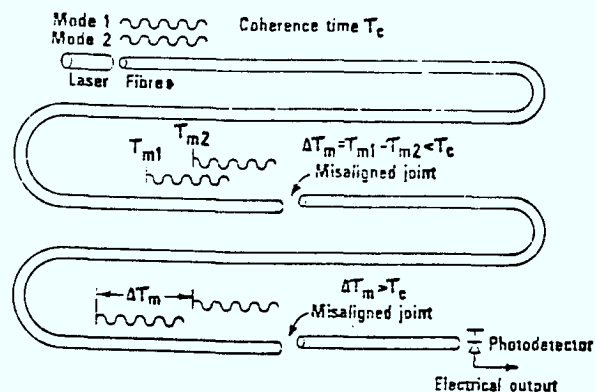


Fig. 5 Simplified explanation of dependence of modal noise on source coherence time τ_c , mode dispersion $\Delta\tau_m$, and position of joint, illustrated for two modes only



Factor	Unwanted amplitude modulation	Mean noise frequency
Source		
High temporal coherence (narrow spectrum)	Increase	Decrease
Good wavelength stability	Increase	Decrease
High spatial coherence	Increase	—
Mode hopping	—	Increase
Longer wavelength	Increase	—
High dispersion (before mode selection)	Decrease	Increase
Vibration of fibre	—	Increase

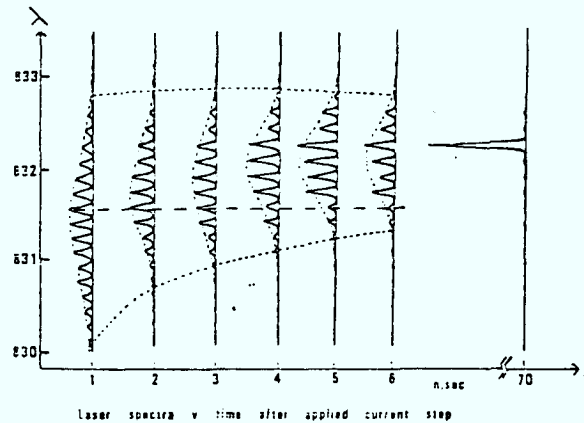
Fig. 6 Factors which influence modal noise: 1. Coherence

Factor	Unwanted amplitude modulation	Mean noise frequency
Low connector loss	Decrease	
High number of modes	Decrease	
Large core	Decrease	
High N.A.	Decrease	
Step V. graded index	Decrease	Increase
Equal distribution of power between modes	Decrease	
Mode selective power dividers/taps	Increase	
Mode selective power dividers/taps with low tap fraction	Increase	
Micro bending loss	Increase	Decrease

Fig. 7 Factors which influence modal noise: 2. Mode Selection

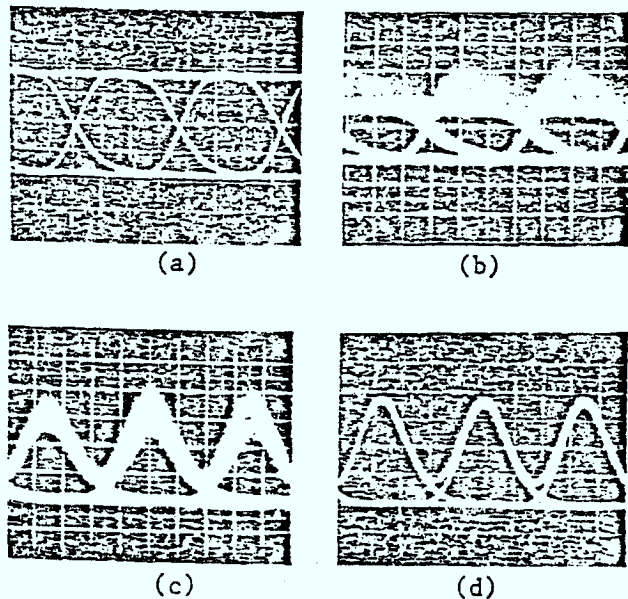
Fig. 8

Showing the effective spectrum broadening that occurs when a nominally single mode laser is modulated from below the lasing threshold

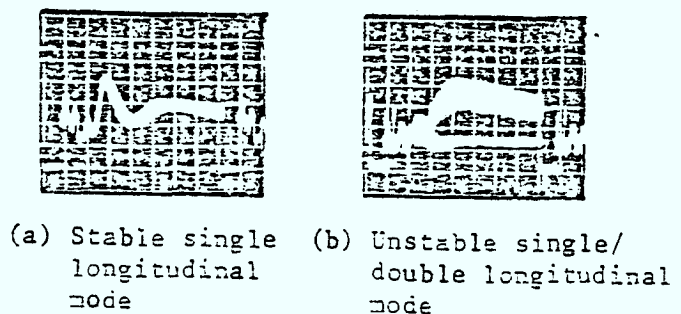
Fig. 9

Showing the reduction in modal noise that is achieved in a practical 140 Mbit/s system by the use of spectrum broadening

- (a) Laser output direct NRZ modulation
- (b) Modal noise induced by misaligned joint (NRZ)
- (c) Modal noise still present with RZ modulation above threshold
- (d) Negligible modal noise with RZ modulation from below threshold

Fig. 10

Repeating modal noise waveforms which appear on low frequency square wave (60 kHz), caused by misaligned joint after 1 km of 50 μ m core G.I. fibre, 15 dB misalignment loss



THE MEASUREMENT OF STATIC AND DYNAMIC COHERENCE

PHENOMENA USING A MICHELSON INTERFEROMETER

R. E. Epworth

Standard Telecommunication Laboratories Ltd.,
London Road, Harlow, Essex.

1. INTRODUCTION

Modal noise is caused by interference between the various modes in a multimode fibre, each of which has experienced a different delay, resulting in broadband noise in the received signal. Its magnitude and spectrum is determined by three factors: source coherence, mode dispersion and mode selective loss. (see Ref. 1, 2) Although modal noise is most readily observed where there is large mode selective loss (such as a misaligned joint or mode selective branching coupler) relatively weak mode selective effects such as the residual microbending losses present even in low loss cables can cause serious effects in some practical systems. If quantitative prediction of modal noise levels is to be a reality then each of these aspects must be understood in considerable detail. The most effective solution to modal noise lies in the use of light sources of as low coherence as is possible without incurring other penalties, e.g. high material dispersion, low launched power.

We have used a Michelson interferometer as an instrument to measure the coherence functions of various optical sources and as a means of simulating the modal noise generated in a two mode fibre system (the worst case) whilst varying the conditions of modulation to gain a fuller understanding of practical modal noise waveforms and their implication for real transmission systems.

2. MEASUREMENT OF COHERENCE USING THE MICHELSON INTERFEROMETER

Fig. 1 shows the interferometer arrangement used for these experiments. Moving one mirror will result in an output current from the photodetector following the curve in Fig. 2. The path difference introduces a delay and the fraction of the light which is coherent over this time will interfere constructively or destructively, depending on the exact phase relationship, resulting in a sinusoidal variation in intensity and hence detector current. The fraction of the light which is incoherent over this delay time will simply generate a DC current y . We can define the degree of coherence as $x - y$, the fringe visibility. Thus we can measure the degree of temporal coherence for different $x + y$ positions of the moveable mirror. When the path difference is zero all light sources will exhibit 100% temporal coherence, but the distance the mirror may be moved and yet coherence still be observed is a function of the spectrum of the source. This is called the temporal coherence length and for a simple source such as an LED, the coherence will fall to approximately one half at $l = \lambda / \Delta\lambda$ where $1/\Delta\lambda$ is the fractional bandwidth. However, for "coherent" sources, the coherence functions (and the spectra, the Fourier transforms of the coherence functions) are more complicated. (3, 4)

3. STATIC COHERENCE FUNCTIONS

(a) Single mode Lasers

The coherence function of a nominally single mode laser (20 μ stripe width) (5) was measured (Fig. 3a, 4a). Mode instabilities caused by feedback were prevented by an attenuator placed between the laser and the interferometer (see section 5). The laser was not entirely single mode (see Fig. 4a) and this accounts for the structure observed on the top of the coherence function, as will become clear later. One mode, however, was dominant and this resulted in a coherence function extending beyond one metre, the present limit of our interferometer. This corresponds to a coherence time > 3 nsec or a bandwidth < 300 MHz, resulting in a measurement of linewidth of $< 6.10^{-3}$ Å. In comparison the resolution of a monochromator of similar overall length would be no better than 0.25 Å, thus making it quite unsuitable for measuring the temporal coherence of injection lasers.

The implication of 3 nsec coherence time in a multimode fibre system is that modal noise can be generated by interference between modes which have a difference in delays less than 3 nsec, thus 3 nsec of dispersion would be insufficient to provide significant reduction in modal noise.

(b) Multiple Longitudinal Mode Lasers

A laser oscillating in more than one longitudinal mode will exhibit a coherence function which is periodic (6). The interference between modes does not usually need to be taken into account for injection lasers as the resultant beat frequency is outside any receiver bandwidth envisaged (~ 100 GHz). The laser resonates where the cavity length is exact multiples of half the wavelength and adjacent lines are thus spaced by $\Delta\lambda$ where $\Delta\lambda = \frac{\lambda^2}{2L}$ where L is the effective laser cavity length.

Such a source exhibits a coherence function with several peaks at multiples of the effective cavity lengths as shown in Fig. 3b, 4b. This is the measured coherence function of a 3 μ stripe width device, the spectrum of which is also shown in Fig. 4b. The actual cavity length was 181 μ m and the measured effective cavity length (i.e. half the spacing of the coherence peaks) was 325 μ m. One might expect these to scale by the ratio of the refractive index of GaAs (~ 3.5) but this is not so. The ratio is 4.5:1 and the difference is accounted for by material dispersion in the laser. This change of refractive index with wavelength shifts the lines unequally moving them closer together in wavelength.

If we assume that all the modes have similar coherence then the envelope of the coherence peaks represents the coherence of a single mode, thus enabling us to measure the mean linewidth of a multimode laser using the interferometer. The width of the coherence peak about zero is a measure of the width of the envelope of the spectrum (which is the measure of spectral width relevant to material dispersion in optical fibre). Furthermore, the greater the number of lines in the spectrum, the lower is the mean coherence level between the peaks.

The modal noise potential of a spatially coherent source is indicated clearly by the temporal coherence function. If for a pair of interfering modes the intermodal delay is known, then the maximum depth of the modal noise modulation can be read off from the coherence function. Intermodal delays corresponding to multiples of the effective cavity lengths will generate significantly more modal noise than other delays. A simple way to compare the modal noise potential of different sources is to compare the total areas under the coherence functions.

The structure on the top of the coherence function of the "single" mode 20 μ stripe laser will now be understood as the contributions of other modes at a fairly low level but yet resulting in discernible multiple coherence (Fig. 4a).

4. DYNAMIC COHERENCE FUNCTIONS

(a) Modulation above threshold

When modulation is applied to a 20 μ stripe laser biased above threshold, not only is the light intensity modulated but so also is the wavelength of oscillation. This FM effect is difficult to observe on a monochromator but is observed easily on the interferometer. Fig. 5 shows the output from the interferometer when a small sinusoidal modulation current is applied to such a laser (it is not necessary to move the mirror). By counting the number of fringes moved during each half cycle and knowing the interferometer path difference, the change in wavelength with current can be measured. We measured this for a range of modulation frequencies, the results being shown in Fig. 6. We then applied a larger amplitude triangular wave modulation to the laser, sufficient to modulate the laser from threshold past the slight kink in the characteristic where the first order transverse mode comes in. The results are shown in Figs. 7a, b, c and d for four different values of interferometer path difference. In each case we have superimposed the trace of the laser output with no interference to show the mean level. Figs. 7b and c show the effects most clearly. For very short path differences, because so few cycles of interference occur it was necessary to vibrate one of the mirrors with a PZT element in order to sweep the waveform through the whole envelope (Fig. 7a). At large spacings (Fig. 7d) the trace begins to get slightly fuzzy due to the FM noise caused by the finite coherence. Careful examination of these photos reveals that the degree of coherence changes with level. Note particularly that except for small path differences the degree of coherence is low in the region just above threshold and also that the coherence falls above the kink (although the total coherent power stays more or less constant above the kink). It is also evident that large path differences could result in such high interference frequencies that a low bandwidth optical receiver might result in a reduction in the observed fringe modulation depth. Thus the coherence may be artificially reduced by the frequency deviation.

The response of the laser/interferometer system to simple square wave modulation is shown in Fig. 8a. Note the bunching up at the leading edge, shown in greater detail in Fig. 3b.

(b) Modulation from below threshold

When a nominally single mode laser is modulated from below threshold, it takes time to settle into single mode operation. Fig. 9 shows the spectra versus time after an applied current step. If the laser is turned on from below threshold and is never on for more than a few nanoseconds, the spectrum will never settle down to a single mode, thus the coherence can be artificially reduced. We have used this technique to greatly reduce modal noise in a practical high bit rate transmission system (1) and we have now measured the coherence function of such a laser modulated in this way, as is shown in Fig. 4c. Note the enormous reduction in coherence that occurs.

5. UNSTABLE MODES

Many nominally single mode lasers can be induced to oscillate in two modes intermittently by a particular choice of temperature and operating current or alternatively by external reflections back into the laser cavity. The interferometer may be used as a comb filter to reject alternate longitudinal modes simply by setting the path difference half way between some multiple of the effective cavity length.

We deliberately induced mode jumping in a "single" mode laser by optical feedback and modulated it with a square wave. Fig. 10a shows its response through the interferometer; note the abrupt jumps between two waveforms. With the feedback removed the response is as shown in Fig. 10b. These waveforms help us to understand the effect of mode instability on modal noise (2). It is clear that such instabilities cannot increase the peak-to-peak modal noise amplitude but will considerably increase its mean frequency. As the optical receiver will have a finite bandwidth it is quite likely that mode instabilities will reduce the effective coherence.

6. THE INTERFEROMETER AS A MODAL NOISE SIMULATOR

Modal noise is generated by interference between modes which occurs at a point of mode selective loss, e.g. a misaligned joint. Fig. 11a shows a typical repeating modal noise waveform generated at a misaligned fibre joint, one kilometre of multimode fibre distant from a single mode laser. The simplest case to understand (and also the worst case) is the two mode fibre in which there is a single value of intermode delay (1). In the interferometer the two modes may be represented by the two paths. Fig. 11b shows the output from the laser via the interferometer when the path difference is set to 500 nm simulating an intermode delay of 1.5 nsec. Note the similarity. The interferometer may thus be used to measure the worst case modal noise potential of transmission system lasers under actual operating conditions.

7. CONCLUSIONS

We have measured the temporal coherence of different types of lasers to assess their potential for generating unwanted modal noise. The multiple longitudinal mode lasers show an enormous advantage (7), not just in the considerably reduced coherence for each mode but also because of the multiple coherence minima induced by the multiple modes. However, a source of the same spectral width, but without line structure in either its spectrum or its coherence function, would further minimise modal noise.

We have used spectrum broadening to minimise modal noise in a practical high capacity digital transmission system (1, 2, 8). We are now using the interferometer to further our understanding of the behaviour of a wide variety of sources under practical system conditions.

I should like to thank the management of STL for permission to publish this paper and Ian Hardcastle for carrying out much of the measurements.

References

1. R.E. EPWORTH, 'The phenomenon of modal noise in analogue and digital optical fibre systems'. Proceedings of the 4th European Conference on Optical Communications, Genoa, Sept '78.
2. R.E. EPWORTH, 'The phenomenon of modal noise in fibre systems'. Fibre Optics Conference, Washington 6,7,8 March '79
3. BORN & WOLF, 'Principles of optics'. 5th Edition, Pergamon Press, 1975.
4. S.G. LIPSON & H. LIPSON, 'Optical Physics'. Cambridge University Press, 1969.
5. P.R. SELWAY, Proc IEE, Vol 123, No 6, 1976
6. COLLIER, BURCKHARDT, LIN, 'Optical Holography'. Academic Press, 1977
7. A.W. DAVIS, R.E. EPWORTH, A.R. GOODWIN, P.A. KIRKEY, 'Narrow stripe lasers for improved performance of optical fibre communication systems'. (To be published)
8. D.R. HILL, 'A 140 MBIT/S Optical Fibre Field Demonstration System. Elec Comm, Vol 54, No 1, April 1979.

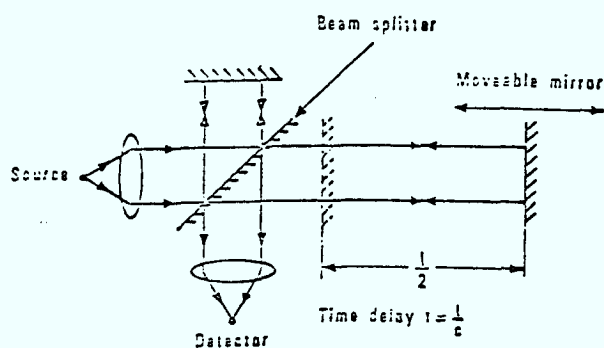


Fig 1 Michelson Interferometer

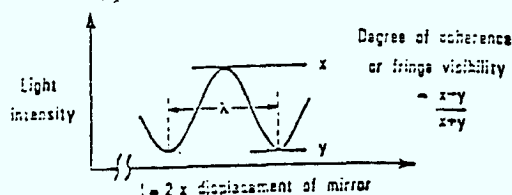


Fig 2 Definition of terms

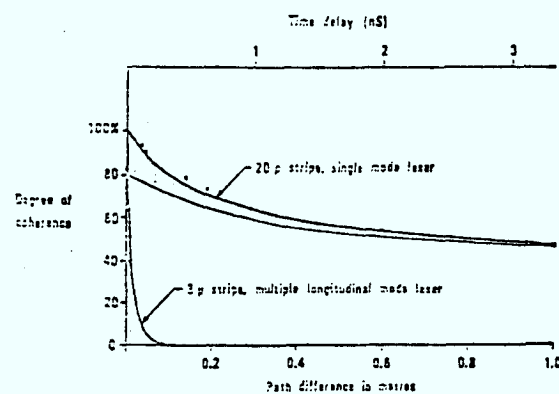


Fig 3 Laser Coherence versus path difference up to one metre.

- a) 20μ stripe, single mode laser
- b) 3μ stripe, multiple longitudinal mode laser

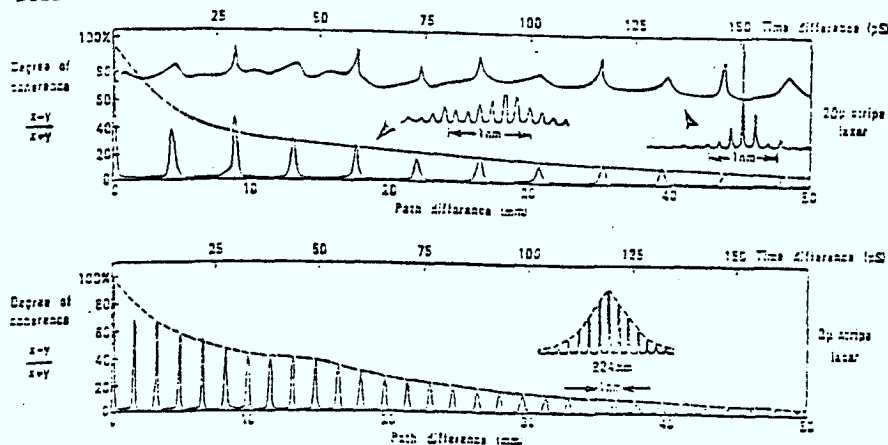


Fig 4 Laser Coherence versus path difference up to 50mm. a) 20μ stripe, single mode laser, b) 3μ stripe, multiple longitudinal mode laser, c) 20μ stripe with spectrum broadening.



Fig 5 Interferometer output with 5mA pk-pk, 2KHz sinusoidal laser modulation current. Path difference = 330mm.

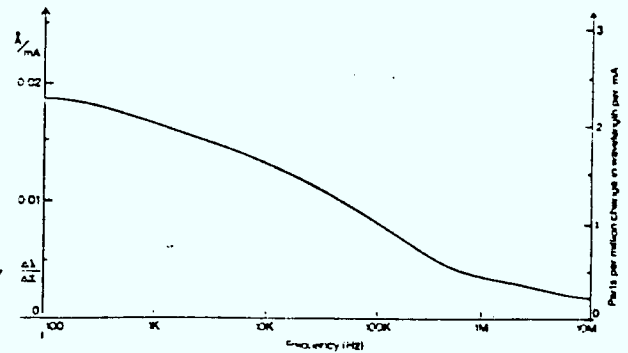


Fig 6 Wavelength deviation versus applied modulation frequency.

Fig 7 Interferometer output for triangle wave modulation for various path differences. 20mA pk-pk modulation.

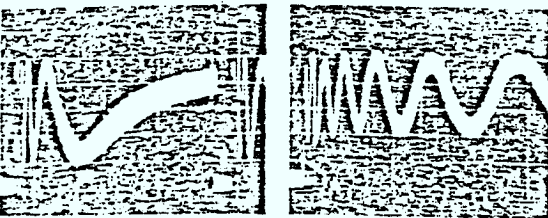
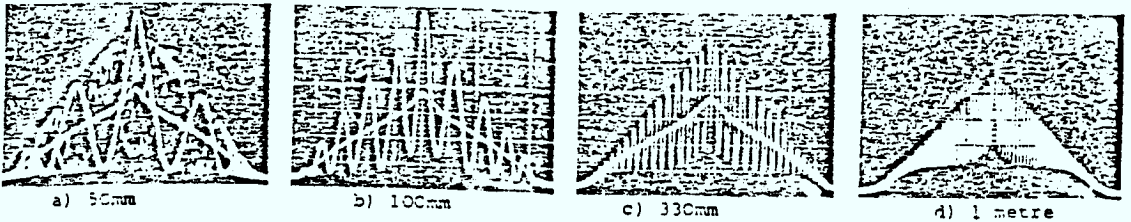


Fig 8 Interferometer output for square wave modulation. 330mm path difference

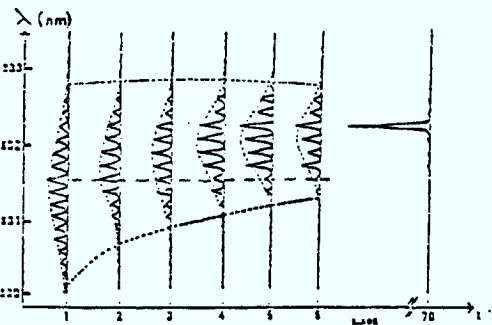


Fig 9 Laser spectra versus time after applied current step from below threshold.

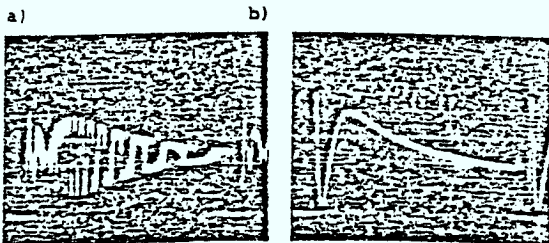


Fig 10 Effect of mode instability on output of interferometer for square wave modulation (2μs/div).

- a) feedback induced mode pumping.
- b) single longitudinal mode.

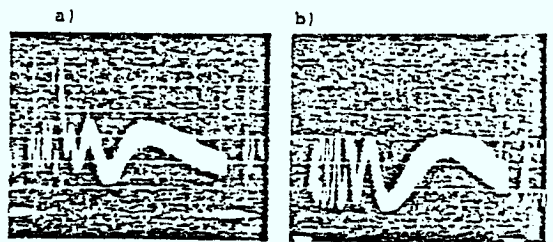


Fig 11

- a) Repeating modal noise waveform induced by misaligned joint 1km of fibre from single mode laser. Fibre: 50μ core, G.I. ~2nSec/Km.
- b) Interferometer simulation of a) for 500mm path difference.



APPENDIX 2

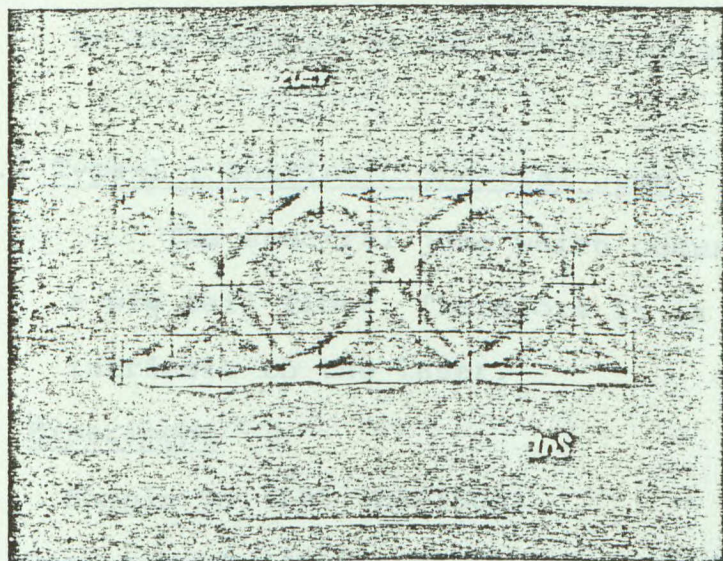
Origin of Delay Noise in High Speed Digital
System Using HLP1500 Injection Laser Diodes

Origin of Delay Noise
in High-Speed Digital System
Using HLP 1500 Injection Laser Diodes

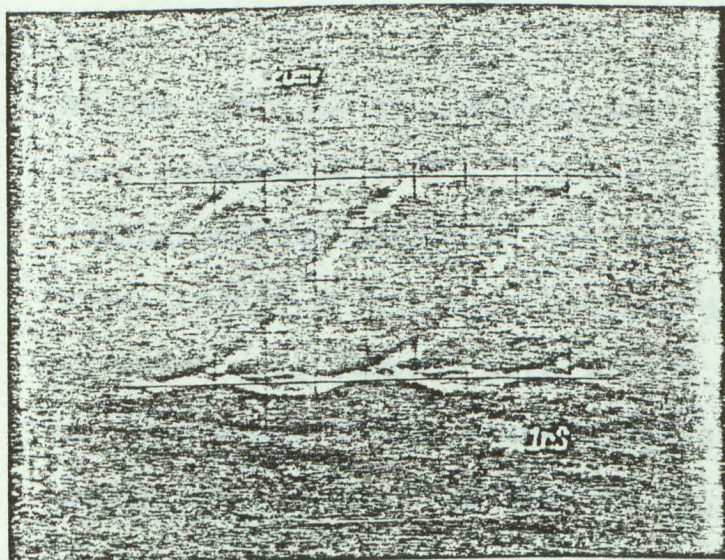
Reference the attached data by Hitachi (attachment #1) on the mode-hop behavior of their HLP 1500 ILD's. With the particular device they tested, they measured up to 27 Å spectral shift during a long pulse. Harris has measured up to 40 Å. However, using the 27 Å figure, the expected change in propagation delay over 4 km of fiber would be:

$$\begin{aligned}
 \Delta T &= \frac{L}{c} (n_1 - n_2) \\
 &= \frac{(4 \times 10^3)}{3 \times 10^8} (5 \times 10^{-5}) \\
 &= .67 \times 10^{-9} \text{ seconds}
 \end{aligned}$$

This is sufficient to cause significant increase in the probability of error at the sampling instant in a 300 mb/s 4km link due to eye closure. This effect is illustrated by the photo (fig.1) taken at the output of a receiver operating in a 4 Km 301 mb/s link. Significant systematic delay noise is seen occurring on the 1/0 transition. Random mode hops also occur, resulting in a falling edge which jitters less systematically.



APPROX. 0.7 NS SYSTEMATIC
DELAY JITTER AT 301 MB/S
NRZ, $2^{15}-1$ PN SEQUENCE,
4.3 KM FIBER LINK.



SAME AS ABOVE,
ONLY ILD TEMP.
CHANGED.

Figure 1

1 Delay Noise

We observed two types of spectral jump which might be the origins of the "delay noise" in your fiber system.

1.1 Type-1 : Intrinsic Spectral Jump

The spectral jump which occurs with and without a pig tail fiber. Therefore it is an spectral jump intrinsic to the laser.

Experiment

Sample No. 277 (HLP1500)

Operation Conditions:

$$I_{\text{bias}} = I_{\text{threshold}} + 10 \text{ mA}$$

$$I_{\text{signal}} = 17 \text{ mA (peak-to-peak)}$$

Measuring System: as described in Fig.1(a)

Results:

As the heatsink temperature was changed, spectral jump occurred at 9.45°C. Above and below the "dangerous" temperature, the mode is single as shown in Fig.2 (a),(c). Another dangerous temperatures, at which mode jumped, were 33.7°C, 18.0°C and 3.15°C on this laser (Temperature range: 2°C-40°C). The amount of the spectral jump is typically 1.1 nm.

1.2 Type-2: Extrinsic Spectral Jump

The spectral jump which is caused by optical reflection from the input facet of the pig-tail fiber. The amount of spectral jump depends on the distance between the laser facet and the fiber-facet.

Experiment

Sample: #3105

Operation Conditions:

Constant temperature 19.1°C

$I_{\text{sig}} = 17 \text{ mA}$ (peak-to-peak)

I_b = changed as described in Fig.3

Result 1 : Fig.3

To groups of modes, centered at 831.5 nm and 834.2 nm are competing. As the I_b was increased, the longer wavelength modes became dominant.

Result 2 : Fig.4 (a-f)

The fiber pig tail of the same laser was removed. Only one group of modes appeared. Thus the spectral jump by an amount of 2.7 nm observed in Fig.3 was concluded due to the reflection from a fiber facet. The 2.7 nm jump well corresponds to the separation of 100 μm between the laser and fiber facets.

1-3 Origin of Double Eye Pattern

In both cases (type-1 & 2), mode jump occurs from shorter to longer wavelength in a single pulse, resulting in pulse shortening at the end of a long distance fiber.

This is supposed to be the origin of your double eye patterns in the 1 - 0 transition. Nevertheless, we have not succeeded in observing double eye patterns in our 2.8 km fiber system.

It may be attributable to the difference in the spectral dispersion of the fibers.

Experiment

Sample: #3105

Operation Conditions:

$I_{sig} = 17 \text{ mA}$ (peak to peak)

Temperature : 19.1°C

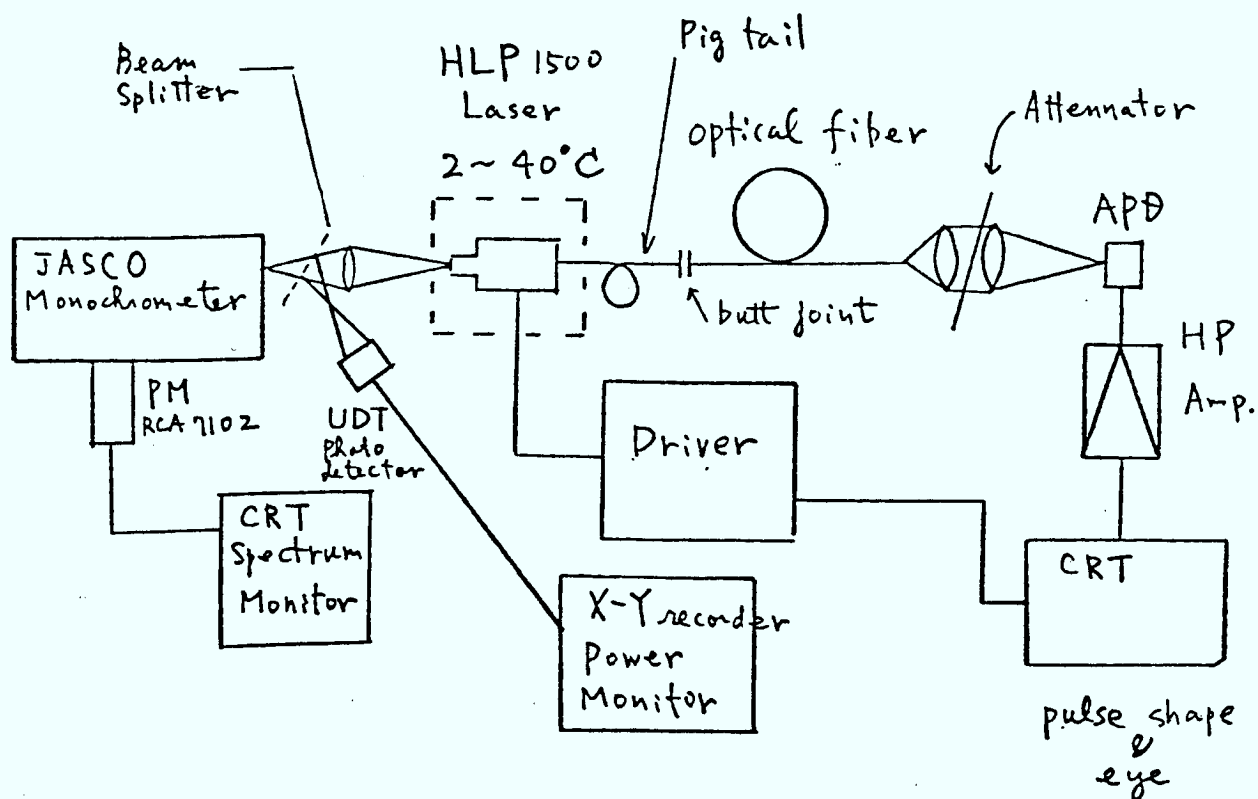
Measuring System : Fig. 1 (b)

Results : Fig.5 (a) $I_b = 75 \text{ mA}$

Fig.5 (b) $I_b = 85 \text{ mA}$

1-4 Future Improvements

The intrinsic mode jump (1.1 nm) seems not harmful in your system. We should appreciate your comment on this. The huge mode jump (3 nm, for example) due to external reflection should be eliminated. We are trying optimization of packaging configuration to minimize the reflection effect.



Bit rate : 200 Mbit/s

Optical fiber : 2.8 km three splices

Signal : NRZ

Spectral Observation : 1 scan / 50 ms


TITLE Fig. 1 (a)
Experimental setup for
longitudinal mode observation

DRAWN
T. Fukuzawa

CHECKED
K. Aiki

APPROVED
K. Aiki

DATE
Nov. 1st 1979

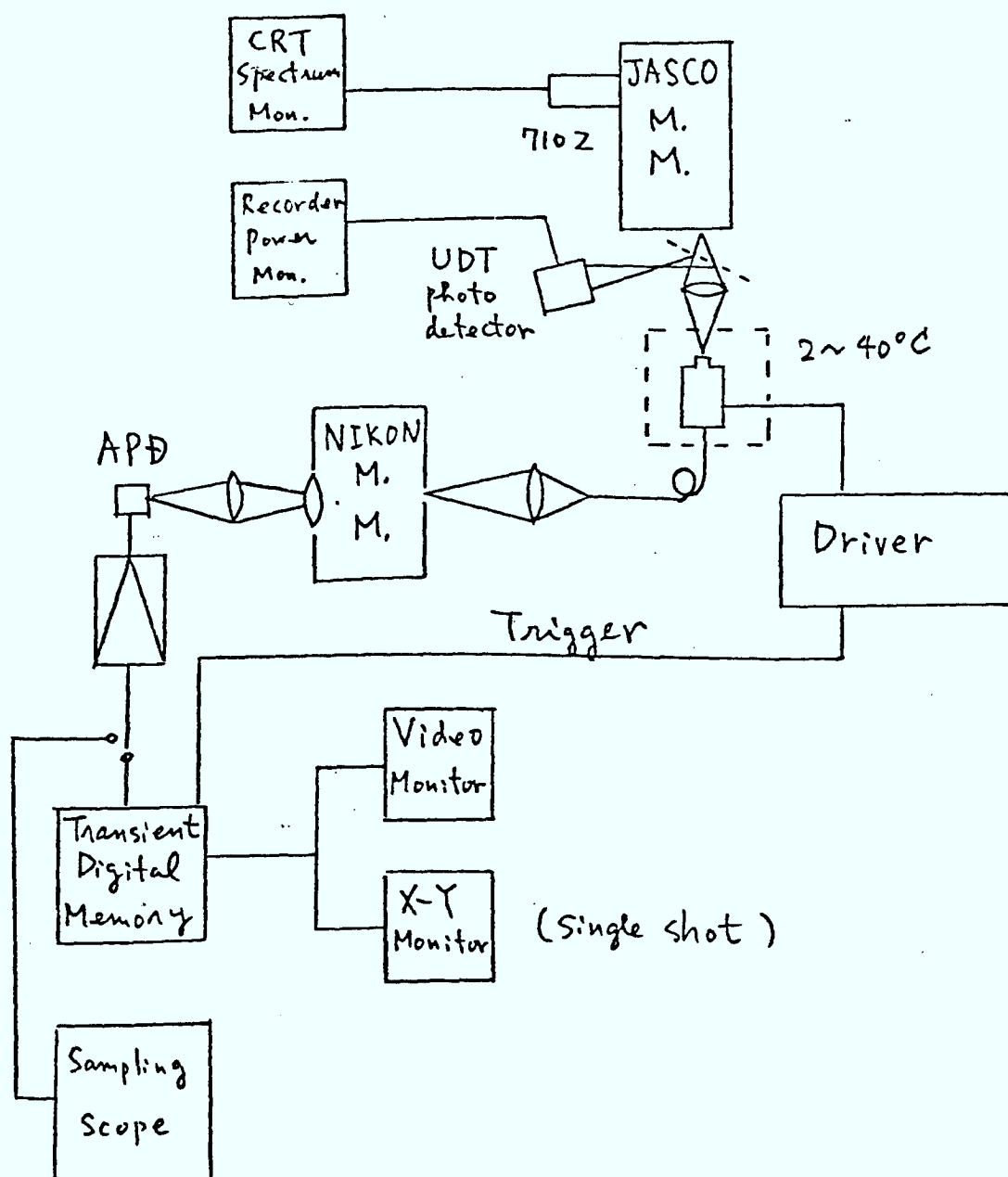
 Hitachi, Ltd. Tokyo Japan

6-2, 2-chome, Otemachi, Chiyoda-ku, Tokyo 100
Telephone: Tokyo (270) 2111
Cable: "HITACHI" TOKYO

DRAWING NO.

9103

REVISIONS



TITLE

Fig. 1 (b)
Experimental setup for transient
characteristics longitudinal
mode observation

DRAWN
T. Fukuzawa

CHECKED
K. AIKI


APPROVED
K. Aiki

DATE
Nov. 1st 1979

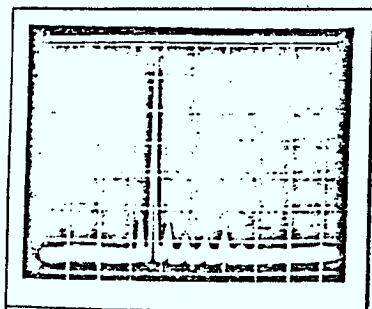
DRAWING NO.

REVISIONS

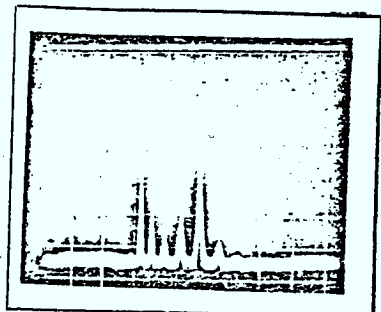
9104

 **Hitachi, Ltd. Tokyo Japan**

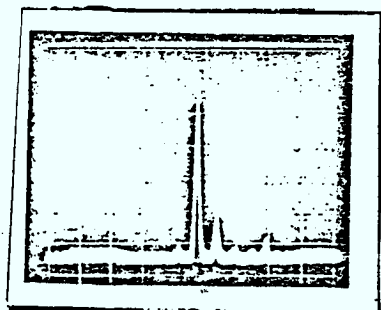
6-2, 2-chome, Ottemachi, Chiyoda-ku, Tokyo 100
Telephone: Tokyo (270) 2111
Cable: "HITACHY" TOKYO



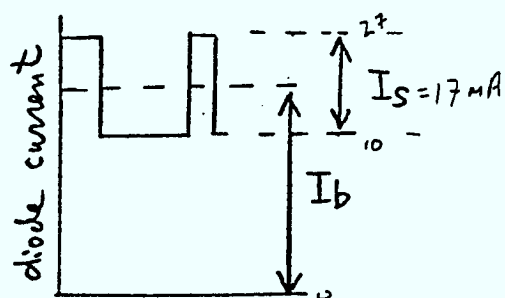
(a) 11.7°C



(b) 9.45°C



(c) 4.35°C



sample HLP-1500 #277

 $I_b = I_{th} + 10 \text{ mA}$ $I_s = 17 \text{ mA (peak to peak)}$


TITLE Fig. 2
Intrinsic spectral jump

DRAWN
T. Fukuzawa

CHECKED
K. Aiki

APPROVED
K. Aiki

DATE
Nov. 1st 1979

 Hitachi, Ltd. Tokyo Japan

6-2, 2-chome, Ottemachi, Chiyoda-ku, Tokyo 100
Telephone: Tokyo (270) 2111
Cable: "HITACHY" TOKYO

DRAWING NO.

9105

REVISIONS

HLP 1500

3105

$I_b = 75 \text{ mA}$

(a)

$I_b = 83 \text{ mA}$

(e)

$I_b = 77 \text{ mA}$

(b)

(g)

$I_b = 79 \text{ mA}$

(c)

(f)

(d)

$I_b = 81 \text{ mA}$

$I_b = 85 \text{ mA}$

$I_b = 87 \text{ mA}$

Temperature $19.1 \pm 0.1^\circ \text{C}$

$I_s = 17 \text{ mA}$ (peak to peak)

TITLE
Fig. 3
Extrinsic spectral jump

DRAWN
T. Fukuzawa

CHECKED
K. Aiki

APPROVED
Y. Aiki

DATE
Nov. 1st 1979

DRAWING NO.

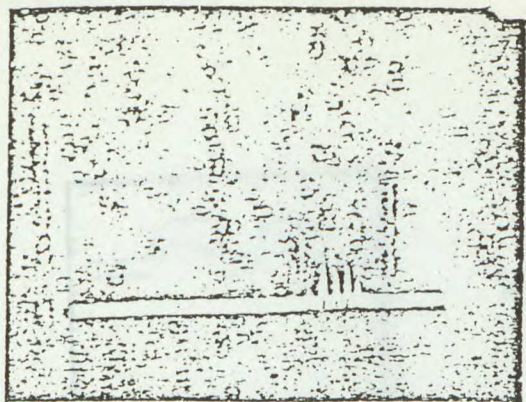
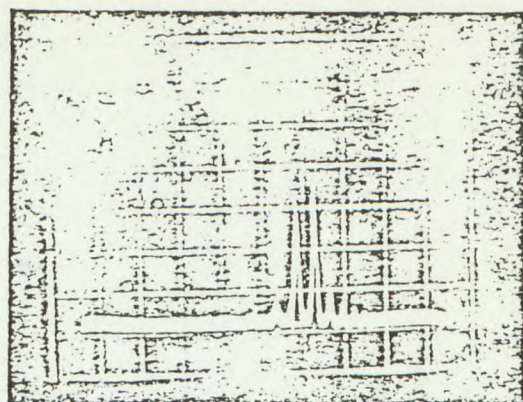
9106

Hitachi, Ltd. Tokyo Japan

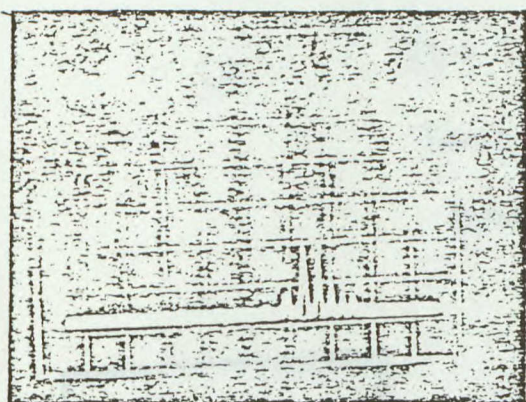
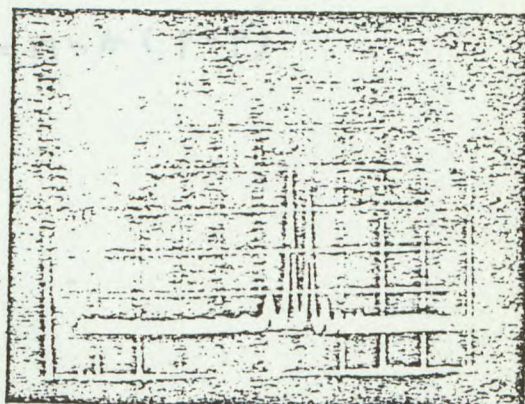
6-2, 2-chome, Oiemachi, Chiyoda-ku, Tokyo 100

Telephone: Tokyo (270) 2111

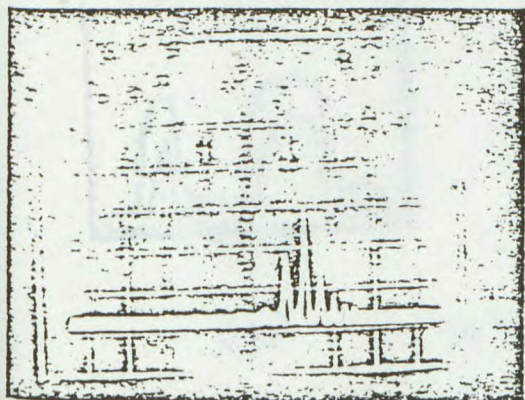
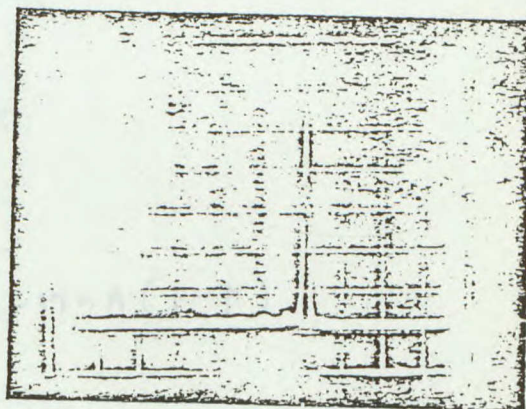
Cable: "HITACHY" TOKYO

(a) $I_b = 70 \text{ mA}$ (d) $I_b = 85 \text{ mA}$

MEMORY

(b) $I_b = 75 \text{ mA}$ (e) $I_b = 90 \text{ mA}$

MEMORY

(c) $I_b = 80 \text{ mA}$ (f) $I_b = 95 \text{ mA}$

TITLE

Fig. 4
Spectral jump for pig tail
removed laser

DRAWN
I. Fukuzawa


CHECKED
K. Aiki

APPROVED
K. Aiki

DATE
Nov. 1st 1979

DRAWING NO.

REVISIONS

 Hitachi, Ltd. Tokyo Japan

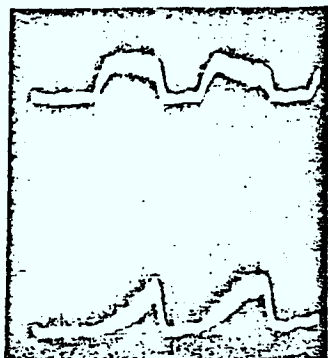
6-2, 2-chome, Otemachi, Chiyoda-ku, Tokyo 100

Telephone: Tokyo (270) 2111

Cable: "HITACHI" TOKYO

Telex: 122305 22422 24401 22227

9107



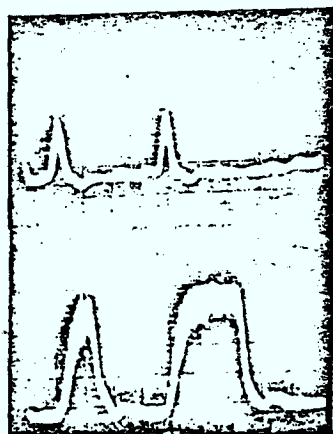
$$\lambda = 829.2 \text{ nm}$$

$$\lambda = 832.3 \text{ nm}$$

$$(a) \quad I_b = 75 \text{ mA} \quad I_s = 17 \text{ mA (P-P)}$$

$$\text{Temp } 19.1^\circ \text{C}$$

$$5 \text{ ns/div.}$$



$$\lambda = 829.2 \text{ nm}$$

$$\lambda = 832.3 \text{ nm}$$

$$(b) \quad I_b = 85 \text{ mA} \quad I_s = 17 \text{ mA (P-P)}$$

$$\text{Temp } 19.1^\circ \text{C}$$

$$5 \text{ ns/div.}$$

TITLE Fig. 5

Transient characteristics

DRAWN

T. Fukuzawa

APPROVED

K. Aiki

CHECKED

K. Aiki

DATE

Nov. 1st 1979

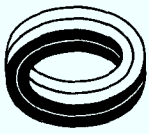
Hitachi, Ltd. Tokyo Japan

6-2, 2-chome, Ottemachi, Chiyoda-ku, Tokyo 100
Telephone: Tokyo (270) 2111

DRAWING NO.

9108

REVISIONS



APPENDIX 3

Study on Mechanical and Transmission
Characteristics of Optical Fibre Cable
During Installation

Study on Mechanical and Transmission Characteristics of Optical Fiber
Cable during Installation

Yutaka KATSUYAMA*, Yukinori ISHIDA*, Chihaya TANAKA*, Kazuhiro HARADA*,
Shigeru TANAKA**, Osamu ICHIKAWA**, Shuzo SUZUKI**

*Ibaraki Electrical Communication Laboratory, NTT
Tokai, Ibaraki-ken, 319-11, Japan

**Sumitomo Electric Industries, Ltd.

1, Taya-cho, Totsuka-ku, Yokohama, 244, Japan

Summary

An installation simulation was conducted for a 240-m long optical fiber cable containing tightly coated multi-mode and single-mode fibers. The cable characteristics during the installation was clarified. The simulation was made by squeezing the cable with curved guides. During the simulation test, optical transmission loss and elongation of glass fiber were monitored. While squeezing cable under 8000 N tension the transmission loss fluctuation was less than 0.01 dB and the residual value of loss increase was less than 0.02 dB/km after six time squeezings. A simple and accurate measuring method was employed to evaluate the fiber elongation during and after installation. The average fiber strain became 0.18% when the optical cable was tested under a tension of 8000 N which is more than double value of the designed tension for installation. However, the maximum residual strain was estimated only 0.07% even after six time squeezings. The residual strain is small enough to guarantee the long-term reliability of fiber strength against the static fatigue.

1. Introduction

Recently optical fiber communication technology has reached the stage of practical use and optical fiber cables have come to be installed in such conventional facilities as conduits and cable tunnels. The optical fiber cable, however, has some innate problems. For example, the optical transmission loss degrades when the glass fiber suffers microbending.^[1] A large elongation of glass fiber during installation causes fiber failures. Furthermore even a small residual elongation of fiber after installation accelerates the static fatigue^[2] of glass fiber and finally results in the fiber failure. Therefore, it is required to clarify the mechanical and transmission characteristics of optical fiber cables during installation and determine the appropriate cable design, installation apparatus and conditions.

This paper describes experimental result of an installation simulation for optical fiber cables which contain the tightly coated optical fibers. The elongation of glass fiber during and after installation test was monitored by employing a newly developed optical method. The optical transmission loss was also monitored at a wavelength of 1.3 μm . Discussion is made on the mechanical and transmission characteristics given by the installation test.

2. Installation simulation

2.1 Cable structure

Fig. 1 shows the fiber coating structure. The glass fiber of 125 μm diameter is tightly coated with silicone buffer of 400 μm diameter and nylon of 900 μm diameter.^[3] Fig. 2 shows the 12-fiber cable used in the installation test. This type of cable was used in

the field trial of large capacity trunk line system by NTT in 1980.^[4]

[5] The cable is composed of two fiber units, two power feeders, and six copper wire quads for subsidiary transmission use. One of the fiber units contains six single-mode fibers and the other contains six multi-mode fibers. The strength member is 7-stranded steel wires of 1.4 mm diameter with polyethylene sheath. The cable diameter is about 25 mm. The average transmission losses of single-mode and multi-mode fibers were 0.54 dB/km and 0.58 dB/km at 1.3 μm , respectively.

2.2 Simulation method

Considering the mechanical forces affecting the optical fiber cable during the installation, the most serious situation is under a squeezing which occurs in a curved part on a installation route, since the optical fiber in the cable is subjected to both tension and bending moment at one time. Therefore, the simulation system of cable installation must be designed to be able to evaluate the squeezing effect on the cable at the curved part.

Fig. 3 shows the simulation system for the cable installation. A 240-m long optical cable was laid on the ground straightly between two poles. The optical cable is able to be loaded with a definite tension up to 8000 N by universal wire stretchers inserted between the cable and the poles. The cable tension was monitored by tension meters at the both ends of the cable. Two curved guides for installation were set up on a truck, which moved from one end of the test cable to the other end to squeeze the cable. As shown in Fig. 3, the optical cable is subjected to two bends in the opposite direction along the curved guides. The bending radius of the cable was 600 mm.

and bending angle was 70 degrees in each guide. Fig. 4 shows the curved guide used in the simulation. The cable contacts with the curved surface of the cushion belt and goes along with rotating the belt. Both rotating cushion belt and base of this apparatus are laminated with teflon sheets to decrease the frictional force.

The advantage of this simulation method is that the squeezing apparatus moves and, therefore, the cable ends keep the same position, which enables the continuous monitoring of transmission loss fiber elongation during the test using optical fibers taken out through the cable ends.

2.3 Monitoring system

The elongation of the glass fibers and transmission loss were monitored. The optical fibers were taken out through the both ends of the cable and were spliced by arc-fusion machine^[6] to form optical links for monitoring at the one end of the cable.

Fig. 5 shows the monitoring system in this experiment. Six single-mode fibers were spliced and formed a 1.44-km long optical link. The optical power at a wavelength of 1.3 μm was detected with APD during the installation. As for the multi-mode fibers, two 0.48-km optical links were formed by splicing two optical fibers, respectively. One optical link was used for the transmission loss monitoring at the wavelength of 1.3 μm in the same manner, as for the single-mode fiber link, and the other for the fiber elongation monitoring. The two multi-mode fibers were left to measure the residual fiber elongation after the installation.

For the precise measurement of fiber elongation, a new optical method^[3] was employed, in which the phase change in the modulation signal was measured. By measuring the change in modulation signal phase $\Delta\theta$ (Fig. 5), the elongation of glass fiber ΔL is obtained by the following equation;

$$\Delta L = \frac{c \cdot \Delta\theta}{2\pi f N} \left\{ 1 - \frac{N^2}{2} [P_{12} - \nu(P_{11} + P_{22})] \right\}^{-1}, \quad (1)$$

where f : modulation frequency,

N : group refractive index of the fiber,

P_{11} : element of strain-optic tensor (= 0.121),

P_{12} : element of strain optic tensor (= 0.270),

ν : Poisson's ratio (= 0.17),

c : velocity of light.

In this experiment $f = 500.0000$ MHz was used. The measurement accuracy of fiber elongation is estimated about 0.005%. This high accuracy is achieved owing to the highly stabilized frequency by the locked-in generator.

2.4 Fiber elongation under static tension

First, the curved guides were removed from the simulation system and the cable was laid straightly and was loaded with a static tension up to 7000 N. Fig. 6 shows the measured fiber elongation under a static tension. It is found that the fiber elongation increased linearly with increasing the applied tension and the maximum value became 0.11% at a tension of 7000 N. After the tension released, the residual fiber elongation of 0.011% was observed and this residual elongation remained unchanged during the observation in further 10 minutes.

2.5 Installation characteristics

Two pieces of cables were used in the squeezing test. Table I shows the simulation conditions. Cable I was squeezed at six times under a tension of 3000 N and successively six times under 6500 N. Cable II was first subjected to the static tension test described in the previous section and then was squeezed at six times under a tension of 8000 N. Relatively high tensions were chosen to investigate the maximum strength of the cable, whereas the designed allowable installation tension is 3000 N for the cable shown in Fig. 2.^[4]

Table II shows the results of squeezing test. The impulsive fluctuations less than 0.01 dB of transmission loss were observed during the installation at tensions of 6500 N and 8000 N for the both single-mode and multimode fibers as shown in Fig. 7. The residual transmission loss after the test was less than 0.02 dB/km for both fibers.

On the other hand, the fiber elongation increased with the increase in the cable tension. Fig. 8 shows the average fiber strain at the stages of (i) before the squeezing and tension loading, (ii) during squeezing, and (iii) after the release of the tension and the return of the truck to the starting position at each time of the test. It was observed that the monitored strain was first revealed under the tension, increased gradually with growing squeezed part of the cable, became maximum when squeezing was finished, and falled down by releasing the tension. The measured values are shown in Fig. 8 schematically. In Fig. 8 the thermal elongation of the optical fiber due to the temperature change is compensated based on the measured temperature dependence of elongation of a fiber in the cable. During the squeezing, the cable is subjected to a bend-tension at the curved guide.

An optical fiber existing in the outer side at bend part of the cable is much subjected to tensile force. Therefore, this fact causes the excess elongation, resulting in the non-uniform distribution of the fiber elongation along the fiber length. The measured strain is to be interpreted as an average value of the monitored optical link. It is found from Fig. 8 that the average fiber strains during the squeezing were 0.06, 0.13, and 0.16% given by subtracting the residual strain from the total strain under the cable tensions of 3000, 6500, and 8000 N, respectively. They are larger than 0.05, 0.10, and 0.125% under the corresponding static tension, respectively, shown in Fig. 6. The average excess fiber strains were, therefore, estimated 0.01, 0.03, and 0.03% at the tensions of 3000, 6500, and 8000 N, respectively. On the other hand, the maximum strains during squeezing are found to be 0.06, 0.15, and 0.18% including residual strain under each tension.

2.6 Residual fiber elongation

After the simulation test, the cables were re-wound on the cable drums and placed in the temperature controlled chamber. The fiber length was measured again in the same way as for the measurement of the initial fiber length before the test by the optical method. The residual fiber elongations due to the squeezing were evaluated by the difference between the fiber length after squeezing and the initial length. The measured residual strains are $0.056 \pm 0.005\%$ and $0.037 \pm 0.005\%$ for Cable I and II, respectively.

3. Discussion

3.1 Transmission loss

3. Discussion

3.1 Transmission loss

The transmission loss increase during and after tests were very small even when the cable tension was more than twice the designed value. The confirmed stability of the transmission loss is consistent with the results of field research using more than 1 km of this type cables. [4][5] The achieved stability during the installation is attributed to the combination of the stable cable structure and the appropriate curved guide. The curved guide is designed to soften the lateral force applied to the cable by adopting rubber blocks for the belt.

3.2 Fiber elongation

(1) Static tension

The fiber elongation under the static tension was found to be linear with the cable tension, which is consistent with the theoretical expectation for the tightly stranded cable. The measured value of fiber strain under a tension of 7000 N is $\epsilon_{\text{mea.}} = 0.11\%$ which is in agreement with the calculated value of $\epsilon_{\text{cal.}} = 0.13\%$ obtained by the following equation:

$$\epsilon_{\text{cal.}} = \frac{1}{\sum_i E_i S_i} \cdot F, \quad (2)$$

where, E, S, and F represent Young's modulus, cross sectional area of the cable constituent, and tension, respectively, and "i" is the suffix distinguishing the cable components.

(2) Installation with bends

In order to prevent the fiber failure during the installation and obtain the long-term reliability against the static fatigue due to the

residual elongation, a smaller fiber elongation is desirable.

The maximum strain within the cable is able to be estimated from the measured fiber strain, when the sinusoidal distribution is assumed for the excess strain,

$$\epsilon(z) = \epsilon_0 + \frac{\Delta\epsilon}{2} \left[1 + \sin \frac{2\pi z}{P} \right], \quad (3)$$

ϵ_0 : fiber strain under a static tension

$\Delta\epsilon$: maximum excess strain

P : stranding pitch in the cable

z : coordinate along the fiber length.

The excess strain is caused by squeezing which consists of bending, lateral force and tension. Bending causes tension and compression sides in the cable, and the fiber strain may be induced sinusoidally in the z -direction, according to the stranding pitch. On the other hand, tension causes constant strain ϵ_0 , and lateral force causes no strain ideally.

Based on eq.(3), the maximum strain $\epsilon_{\max.}$ ($= \epsilon_0 + \Delta\epsilon$) is estimated 0.07% by substituting $\epsilon_0 = 0.05\%$ and $\Delta\epsilon = 0.02\%$ during the squeezing at a tension of 3000 N. The maximum residual strain is also estimated about 0.2% after six time squeezings at a tension of 8000 N.

In field, these cables are installed with the tension smaller than 3000 N and with a few curved guides per km. Therefore, a much smaller residual strain of optical fiber than the above value is expected in the actual application.

Fig. 9 shows the estimated fiber lifetime without failure as a function of proof test strain.^[8] It is found from Fig. 9 that the sufficient long-term reliability can be expected with this cable when the installation conditions and the proof testing of optical fibers

are appropriately designed.

4. Conclusion

Installation simulation was conducted for an optical fiber cable, monitoring the transmission loss and the elongation of glass fiber. To investigate the maximum cable strength, the cable tension was raised up to 8000 N, which is more than double value of the designed tension. The transmission loss change during and after installation was less than 0.01 dB and 0.02 dB/km, respectively, for both single-mode and multi-mode fibers. The fiber elongation, on the other hand, increased with the increase in cable tension. The average fiber strain became 0.06% and 0.18% when the cable tensions were raised up to 3000 N and 8000 N, respectively. The maximum residual strain of the glass fiber was estimated as 0.07% even after six time squeezings under a 8000 N tension, which is considered to be small enough to guarantee the long-term reliability against the static fatigue. As far as the tested cable is concerned, the maximum allowable installation tension is considered to be determined by the fiber elongation during and after installation rather than the transmission loss stability.

Acknowledgment

The authors thank N. Uchida and M. Hoshikawa for their effective suggestions and discussions, and H. Fukutomi and Y. Kato for their encouragements throughout this work. Thanks are also due to K. Saegusa for this experimental assistance.

References

- [1] W. B. Gardner, "Microbending loss in optical fibers", BSTJ 54, p 457-465 (1975)
- [2] See, for example, D. Karish and B. K. Tariyal, "Static and dynamic fatigue of a polymer-coated fused silica optical fiber", 61, p. 518 - p.523 (1978)
- [3] T. Nakahara and N. Uchida, "Optical cable design and characterization in Japan", Proc. IEEE 68, pp. 122 -1226 (Oct. 1980)
- [4] N. Uchida, Y. Ishida, and K. Ishihara, "Single-mode and graded-index multimode optical cables for use in long wavelength transmission systems", ICC'81, 27.5.1, Denver, (June 1981)
- [5] Y. Ishida, M. Tokada, S. Seikai, M. Nakahira and K. Harada, "Construction and characteristics of large capacity optical transmission line", IECE of Japan, CS81-2, p.7~12, (1981) [in Japanese]
- [6] M. Miyauchi, M. Matsumoto, M. Hirai, and K. Takahashi, "Practical fiber splice techniques for optical cables" Rev. Electr. Commu. Lab. (1981), to be published
- [7] S. Tanaka, M. Hoshikawa, N. Kurauchi, Y. Katsuyama, and T. Horiguchi. "Precise measuring method of elongation and residual strain of optical fiber due to cabling process", 7th ECOC 6.6 Copenhagen, (Sep. 1981)
- [8] Y. Katsuyama, Y. Mitsunaga, S. Tanaka, Y. Kameo, and M. Hoshikawa, "Lifetime design of optical fiber cable for long-term use", 7th ECCC, P.21, Copenhagen, (Sep. 1981)

Table I Simulation conditions

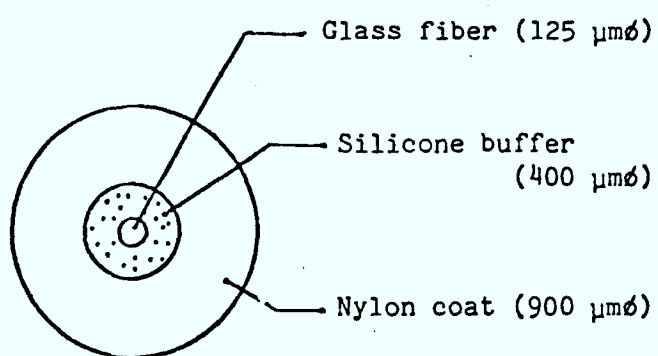
	Tension	Squeezing
Cable I	3000 N	6 times
	6500 N	6 times
Cable	(7000 N)*	-
	8000 N	6 times

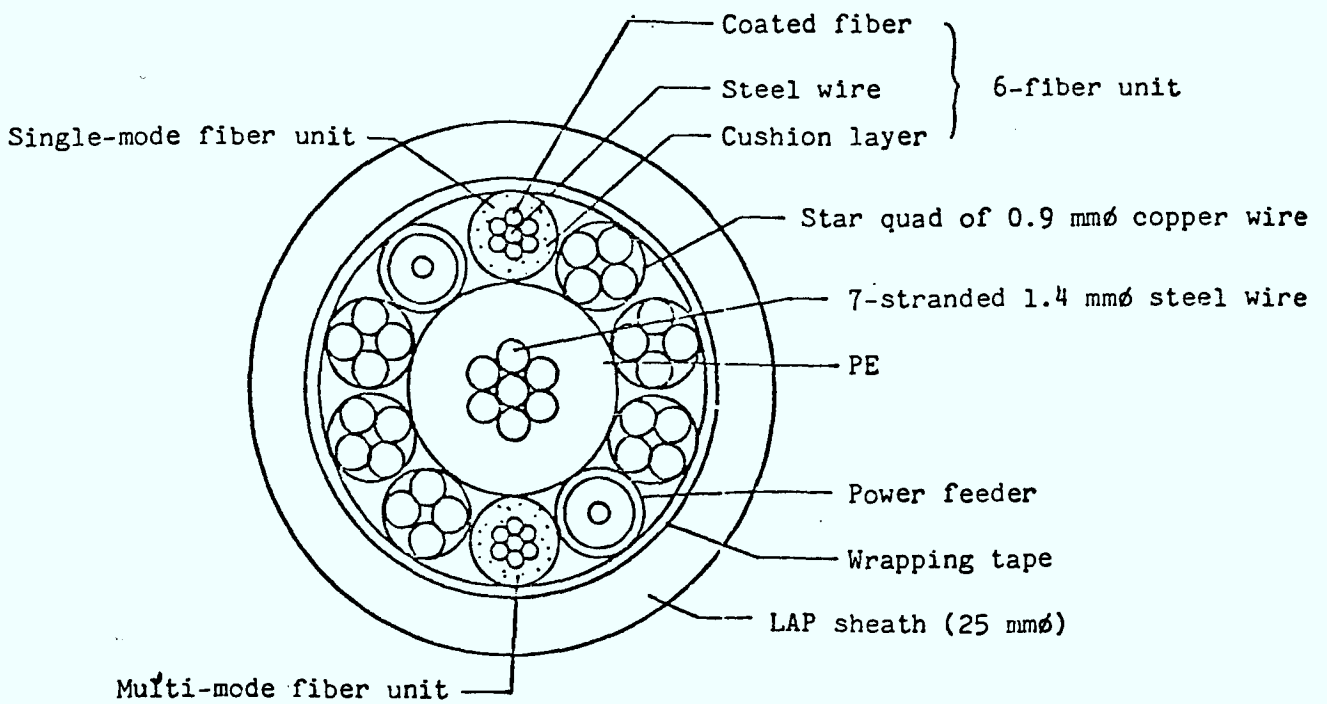
*static tension without curved guide.

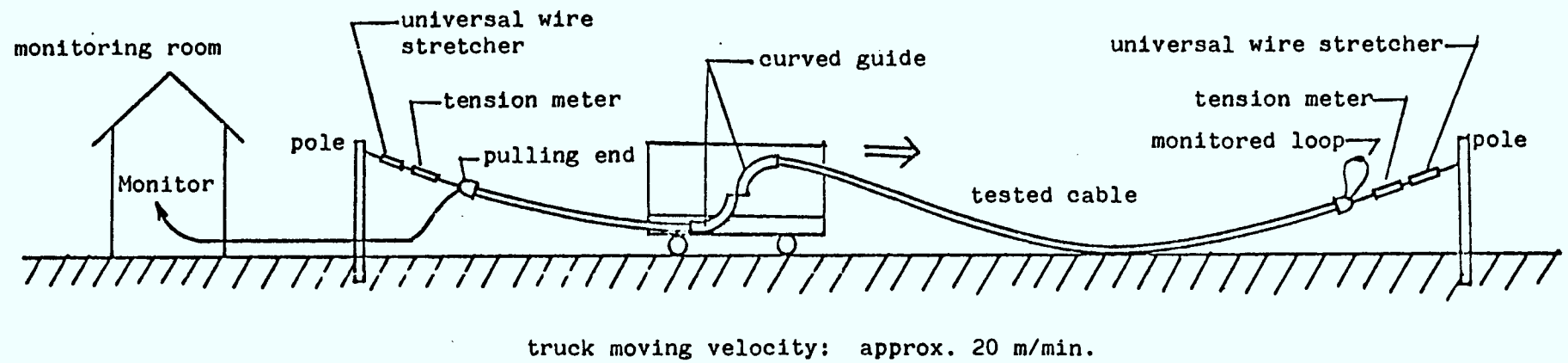
Table II Test results of transmission loss at 1.3 μm

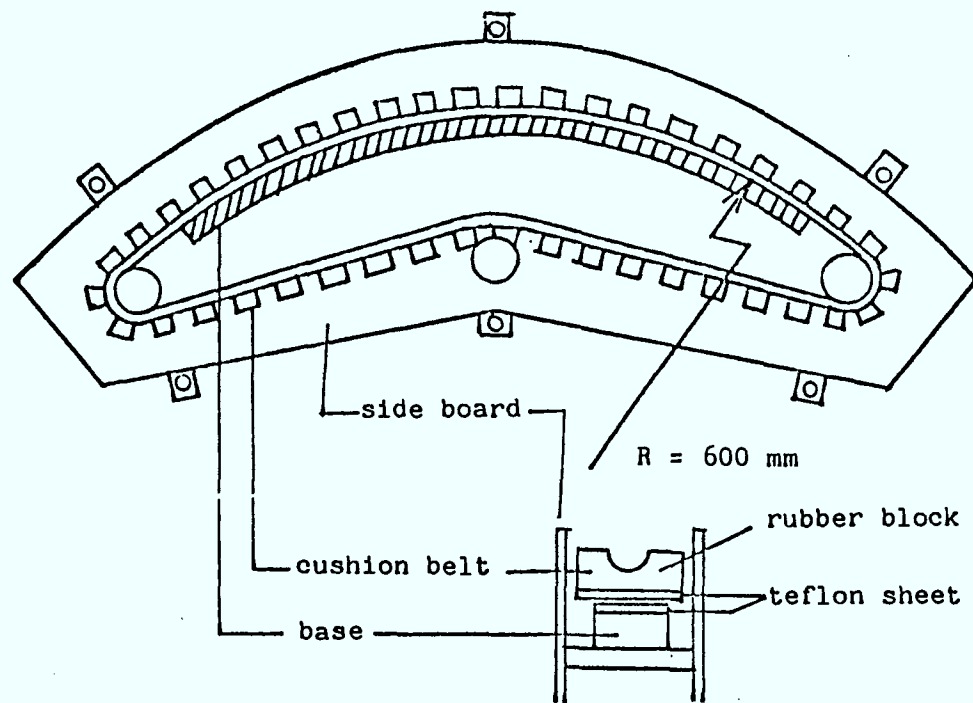
	Tension		Residual transmission loss		Transmission loss fluctuation during squeezing
	Higher side*	Lower side*	single-mode fiber	multimode fiber	
Cable I	3000 N	700 N	-0.009 dB/km	-0.004 dB/km	-
	6500 N	1100 N	0.009 dB/km	0.016 dB/km	less than 0.01 dB
Cable II	8000 N	1200 N	0.017 dB/km	0.010 dB/km	less than 0.01 dB

* Cable tension in the right side of the curved guide in Fig. 3 is lower than that in the left side because of the tension resistance at the curved guides. The higher tension in the left side cable corresponds to the pulling tension during the actual installation.

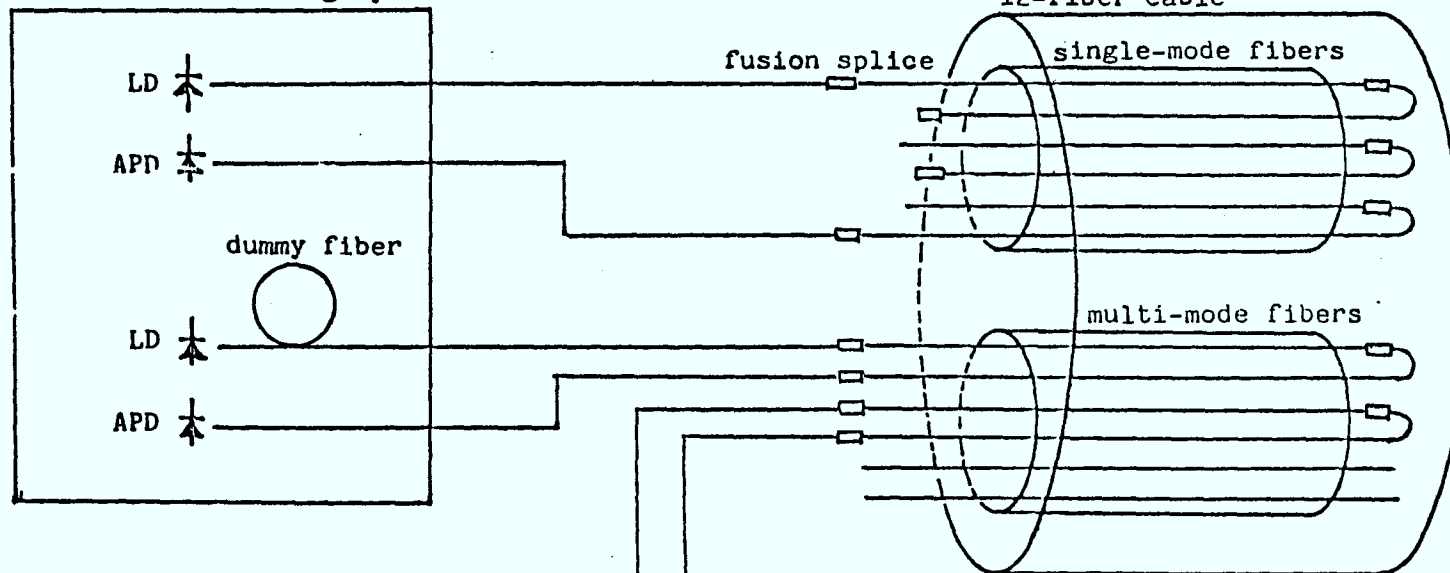




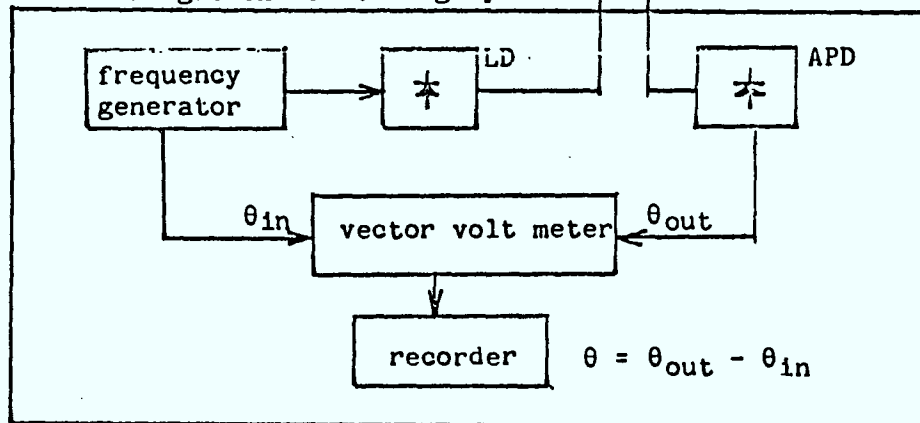


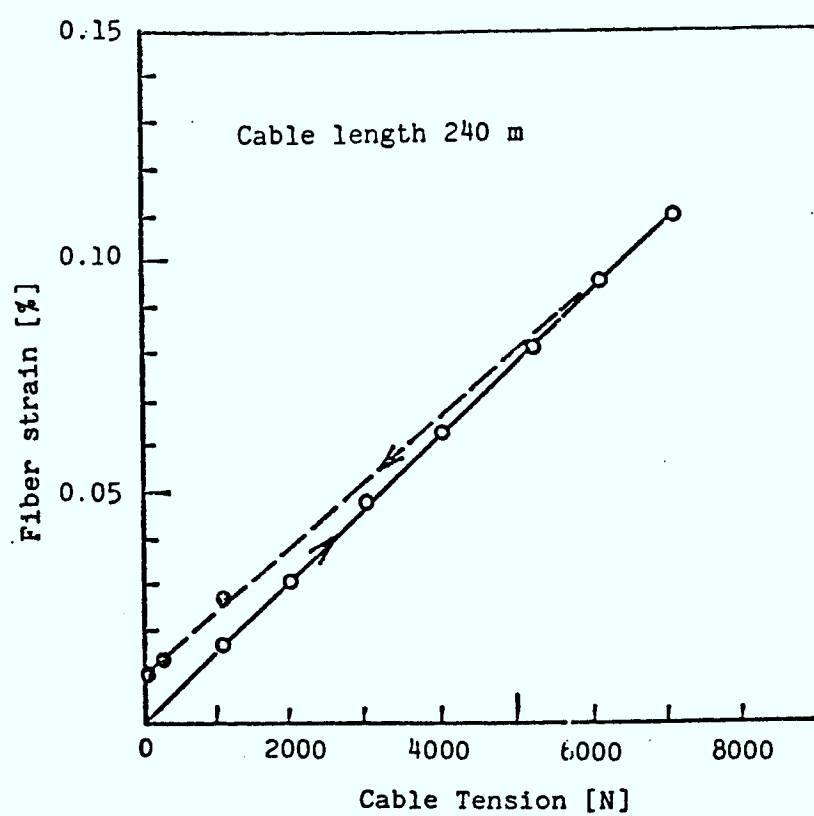


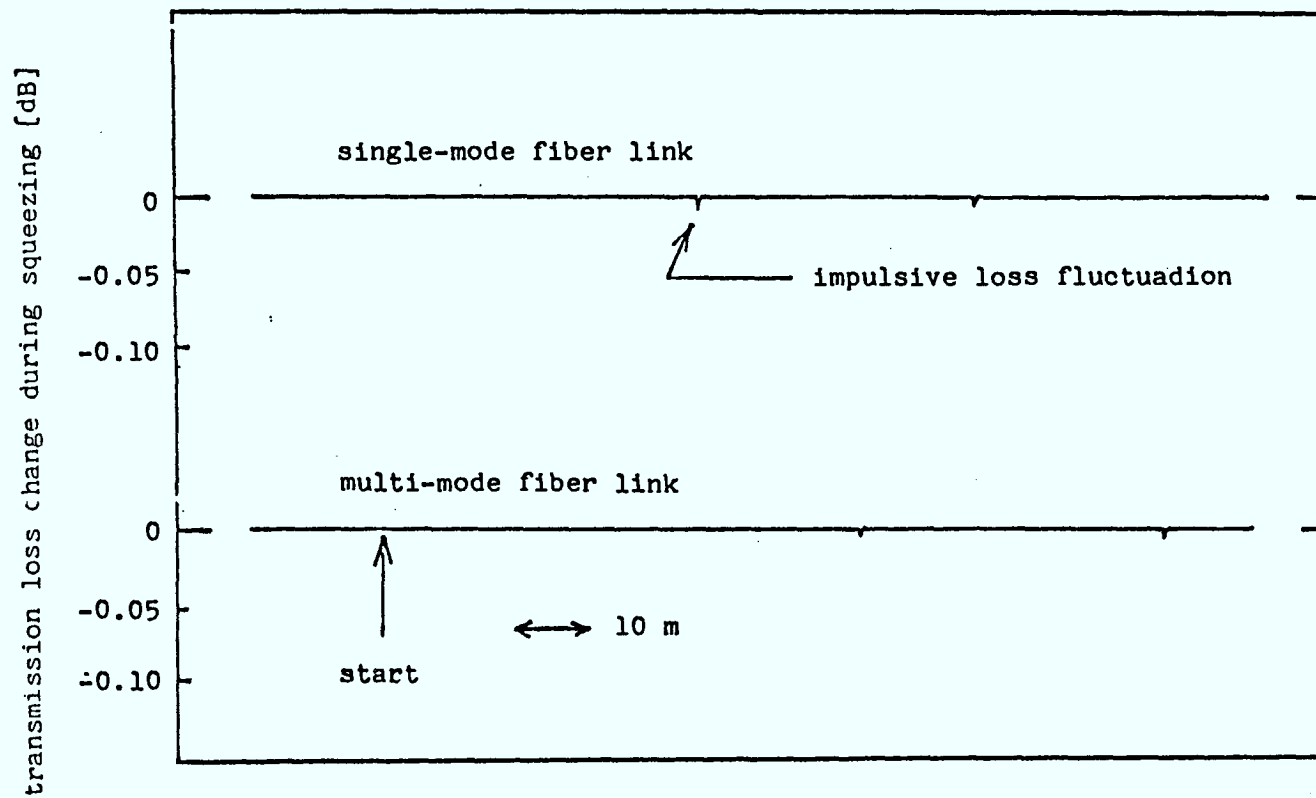
transmission monitoring system

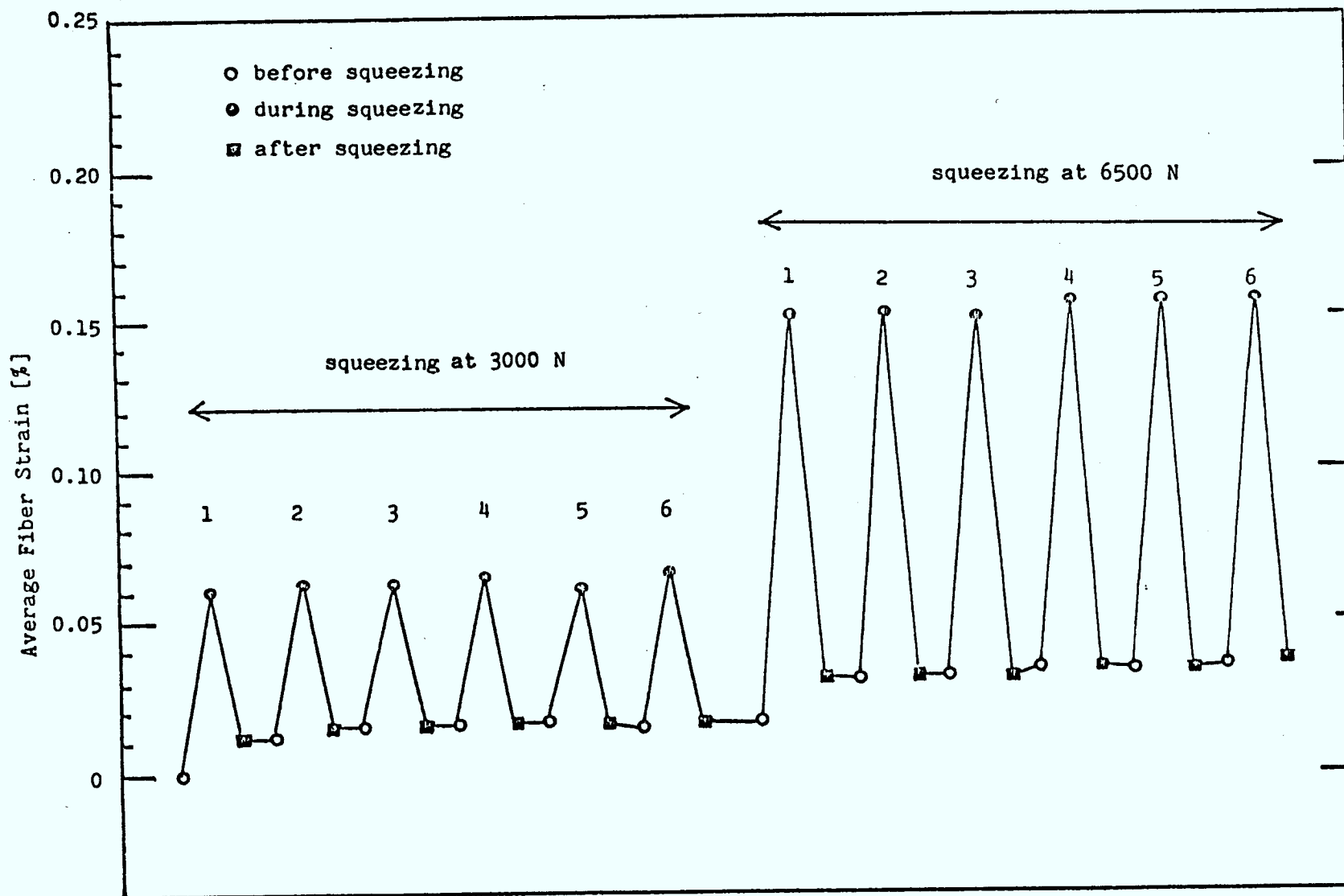


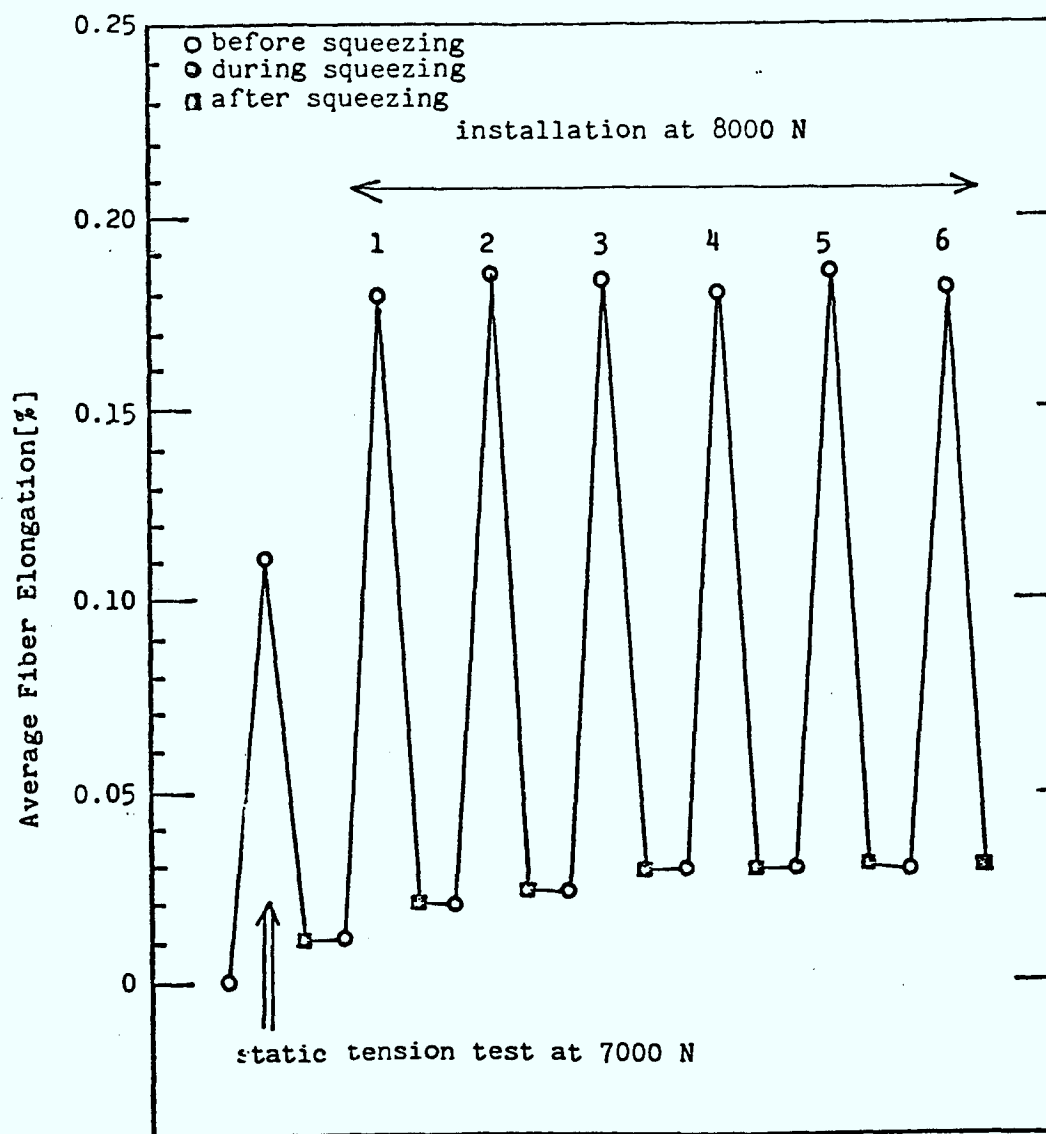
fiber elongation monitoring system

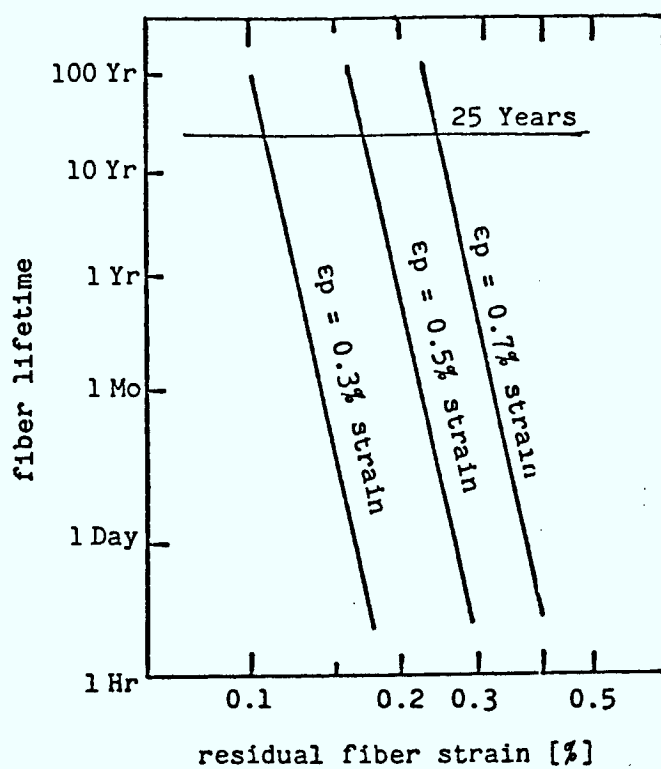


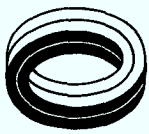












APPENDIX 4

Modal Noise in Optical Fibres: Open and Closed
Speckle Pattern Regimes by: Y. Tremblay,
B.S. Kawasaki and K.O. Hill

Modal noise in optical fibers: open and closed speckle pattern regimes

Y. Tremblay, B. S. Kawasaki, and K. O. Hill

Modal noise generation in multimode optical fiber is identified as occurring in two statistically differing regimes, that in which there is independence of the speckles (open regime) and that in which the speckles have an interdependency related to the constancy of the total light power in the core modes (closed regime). We derive statistical expressions for modal noise generation in the closed regime and verify them with experiment.

1. Introduction

In a series of publications that have appeared recently in the literature,¹⁻³ there is an apparent discrepancy in the measurements and theoretical treatment of modal noise in optical fibers as reported on the one hand by Daino *et al.*¹ and Rawson *et al.*³ and on the other hand by Hill *et al.*² All approaches predict the level of modal noise as a function of the detected portion of the total exit pattern of light from the fiber core but quantitatively they differ considerably. In particular, the treatments of Refs. 1 and 3 predict a maximum ratio of signal to modal noise equal to the square root of the number of guided modes, whereas treatment 2 predicts negligible modal noise when all of the core-guided light is detected. This discrepancy would lead to large differences in the predicted modal noise performance of fiber systems. Since modal noise acts to reduce the performance of an optical fiber link by increasing the error rate in the case of digital transmission and decreasing the fidelity in the case of analogue transmission, it is important to remove the discrepancy and thereby quantify modal noise in a unified manner as an aid to fiber-based communication system design.

In this paper, we resolve this apparent discrepancy by explicitly recognizing two statistically differing speckle pattern regimes which we term the open and closed regimes. It is, of course, the statistical properties of speckle patterns as they are related to and are dependent on the modal properties of optical fibers and

the coherence properties of the sources used to excite them that give rise to modal noise.⁴ Statistically closed speckle patterns are characteristic of an electromagnetic field (for example, that of the core-guided light) that does not exchange energy with one or more other energy fields (for example, the set of cladding modes). On the other hand, the occurrence of such energy exchange would lead to statistically open speckle patterns. A speckle pattern is fully open when all of the speckles are statistically independent. Thus, if we are concerned with the modal noise properties of the core-guided light of an optical fiber, we must determine at the outset whether the core light can, on a mode-selective basis, couple to the cladding modes of the fiber. To the extent that such a process can occur, the core-light speckle pattern will be open. In the open speckle pattern regime, the probability density function (PDF) of the power transmitted by a finite aperture placed within the speckle field as the fiber or the source exciting it is perturbed cannot be determined in general; the details of the energy exchange process between the interacting fields are normally not known in such instances. However, in the case of nonpolarization maintaining multimode fibers, a class which at present includes all multimode fibers, it is possible to study fiber speckle statistics conveniently in a regime that is approximately open by considering the power of the core-guided light that is contained exclusively by one of the two orthogonal states of linear polarization. Here, there need be no deterministic power level changes as the statistics of the process can be invariant. This approach was taken implicitly in Ref. 3 where a polarizer was inserted between the fiber output optics and the detector. In this case, the speckle pattern transmitted by the polarizer is approximately open because perturbation-induced energy exchange can occur along the length of the fiber between the fields that give rise to the orthogonally polarized output fields. It is not fully open, however,

The authors are with Department of Communications, Communications Research Centre, Ottawa, Ontario K2H 8S2.

Received 22 November 1980.

0003-6935/81/091652-04\$00.50/0.

as our following analysis will show, because the total energy in the two orthogonally polarized fields is constant in the absence of mode-dependent losses.

In this framework of modal noise existing in two basically different regimes we can categorize previously presented experimental results and theoretical treatments. The theoretical treatments of Refs. 1 and 3 describe the fully open regime and predict the maximum obtainable SNR equal to the square root of the number of degrees of freedom in the pattern transmitted by the restricting aperture. Furthermore, as pointed out in Ref. 3, in these conditions, the statistics of the light transmitted by the aperture is given by the gamma distribution whose parameter is equal to the number of degrees of freedom of that portion of the speckle pattern falling within the aperture. This distribution results from the assumption of statistical independence of the individual speckles. On the other hand, Ref. 2 describes the case of a closed speckle pattern (or no coupling to cladding modes) and predicts the variation of modal noise as a function of that portion of the speckle pattern detected; it does not present a derivation for the PDF of the transmitted light. Prediction of the statistics of the light transmitted by a restricting aperture for the closed regime is made complicated because the speckles are interdependent. However, we demonstrate in the following section that the statistics of the transmitted light are closely approximated by those of a gamma distribution and a transformed gamma distribution for typical multimode fibers.

II. Analysis

A. Open Speckle Pattern

In the case of a maximum-contrast speckle pattern, the speckle pattern amplitude PDF is Rayleigh and the intensity PDF is exponential.² If we further assume that the speckles have the same average intensity, it follows directly from the assumption of statistical independence between speckles that the PDF characterizing the optical power contained by that portion of the speckle pattern having n degrees of freedom (corresponding directly to M' of Ref. 3) is the gamma distribution.

$$p(P) = \frac{(P/b)^{n-1}}{b\Gamma(n)} \cdot \exp(-P/b). \quad (1)$$

In this expression P is the transmitted optical power and, for this case of an open speckle pattern, b is the power associated with one degree of freedom of the transmitted pattern. The mean of the distribution is nb and the variance is nb^2 . The ratio of the mean to the standard deviation is thus

$$R_0 = \sqrt{n}. \quad (2)$$

B. Closed Speckle Pattern

As we indicated in the Introduction this situation is complicated to characterize analytically because of the interdependency of the speckles in the closed regime of speckle patterns. If we make a number of assumptions,

however, about the case we are considering, we can deduce the form of the PDF in a piecemeal fashion. These assumptions are:

(1) N_{\max} , the maximum number of degrees of freedom of the unrestricted fiber output speckle pattern, is much larger than 1.

(2) There are no time-dependent mechanisms present in the fiber leading to time-dependent attenuation of the core-guided light. This condition, in effect, distinguishes the closed from the open speckle pattern regimes.

(3) The speckles have the same average intensity.

We can deduce the form of the PDF for the closed regime in the limiting cases of almost zero or almost complete transmission of the fiber output speckle pattern as follows. In the case of the closed speckle pattern a portion of the total speckles N_{\max} can be considered statistically independent if that portion is very small compared to N_{\max} . Therefore, in the case of a closed speckle pattern, the PDF of the power transmitted by a portion of the total pattern will be given closely by the gamma distribution, as for the open speckle pattern, when that portion is very small (this conclusion follows because the covariance is small; the covariance for two independent samples of intensity taken at the same instant is $-\sigma^2/N_{\max}$, where σ^2 is the variance of the intensity distribution of a single sample). Since the total of the light intensity is constant, it follows that the PDF of the power in the complementary speckle pattern (that portion of the speckle pattern that was not observed) will have a mean of $P_T - nb$, where P_T is the total power of the speckle field, and a variance of nb^2 . Also this PDF will be characterized by a skew reversed in direction from that of the function describing the transmitted portion of the light. What we are describing is, by symmetry, not only the PDF of the blocked light when a small portion of the pattern is transmitted but also that of the transmitted light when only a small portion of the pattern is blocked. The PDF for the transmitted light when almost all the speckle pattern is transmitted is thus given by

$$p(P) = \frac{[(P_T - P)/b]^{n-1}}{b\Gamma(n)} \cdot \exp(-(P_T - P)/b), \quad P_T - P > P > P_T/2. \quad (3)$$

We will call this the transformed gamma distribution. It is the mirror image of the previously described gamma distribution with the mirror plane located at $P_T/2$.

We would therefore expect the PDF for the closed speckle pattern to be gamma in shape in the region $P \sim 0$ and transformed gamma in the region $P \sim P_T$. We can, moreover, deduce the exact value of the variance for the closed speckle case because Ref. 2 provides us with the precise value of the ratio of the mean to the standard deviation for any portion of the transmitted light as deduced from a fundamental perspective. It is

$$R_1 = \left(\frac{n}{1 - n/N_{\max}} \right)^{1/2}, \quad (4)$$

where n is again the number of degrees of freedom in the

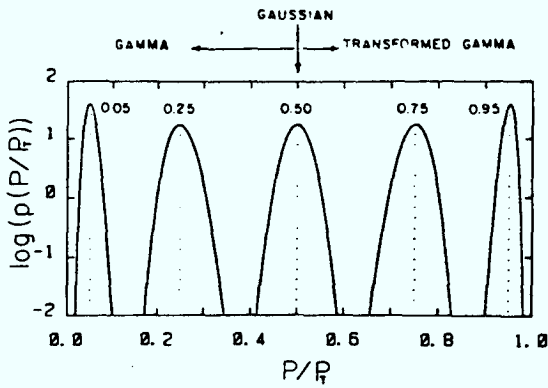


Fig. 1. Probability density function of the transmitted portion of a closed speckle pattern. The vertical scale is logarithmic, and the dotted lines indicate the respective means of the transmitted power. The curves are drawn for $N_{\max} = 500$. The areas of applicability of the piecemeal PDFs are also indicated.

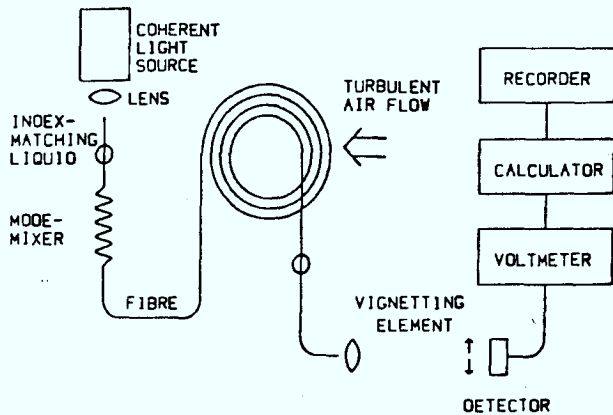


Fig. 2. Experimental apparatus arrangement.

transmitted portion of the light. For the closed speckle regime the effective power per degree of freedom β is substituted for b in Eqs. (1) and (3) as

$$\beta = (1 - n/N_{\max})b, \quad (5)$$

where b remains the power per degree of freedom; we can therefore approximate the PDF of the transmitted light in the closed speckle pattern regime by using Eqs. (1) and (3) with n' , now the effective number of degrees of freedom, substituted for n as

$$n' = n(1 - n/N_{\max})^{-1}. \quad (6)$$

These PDF's are only approximations, however, since it follows from the symmetry argument used to deduce Eq. (3) that the PDF for the closed speckle pattern case must be symmetric at $\bar{P}/P_T = 0.5$; it is readily shown that neither Eq. (1) nor Eq. (3) is symmetric at any point. We will show later nevertheless that the approximation is, for typical multimode fibers, a very good one even very close to $\bar{P}/P_T = 0.5$. At $\bar{P}/P_T = 0.5$, when both the transmitted and complementary speckle patterns contain on the average the same number of

speckles, the PDF can reasonably be expected to be Gaussian with a mean to standard deviation ratio given by Eq. (4).

To summarize our approximation: for the closed speckle pattern regime Eqs. (1), (5), and (6) give the PDF for the region $\bar{P}/P_T < 0.5$ and Eqs. (3), (5), and (6) give the PDF for the region $\bar{P}/P_T > 0.5$.

This situation is shown graphically in Fig. 1 in which the PDFs of \bar{P}/P_T , the portion of the total power in the speckle pattern, described by Eqs. (1) and (3) are plotted for four values of \bar{P}/P_T , the normalized average transmitted power. Equation (1) is plotted for $\bar{P}/P_T < 0.5$ and Eq. (3) for $\bar{P}/P_T > 0.5$. The curve at $\bar{P}/P_T = 0.5$ is Gaussian. The dotted lines mark the average transmitted powers at which the PDF's are calculated. The reversal of the skew from a right-side skew to a left-side skew for $\bar{P}/P_T < 0.5$ and $\bar{P}/P_T > 0.5$ is apparent.

III. Experiment

The validity of our analysis for the closed speckle pattern regime of modal noise was investigated using the experimental arrangement shown in Fig. 2. The source was a single-mode laser diode with an $0.894\text{-}\mu\text{m}$ wavelength and 2-mW output power. The test fiber was 10 m of step index glass clad fiber with a $100\text{-}\mu\text{m}$ core diam and a measured numerical aperture of 0.16. A major portion of the test fiber was configured into ten 20-cm diam loops which were loosely supported in a turbulent airstream giving rise to a dynamic, continuously changing speckle pattern at the output of the fiber. This output was imaged through a vignetting element onto a large area detector. The vignetting element, located in the image plane, consisted of an adjustable iris together with a movable cutting edge. The fluctuations in the photocurrent were processed with a combination of a sampling voltmeter and microcomputer.

Several measures were necessary in order to obtain repeatable results. The spectrum of the laser was monitored occasionally to ensure single-mode operation, and the launching was adjusted and a mode scrambler inserted to excite the core modes uniformly. To ensure that no unwanted time-varying elements were entering our measurements and that we were truly operating in the closed speckle pattern regime we monitored the overall stability of the total light in the core of the fiber. A cladding mode stripper followed the mode scrambler.

A. Ratio of Transmitted Power to Modal Noise in Closed Speckle Pattern Regime

Figure 3 shows a comparison between the calculated and measured levels of modal noise generation in the fiber strand as a function of $a = n/N_{\max}$ ($= \bar{P}/P_T$). The solid line indicated as R_1 gives the ratio of the transmitted power to the standard deviation of the power predicted by Eq. (4) with $N_{\max} = 1600$. To provide a universal curve the value of R_1 is R_1 divided by $(N_{\max})^{1/2}$. The experimental points were determined for 50,000 readings; the spread of the points gives a measure of the repeatability of the measurements. The

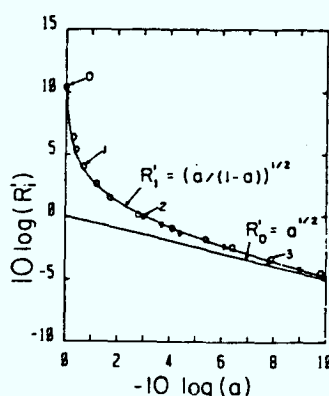


Fig. 3. Calculated and measured levels of modal noise as a function of the fraction of the speckle pattern transmitted. R'_1 gives the ratio of transmitted power to the standard deviation of the power for a closed speckle pattern with $N_{\max} = 1600$. R'_0 gives the equivalent curve for an open speckle pattern. Both curves are normalized to $(N_{\max})^{1/2}$. The experimental points are determined for 50,000 readings.

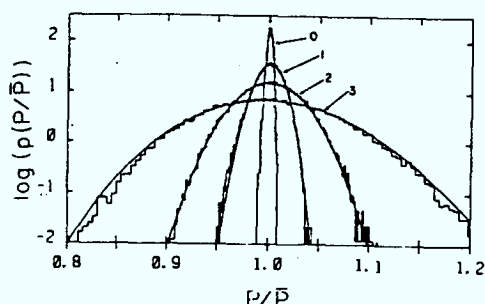


Fig. 4. Probability density functions of transmitted light for the four experimental points indicated on Fig. 3. Curves 1, 2, and 3 show a comparison between calculation (smooth solid lines) and measurement. Histogram 0 is a measure of the system stability.

measurements were taken in two different forms. The circles indicate measurements in which the aperturing was done with only the vignetting element. The stars indicate the measurements in which a polarizer was placed in front of the detector in addition to the vignetting element. The fit between experiment and theory is quite convincing in both cases. As expected, the polarizer acted merely as a 3-dB attenuator eliminating one-half of the degrees of freedom of the speckle pattern. On the figure the theoretically predicted value of $R'_0 [= R_0/(N_{\max})^{1/2}]$, the ratio of transmitted power to standard deviation that would be obtained in an experiment in the regime of a statistically open speckle pattern, is also shown. The two regimes closely resemble one another in the generation of modal noise for attenuation levels above 3 dB but diverge greatly toward lower attenuations.

B. PDF Shapes for Closed Speckle Patterns

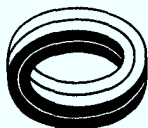
Figure 4 shows the PDFs of the transmitted light corresponding, respectively, to the four experimental points indicated by numbers in Fig. 3. These histograms were constructed by taking 50,000 samples of the detected voltage signal. The corresponding calculated curves, with power normalized to each average power, are indicated by solid smooth lines. Curves 1 and 3 were calculated using Eqs. (3) and (1) respectively, and curve 2 is a Gaussian. Histogram 0 corresponds to the system stability since all of the light was detected. The fit between theory and experiment is gratifying. The reversal of the skew predicted for the PDF from a left skew in curve 1 to a right skew in curve 3 is shown by the experiment, and curve 2 is symmetric as expected. This fit is convincing evidence of the validity of the approximation for PDF's for the closed speckle regime in this set of experimental conditions.

IV. Conclusions

In conclusion, we have resolved the apparent discrepancy in some previous treatments of modal noise generation in fiber by demonstrating that modal noise in fiber should be treated differently for two cases, that of open speckle patterns and that of closed speckle patterns. We have shown precise experimental confirmation of a mathematical treatment of the closed speckle pattern condition by demonstrating an accurate fit between experiment and theory for the ratio of mean transmitted power to standard deviation and also for the shape of the PDF of this power.

References.

1. B. Daino, G. DeMarchis, and S. Piazzolla, *Electron. Lett.* 15, 755 (1979).
2. K. O. Hill, Y. Tremblay, and B. S. Kawasaki, *Opt. Lett.* 5, 270 (1980).
3. E. G. Rawson, J. W. Goodman, and R. E. Norton, *Opt. Lett.* 5, 357 (1980).
4. R. E. Epworth, in *Technical Digest, Fourth ECOC, Genoa, Sept. 1978*, p. 492.



APPENDIX 5

Optical Transmission Channel Noise Phenomena
For High Bit Rate Fibre Optic Systems by:
E.J. Miskovic and P.W. Casper

OPTICAL TRANSMISSION CHANNEL NOISE PHENOMENA FOR HIGH BIT RATE FIBER OPTIC SYSTEMS

BY

E.J. MISKOVIC AND P.W. CASPER
HARRIS CORP.
MELBOURNE, FLORIDA

ABSTRACT

The present trends toward higher data rate and longer transmission distances have resulted in increased attention toward the characteristics of the electro-optical interfaces and the transmission channel. Due to the quasi-dynamic characteristics of the transmission channel, the combination of high data rates and larger repeater spacings compound signal propagation problems ultimately affecting the performance of an optical link. Four basic noise sources, referred to as "spurious noise", (laser, partition, modal and delay) are responsible for this performance limitation. This paper identified these various noise phenomena associated with the transmission channel and discusses their effect on overall channel performance. This paper is a consolidation of work done by Hitachi, STL, NTT and others along with studies and experiments performed at Harris particularly in the area of delay noise.

INTRODUCTION

As the technology advances in the area of optical transmission systems with regard to data rates and repeater spacings, noise phenomena associated with the transmission channel have become a more significant factor in evaluating the performance of the link. The transmission channel consists of the Injection Laser Diode, cable, connectors, splices and Avalanche Photodiode.

There are four basic noise sources associated with the transmission channel:

- 1) Laser noise - Total spectral intensity fluctuation emitted by the laser.
- 2) Partition noise - Individual wavelength intensity variations with constant total spectral intensity.
- 3) Modal noise - Amplitude noise generated at points along the channel where fiber-mode selective losses occur.
- 4) Delay noise - Jitter in the time of arrival of optical pulses transmitted through long optical fibers.

Rather insignificant in low-data rate, short distance systems, these noise sources became increasingly important as the data rate and distances increase. Up to the present, only the first three noise sources have been identified by others. Delay noise is a phenomenon that may cause severe limitations to high data rate systems using present technology lasers in the 0.83 μ m region.

LASER NOISE

The existence and characteristics of laser noise have been known for some time and it is continuously being studied to gain a better understanding of the cause and effect relationship between the transmission channel and the laser's noise output. Laser noise is an intensity fluctuation of the total spectral pattern and can occur with either single or multi-mode emission (optical "1" or "0" state).

Laser noise is stimulated by reflections back into the laser cavity from the laser/fiber and fiber/fiber interfaces. The phase, amplitude and frequency of these reflections all contribute, either constructively or destructively to laser emission. Tests indicate that relative reflection magnitudes as low as 10^{-7} can have an effect on the primary emission intensity. Because the intensity of the laser output varies, the laser noise can be detected at the rear facet of the laser.

Figure 1 (taken from Y. Ohgushi, et al, ref. 1) shows the effect of fiber on laser noise. Above threshold, the noise drops off significantly with no external reflections. However, in the presence of various amounts of reflection, the noise floor increases significantly. By intentionally increasing the end reflections with a mirror or decreasing them with index matching fluid, a 10dB difference in noise performance was observed when using a 1 meter fiber. From a laser noise standpoint, it appears advantageous to index match the output of the fiber pigtail.

The efficiency of the laser/fiber interface, as would be expected, also influences the laser noise performance. Data taken of the noise level for various laser/fiber coupling losses indicates that the noise floor decreases by approximately 10dB for large coupling losses (>5dB) (ref. 1). A lossy interface, although decreasing coupled signal, can provide better stability in other aspects of laser performance due to the reduction in reflected power entering the laser cavity.

PARTITION NOISE

As a multi-mode laser is modulated, the intensity of each wavelength can fluctuate, redistributing its energy to other modes. Partition noise refers to the phenomena that, although the total emission intensity remains constant, the spectrally-resolved output is shown to be characteristically dynamic.

Prerequisites for partition noise are: 1) multi-mode (longitudinal) emissions from the laser, 2) individual mode amplitude fluctuations and 3) wavelength dependent losses within the transmission channel. These modal intensity perturbations are influenced by laser thermal conditions, signal reflections into the laser cavity, aging, operating point and other laser-related conditions.

Under total detection conditions (no wavelength-selective losses), the mode partitioning has no effect on the detected signal. However, once the light passes through mode-selective loss mechanisms, the relative amplitude of the various modes changes from the initial conditions and, during summation at the detector, results in noise in the form of signal amplitude variations.

Partition noise occurs primarily in the optical "1" state where the laser is in its high spectral purity state. In this condition, the few spectral components of the signal are subjected to these wavelength-selective losses, including material dispersion. In the optical "0" state, generally the spectrum is wide enough where signal averaging reduces the overall effects of the wavelength-selective losses. Work done by Tanaka of Hitachi (ref. 2) indicates that a fiber/fiber connector has associated with it a wavelength - dependent loss mechanism which is cyclic in a lossy connector for a large (≈ 10 nm) multi-mode spectral output.

Figure 2 (from Okano, ref. 3) shows an example of the spectral output of a multi-mode laser along with the signal contributions of several of the dominant modes. Notice that under total spectral detection, the output is a well-defined pulse. However, the individual mode intensities violently fluctuate. When observing the spectral output from a laser with two dominant modes (optical "1" state), the effect of mode partitioning becomes more pronounced. The individual mode intensities oscillate between each other (mode competition, ref. 4) even though, under total spectral detection, the pulse is well-defined.

Okano, of NTT (ref. 3) demonstrated the effect of signal partitioning on the noise floor of the detected signal over a long fiber (7km). His tests and analysis indicate that as the spectral width of the laser increases, the maximum transmission distance must be decreased to maintain a constant BER. Because each simultaneous longitudinal mode is separated by the material dispersion of the fiber, the increase in spectral width results in increased detected noise.

Although partition noise can be categorized and characterized, it does not appear to have a significant influence on the limitations of high speed data links operating over less than 7km.

MODAL NOISE

Modal noise refers to the noise induced by the transmission medium (fiber, connectors and splices) where fiber mode-selective losses occur. The result is a random amplitude modulation of the received signal (similar to partition noise). Modal noise is the result of a combination of various dynamic parameters within the optical channel which have, as a common element, fiber mode-selective losses. Connector and splice imperfections and over-illumination of the detector constitute the bulk of these fiber mode-selective loss mechanisms.

In order for modal noise to occur, one of two channel characteristics must change, in conjunction with the mode-selective losses. Either the laser spectrum must be dynamically changing or there must be some relative phase and/or amplitude disturbance of the propagating fiber modes. In either case, the result is a perturbation in the speckle pattern generated at the fiber end.

Figure 3 shows the relationship between a fiber/fiber interface and the speckle pattern. Under stable conditions, the result of fiber misalignment is a fixed attenuation. However, as the speckle pattern changes, the coupled mode intensity varies causing a dynamic variation in connector attenuation.

One of the larger factors affecting the amount of modal noise generated at a given fiber interface is the spectral purity of the laser source. As the spectrum approaches a single-mode state (such as can be expected in the optical "1" state), the resultant speckle pattern becomes more defined. At the other extreme, as the spectrum broadens and approaches a LED type distribution (optical "0" state), the speckle pattern diminishes. It is then obvious that under typical conditions, the optical "1" state is affected more by modal noise than is the optical "0" state.

Figure 4 shows a photo of a 301 Mb/sec NRZ pattern with and without modal noise present. The top trace shows the effect of introducing an intentional connector air gap loss into an otherwise modal noise-free link (bottom trace).

There is an obvious relationship between coherence length (spectral purity) and modal noise. It is important to understand that interference between two rays (modes) can exist only if the difference in (differential phase relationship) is less than the coherence length of the source. Therefore, if the mode-filtering element (connector) were outside the coherence length of the source, no interference pattern would result. Under those conditions, modal noise would not exist. However, localized changes in the index of refraction due to slight fiber disturbances cause large differential phase changes in the propagation signal. If this change is time-dependent, the result at a fiber/fiber interface is a dynamic change in attenuation because of the interference pattern generated. This then leads to the fact that modal noise, initiated from source fluctuations, diminishes as the fiber length before an interconnection becomes longer. But fiber perturbation induced modal noise is rather insensitive to connector spacing.

Figure 5 shows a diagram of the transmission channel characteristics in relation to modal noise. As shown, it is a rather complex phenomena that is dependent on nearly every aspect of the channel. In understanding this phenomenon, a great deal about the performance and component interrelationships will be learned.

DELAY NOISE

Delay noise is in reality a special case of partition noise. Recall that partition noise is an amplitude effect due to, first, the spectral distribution of the energy and, second, the selective wavelength attenuation on propagation delay mechanisms in the transmission channel. If one were to consider a light source whose spectral width was not only large but was also time-variant, the basis for delay noise would become evident.

Delay noise, in essence, is jitter in the time of arrival of optical pulses transmitted through long optical fibers. It is caused by the time-varying spectral components and is transformed into signal transition jitter by the wavelength - dependent index of refraction of the fiber core. Although based on optical partitioning, it has very different effects on the system performance than does partition noise.

Illustration of delay noise calculation:

$$\text{Propagation of } \lambda_1 \text{ thru fiber} = \tau_1 = \frac{N_1 L}{C}$$

$$\text{Propagation of } \lambda_2 \text{ thru fiber} = \tau_2 = \frac{N_2 L}{C}$$

$$\text{Differential delay} = \nabla_{12} = \frac{L}{C} (N_1 - N_2)$$

$$\text{for } \lambda_1 - \lambda_2 = 4 \text{ nm (both in } 0.83 \mu\text{m region)}$$

$$N_1 - N_2 = 6.45 \times 10^{-5} \text{ (ref. 7)}$$

$$\text{thus for } L = 4.3 \text{ km}$$

$$\nabla_{12} = 4.3 \times 10^{-3} \times 6.45 \times 10^{-5}$$

$$\nabla_{12} = 0.924 \text{ nsec}$$

As shown above, the differential delay can be extremely significant when transmitting at high data rates. Figure 6 shows the effect of delay noise on the received "eye" diagram of a 301 Mb/sec NRZ PN sequence through 4.3 km of fiber. The measured delay is approximately 0.7 nsec.

Initially considered to be caused by instantaneous junction temperature changes as a function of data format, recent tests indicate that the spectral output of the laser changes with time (in the region of nanoseconds) resulting in an unstable spectral condition for high bit rate systems. Time resolved spectroscopic experiments have shown significant wavelength contributions to short data pulses, extending more than 4.0 nm from the stable, single longitudinal mode. These findings substantiate the cause and effect relationship between dynamic laser instability and delay noise.

Figure 7 shows the output of three adjacent wavelengths in response to an input pulse. (It should be noted that under static conditions, both the optical "0" and "1" states exhibited stable, single mode performance). Notice that two of the wavelengths die out within the first 10 nsec with the majority of the signal being carried by a single longitudinal mode. This occurrence is common among all lasers tested and forms the basis behind the delay noise phenomenon.

Delay noise generally occurs on the optical "1" to "0" transition because of the relatively high spectral purity of the "1" state as compared to the "0" state - generally near threshold. Because the dynamic spectral condition has a short lifetime, delay noise is insignificant in low data rate systems. Even at high data rates, transmission distances of several kilo-meters are required to observe this phenomenon.

The existence of delay noise does not appear to be a significant function of reflection back into the laser cavity nor is it highly affected by fiber mode coupling along its length. It is, however, very strongly related to the thermal condition of the laser. There exists a set of operating conditions, thermally related, that cause the laser to become dynamically unstable resulting in a larger spectral width.

SUMMARY

Four "spurious noise" sources (laser, partition, modal and delay) have been defined and characterized. These noise sources can have very severe effects on high data rate, long distance systems. Laser and partition noise phenomena result in an effective increase in the noise floor of the detected signal. Modal and partition noise phenomena introduce dynamic signal amplitude variations into the propagating signal. Both noise sources are related to the optical efficiency of the transmission channel. As the channel becomes more optically transparent, the effects of those disturbances decrease. Delay noise phenomena results in received signal transition jitter (optical 1-0 transition) when transmitting pseudo-random NRZ data patterns. A cause and effect relationship for each of these noise sources has been established.

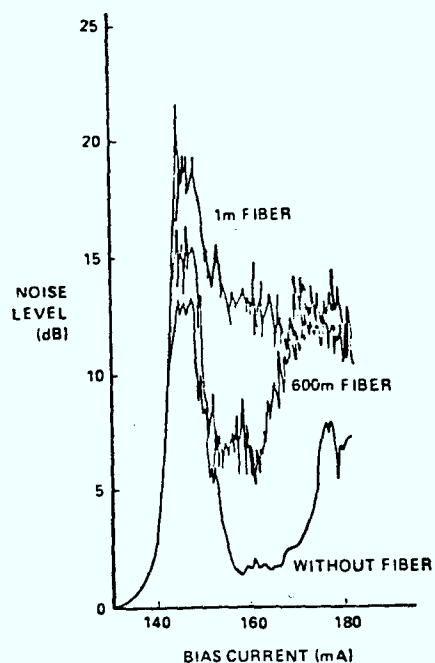
Of these noise sources, modal and delay noise have the most significant effects on system performance. Modal noise can be controlled in two ways. First, if the coherence length of the laser were decreased, the interference effect of differential phase changes would be lessened. Second, by improving fiber/fiber interfaces (connectors and splices), the speckle pattern changes would result in small dynamic connector attenuation variations.

The delay noise phenomena presently appears to be mainly related to the dynamic characteristics of the injection lasers. Under appropriate conditions (operating transmission channel) does not have some influence on the magnitude of the dynamic spectrum but its affects presently appear to be second order.

Extensive work is being done in both the modal noise and delay noise area in an effort to obtain a greater understanding of the problems and to determine system design considerations that may minimize or eliminate these noise sources.

REFERENCES

1. Y. Ohgushi, et al., "Laser Diode Noise In Fm Signal Transmission System".
2. M. Tanaka et al., "New King of Noise Performance in Optical PCM 200 Mb/s Transmission Systemes".
3. Y. Okano et al., "Laser Mode Partition Noise Evaluation for Optical Fiber Transmission".
4. M. Ito, T. Kimura, "Longitudinal Mode Competition in a Pulse Modulated AlGaAs DH Semiconductor Laser", IEEE Journal Quantum Electronics, Vol. QE-15, July 1979.
5. R.E. Epworth, "The Phenomenon of Modal Noise in Analogue and Digital Optical Fiber Systems".
6. N. Kashima, N. Uchida "Relation Between Splice Loss and Mode Conversion In A Graded-Index Optical Fiber", Electronics Letters, June 7, 1979 Vol. 15, No. 12.
7. I. H. Malitson, "Interspecimen Comparison of the Refractive Index of Fused Silicia", Journal of the OSA, Vol. 55, No. 19, October 1965.



(TAKEN FROM DHGUTHI, ET. AL.)

FIGURE 1 THE EFFECT OF FIBER LENGTH ON LASER NOISE ($I_{TH} = 145\text{mA}$)

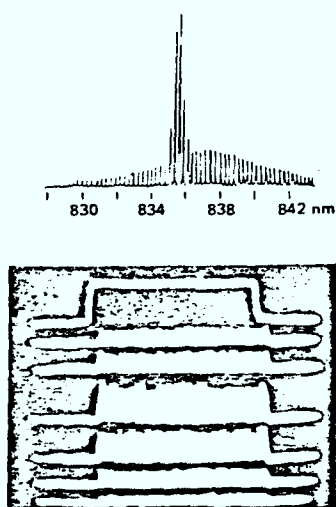


FIGURE 2 LASER OUTPUT SIGNAL CHARACTERISTICS IN MULTI-MODE OSCILLATION
(a) SPECTRAL CHARACTERISTICS
(b) TIME DOMAIN FEATURES

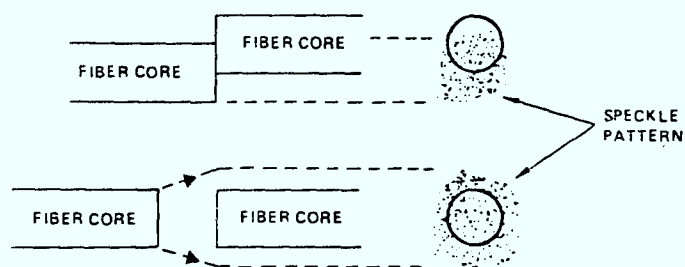
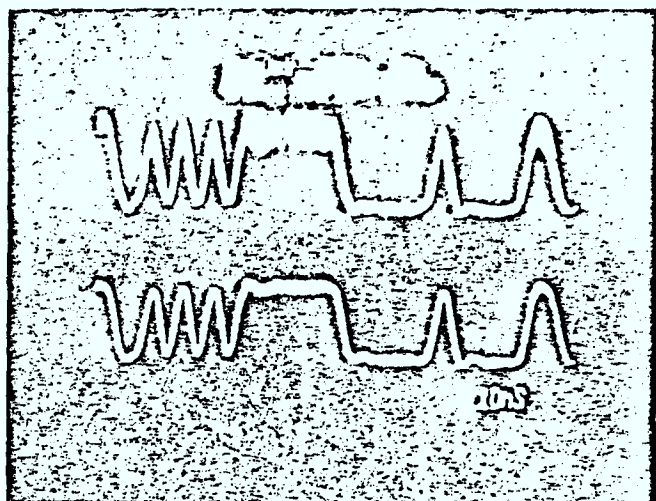


FIGURE 3 INTERFERENCE PATTERN AND EFFECT OF FIBER MISALIGNMENT



WITH CONNECTOR AIR GAP

WITHOUT AIR GAP

FIGURE 4 301 Mb/sec. DATA PATTERN

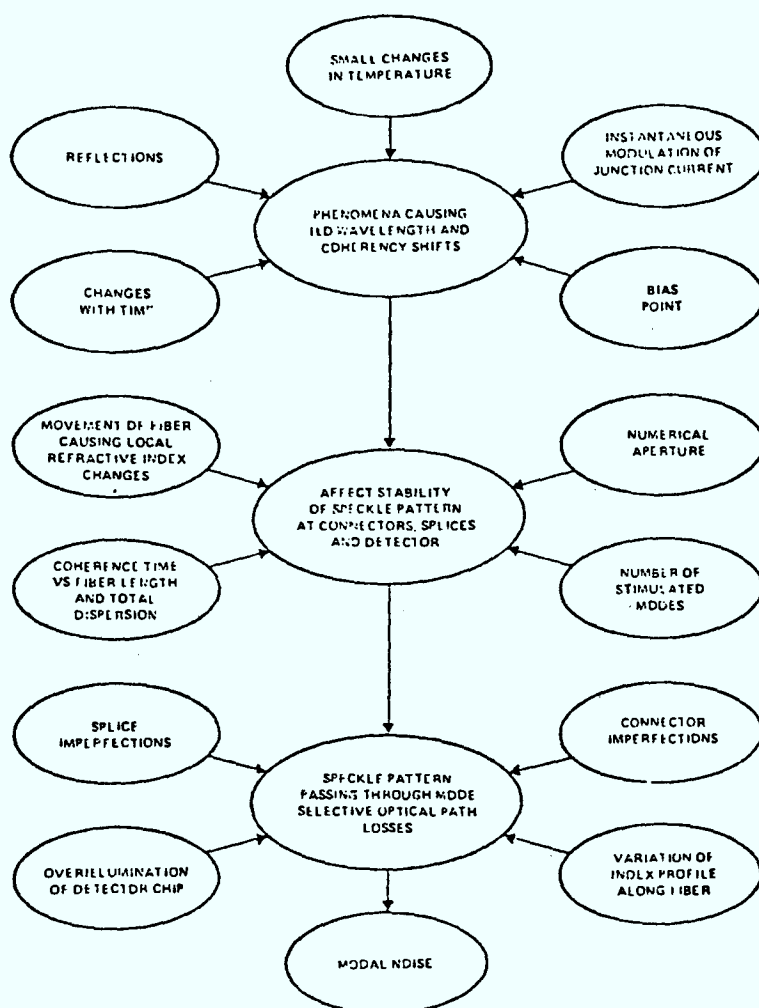


FIGURE 5 INTERRELATIONSHIP OF PHENOMENA AFFECTING MODAL NOISE

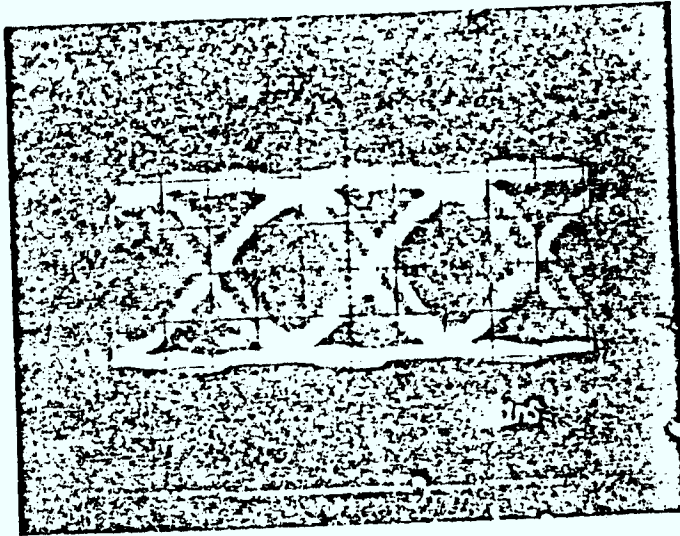


FIGURE 6 "EYE" DIAGRAM OF 301 Mb/sec.
NRZ PN SEQUENCE CABLE DISTANCE = 4.3 km

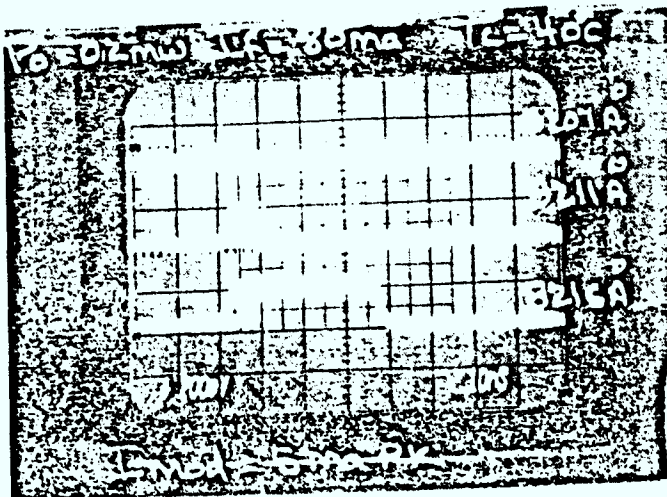


FIGURE 7 TIME DEPENDENCE OF ILD
WAVELENGTH TO INPUT PULSE

FRANK, LEON.
--Broadband communications
network (BCN) project :
final report.

LKC
P91 .C655 F7 1982
Broadband communications
network (BCN) project :
final report

DATE DUE
DATE DE RETOUR

JUL 28 1988

LOWE-MARTIN No. 1137

CRC LIBRARY/BIBLIOTHEQUE CRC
P91.C655 F73 1982 c. a
INDUSTRY CANADA / INDUSTRIE CANADA



220416

